Acknowledgement

I dedicate this work to my parents.

Summary and Conclusions

The topic of this thesis is damage of hydraulic machinery due to sand erosion. This is a very broad topic in which all the aspects of design of hydraulic machinery namely material selection; mechanics of material and hydraulics are involved. The issue of sand erosion is equally important for operation and maintenance of hydropower plants.

The erosion damage of turbines of hydropower plants in Himalayan Rivers, in particular in Nepal, due to high sediment contents in river is a motivating factor for this research. The findings of this study are believed to help to reduce erosion of turbine components, increase their life time and improve maintenance procedure.

The objectives of this study are to:

1. Study the erosion process on different materials and compare lifetime of turbine material with hard surface coating.
2. Study the flow in the turbine and identify the region of highest velocity and acceleration where most serious sand erosion occurs.
3. Study erosion rate of turbine as a function of operating parameters (head and speed), particle characteristics and turbine material.
4. Assess loss of efficiency and to analyze repair method and repair interval that gives optimal economy of the hydropower plants.

The goals laid out in the objectives are achieved by understanding the theory of erosion of material through literature, investigating the nature of turbine damage from field observation and finally by experiments to study effect of variables of erosion rate and investigation of particle separation process in rotational flow.

Erosion

Erosion, cavitation pitting and corrosion are major material removal procedures in hydraulic machinery. Erosion is caused by impacts of solid particles against the surface. It is often misunderstood as one class of abrasive wear. Cutting, fatigue and brittle fracture are basic mechanisms of solid particle erosion. The factors affecting erosion rate are as follows:

1. Factors associated with operating conditions – velocity, acceleration, impingement angle, flux rate, medium of flow and temperature
2. Factors associated with eroding particles - size, shape, hardness and material
3. Factors associated with substrate (base material) - chemistry, material property and morphology

The models for erosion rates generally incorporate these factors and such models are useful for design of turbine components, sediment settling basin, and optimization of power plants in sand-laden river. Erosion models are developed on the basis of individual particle

dynamics or from empirical relations based on experiment and field experience. The erosion mechanism is complicated when erosion, cavitation and corrosion act together. The synergies between these factors generally enhance the damage and prediction of such a combined effect is difficult.

The material in the eroded components can be broadly classified as metals, ceramics and polymers in terms of their distinctive erosion behavior. The metals have large range of toughness and hardness to suit variety of operating conditions. Steel is most common structural material. Historically, austenitic steel, 18Cr8Ni, was used as turbine steel that is later replace by martensitic steel 13Cr1Ni. Most of the modern turbines are made from martensitic-austenitic steel 13Cr4Ni or 16Cr5Ni. Ceramic and ceramic-metallic (cermets) are hard, sustain high temperature and are resistant to corrosion. They have poor toughness and suffer with high erosion in brittle mode. Tungsten carbide (WC) coatings with Co, Ni, Cr, Mo as binder are widely used in turbine industry. Such coatings are applied by thermal spray. The quality of coating depends on powder properties and spray process. Cladding, plasma nitriding and laser treatment are some other processes for improving erosion resistance of materials, but they have not shown promising performance in hydropower turbines.

Erosion of hydraulic turbine

High head Pelton and Francis turbines are most affected by sand erosion. Low head reaction turbines will be eroded only in case of extremely high sediment concentration. The erosion of hydraulic machinery can be classified in to: (i) micro erosion due to fine particles (<60 μm) at high velocity (ii) secondary flow vortex erosion caused by obstacles or secondary flow (iii) acceleration of large particles (> 0.5mm) (Brekke, 2002).

Nozzle, needle and buckets are most affected components of Pelton turbine. Basic design criteria for Pelton runners operating in sand laden water are: (i) buckets with largest possible curvature and size (ii) lowest number of jet and (iii) largest hydraulic radius. Runner, guide vanes, facing plates and labyrinth seals are most affected components of Francis turbine. Smooth acceleration in guide vane, stay vane outlet angle to keep guide vane at neutral position in normal operation condition are important design criteria for Francis turbines.

Pelton turbines are preferred to Francis in overlapping zone of turbine selection diagram because of shorter repair time. Lowest number of units and lowest possible speed should be selected to minimize effect of sand erosion. Low maintenance cost, ease of dismantling and replacement of components are factors for turbine selection.

The efficiency of eroded turbine decreases and turbine becomes structurally weak. The turbine efficiency drops due to leakage of the water, incorrect direction of flow and secondary flow or friction loss. Because of sand erosion, Francis turbine has largest drop in efficiency at part load and Pelton turbine has largest loss at best efficiency point (BEP). The causes of efficiency loss in Pelton turbine are: (i) water bypassing from eroded entrance lip without doing useful work, and (ii) change of flow direction and braking effect due to back hitting. The increase in clearance between guide vane and face plates, leakage through

labyrinth seals and friction loss in eroded surface are main reasons for loss of efficiency in the case of Francis turbine.

The operational strategies to minimize effect of erosion are: (i) deeper submergence of Francis turbine to avoid cavitation pitting (ii) plant shut down at high sediment concentration (iii) reduce operation time at off design point to avoid higher relative velocity at the runner outlet, secondary flow and vortices leading to local erosion (iv) minimum start and shutdown sequence to avoid mass oscillation and sweeping of sand particle from tunnel floor.

The appearance of cavitation damage has pit holes with sharp edges which bleeds finger. Sand erosion surface are with shinning luster and wavy scales or ripples. But the appearance in combined effect of these two is not clear. The shape and size of ripples reflect local erosive condition, which is a function of flow pattern, particle size & shape and concentration. These ripple pattern can be used as inspection indicator in the hydraulic turbines.

Field study in Nepal

The climatic and physical conditions are highly favorable for erosion and sedimentation. Excessive sediment in the Himalayan River is due to presence of weak rocks, extreme relief and heavy monsoon rain. Multidimensional approaches, such as management of catchments area to avoid sediment production, settling basin management to screen large particles and enhancing erosion resistance of underwater components are needed to tackle with the sediment problems.

Out of 19 power plants (>2MW) in operation in Nepal, almost all have sand erosion problem. The 1.83 million tons/year average sediment load is damaging Francis turbine components of 3X23 MW Marsyangdi hydropower project (MHP). More than 80% of particles in the suspended sediment passing through turbine are smaller than 0.05 mm and about 90% of this is quartz and feldspar (Kayastha, 1999). The repair cycle for each unit is three years. The 3X4MW Francis turbine components of Jhimruk hydropower project (JHP) is severely damaged by about 9300 tons of sediment through one unit with in one monsoon season. Around 83% particles are smaller than 0.09 mm consisting 85% quartz. The repair cycle of this turbine is only 1 year. The 5X12 MW Pelton turbine of Khimti hydropower project (KHP) is also eroded due to fine sediments. The maintenance cost is less than 10% of replacement cost at JHP and 15% at MHP. Hence maintenance is preferred in power plants in Nepal even if efficiency of system is degrading.

The thermodynamic efficiency measurement at JHP revealed 4% loss at BEP and 8% loss at 25% load for operating time from Sept-Nov, with only 9600 tons of sediment. The leakage loss is 50% of total efficiency loss. The provision to prevent sand laden water through labyrinth can reduce this loss. One of such provision could be inserting clean water through these seals. Relative efficiency measurement was not successful because of blocking of pressure tap by sediment.

High velocity jet erosion test rig

High velocity jet erosion test rig at NTNU/SINTEF is selected for investigation of factors influencing erosion rate because of low test cycle time, possibility to carry out test at different impingement angles and easy control of variables like velocity and sand concentration. Baskarp-15 foundry sand with 67% free quartz and mean particle size 0.15mm is used as eroding particles. The concentration in between 0.38% to 0.08% by weight can be obtained in the jet velocity range 20 m/s to 80 m/s. The erosion tests by sand sample from Nepalese rivers were carried out on 16Cr5Ni specimen on jet type of test rig at Kathmandu University laboratory. Sediment samples of bed material from 30 locations were collected covering main basins, rivers, tributaries, hydropower plants of all over Nepal. Erosion tests were carried out by particles of sizes <90μm, 90-212 μm, 212-300 μm, 300-425 μm, 425 -500 μm and >500 μm.

Ductile materials have maximum erosion at low impingement angle in between 10° to 30° and brittle material have maximum erosion around normal. Aluminum and austenitic steels have shown ductile mode of erosion, but martensitic steel and ceramic coatings have shown brittle mode. The difference of erosion rate at 45° impingement angle and highest erosion rate was found to be moderate. Hence estimation of erosion rate at 45° can be conservative and realistic prediction of turbine erosion because actual impact angle in turbine is also small.

The most general expression for relation between erosion rate and velocity of particle is *Erosion* $\propto$ *Velocity^n*, where the value of exponent n may vary depending on operating conditions. The kinetic energy of particles gives this exponent value as 3. The experimental data of erosion rate against impact velocity also follows power law. For hydraulic turbines, exponent value is proposed in between 3-4 based on experimental observation. The higher value of velocity exponent for actual turbine components is proposed because of complex operating condition of hydraulic turbines.

The value of velocity exponent for garnet, aluminum oxide and sand particles at same test condition varied in between 3.3-3.8. The values of velocity exponents for these particles are increasing with the increase of density of particles. Hard particles have irregular shape and give high value of velocity exponent. The difference in erosion rate is large at high velocity region, which indicate need of careful mineralogical analysis for high head projects.

The erosion of actual hydropower turbine increases with increase in sediment concentration. In laboratory measurement there is no significant difference in erosion rate for increasing concentration. This is because, after certain limit there will be interference between particles and the erosion rate is presented in term of weight of striking particles.

Turbine steel 13Cr4Ni and duplex steel SAF 2304 have shown better erosion resistance with erosion rate less than 10 mg/kg in all operating condition. Turbine steel 13Cr1Ni has shown poorest erosion resistance which has minimum erosion rate around 15 mg/kg. Turbine steel 16Cr5Ni have shown relatively higher erosion rate than 13Cr4Ni and duplex steel.

The ranking of erosion rate of ceramic coatings in term of volume loss per unit striking particle is $75Cr_3C_2$-$25NiCr$>$86WC$-$10Co$-$4Cri$>$86WC$-$6Co$-$8Cr$. The better erosion resistance of $86WC$-$6Co$-$8Cr$ could be due to uniformly distributed fine carbide particles in the matrix. The polished coatings have shown better erosion resistance. But ceramic-metallic coatings are normally used in as sprayed condition in hydraulic machinery.

Polymers have ability to absorb energy of striking particles and also have good erosion resistance in corrosive media, but their use is restricted to low temperature applications. Erosion resistance of soft material (elastomer) coatings is found very poor in high velocity jet erosion test. Such coatings are not appropriate for hydropower turbine components.

The morphology of surface changes due to erosion and on the other hand, erosion rate is normally high on rough surface. The combined effect of erosion and cavitation can take place due to rough surface at high velocity. Any logical trend or relationship of erosion rate with respect to specimen surface roughness could not be traced due to uncertainty in test specimen.

The stress will be induced under the point of particle strike. The deformation of material and hence also the erosion should be dependent on pre-stress in the surface. But no specific conclusion was obtained from the test on pre-stressed specimen. Bending of specimen with four point bend clamp may have neutralized pre-stress during rolling or machining.

The velocity and impact angle depend on shape and size of jet in this test rig. The hitting of specimen edge by jet has significant contribution in the error in the result. This effect is pronounced in low impact angles. Recirculation and secondary flow within the tank is another source of main error.

The extrapolation of relation between erosion rate and velocity can be used to obtain weight loss of turbine. Erosion estimate from experimental measurement is found about 3.5 times higher than the one estimated by inspection of eroded turbine of JHP. This can be because all particles passing through turbine conduit will not necessarily strike surfaces. This is a cause of difference of experiment and field observation. The ratio of wetted surface to volume of water may give indication of this factor, which depends on turbine type and size. This relation is not yet clearly understood, but this is important for experimental as well as numerical investigation of erosion of turbine. The experimental measurement from high velocity jet test rig gives close estimation of material removed from the turbines.

Quartz is found as main constituent of the sediment in Nepalese rivers. On average, nearly 70% of the constituent of the sediment are hard mineral content with hardness more than 5 Moh's scale. The overall trend of erosion rate is found to be increasing from western river basins to east, which is in accordance with the content of quartz in the sample. The erosion capacity of particle was decreasing when they traveled long distance. The erosion rate has linear and slightly increasing trend with respect to percentage of hard particles. The significance of shape of particle, not only percentage of hard mineral contents was also observed from this test.

Rotational flow

The experience of erosion of Francis and Pelton turbines by particles of different size have confirmed phenomenon of particle separation. The observation of particle rotating in swirl flow by naked eye and with high speed video camera on the newly developed test rig at NTNU verified the concept. Following conclusions are drawn from the experiment:

- The equilibrium of particle in between centrifugal force and drag force holds true in case of swirl flow.
- Theory of swirl flow is true in case of test rig. The measured and computed pressure distribution in the swirl flow is very close.
- The visualization of flow direction in the swirl flow confirms assumption that flow direction is same in all radial positions.
- The radial position of rotation of particles of various sizes confirms drag coefficient is function of Reynolds number. The experimental observation reveals that drag coefficient for particles at high Reynolds number, for example higher than 10^5, is in between 0.1-0.2.

Sand particles of diameter higher than 2 mm will stay rotating in the swirl flow and damage guide vanes of Francis turbine of radius 1 m positioned around 10°. This study also indicates that smaller turbines are more likely to be damaged by sand erosion because of smaller critical diameter, for example particles as small as 0.35 mm may remain rotating in the turbines of inlet diameter 800 mm. This is a likely case at Jhimruk hydropower project in Nepal. This research suggests guidelines for operating strategy for Francis turbine operating with large sand particles. If the particle size in the water increases critical particle sizes, the turbine should not be operated at low guide vane opening.

List of symbols

ρ	density of liquid (fluid)
α	impingement angle
ε	deformation wear factor
λ	ripple wavelength
β	turbine coefficient (constant)
$f(\alpha)$	function of angle α
θ_p	angular position in cylindrical co-ordinate
ρ_p	density of particle
$\Delta W_{Corrosion}$	corrosion synergy due to erosion
$\Delta W_{Erosion}$	erosion synergy due to corrosion
a	average grain size coefficient
B_s	ratio of hardness to fracture toughness
c	concentration of particles
C	velocity of fluid
C_D	drag coefficient
C_u	peripheral component of absolute velocity
Cw	ratio of weight of solid to mixture
D	characteristic dimension
d	diameter of particle
F_c	centrifugal force
F_D	drag force
g	gravitational constant
h	water head
H_n	net head
H_v	hardness
K	constant expressions
k	intrinsic constant
Kl	constant expressions
k_1	shape coefficient
k_2	hardness coefficient
k_3	abrasion resistant coefficient
K_c	fracture toughness
K_{env}	constant depending on environment
k_i	constant velocity at inlet
K_{mat}	constant depending on material
k_n	constant velocity at nozzle
K_T	threshold velocity
k_v	constant velocity at valve
M	total mass of particle
n	exponent of velocity
N	rotational speed
P	plastic flow stress

ix

p	pressure
Q	total volume removed by cutting wear
q	hard particle content
r	radius of particle
R	radius of rotation
R_c	radius with highest C_u
Re_p	particle Reynolds number
r_p	radial position in cylindrical co-ordinate
S	amount of sediment
t	erosion time
U	peripheral velocity
V	velocity of particle
$V_\perp$	normal velocity component
V_θ	relative gas velocities in the circumferential directions
V_{ll}	parallel velocity component to surface
V_r,	relative gas velocities in the radial directions
V_z	relative gas velocities in the axial directions
w	erosion rate (thickness loss/time)
W	erosion rate (weight loss/particle weight or loss of thickness/year)
W_c	cutting wear
W_C	corrosion rate
W_D	deformation wear
W_t	total wear (cutting and deformation)
W_T	total wear rate (erosion and corrosion)
x, y and z	exponent value
Z	height
z_p	axial position in cylindrical co-ordinate
η_m	efficiency due to mixture
η_w	efficiency due to clean water
v	kinematics viscosity
ς	cutting wear factor

Table of Content

List of figures

List of tables

Chapter 1

Introduction

1.1 Background

Nepal has numerous rivers and streams with perennial supply of water from the glaciers of the Himalaya. Himalayan topography and continues sources of water have favored the country with a huge hydropower potential. It is estimated that around 42130 MW could be economically harnessed (MWR, 2003). Less than 2% of that is developed so far. Until 2004 nearly 550 MW of hydropower generating capacity is installed (NEA, 2002/03). Per capita energy consumption in Nepal is one of the lowest in the world, but energy demand is growing day by day. Apart from this, there are tremendously large neighboring markets like India, China, and Bangladesh, where electricity demand is high and electricity can be exported. The prospects for hydropower development in Nepal are thus very good. But it is important that all the challenges concerning this important development are dealt with.

One of such challenge for hydropower development, specific for the Himalayan region, including Nepal and some other regions of the world is withdrawal of clean water from sand-laden rivers (Støle, 1993). Most of the Himalayan River contains very high sediment concentration, especially during the monsoon season. Major components of this sediment are hard abrasive sand and silts.

There are two main problems concerning sediment aspect of hydropower development. The first is efficient operation of hydropower plants to meet the electricity demand by storing energy in reservoirs that will be filled with sediments over a period of time. This problem must be taken care of by sediment settling systems in power plants. However, huge amount of unsettled sediment pass through the turbines every year and turbine parts operating in such water are exposed to severe erosion. This represents second challenge. The impact of sediments in the water passing the turbines at high velocity causes severe erosion of turbine components. That will be the main concern in this thesis.

Special headwork, sediment settling basins and sediment-flushing system are designed to remove sediment particles and isolate mechanical and structural components from impact by sediments. Design of civil structures and mechanical components as well as selection of materials are often dictated by the demand to reduce the erosion of turbine. Sediment settling basins increase the cost of the hydropower projects significantly. Hence they are designed to removing only coarser sediment particles. In principle, smaller particles are allowed to pass through the turbine. Settling of particles smaller than 0.2 mm is costly. However, even with the particles less than 0.2 mm severe erosion of turbine components are observed in high head turbines.

The loss of material from component over a period of time means a geometrical change of the turbine parts. This is caused by erosion, cavitation pitting and corrosion. The eroding particles present in the moving fluid possess high kinetic energy. When these particles strike surface, wear of material takes place by cutting or deformation of the surfaces. This type of wear is called erosion. There are industries, which are working in aggressive environment or handle aggressive materials. Examples of such industries are marine, offshore, process, mining and manufacturing. Components used by such industries are exposed to erosion. The working principle of erosion is same as that of abrasive water jet machining. The rate of erosion are dependent on (i) properties of sand particles (grain size, shape, hardness, material), (ii) properties of substrate materials (chemistry, elastic properties, hardness, surface morphology) and (iii) operating environment (velocity, impingement angle, flux rate or concentration, medium of flow, temperature). The result obtained in this thesis may thus be of use to applications other than those met in hydropower turbine constructions.

High head Francis and Pelton turbines are highly affected by sand erosion. Even low head Kaplan turbine and propeller turbines are also found eroded in rivers with high sediment contents. Bucket, nozzle and needle are the most affected parts of impulse turbines. Guide vanes, faceplates, runner blades and seal rings are vulnerable parts in reaction turbines. Components with comparatively low velocity region, such as inlet valves, spiral casing, draft tube and wheel pits are also to a certain extent will be eroded by sand-laden water. Normally the erosion of small unit is worst than for larger units when comparing turbines operating at the same head with the same water velocity. This is due to small radius of curvature and smaller hydraulic radius bringing more particles in contact with the surface with a higher acceleration.

In addition to the skill of design, knowledge of the erosion mechanism is of large importance for engineers working with operation and maintenance, where sand erosion plays a decisive role. The decision to be taken between repairs versus replacement of turbine is always a challenging task. The optimization of time period and economy of refurbishment is a complex task where the cost of the repair technology, investment, downtime during repair and routine maintenance cost have to be considered.

Yet, very little attention is given in Nepal to study the theory of wear, methods to improve the wear resistance of material and methods for maintenance. Corrective maintenance is the normal approach followed in Nepal for the repair of worn out turbines, mostly on a hit and trial basis although sedimentology is gaining attention in Nepalese hydropower projects. Surface of the turbine components have been coated with the high erosion resistant coatings as a preventive maintenance. The damaged turbine components are repaired by welding with suitable electrode, machined and grinded in order to obtain the correct profile of blade or bucket. This is a quite labor-intensive process and labor cost is significant in total maintenance cost. The maintenance cost in Nepal (and in developing countries) is low compared to replacement cost due to cheap labor cost. The hydropower companies normally prefer to repair the turbine rather than frequent replacement; hence focus should be directed on method of repair and maintenance. The challenge for the repair of the eroded turbine is to select and use proper type of welding and coating material to get best performance from the turbine.

Sand erosion is not a major problem in Norway and other parts of the world with stable geology and old rocks, where soft rock has been removed by moving glaciers. The water in these regions is clean and turbine runner can sustain the lifetime of the project. However, some cases of sand erosion are reported also in Norway with very fine sand coming in to the river from glaciers (Bjordal 1995, Brekke 1988). Though this problem seems to be more crucial for Himalayan region and Andes Mountain in South America, it has an application throughout the globe for example Alps in Europe.

Hydraulic turbine and pump work in similar principle and constructions of these two are also similar in many aspects. But operating environment of these two machines can be different. Mostly turbines are expected to run in clean water, but pumps may have to operate at different environmental conditions such as corrosive fluids, chemicals and solid slurries. Hence erosion of pump component is possible when it is handling fluid containing abrasive particles.

Beside solid particle erosion, corrosion and cavitation erosion are other types of material removal mechanism in hydraulic machinery. These three types of material removal processes can take place singly or they can act together. The synergy between sand erosion, cavitation and corrosion can be significant, and lifetime of the hydraulic machine could be reduced considerably.

1.2 Objective

The main aims of this Ph.D. study are more specifically:

1. To study the erosion process on different materials and compare lifetime of turbine materials with hard surface coatings.
2. To study the flow in the turbine and identify the region of highest velocity and acceleration where most serious sand erosion occurs. This work is concentrated on high head Francis and Pelton turbine.
3. To study erosion rate of turbine as a function of operating parameters (head and speed), particle characteristics and turbine material.
4. To assess the loss of efficiency due to erosion and to analyze repair method and interval that gives optimal economy of the hydropower plants.

1.3 Research Methodology

This study of the effect of sand-laden water in the hydraulic machinery is basically aimed to contribute to the knowledge for: (i) operation strategy of hydropower plants (ii) selection and design of turbine (iii) selection of appropriate material for turbine construction and maintenance (iii) maintenance of eroded turbine and maintenance scheduling. Hence all technical, management and economical aspects are considered in this study. Realizing the fact, that the knowledge of all these areas is necessary to achieve the aim of the project, this study includes literature study, field study, simulation and experimentation.

Very little literature is published on specific problem of sand erosion in hydraulic machinery. Much more is available on erosion mechanism from the point of view of

material science for different applications. The findings reported in such literature applied to erosion problem in hydraulic machinery are in this thesis.

The second part of the thesis describes a field study in Nepalese and Norwegian hydropower plants. Inspections of effect of sand erosion in various types of turbines in different operating conditions were made. The technology used to repair turbines erosion and management of maintenance activities were investigated during the field study. The field investigation also includes the investigation of efficiency of turbine damaged by sand erosion which was done at Jhimruk hydropower project, Nepal by thermodynamic efficiency measurement.

In the third part, the erosion damage at the location of highest velocity and acceleration is investigated on the basis of hydraulics, empirical relations and experimental measurement as a function of head, speed and other variables such as concentration, particles and material properties.

One of the important contributions of this study is the investigation of the erosion of different turbine steels and erosion resistant coatings by laboratory experiment. This test is carried out on high velocity jet erosion test rig at NTNU/SINTEF at controlled environment. The study of other variables like velocity, concentration, and impingement are also done in the same rig.

The effects of particle shape, size and mineral contents on erosion of turbine components are studied by collecting actual river sand from different rivers of Nepal. The test facility with high velocity jet erosion test rig was developed at Kathmandu University (KU) laboratory. The erosion tests with sand samples from Nepalese rivers were carried out at KU laboratory.

The study of separation of large particles accelerating normal to surface and particles rotating in swirl flow is studied by developing new test rig at NTNU water power laboratory. The particle trajectory is analyzed by using high speed video camera.

These research activities of literature study, field visit and measurements contribute to achieve the goal of one or more of the aim setup in section 1.2.

1.4 Outline of thesis

First part of this thesis from chapter 1 to 5 is background information and the theoretical part, containing introduction of the problem, wear, erosion, material and sand erosion in hydraulic machinery. This part is basically based on literature study and outlines the different types of wear and erosion mechanisms, their effect and factors affecting the erosion rate. Effects of erosion on hydraulic turbine components and materials are basically presented on the basis of experience that the author has acquired from hydropower projects and cases reported on literatures. Some of the observations of field inspection in Nepal and Norway are also reflected in the chapter 5.

Rest of the thesis from chapter 6 to 11 gives contributions to the problems at hand. Chapter 6 is based on the study and field visits on different hydro power plants in Nepal. The status

of Nepalese hydropower industry is presented and the status of erosion problem and methods followed to repair turbine components are discussed in this part. The results of efficiency measurement at Jhimruk hydropower project, Nepal to study the effect of sand erosion on performance on Francis turbine are also presented in this chapter 6.

Chapter 7 and 8 are introduction and presentation of findings of experiment on high velocity jet erosion test rig at NTNU/ SINTEF and Kathmandu University. These two chapters in combination are self-contained including background introduction on experimental investigation of erosion, objective of experiment, material, method and discussion on findings. The results of erosion tests from sand of rivers and hydropower projects in Nepal are also included in chapter 8.

Chapter 9 and 10 is about the newly developed test rig at Water Power Laboratory to study effect of particle motion in curved path or rotational motion. This test rig was developed based on some of the observation erosion test on curved specimen presented in chapter 8 and experience of power plant in Nepal and other countries. This chapter is also original contribution to the problem of sand erosion of hydraulic turbines. This include proposition of concept of large particle separation in rotational flow in between guide vane outlet and runner inlet. The description of newly developed test rig, test procedure and observation of particle separation from naked eye and high speed video is presented.

Finally, on the basis of conclusions from this research, the suggestions for further study are proposed in chapters 11.

1.5 Earlier work

Basically earlier erosion studies are carried out from material point of view. Truscott (1972) presented the literature survey on wear test of materials, wear test on pumps and service experience of pumps. His paper summarized the factors affecting wear and theory of wear together with discussion on hydraulic performance and expression for pump life. Finnie (1960) and Bitter (1962) have developed most fundamental erosion model for ductile and brittle materials. The work of Duan (1981) is one of the pioneer collection (in Chinese) in the field of sand erosion problem in hydraulic machinery where he presented mechanisms of erosion, damage of turbine parts, turbine design criteria and erosion resistance of materials. Duan and Karelin (2002) further edited the work of several researchers to incorporate recent advancement in the knowledge of sand erosion in hydraulic machinery. The work of Prof. Hermod Brekke related to sand erosion for instance on choice of turbine (Brekke, 1978), performance of eroded turbines (Brekke, 1988), Norwegian research work on erosion resistance coating materials (Brekke, 1994), Pelton turbine design (Brekke, 1994) and design and material quality for high head turbines (Brekke, 1986) are summarized in the chapter "Design of hydraulic machinery in sand laden water" in Duan and Karelin (2002). Naidu (1996) and Naidu (1999) have presented sand erosion problem in hydropower plants in India with remedial measures. The contribution of researcher in the field of sand erosion is referred extensively in chapters 2-5. However, the literature survey of experimental study of erosion is presented separately in appendix A.

Chapter 2

Wear of materials

2.1 Introduction and definition

Wear of water turbine due to sediment, denoted as erosion, is one of many forms of wear. Many different terms are used in literature to describe the material removal mechanism from hydraulic machinery. Hence it is essential to have the general knowledge of wear, its types and mechanisms before actually dealing on the topic "Sand erosion in hydraulic machinery".

It is however difficult to formulate precise, vivid and self-explanatory definition of wear. Most general definitions of wear are more concerned on the progressive loss or destruction of material from mechanical interaction between components. Wear is defined as (ASTM G40 - 88) "damage to a solid surface, generally involving progressive loss of material, due to relative motion between that surface and a contacting substance or substances ". On the other hand, Bhushan (2002) emphasize that the material displacement on a given body, with no net change in weight or volume also should be considered as wear.

2.2 Classification of wear

Wear can be classified and characterized in many ways. Before 1950's only adhesive, abrasive, surface fatigue and corrosion were considered as major and principal types of wear and more than 95% wear experienced in the machinery of that period were expected due to one or more of those four major wear type (Burwell, 1957). Summarizing the literatures (1957- 2001), Bhushan (2002) identified six principal wear mechanisms, which are quite distinct phenomenons, but have only one thing in common, that is 'removal of solid material from rubbing surfaces'. He added erosion by solid particle and droplet impact in the classification of Burwell (1957). Meng and Ludema (1995) found only nominal agreement on the meaning of the terms used by most of the researcher on mechanisms, mode or process of wear. A list of the frequently discussed wear mechanisms are presented in Table 2.2.1 together with definition of all types.

The wear of hydraulic machinery due to the sand laden water is erosion. Even if minor abrasion may take place in certain parts of turbine due to entrainment of particles such as in bearings, erosion is the main cause of damage and this is the main area of study in this thesis.

2.3 Wear rate

The mechanism, means, location and magnitude of damage varies in different types of wear. Hence wear process is generally quantified in term of wear rate, but because of above-mentioned differences, it is really hard to use a common method for defining wear rate. The traditional way of defining the wear rate of the surface is the depth or volume of material removed per unit of sliding or rolling distance (Bhushan 2002).

General definition of wear rate is (ASTM G40-88) "the rate of material removal or dimensional change due to wear per unit of exposure parameter, for example, quantity of material removed (mass, volume, thickness) in unit of distance of sliding or unit of time".

Most of the wear rate data are developed on the basis of friction and wear. Such data depends on material pair, which is normally presented in term of dimensionless wear coefficient. The usefulness of the wear data presented in the literature lies more in their relative magnitude than in their absolute values (Bhushan, 2002). Hence it is difficult to use those data for the purpose of erosion rate of hydraulic machinery, where nature and rate of material removal is different. The rate of material removal due to erosion is termed as erosion rate, which is discussed separately in section 3.4.

2.4 Factors influencing the wear rate

Several factors are associated with different types of wear and among them some are common in nature. These factors may be acting individually or in combination. The general influencing factors are listed below:

- Macro-geometry: the interacting surfaces - point, line or surface contact
- Type of interaction: sliding, rolling, impact, adhesion, and abrasion or force transfer through a fluid film
- Materials and material properties: surface hardness and hardness difference between interacting surfaces, elastic modulus, fatigue strength, chemical composition, microstructure
- Load and surface pressure: external load, resistance load, and direction of load
- Environment: temperature, humidity, atmosphere
- Surface properties: surface treatment, surface roughness (micro-geometry), coefficient of friction, elastic or plastic deformation of surface
- Relative velocities between interacting surface
- Lubrication: types, properties of lubricants, contaminants in lubrication
- Debris escape

Some of these factors are applicable also to erosion of hydraulic machinery, which will be discussed separately in section 3.3.

Table 2.2.1: List of frequently discussed wear mechanisms with some definitions (after Meng and Ludema 1995)

Mechanism	Definition by common usage in the literature
Adhesive wear	Apparently refers to a state of sufficient local traction to cause local failure but not enough to prevent separation of derbies from the system
Diffusive wear	Transfer of single atoms from one body to another
Abrasive wear	Some combination of cutting. Fatigue failure and material transfer
Cutting wear	Indentation by sharp body, followed by fracture of material
Deformation wear	Usually not defined, but implies fracture of material
Fatigue wear	Failure of material after cyclic straining
Sliding wear	Perhaps intended to separate out erosion but not corrosion
Cavitation	Fatigue failure induced by collapsing bubbles in liquid
Impact wear	Combination of fatigue failure and loss of surface oxides
Erosion	Cutting, Fatigue and melting by impinging particles
Fretting	Fatigue failure of oxides and substrate material
Scuffing	A form of catastrophic surface failure of lubricated sliding members
Chemical wear	As enhancement of other forms or formation of new substances that are more readily removed than the substrate is
Corrosive wear	Probably implies loss of material without formation of new substances
Oxidation wear	Same as chemical wear, only oxides form
Thermal wear	Could cause melting or could influence chemical activity

Method of separating material as wear debris

a. Mechanical action
  1. Single action — Ductile failure / Brittle failure
  2. Repeated action — High cycle (elastic fatigue) / Low cycle (plastic fatigue)

b. Chemical action
  1. Loss by simple chemical dissolution
  2. Reduction with substrate materials to form a substance which is readily removed by sliding

3. Thermal action
  1. Melting
  2. Change in material properties to allow high wear rate

Chapter 3

Erosion

3.1 Introduction

Erosive wear, commonly known as *erosion* is caused by impacts of solid or liquid particles against the solid surface. These particles are contained in flow medium and possess kinetic energy that is sufficient to damage even metallic surface. The gas medium carries liquid particles in liquid particle erosion whereas liquid or gas medium carries solid particles in solid particle erosion. In general erosion can be classified into solid particle erosion and liquid droplet erosion.

Though erosion has emerged as a separate type of wear mechanism, it is still misunderstood as one class of abrasive wear. Erosion occurs in a wide range of machinery within power, aviation, process, and mining industry and so on. High temperature applications such as gas turbines of coal burning power plant will be eroded by fly ash (Tabakoff et al., 1992) and steam turbine blades will be eroded by water droplets (Krzyzanowaski et al., 1994). The military aircrafts and missiles experience both sand and rain erosion (Jilbert and Field, 2000). The turbine runner and other components of hydropower plants will be eroded due to sand in water. Pumps operate in different environmental condition and handles variety of aggressive liquid and solid slurries. Other components such as pipes, valves and sensors in off-shore industries, process industries, sewage system and mining industry are also affected by erosion. Even though erosion is normally harmful for the machine components, the same mechanism has beneficial use in unconventional manufacturing techniques. Water jet machining, sand blasting, erosive drilling and rock cutting are some examples of beneficial application of erosion mechanism.

Complete elimination of erosion of component is impossible, but the study of material characteristics and failure mechanisms help in understanding cause of material failure and this helps to minimize the damage of the material.

3.2 Mechanisms of particle erosion

Mechanical, chemical and thermal actions are the root cause of material separation as debris in erosion, but means for reaching those actions are different. Cutting, fatigue, brittle fracture and melting are four basic mechanisms for solid particle erosion. Cutting actions can also be divided into; cutting by penetration of cutting edge or plastic deformation to failure. Figure 3.2.1 shows the hierarchy of these processes. Stachowiak and Batchelor (1993) have discussed abrasive erosion, surface fatigue, brittle fracture, ductile deformation, surface melting, macroscopic erosion and atomic erosion as seven different possible mechanisms for solid particle erosion. But among all these, from the point of view

9

of erosion of hydraulic machinery, only first four (abrasive erosion, fatigue, plastic deformation and brittle fracture) are applicable.
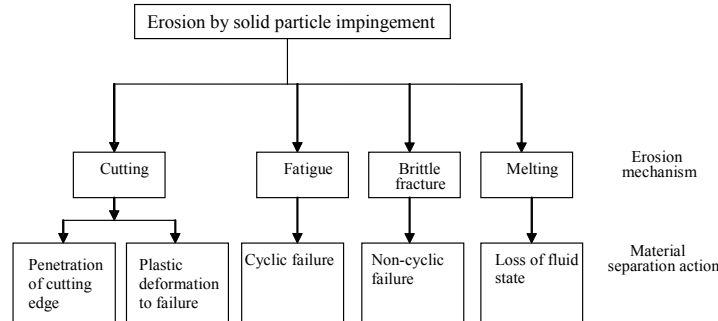
Figure 3.2.1 Mechanism of solid particle erosion (after Meng and Ludema, 1995)

Cutting (abrasive) erosion

When particles strike the surface at low impingement angle (figure 3.2.2) and remove the material by cutting, the erosion mechanism is called abrasive erosion. The abrasive grits roll or slide when they strike on the surface and cause erosion by abrasion or cutting mechanism. The material is removed by scouring or scrapping by sharp edges of the particles forming short track-length scars.

Surface fatigue

This mechanism of erosion is similar to wear due to surface fatigue on rolling surfaces. When the particles strike the surface with large impact angle but at low speed as shown in figure 3.2.3, the surface can not be plastically deformed. Instead the surface becomes weak due to fatigue action and cracks are initiated in surface after repeated hitting. The particles will be detached from the surface after several strikes.

Plastic deformation

Plastic deformation of the surface takes place due to formation of the flakes around the striking point when the particles strike the elastic surface with medium speed and large impingement angle as shown in figure 3.2.4. With repeated strike on the flakes, the material will detach as debris.

Brittle fracture

When particles strike the brittle surface with large impingement angle in medium velocity, erosion takes place by brittle fracture (figure 3.2.5). If the particles are sharp, then brittle fragmentation is more likely and the particles detach from the material by subsurface cracking.
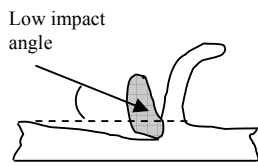
Figure 3.2.2: Cutting (abrasive) erosion mechanism
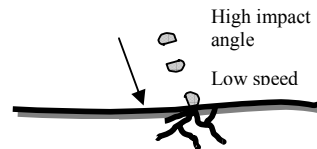
Figure 3.2.3: Fatigue erosion mechanism
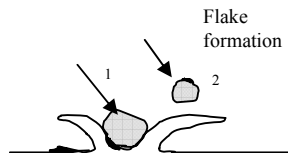
Figure 3.2.4: Plastic Deformation
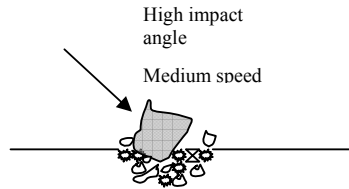
Figure 3.2.5: Erosion by brittle fracture

3.3 Factors affecting erosion

There are several factors, which differentiate types of erosion mechanism and control erosion rate. These factors can be grouped in three distinct categories. They are factors associated with:

1. Operating conditions - velocity, acceleration, impingement angle, flux rate or concentration, medium of flow, temperature
2. Eroding particles (sand or liquid droplets) - size, shape, hardness, material
3. Substrates (target materials)- chemistry, elastic property, hardness, surface morphology

3.3.1 Factors associated with operating conditions

Velocity, impingement angle and particle concentration are most important among all other factors and applicable to all type of components where erosion occurs. These terms also appear in almost all models of erosion.

Impingement angle

The impingement angle is defined as the angle between the eroded surface and the trajectory of the particle just before the impact (figure 3.2.2). If the particles are moving parallel to the surface, impingement angle is almost 0° and hence only minor erosion may take place. When particles are moving normal to the surface the impingement angle is 90°. Ductile and brittle material show different erosion behaviour against impingement angles.

Ductile materials have severe erosion in low impingement angle. Maximum erosion rate is observed between 10° to 30° in ductile material, whereas lower erosion rate is observed around normal impact. The erosion behavior of the ductile material is similar to abrasion in the case of very small impingement angle. For the brittle material the erosion rate increases as the angle of impingement increases and is highest at normal impingement. The erosion can be termed as *ductile mode of erosion* for the cases where erosion rate is maximum at low impingement angle and conversely *brittle mode of erosion* if erosion rate is maximum at normal impingement angle, irrespective or type of material is either ductile of brittle.
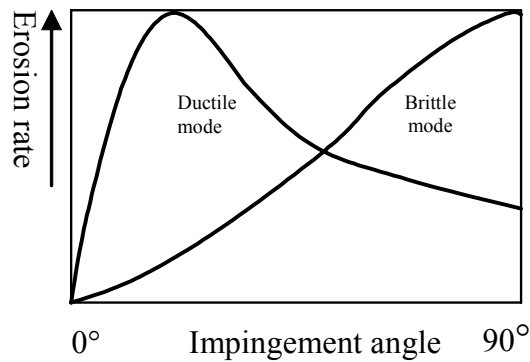
Figure 3.3.1 Schematic representation of erosion rate as a function of impingement angle for brittle and ductile material (Bardal, 1985)

Figure 3.3.1 illustrates the variation of erosion rate against impingement angle for ductile and brittle material. This curve is normalized for maximum erosion rate for both ductile and brittle materials. There are differences in the ways of presenting the relation of erosion rate with respect to impingement angle. Bhushan (2002) have shown maximum erosion rate for brittle material is higher than that for ductile material. On the other hand Matsumura and Chen (2002) have shown higher erosion rate for ductile material. Similarly, Bhushan (2002) has shown no erosion up to certain low impingement angles and on contrary, Stachowiak and Batchelor (1993) have shown erosion rate (about 10% of maximum) even at zero degree impingement. These differences in the presentation could be due to way of defining the impingement angle of actual particles. Normally the jet angle is considered as impingement angle of particles for practical purpose, but that is not the true impact angle. The flow of particle in the straight pipe or parallel plates can be considered to have impingement angle zero but even in such flow erosion can be expected. In such cases, if the flow is turbulent, the particles could be dancing or oscillating within the boundary layer in the direction normal to the flow and hence effective impingement could be even close to 90°.

Speed of erosive particle

In actual practice, material damage due to plastic deformation and cutting occur simultaneously and the ratio of these damage mechanisms depends on velocity of particle and impingement angle together with other parameters. Up to certain velocity, also referred

as critical velocity or threshold velocity, the particle can not skid in the surface due to friction and cutting action does not take place. Yabuki et al. (1999) found this critical velocity for silica sand and carbon steel pair as 2.5 m/s for 0.26 mm particles. As the velocity increases higher than critical velocity, both cutting and plastic deformation component increases, which amplify the erosion rate drastically. The modes of erosion also vary depending on velocity of the particles. At low velocity, the particles do not have enough energy to erode the material by cutting action, but elastic deformation or fatigue effect may be observed.

Most often quoted expression for relation between erosion and velocity of particle is *Erosion $\propto$ Velocity^n*, where the values of exponent n vary depending on material and other operating conditions. Considering the impact of particles due to kinetic energy as cause of material removal, theoretically value of n is 3. However, the view and finding of different researchers on the value of this exponent n are not alike. Truscott (1971) reported different values of the exponent, for instance n=1.4 for steel St 37 to n=4.6 for rubber tested on sand-blast apparatus. The value of the exponent will be lower in the case of combined effect of corrosion and erosion with higher corrosion intensity. However, sudden increase in this value can be observed in some velocity range when corrosion scales are removed. In the combined case of solid particle erosion and cavitation, Zhang et al. (1996) found the erosion rate proportional to peripheral speed of disc with exponent value in between 3 - 4.5 for non-metallic coatings. Similarly Arnold and Hutchings (1990) found the velocity exponent for unfilled elastomer in between 2.9 and 5.1 for impingement angels 30° and 90° respectively. It may be due to particle erosion at higher velocity is more significant than synergy due to cavitation and erosion. Karelin et al. (2002) observed different values for different type of test rig for instance n = 2.5 ~ 3.0 for rotary type stand, n = 1.8 ~ 2.7 for disc stands and n = 2.0 ~ 2.2 for water jet impact. There are big differences in values of the velocity exponent and it makes difficult for uniformity in erosion rate prediction and simulation.

Most often, particle velocity is considered same as fluid velocity which is estimated on the basis of continuity equation (Wood, 1999). This is not true in actual practice because generally particle velocity is less than the fluid velocity. Zahavi and Schmitt (1981) found sand velocity one third of air velocity in jet type of erosion test rig. The accuracy of particle velocity is important in erosion models, but measurement of that is difficult in practice. Chevallier and Vannes (1995) have mentioned light speed photography, optic gates and double rotating disc for measurement of particle velocity. Bjordal (1995) used the velocity based on rotational speed of specimen. In the experimental part of this research, velocity of the particles will be computed by considering continuity equation of the mixture.

Particle flux rate

The mass of impacting particles per unit area and time is defined as particle flux rate. The erosion rate is proportional to the flux rate of particle up to a certain limit and reduces beyond the limit due to interference between rebounding and arriving particles. This is more significant for high impingement angle. Arnold and Hutchings (in 1989) found that the limiting particle flux rate is highly variable, ranging from as low as 100 kg/m^{2}s for elastomer to as high as 10000 kg/m^{2}s for erosion against metals by large particles (in Stachowiak and Batchelor, 1993).

13

Concentration is also used in most of practical applications to represent this factor. It is a mass (or volume) of particle present in the unit mass (or volume) of fluid. It can also be represented in terms of percentage of particles in a given fluid mass (or volume). Especially for river sedimentation, concentration is presented in term of PPM (parts per million), which is equivalent to mg/litre or kilogram of particles in 1000 m^3 of water (1000 PPM is equivalent to 0.1%).

Mostly erosion rate is considered linearly proportional to concentration. Bjordal (1995) found *erosion rate $\propto$ concentration*$^{0.25 \text{ to } 1.27}$ for different metals and coatings. But for most of the materials, when tested for longer period of time, this value is close to 1. Hence considering erosion rate direct proportionality of concentration with respect to velocity is a satisfactory approximation.

Temperature

The mechanism and erosion rate are influenced by the change in temperature. At elevated temperature the material will be softened and hence erosion rate increases. With in 600°C erosion rate of stainless steel does not change significantly. This is a softening temperature and beyond this temperature, erosion rate increases rapidly. Shida and Fujikawa (1985) found strong correlation between erosion rate and mechanical properties of the material. Figure 3.3.2 shows the erosion behavior of stainless steel 310 with respect to temperature. The effect of temperature on erosion does not have significance in erosion of hydraulic turbine but it has importance in pumps conveying hot liquids, gas turbines, steam turbine and other similar applications.
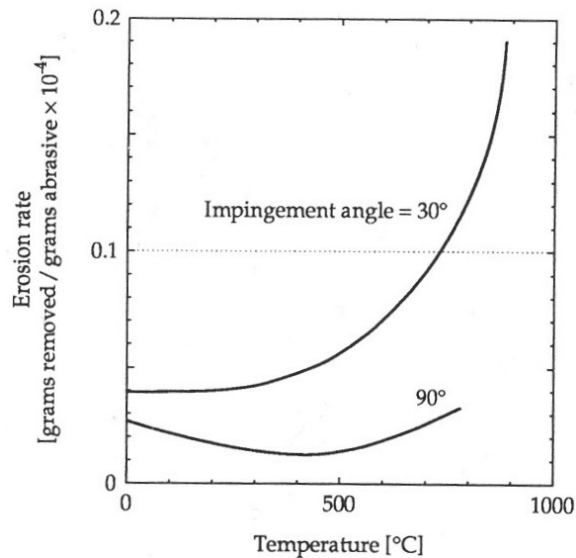
Figure 3.3.2 Effect of temperature on erosion of stainless steel (Levy and Man, 1986)

Effect of media

The erosive particles are conveyed by fluids such as air, water, hydraulic oil and lubricating oil. The characteristics of conveying medium have strong effect on erosion rate. The following factors or properties of the conveying medium affect the final erosion rate.

- Bulk properties of fluid: density, viscosity
- Nature of flow: laminar or turbulent
- Microscopic properties: corrosivity, lubrication, cooling effect

The viscous fluid imposes drag force on the eroding particles and affect erosion rate by altering the impingement angle (Hojo et al, 1986). The trajectory of particles and effect of viscosity on impingement angle is demonstrated in figure 3.3.3. The effect of erosive medium is assessed in terms of "collision efficiency", which is a ratio of particles that actually hit the eroding surface in presence of eroding medium to the theoretical number of particles that hit the eroding surface in absence of the medium. Particle trajectory is affected by flow medium. Comprehensive analysis of particle trajectory can determine the exact erosion rate and locations of damage. Erosion at the back side of the Pelton turbine bucket and gas turbine blade are examples of the effect of the particles that rebound from preceding blades or buckets.

When the flow direction is parallel to the surface, but flow is turbulent, the erosion rate of the material is higher compared to laminar flow. In turbulent flow more number of particles are likely to come in contact with the surface and same particle can repeatedly hit the surface. In laminar flow, the particles will try to follow the streamline and may escape without striking the surface, and hence reduce erosion rate. When the fluid flow is directed normal to the surface, the opposite will be the case, i.e. erosion rate will be higher for laminar flow than for turbulent flow. The illustration of behavior of particles in laminar and turbulent flow is shown in figure 3.3.4.

Small addition of lubricant in the liquid medium provides cooling during particle impingement restricting the change in material properties and hence reduces erosion rate significantly (Stachowiak and Batchelor, 1993). Arnold and Hutchings (1990) found that the lubrication of elastomer surface during erosion process reduces erosion rate due to reduction of surface tensile stresses associated with impact.

3.3.2 Factors associated with eroding particles

The rate and mechanism of erosion can alter depending on characteristics of the particles. The particle characteristics may remain same as in origin or it can change depending upon operating condition. Hence knowledge of particle characteristics is very important for estimation, reduction and prevention of erosion. Some of the particle characteristics and their effects are discussed here.
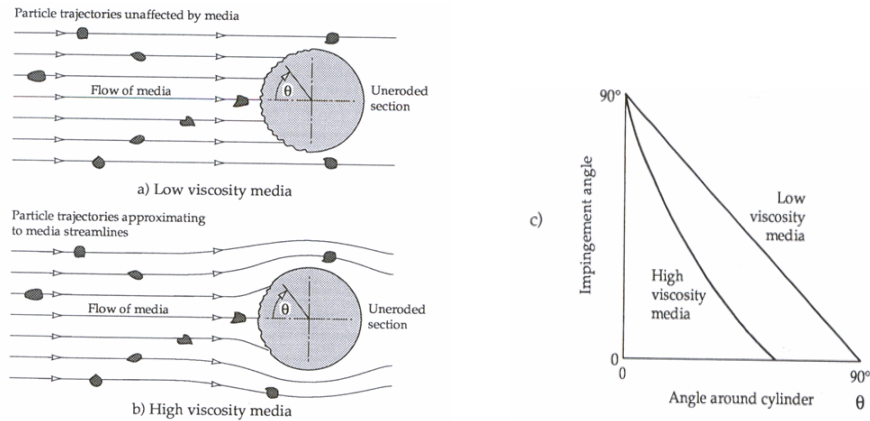
Figure 3.3.3 Effect of medium on impingement angle (Stachowiak and Batchelor, 1993).
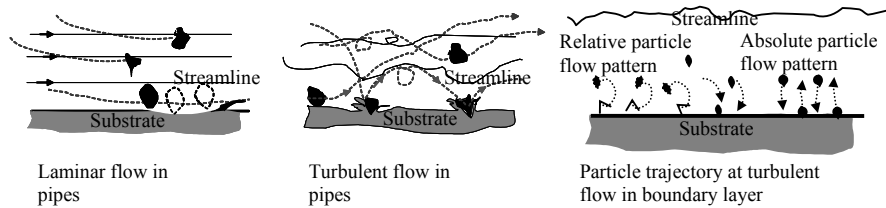
Figure 3.3.4 Effect of fluid flow condition on erosion effect

Particle size

Particle size can be characterized mainly in two basic dimensions mass and length. For a given velocity, kinetic energy of particle is directly proportional to mass and mass of spherical particle is proportional to (diameter)^3. Hence in theory *erosion rate $\propto$ diameter^3*.

Sheldon and Finnie (in 1966) observed the change of ductile mode of erosion to brittle mode when particle size is changed from small to larger (in Stachowiak and Batchelor, 1993). In the experiment with small and larger size particles, maximum erosion rate shifted from impact angle 30° to 80°. Small size particles have more cutting effect while bigger particles deform material by elastic deformation and fatigue. Along with the change in mode of erosion, there was dramatic change in erosion rate and ranking of erosion resistance as shown in figure 3.3.5. The erosion rate ranking depends on hardness in case of erosion due to small particles, whereas in case of large particles, it is dependent on toughness of material.
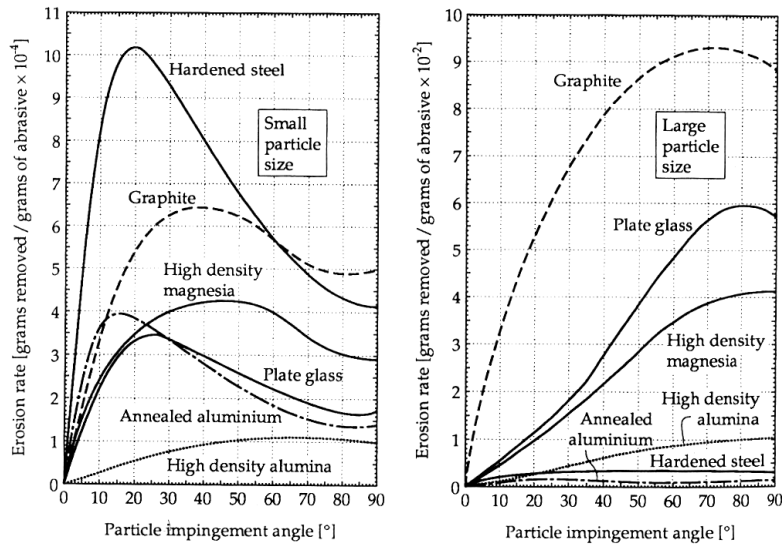
Figure 3.3.5 Erosion resistance ranking based on erosion test by Sheldon and Finnie with silicon carbide at velocity 152 m/s (Stachowiak and Batchelor, 1993).

Bahadur and Badruddin (1990) have discussed several approaches for particle characterization; which are self explanatory from figure 3.3.6. Some commonly used characterization parameters are:

- Maximum separation length L' along a straight line between two points (figure 3.3.6 a)
- Considering the plane of maximum stability: length , width and thickness (figure 3.3.6 a)
- Diameter of a circle of equal projected area d_a or alternatively equal projected perimeter d_p (figure 3.3.6 b)
- Diameter of sphere of equal surface area d_s or equal volume d_v (also called nominal diameter)(figure 3.3.6 c)
- Aperture A of sieve or equivalent round aperture (sieve diameter)
- Elongation ratio = L/W and flakiness ratio = W/T
  These ratios are unity for regular bodies (e.g. sphere). The reciprocal of elongation ratio is called "Aspect Ratio".
- The ratio of the square of perimeter to area of the particle (P^2/A) also provide quantitative measure of the deviation in shape of an irregular particle from that of known geometry.

Most often, non-cohesive natural sediments are characterized in term of particle diameter in river hydraulics. This method can be acceptable for other particles which have shape and density similar to natural sediments. Sediment particle sizes are defined in terms of *sedimentation diameter, standard fall diameter,* nominal diameter or sieve diameter. Sedimentation diameter of a particle is the diameter of sphere that has the same specific gravity and has the same terminal settling velocity as the given particle in the same fluid under the same condition. The standard fall diameter of a particle is the diameter of sphere

that has a specific gravity of 2.65 and has the same terminal settling velocity as the given particle in quiescent distilled water at 24°C.
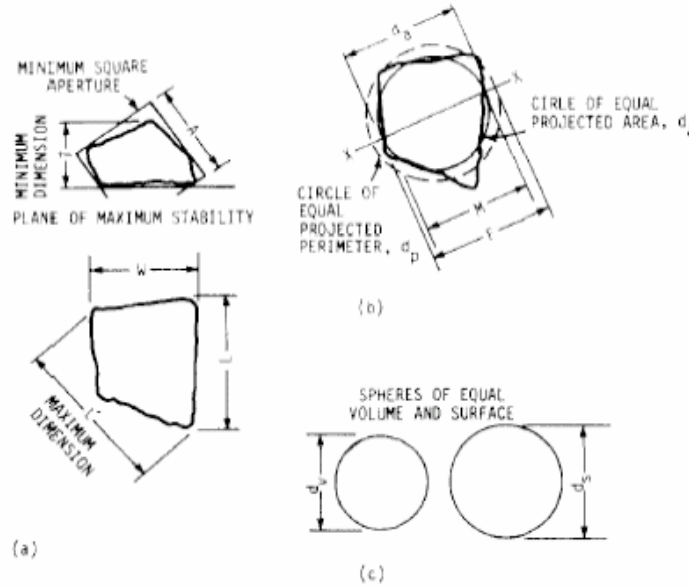
Figure 3.3.6 Definition of particle shape (Bahadur and Badruddin, 1990)

Particle shape

The shape of the particles is also one of the important factors which control erosion rate, but there are only limited studies on relation between erosion rate and particle shape. Beside erosion rate, the shapes of eroding particles are of interest because of its influence in shear strength, density, permeability, compressibility and capacity of sediment transport (Drolon, 2000). Generally particle shapes are described qualitatively such as round, angular and semi-round based on visual observation. The basic shapes found in the nature are generally uniform, but due to several reasons, actual shapes of particles are sharp and complex, which can not be described in simple mathematical terms. The shape of the particle is a good indicator of erosion process, for instance, irregular shape with sharp edge increases erosion rate, whereas blunt particles with round edges retard that in general. Most of the erosion models have incorporated the effect of shape; hence quantification of the shape parameter is essential for the estimation of erosion by solid particles. Together with the some of the approaches suggested by Bahadur and Badruddin (1990), roundness factor (Perimenter^2 / 4 π Area) and other statistical parameters are also used to describe the shape of the particles. Correlating the ductile erosion with cutting by single point cutting tool, the shape of particles can also be defined in term of "Rake angle", which is the angle between the front face of particle and normal to the target surface. Winter and Hutchings (1975) also used this concept. Drolon et al. (2000) used Multiscale roughness Descriptor (MDA) technique, based on harmonic wavelet transform for sediment particle analysis. Stachowiak (2000) used "Spike Parameter-Linear Fit" based on projected particle boundary and "Spike Parameter-Quadratic Fit" based on curve fitting for major boundary to describe the

angularity of the particles and studied their relation with erosion rate. These parameters are based on representing the particle boundary by set of triangles, which is directly related to particle erosivity. The erosion experiments by different particles have shown linear relationship between "Spike Parameter-Quadratic Fit" and erosion rate.

Chen and Li (2003) simulated erosion using computer model (Micro-scale dynamic model, MSDM) and investigated the difference in erosion rate by three basic shapes; triangle, square and circle as shown in figure 3.3.7. The highest erosion loss in single particle impact is by triangular particle followed by circular and square. This observation is in agreement with stresses induced by contact area. The erosion loss changes when square particle is rotated at 45° and contact are becomes smallest. In reality, several particles strike the surface and the ranking of erosion will be different in that case as show in impacts by 50 particles. In this case, erosion by square shape particle is bigger than circular, because of plastic deformation after subsequent strikes is in larger area. In general, the erosion rate by triangular or square particles may be 1.5 times higher than the circular particles.

Impact by 1 particle

Impact by 50 particles
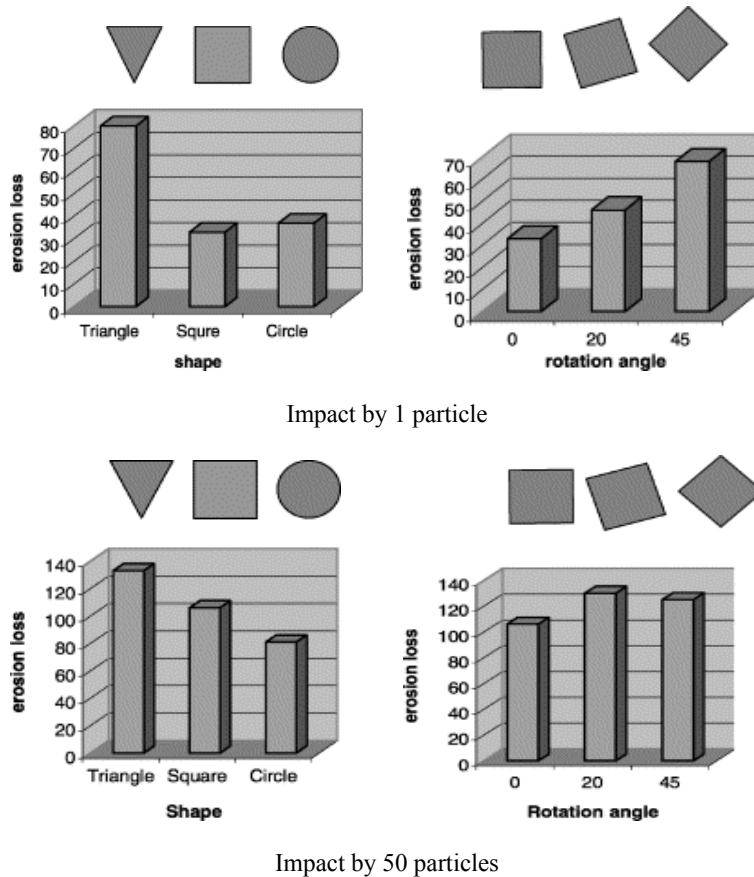
Fig 3.3.7 Erosion rate due to particles of different shapes (Chen and Li, 2003)

Hardness

The shape and hardness of particle complement each other. Even hard but relatively blunt particle may not cause severe erosion. Hard particles tend to have the sharp profile; in contrast, edges of soft particle round off even with slight impact. If the particles are harder than substrate, severe erosion occurs, but if particles are softer, erosion occurs only if the substrate has low fracture toughness. Hence the ratio of hardness of particle and substrate is very influencing in the erosion rate. Generally hardness of the minerals is represented in relative term of Moh's hardness scale between 1 for talk powder to 10 for diamond. Hardness of the knife edge in Moh's scale is 5.5 and that of steel needle is 6.5.

Sediment

The particles causing erosion of turbine components in hydropower plants are river sediments. The river sediments are in the form of clay, silt, sand and gravel with specific gravity approximately 2.6. In the river hydraulics, sediment particles are classified in to bed load and suspended load based on transport of sediment. All the particles, which move close to the bed by sliding, rolling or jumping are called bed load. These particles have much lower velocity than flowing water, whereas all those particles which are carried away in suspension by flowing water is called suspended load and they have more or less same velocity as flowing water. Fraction of suspended load is settled down in the settling basins or reservoirs and rest will pass through turbines causing erosion of components.

Sediments are made of fragmentation of rock due to chemical and mechanical weathering. The sediments in river are mixtures of different particle size as shown in table 3.3.1. Basically it is a sand fraction of the sediment which causes turbine erosion. The sand fraction can be further classified in to fine (0.06-0.2 mm), medium (0.2-0.6 mm) and coarse (0.6-2 mm).

Together with particle properties, particle transport mechanisms also have a role in erosion models. The movement of such particles basically depends on particle characteristics (density, shape, size) and fluid characteristics (velocity, turbulence, viscosity). Several forces acting on the particles for stabilizing and destabilizing its position in the bed are schematically shown in figure 3.3.8.

Table 3.3.1 Classification of river sediment (Lysne et al., 2003)

Particle	Clay	Silt	Sand	Gravel	Cobbles	Boulders
Size (mm)	<0.002	0.002-0.06	0.06-2	2-60	60-250	>250

In standstill water, the particles sink due to gravity and this is countered by buoyancy or up-thrust. The speed of sinking depends on mass of particle and fluid viscosity. The turbulence in the flow detaches particles from the rest and lift from bed, while transit velocity move particle in the flow direction. Low value of Reynolds number (Re) gives laminar flow which is a favorable condition for settling of particles. Similarly, water flowing around the particle exerts the drag force in the direction of flow. Solid friction between the particle and bed opposes forward movement. Dissolved air or air bubbles may also prevent the particles to settle down and suspension of particles cause coloring of water. When particles move

along curved path, the centrifugal force and if the system is rotating (including global rotations) the Coriolis force are pertinent destabilizing force. Exact interactions between all associated factors are complicated for numerical analysis. Sediment transport analysis may give indication on location of attack on turbine, which can be useful to focus on an optimal location of erosion resistant coating in turbine.

Centrifugal and Coriolis force

Drag

Viscous force

Transit velocity

Cohesive force

Legend

Sediment

Destabilising forces

Conduit wall or river bed

Turbulent force

Up-thrust

Solid friction

Gravitational force

Stabilising forces

Lift
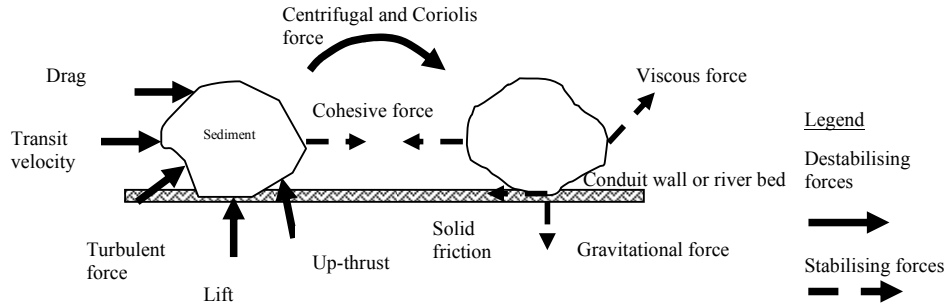
Figure 3.3.8 Forces acting on the particles in the flow field

3.3.3 Factors associated with substrate

The materials such as metal, alloy, ceramic, and polymer used in different applications are exposed to erosive environment. The characteristic of these materials have strong effect on erosion. Chemical composition, elastic property, hardness and surface morphology are some of the major parameters of the substrate material which affect the erosion rate. Erosion resistance of materials is separately discussed in Chapter 4.

3.4 Erosion Rate

The term erosion rate is often used for presenting the results of experimental observation and comparing erosion performance of various materials operating at different operating conditions. There is no standard and well agreed general definition for erosion rate. Hence erosion rates are presented in several forms in the literature.

With the analogy of definition of wear rate, erosion rate can also be defined as dimensional change of substrate per unit exposure parameter. Stachowiak and Batchelor (1993) has used the negative ratio of change of mass to the duration of process (-dm/dt) as erosion rate to show the relationship between variables of erosion process for medium to high speed particles. Wood (1999) has used the term erosion rate as ratio between volume losses per impact, which has the advantage over the commonly used ratios of target material loss to unit mass of erodent. This is because the number of individual particle impact varies with change in particle diameter for the same mass of erodent. The erosion at early stage may be negligibly small at low velocity. The impact energy is expended for elastic deformation or initiation of fatigue crack. Erosion rate may increase suddenly after some time and this can be considered incubation period.

Based on empirical expression from wide range experiments and observations, there is a general agreement to represent erosion rate as ratio of weight loss of material to mass of erodent (Bardal, 1985). If the densities of eroded material are considerably different, erosion rate should be represented as volume loss to mass of erodent. Erosion of turbine component is difficult to measure in term of weight loss. Hence loss of volume or reduction of thickness is practical way to represent erosion rate. In number of cases, erosion is represented in term of operational time based on inspection for failure or identification of efficiency, power output or pressure drop by certain value.

3.5 Models of erosion

Erosion models are useful for design of turbine components, sediment settling basin and optimization of hydropower plant operation in sand-laden river. Most often, individual particle dynamics are used for developing erosion models. Empirical and statistical relations are also often developed from experiments and field experiences. As erosion studies are heading toward numerical modeling and simulations, the importance of analytical models are increasing day by day. Truscott (1972) on his literature survey of publications of 20 years on abrasive wear of hydraulic machinery has found that the most often quoted expression for erosion is *Erosion $\propto$ (velocity)^n*.

There are several other fundamental studies of erosion behaviors. The erosion equations of most prominent researchers (Sheldon and Finnie, 1966, Head and Harr (1970), Tilly (1973), Grant and Tabakoff (1973), Williams and Lau (1974) Hutchings (1976), Evans (1979) Ruff and Wieherhorn (1979), Routbort (1980), Sundarajan and Shewmon (1983) Beckmann (1981) and others can be found in Meng and Ludema (1995). General erosion model and two of the most fundamental models of erosion studies by Finnie (1960) and Bitter (1962) are presented in the following section.

General erosion model

As it is discussed throughout this chapter, simplest way of writing equation for erosion is:

Erosion $= f$ (operating condition, properties of particles, properties of base material)

Generally, this expression is given as a function of velocity, material hardness, particle size, and concentration. Bardal (1985) describes the most general formula for pure erosion as:

$$W = K_{mat} K_{env} c V^n f(\alpha) \hspace{4cm} 3.5.1$$

Here, W is erosion rate (material loss) in mm/year, K_{mat} is material constant and K_{env} is constant depending on environment, c is concentration of particles and $f(\alpha)$ is function of impingement angle α. V is the velocity of particle and n is the exponent of velocity.

Finnie's Model

Finnie (1960) derived two expressions for ductile materials by considering ideal case of hitting by single particle and solving the cutting wear and that equation is further extended

to the equations for impacts by several free moving particles of total mass, *M*. These two expressions for total volume removed by cutting wear, *Q* is given by:

$$Q = \frac{MV^2}{8P}\left(\mathrm{Sin}\,2\alpha - 3Sin^2\alpha\right) \text{ if } \alpha \leq 18.5^0 \qquad\qquad 3.5.2$$

$$Q = \frac{MV^2}{24P}\left(Cos^2\alpha\right) \text{ if } \alpha \geq 18.5^0 \qquad\qquad 3.5.3$$

Here *V* is velocity of particles, α is impingement angle and *P* is plastic flow stress (constant horizontal pressure between particle and substrate)

Finnie assumed the target material as plastic and eroding particles as rigid with sharp edge. For impact angles lower than 18.5°, it is assumed that the particles will leave the surface while they are still in the cutting action, whereas in higher angles the horizontal motion of particles ceases. The ratio of the vertical to horizontal force component in particle face is assumed 2 with the experience of grinding and the ratio of length to depth of the scratch is assumed 2 from the analogy from metal cutting experiment. The above equations consider that only 50% of the total impinging particles will have cutting effect.

The equations 3.5.2 and 3.5.3 have angular dependence, which agrees well with the experimental results at low angle, but have limitation of underestimating erosion above 45°. At normal impact the equation shows no erosion, which is contradictory to the real life experience. This deviation could be due to deflection of impinging particles to smaller angles because of rebounding particles or irregularities of surfaces at micro-level. Similarly, impacts at high impingement angle may cause fracture of work hardened surface and hence may have brittle failure. The erosion of brittle materials cannot be estimated by this equation, since material failure mechanism is different than the one assumed by Finnie.

Bitter's Models

Based on observation of hitting of silver plate by cast iron pellets at different angles, Bitter (1962) defined following two modes of erosion based on visual appearance of surface of silver plate:

- Deformation wear (W_D), deformation due to repeated impact of particles normal to target
- Cutting wear (*Wc*), cutting action by free-moving particles striking surface on acute angle

In most of the practical cases, deformation wear and one of these cutting wears occurs simultaneously. Cutting wear component is negligible in erosion of brittle materials whereas deformation wear component is negligible in ductile materials. Bitter developed the erosion formulae as a function of mass and velocity of particles, impingement angle and properties of both erosive particles and substrates by using the energy approach. Figure 3.5.1 shows total wear curves for soft and ductile material and hard and brittle material based on Bitter's model.

23

Deformation wear

Bitter (1962) also explained the contour of the stress concentration under the surface of particle hitting. The plastic deformation of material takes place when collision exceeds elastic limit and upon repeated hitting, elastic limit increases because of hardening of plastically deformed surface. Once the surface becomes relatively hard and brittle, it cannot be deformed plastically anymore with increasing load and surface layer will be destroyed by detachment of fragments. Bitter derived the equation for deformation wear (W_D) based on deformation wear factor (ε), which is the ratio of energy absorbed by the surface layer during collision and amount of energy needed to remove one unit volume of material.

$$W_D = \frac{\frac{1}{2}M[V\text{Sin}\,\alpha - K]^2}{\varepsilon} \qquad\qquad 3.5.4$$

Equation 3.5.4 is valid *if V Sin* $\alpha \geq K_T$, where K_T represents the maximum particle velocity at which collision is still purely elastic, hence no deformation wear occur. The influence of mechanical properties on deformation wear is related in term of value of K_T, which is also considered as threshold velocity, below which deformation wear does not takes place.

Cutting wear

When particles strike the horizontal surface in acute angle, the material is subjected to shear stress and indent through surface. When this stress exceeds material shear strength, material is removed by scratching, which is known as cutting wear. The magnitude of scratching depends upon velocity and impingement angle of particles. The velocity of impinging particles can be resolved in two components:

- normal to the surface ($V_\perp$) and as result of this component the particle indent in to the body
- parallel to surface ($V_{\parallel}$) and this causes scratching action

As long as $V_\perp$ does not exceed the constant expression K_T, no damage occurs as a result of $V_{\parallel}$. The energy possessed by particle is expended during deformation and scratching resulting decrease in both horizontal and vertical component of particle velocity. There are two possibilities of particle velocity after scratching the surface and corresponding erosion are:

- Wc_1 in which horizontal velocity component are still present when particle leaves the body surface
- Wc_2 in which particle horizontal velocity component vanished during the collision

Bitter has developed different models of erosion for two above-mentioned conditions with cutting wear factor ς.

Cutting wear equation when $V_{\parallel} \neq 0$

$$W_{c1} = \frac{2MK(VSin\alpha - K_T)^2}{\sqrt{(VSin\alpha)}}\left[VCos\alpha - \frac{K(VSin\alpha - K_T)^2}{\sqrt{(VSin\alpha)}}\varsigma\right] \qquad\qquad 3.5.5$$

Cutting wear equation when V_{ll} becomes zero.

$$W_{c2} = \frac{\frac{1}{2} M \left[V^2 Cos^2 \alpha - K_1 (VSin\ \alpha - K_T)^{3/2} \right]}{\varsigma}$$
3.5.6

Here, K and K_1 are constant expressions and K_T is threshold velocity, which are dependent on material properties.

The total wear at any instant is $W_t = W_D + W_{c1}$ or $W_t = W_D + W_{c2}$
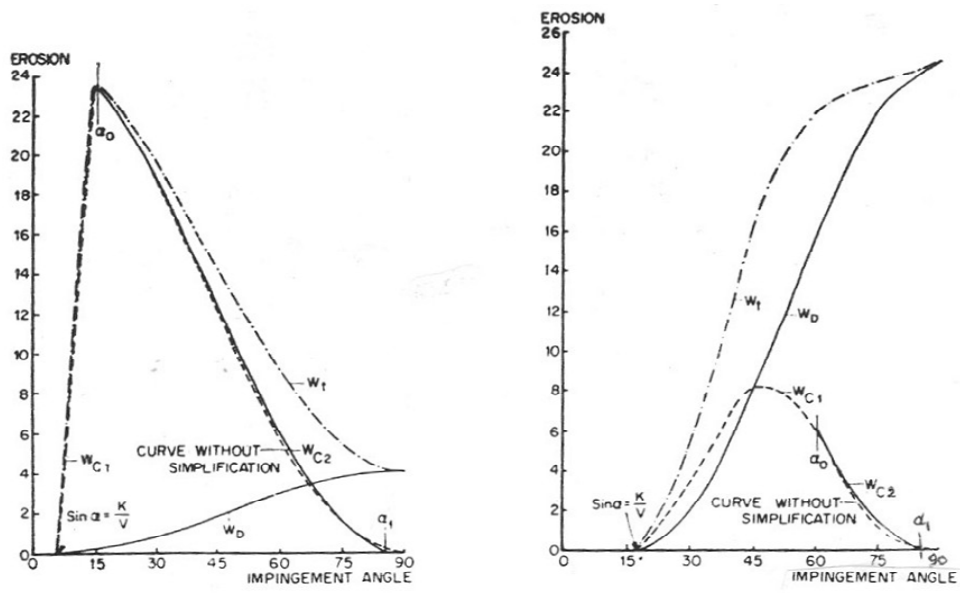
Figure 3.5.1 Total wear curves for soft and ductile material (left) and hard and brittle material (right) based on Bitter's model (Bitter, 1962)

Dimensional analysis

Dimensional analysis can also be used to develop the model to predict erosion. Head and Harr (1970) developed the functional relationship of the erosion process between the variables such as erosion rate, velocity, impingement angle, particle shape; hardness ratio and erosion resistance using Pi-theorem. This relation was developed for erosion by dust particles in air. Due to lack of sufficient data to verify the relation for erosion of hydraulic turbines, this technique is not used. However this technique can be used to establish erosion model once sufficient data of erosion of turbine component is available.

Erosion models for hydraulic machinery

The erosion models are basically developed for specific purpose or condition. For example, Bitter's model is developed for dry condition, hence it is not clear whether this equation realistically predict erosion rate for wet condition or not. Few researchers have presented models specifically for hydraulic machinery. Truscott (1972) presented the equation of Bergeron (in 1952) to predict the erosion rate of pump with simplified assumptions such as pure sliding of spherical particles over the surface. He presented equation for erosion as:

$$Erosion \propto \frac{V^3}{D}(\rho_P - \rho)d^3 pK \qquad\qquad 3.5.7$$

Where V is the characteristic velocity of liquid, D is the characteristic dimension of the machine, ρ_P is density of particle, d is diameter of particle, p is number of particles per unit surface area, ρ is density of liquid and K is experimental coefficient depending upon nature of abrasive particles. This equation is proportional to experimental coefficient, which is dependent on abrasive nature of particles.

Karelin et al. (2002) established the equation for surface erosion based on impact effect of particles considering kinetic energy of single particle. They have anticipated deviation on erosion estimated by equation due to uncertainties like non-homogeneous particles, variable concentration, continuous alteration and pulsation of velocities and pressure, non-uniform flow distribution and so on. On the contrary to laboratory tests, Tsuguo (1999) established the relationship of factors concerning erosion of turbines based on 8 years erosion data of 18 hydropower plants. The repair cycle of turbine is determined according to calculation of turbine erosion from equation 3.5.8, which gives erosion rate in term of loss of thickness per unit time *(w)*.

$$w = \beta c^x a^y k_1 k_2 k_3 V^n \qquad\qquad 3.5.8$$

Where β is turbine coefficient at eroded part; c is the concentration of suspended sediment, V is relative velocity. The term *a* is average grain size coefficient on the basis of unit value for grain size 0.05 mm. The terms k_1 and k_2 are shape and hardness coefficient of sand particles and k_3 is abrasion resistant coefficient of material. The *x, y* and n are exponent values for concentration, size coefficient and velocity respectively. The value of *x* and *y* are close to the unity and any deviation of this linear proportionality is determined from plot of wear versus parameter. The values of n are proposed for different turbine components based on relation between relative velocity and erosion. Minimum value of n is proposed as 1.5 for Pelton bucket and maximum value is 3 for Francis turbine runner. Similarly for Francis turbine guide vanes and Pelton turbine needle this value is proposed as 2.5. The equation similar to this for the purpose of hydraulic turbines will be established in experimental part of this research.

3.6 Synergy between particle erosion, cavitation and corrosion

The velocities in the hydraulic machinery and offshore industry components are ever increasing, which lead to premature failure of components by combination of flow dependent erosion and corrosion. The presence of solid particles in the flow and cavitation further complicates the situation. Combined erosion-corrosion is one of top five corrosion related concern in offshore industries (Wood et al., 2002). Hydraulic machineries can also have combined effect of sand erosion, cavitation and corrosion. Even though there could be mixed response of combined effects it may damage protective layers in most of the cases and increase corrosion rate.

Figure 3.6.1 schematically shows possible interaction between various flow regimes and corrosion. The area between corrosion-slurry impingement, corrosion-cavitation and corrosion-turbulent flow are generally referred as erosion-corrosion. But Wood et al. (2002) defined interaction between turbulent and laminar flow as flow-induced corrosion and rest with erosion-corrosion, where mechanical effects are predominant. As flow velocity increases, erosion is more significant than cavitation and corrosion.

The interactive effect, in which liquid and liquid-solid erosion corrosion conditions describes the increment in the total weight loss that can not be accounted for pure corrosion (without solids) or pure erosion (mechanical effects - with solids) is termed as synergic effect (Wood et al., 2002). The definition of synergy between erosion and corrosion are available in the literature (Bjordal, 1995), but the relation for erosion and cavitation is not found, even though some studies have been done on this issue (Wu 1996, Hengyun et al. 1986, Kang et al. 1993). The synergism in erosion-corrosion can be split in to erosion enhanced corrosion ($\Delta W_{Corrosion}$) or corrosion enhanced erosion ($\Delta W_{Eroiosn}$) and hence total erosion can be written as:

$$W_{Total}=W_{Erosion}+W_{Corrosion}+\Delta W_{Eroiosn}+\Delta W_{Corrosion} \qquad \text{where } \Delta W_{Erosion}+\Delta W_{Corrosion}=\text{Synergy}$$

Total synergy is the sum of $\Delta W_{Erosion}$ and $\Delta W_{Corrosion}$, among which $\Delta W_{Erosion}$ is dominating in case of transport of solid slurry. In the case of cavitation, combined effect can be included in ΔW_E as erosion or mechanical effect synergy. For the case of hydropower turbines, river water is normally none corroding and hence synergic effect of erosion-corrosion is negligible. But corrosion effect can be influential in the case of galvanic effect due to poor selection of materials with highly different electrochemical potentials.

Particle erosion can strip corrosion film and influence on corrosion rate by different mechanisms, such as:

- Increased mass transport by high turbulence levels caused by surface roughening
- Removal of oxides or corrosion scales exposing fresh reactive material, prohibiting film formation and acceleration corrosion rates
- Local acidification in erosion pits
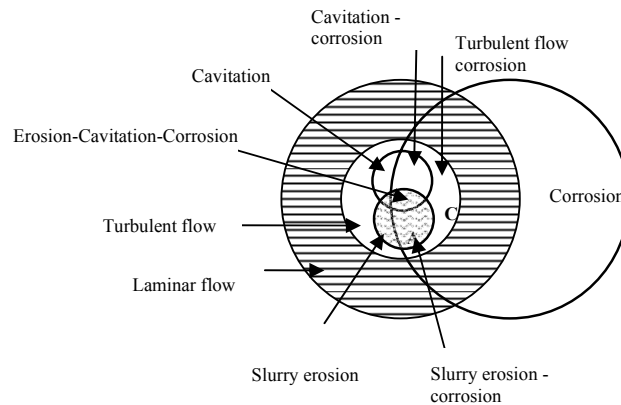
Fig 3.6.1 Interaction of erosion-cavitation-corrosion (Wood, 2002)

Similarly, some of the effects of corrosion on erosion are as:

- Corrosion removes work hardened surface
- Preferential corrosive attack on grain boundaries
- Corrosion can lower fatigue strength
- Corrosion can introduce micro pits, which can be easily damaged by particles and increase stress concentration

Most of the above mentioned mechanisms give positive synergy. However in certain cases negative synergy can be possible. Some possible mechanism for reduction of mechanical erosion ($-\Delta W_E$) are:

- Increased work hardening due to corrosion mechanisms
- Shot-peening by high velocity particles
- Presence of soft or loosely adherent corrosion particles
- The reduction of corrosion synergy ($-\Delta W_C$) may be due to rapid corrosion film growth or the formation of passive film

Zhang et al. (1996) found that ratio of erosion rate of different non-metallic coatings with reference to 0.45%C-steel in between 0.15 to 7.9 in the combined solid particle-cavitation erosion. Similarly the ratio of combined erosion to pure particle erosion was found in between 0.67 to 2.10 for those coatings. Hence mixed and complex reaction of combined effect of solid particle-cavitation erosion can be expected. Except few cases the combined cavitation and particle erosion was more than pure particle erosion. This could be due to particles acting as cavitation nuclei and increasing bubble formation rate. Similarly, surface damaged by erosion make condition favorable to cavitation for example severe damage of Pelton needle. On the other hand, particle erosion can be enhanced due to pitting effect and plastically deformed surface because of cavitation. The failure of material from surface damaged by cavitation is easy. Nanda (1999) reported erosion with medium silt content cause 4 times higher than cavitation in clean water and the combined effect of cavitation and erosion is 16 times higher than cavitation alone.

28

Chapter 4

Erosion resistance of material

4.1 Introduction

The erosion resistance is related to mechanical property of material in general. But the difference in erosion resistance of steel of different hardness and alloy is not significantly large (figure 4.1.1). The material can be broadly classified as metals, ceramics and polymers in terms of their distinct erosion behavior. The erosion mechanism in metal and alloy is generally scratching, whereas that for pure ceramic is breakout of particles. On the other hand, erosion of cermets is by removal of binding matrix.

The erosion resistance of material can be improved by either making material surface extremely hard (for example metals and ceramic) or by making the surface tough but with extremely low elastic modulus so that kinetic energy of particle harmlessly dissipate such as in rubber. Rubber and polymers absorbs some of particle energy upon impact. The erosion behaviors of these three groups of materials are discussed in the following sections.

Steel

Steels are most common structural material and exposed to variety of eroding environment. Levy (1981) found that maximum erosion of ductile material at low impingement angle (around 30°) is due to subsurface and surface cracking. This suggests that erosion resistance of steel is limited by lack of ductility. The effect of microstructure on erosion rate suggest that ductile steel is most erosion resistant and hardening of steel to form martensite offers little improvement except at low impingement angle and formation of massive carbides reduces erosion resistance of steels (Stachowiak and Batchelor, 1993). Alloying of steel or cast iron to obtain significant retained austenite is also effective way to reduce erosion. Addition of appropriate amount of silicon to carbon steel or cast iron results improved erosion resistance (Stachowiak and Batchelor, 1993).

Polymer

The erosion resistance of polymers is generally inferior to steels, but the developments of newer polymers are rather fast and in future, polymers could be substitute for erosion resistant materials. Polymers show brittle mode of erosion in general, but when they show ductile mode, that is comparable with steel (figure 4.1.2). The ranking of erosion resistance

of commonly used polymers are in the following order: Polyurethane > fluorocarbon > polycarbonate > ploymethylmethacrystalate > nylon (Stachowiak and Batchelor, 1993).

The erosion of these soft materials can be due to slow fatigue processes and hence soft materials may have better erosion resistance (Arnold and Hutchings, 1990). But in actual practice, the strikes at low impingement angle cause damage of such soft material by tearing of the surface due to the particles sharpness. Oxidation may accelerate erosion of elastomers and that may enhance at higher temperatures.
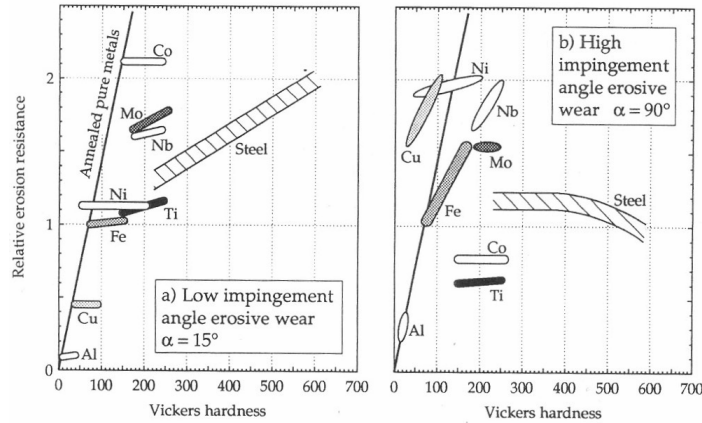
Figure 4.1.1 Relation between relative erosion resistances with primary material character based on Gahr, 1987 and Kleis, 1984) (from Stachowiak and Batchelor, 1993)
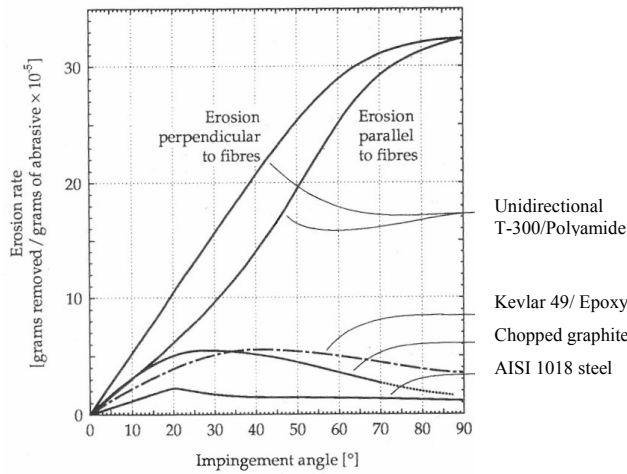
Figure 4.1.2 Erosion of reinforced polymer and carbon steel based on Pool et al., 1986) (from Stachowiak and Batchelor, 1993)

Ceramic

Ceramics have advantage at high temperatures against poor erosion resistance of common metals. Some of the common ceramics in use are alumina, zirconia, silicon nitride and silicon carbide. Ceramics become ductile at high temperature and erosion rate is reduced. On the other hand, ceramics have certain disadvantages like brittleness which may accelerate erosion. Oxide ceramics such as alumina and zirconia are found better erosion resistance compared to silicon nitride and carbides (Srinivasan and Scattergood, 1991).

Cemented carbides or cermets are composite materials consisting of carbide particles glued together with a metallic matrix. Carbides provide good erosion resistance, whereas metals in the matrix are binder. Tungsten carbide-metal coatings, WC-M (where M stand for Co, Ni, Cr, Mo or combination of these) have better erosion resistance than pure metals. Tungsten carbide grains with a cobalt as binder is widely used in turbine industry. But in corrosive media when WC-Co is in contact with stainless steel (SS), Co acts as anode and SS acts as cathode and hence corrosion rate increases in Co phase. Corrosion resistance of such matrix is improved by adding Cr to the binder.

Large volume fraction of finely distributed tungsten mono carbide (WC) particles improves erosion resistance (Berget, 1998). During spraying, the decarburization of WC can occur at high temperature forming W_2C, which is harder than WC but is more brittle. This decarburization also detaches C from WC and liberated C oxidizes to form CO or CO_2 gas. The diffusion of CO in a matrix is one of the main causes of poor coating quality (Berget, 1998). The decarburization reaction depends on time, temperature, powder and spray parameters. Decarburization can not be completely eliminated, but can be controlled by spray parameter. Hence it is not only coating composition, spray process and parameters have also significant role for good coating. If the carbides are very small compared to abrasive particles, the hardness of overall metal matrix will increase. On the other hand, if the size of carbide is large, hardness of carbide itself is effective in combating erosion.

4.2 Effect of material defect in erosion

The defect such as holes and cracks in the material and their average spacing of defects causes change in erosion modes. If striking particles are fine, only few impingement sites will coincide with defect. The impingement site is a zone of highly stressed area which is almost equal to the size of particle just beneath the point of impact. Slow plastic deformation of substrate is predominant for erosion in absence of material defect. On the other hand erosion could be due to brittle failure when big particle strike the point of defect. Crack formation and propagation is rapid process in brittle material and hence brittle mode is very destructive. Any insertion of particles in the larger cracks in cyclic loading may cause abrasion. The effect of crack and fracture mechanics in hydraulic turbine can be found in Brekke (1986 and 1998). The static working pressure at the pressurized parts of turbines made from high tensile strength material should be limited to value which gives a critical crack size large enough to obtain leakage before rupture and acceptable defect size should not grow beyond critical size within 20000 to 50000 loading cycles (Brekke, 2000).

4.3 Materials for hydraulic turbines

The materials for hydraulic turbine are selected according to criteria and requirements as shown in table 4.3.1. Higher stresses, improved fatigue, cavitation and corrosion resistance have been the most important criteria for the selection of material for rotating parts exposed to high velocity. The improvement of material quality has allowed increase in turbine capacity and speed with less weight per generation capacity. Erosion is normally not considered for material selection for turbines such as for cavitation and fracture. But in the cases where failure of turbine due to erosion is foremost, material selection process should be dominated by erosion resistance of materials.

Table 4.3.1 Turbine material requirement and selection criteria (Brekke, 2000)

Requirements to be fulfilled	Criteria for the choice of material
1. Operational Condition	Static load Dynamic load (fatigue) Temperature Corrosion/Abrasion/Erosion/Cavitation
2. Operational Requirement	Reliability Maintainability (Repair time and cost) Life time
3. Production feasibility	Weldability Availability in market Machinability
4. Price and delivery time	Material cost and labor cost (Interest rate) Delivery time Quality

Basically steels are used for high head turbines, except few low head small turbines are made up of cast iron and bronze. The development of turbine steel is not very old as compared to other technological development. Before 1950's cast iron was used for turbine components, which was later replaced by cast steel and riveted plates due to higher requirement of strength and toughness. Cast steel is replaced by fabricated steel after 1950's because of weldability and development in fine grain steel.

Austenitic steel 18Cr8Ni with less than 0.2% Mo has good resistance to corrosion and cavitation, but their fatigue and creep resistance are poor. It also has self hardening effect caused by mechanical abrasion; hence this steel is not recommended for runners, guide vanes, and other movable parts of turbine. But it is still in use for constructing micro hydro turbines in Nepal. This steel was used to fabricate the turbine runner also in Pathri hydropower plant (Uttar Pradesh) and Mattur hydropower plant (Tamilnadu) in India (Goel and Sharma, 1996). Martensitic steel 13Cr1Ni was developed as substitute for 18Cr8Ni, but corrosion, cavitation and sand erosion resistance of this steel is poor because of low hardness, toughness and less Ni content. The weldability of this steel is also poor, which needed preheating up to $200°_C$ and stress relieving up to 600°C. Swedish quality steel 13Cr6Ni was patented in late 60's but the restriction of its use due to patent right favored

the development of 13Cr4Ni, 16Cr5Ni and 17Cr4Ni stainless steels, among which 13Cr4Ni and 16Cr5Ni are widely used in turbine industry.

Both 13Cr4Ni and 16Cr5Ni are austenitic-martensitic steel with δ-ferrite and about 20-25% stable austenite. The normalization followed by annealing at 580°C creates tough structure with martensite. Corrosion resistance is satisfactory in both steels and cavitation resistance is found better in both, but marginally better in 16Cr5Ni, which is making this steel first choice in modern turbine industry. These materials are occasionally cladded with weld alloy overlaying to enhance surface properties.

Ferrite austenitic duplex steel is developed for offshore and oil industries for better corrosion resistance. Pumps and pipe line components will be eroded by sand particles present in the crude oil. Its erosion performance is also investigated (Bjordal, 1995 and Berget, 1998) and erosion properties are continuously being developed. There is no report of use of this steel in turbine industry. In spite of development effort of steel industry, none of these steels have shown excellent performance on resistance against sand erosion. Some of the properties of turbine steels are given in table 4.3.2.

Table 4.3.2 Properties of turbine steels (Jain, 1999)

Stainless steel	Tensile strength (MPa)	Yield strength (MPa)	Elongation %	Impact strength (J)	Microstructure	Nature
13Cr1Ni, 0.06 C, 0.4 Mo	630	470	18	39	Martensite	Hard and brittle
13Cr6Ni, 0.06 C, 0.4 Mo	800	550	16	70	Martensite-70 Austenite-30	
17Cr4Ni, 0.06 C	880	650	12	59	Martensite+ Austenite+ Ferrite	Hard and ductile
13Cr4Ni, 0.04 C 0.4 Mo	823	686	23	81	Martensite	Hard
16Cr5Ni, 0.05 C, 1.5 Mo	880	600	21	100	Martensite-65 Austenite-35	Hard and ductile

The use of expensive materials like Stellite and titanium show improved results which may not be cost effective for turbine industry. Present trend of improving erosion resistance is by coating the steel surface by hard materials like ceramic or cermets.

Francis turbine parts are classified in two categories as: (i) pressurized static parts: such as spiral casing, head covers, draft tube and (ii) movable stressed parts: such as guide vanes, shaft, runner with labyrinth seals and bearings. For high head turbine, stress carrying parts are made from *fine grain high tensile strength carbon steel* (micro alloy steel) to increase

stress without increasing the danger of fracture. Maximum stress and number of cycles for pressurizing are basis for design. The covers and draft tubes are made from *fine grain low tensile stress with low carbon content steel* for defect free welding. Pelton turbines normally operate at high head and its parts can be exposed to very high kinetic energy. Stress carrying fabricated parts such as manifold is made from *fine grain high tensile stress steel* plates to reduce thickness. The summary of Norwegian experience of turbine material for Francis and Pelton turbine are presented in table 4.3.3 (a) and (b).

Table 4.3.3 (a) Material for Francis Turbine

Part	Operating condition and requirement	Material
Guide vane	high velocity, prone to cavitation, corrosion, sand erosion	13Cr 4Ni
Runner	high velocity, prone to cavitation, corrosion, sand erosion	16Cr 5Ni
Upper part of draft tube	High velocity, prone to cavitation and corrosion, welding at site	16Cr 5Ni
Facing plates	Abrasion or adhesion between guide vanes and facing plates	16Cr 5 17Cr 1Ni
Labyrinth (static)	Minimum gap to avoid leakage loss, replaceable	Ni-Al bronze (steel in case of erosion)
Labyrinth (rotating)	Minimum gap to avoid leakage loss	16Cr 5Ni

Table 4.3.3 (b) Material for Pelton Turbine

Part	Operating condition and requirement	Material
Needles, Nozzles	high velocity, prone to cavitation, sand erosion	16Cr 5Ni 13Cr 4Ni
Runner (bucket and disc)	high velocity, acceleration, prone to cavitation, corrosion, sand erosion	13Cr 4Ni
Shaft of needle servomotor	Low friction	SS with hard chrome surface
Turbine housing	Weldability at site	low carbon mild steel of fine grain quality
Inlet pipe of injectors		fine grain cast iron

Matsumura and Chen (2002) reported research by Prof. Duan to compare the erosion performance of several turbine steels and coatings at different locations of Francis turbine. The relative index of erosion resistance is presented considering cast carbon steel as reference material. Most of the steels have shown better erosion resistance compared to cast

carbon steel and ceramics have shown overall better result. Moreover synthetic rubber coatings have shown extremely better results. On the other hand protective resin paints have shown extremely poor performance. Same materials have shown large variation in the index at different locations for example cast SS has relative index 1.91 at runner and only 0.46 at bottom ring. Hence it could be misleading to make general ranking of the erosion resistance of the materials merely on type of material.

4.4 Thermal spray coating

Thermal spray involves different processes of applying coating to improve the erosion resistance and other surface properties. Raw materials for such coating are in the form of powder or wire, which are melted by heat source and sprayed in to the substrate with sufficient adhesion. There are several thermal spraying processes. Most important and general components in these processes are as follows:

- Gun (melting of particle and accelerating towards substrate)
- Control unit (combustible gas control console or electric power control)
- Coating material (wire or powder) feeding mechanism

The molten coating material is accelerated in the thermal spray system and strikes the substrate. Due to heat and impact, the particles flatten in the form of thin platelets and bind together with the substrate. These layers of flattened particles act as a protective coating. The quality of thermal spray coating depends on both coating material property and spray process parameters. Following are some of the important factors influencing thermal spray coating properties (in the case of powder as feed material):

Powder properties:
- Chemical composition
- Melting point
- Morphology
- Particle size distribution
- Shape

Spraying process control:
- Flame temperature
- Gas pressure
- Powder flow rate
- Geometry of nozzle
- Spray distance
- Surface preparation (chemical or mechanical)

The most common thermal spray processes are summarized and compared in table 4.4.1.

Table 4.4.1 Comparison of different thermal spray processes

Spray process	Particle Velocity (m/sec))	Temp. (^{0}C)	Adhesion (MPa)	Porosity (%)	Fuel/ Power	Carrier Gas	Example
Flame Spraying (Powder)	60-70	3100	6-10	7-12	Fuel gas (acetylene or propane) + oxygen	Same fuel gas	Al, Zn for corrosion protection
Flame Spraying (Wire)	120-140	3100		5	-do-	-do-	
Arc Spraying	100-170	7000	10-20	3-15	Electricity	Compressed air	
Plasma Spraying (W-cathode, Cu-anode)	150-600	15000	20->70	1-8	Electricity	Ar, H_2, N_2 or mixture	Ceramic coating
Detonation Gun Spraying	600-800	4200	60	<1	Acetylene + oxygen	-do- , N_2 for purging	
High Velocity Oxygen Fuel (HVOF)	600-1200	2750	>70	1-2	Oxy-propylene or oxy-hydrogen or kerosene	Compressed air	Ceramic-metallic or metallic coating

Source: Berget (1998), Bjordal (1995) and internet

4.5 Welding repair of eroded turbine

The eroded turbine runners and other components are normally repaired by welding to improve its structural and hydraulic requirements. Even though normally repair welding of highly stressed component is not recommended, still it is a feasible option in developing countries due to high cost of imported turbine runners in one hand and cheap labor cost for welding and grinding on the other hand. The turbine components are welded with protective coating to save precious turbine steels from erosion during manufacturing or for build up of eroded portion in repair sites.

Matsumura and Chen (2002) has discussed the bead and paving welding as two types of welding used against turbine erosion. Bead welding is used to protect the flow passage of hydraulic turbines from erosion whereas the paving welding is the method of attaching anti-erosion plates to the surface by spot or braze welding. The preparation of the surface for erosion repair, selection of appropriate welding process/electrodes, adjustment of welding parameters are very important to have good weld quality.

The problem of welding in turbine steels can be realized by taking example of 13Cr4Ni stainless steel. Its weldability is poor because martensitic steels are hard and strong. They are less ductile even with heat treatment. Metallurgical change occurs due to the heat input

to welding, which is localized in the weld area. The chromium content added to improve erosion and corrosion properties of martensite also acts as ferrite former; hence higher percentage of carbon content is needed to ensure formation of martensite. With higher carbon contents, cracking at heat affected zone (HAZ) becomes more serious. Poor thermal conductivity during phase change makes this steel vulnerable to cracking. Post heat treatment is also needed to relief residual stresses. Sharma (1996) have found the linear relationship between cumulative erosion and time of exposure for welded layer by hard facing deposition of 13Cr4Ni0.5Mo (welding electrode D&H 444L) and HAZ. In the laboratory test, he observed constant erosion rate for both weld layer and HAZ for long term tests, even though they show different behavior at early stage. He also found that 300°C preheating is optimum for mechanical properties and microstructure of 13Cr4Ni for better erosion resistance in weld layer.

The welding of eroded Pelton turbine is analogous to the repair of casting defects and cavitation repair. Welding repair of eroded turbine can be classified in to three categories as: (i) minor repair in non-critical areas of thicker section or at outer portion of the bucket (ii) minor repair in critical areas such as inside the bucket and (iii) major repairs in critical areas such as welding at splitter root where bending moment is maximum or in the thin section of the lip or splitter, which hardens easily.

Goel and Sharma (1996) have collected the weld repair data including type of electrodes used for different type of stainless steels used for different materials. Most of the electrodes were A.W.S equivalent E309-15, E309-16, E308-16, E410-15 and so on. Some of these electrodes were also with small percentage of Mo and Cb. Since data are collected from many of the hydropower plants in Himalayan region of India, those experiences will be very useful to hydropower plants in Nepal as well.

4.6 Other processes against erosion damage

Improving one or few mechanical and chemical properties hardly improves erosion resistance of material. Heat treatment is one of the methods to change surface properties of material to improve erosion resistance. This is mainly achieved by increasing the hardness of metal. But together with the hardness, ductility of the component is equally important in the case of hydraulic machinery. Hence the efforts are made to change the material property only at the surface by retaining the properties of bulk material as original. Surface engineering is becoming popular in production process and for improvement of the properties of all kind of surfaces. Together with conventional heat treatment techniques, laser beam and plasma techniques are becoming popular for better surface properties and optimization of the process.

Laser beam can be used to improve erosion properties. The thickness of treated layers ranges from nanometer to several millimeters by different laser treatment techniques. Even though laser techniques are developed for improving properties like abrasion and friction, some of the laser techniques can be equally used for the purpose of erosion.

Laser can be used for transformation hardening of iron base alloy involving austenitisation. Similarly self-quenching can be applied for martensitic transformation. The depth of hardening and temperature profile can be determined by energy density and spot speed. It has an advantage of local treatment with minimum heat affected zone on the bulk volume. But it has limitation in case of overlapping which causes tempering effect. Similarly laser melting process can be used to refine microstructure of metals and formation of metastable crystalline and non-crystalline phases for certain alloys.

Whenever surface melting by other process is not sufficient to provide required properties, laser technology can be used to change the composition of surface layer, known as laser surface alloying. Solid particles like carbides can be injected in to the laser melted pool in laser dispersion hardening method. These methods are generally used for Ti, Mg, Al, Cu alloys, but may be used to improve erosion resistance of steels as well.

Cladding and melting of different alloys in the surface gives good metallurgical bonding providing best possible adhesion of coatings. Cladding can be done by melting a deposit on the surface or feeding powder or wire into the laser beam. WC/Co can be coated in thickness between 0.1-2 mm using laser technique.

Plasma treatment and ion implantation produces thin layer (nm-μm) with high hardness. Plasma is generated surrounding the work piece in particular gas sphere, ionized gases such as N, O, C at temperature about 550°C for more than 24 hours The accelerated ions either diffuse or react with the surface producing hardness up to 1000 HV in steels within few micron thicknesses. The advantage of this method is that it does not change the dimension of component and chances of distortion of component are low. This gives better resistance, but due to high hardness, once erosion process starts it is very dangerous and it is difficult to repair such surface by welding. This method was tried at tried at Jhimruk hydropower project, Nepal but it was not successful.

Ceramic tiles (Aluminum-talc-clay) of size 10x10x1.5 mm was fixed in the Kaplan turbine (Chilla Hydropower Project, India, H_n = 32.5 m, N = 187.5 rpm) blade with epoxy adhesive to prevent erosion, but these tiles were washed away very soon (Chopra and Arya, 1996). The pre-hardened 'wear plate' is also available from the manufacturer of steels and coating companies which can be used as replaceable components. They can be simply bolted to the main component to improve the erosion resistance. It has several advantages over conventional welding overlay of hard surface, such as no heat input to the component, less maintenance time, consistent surface quality and so on.

The welding and coating materials and erosion resistance improvement processes used to protect or repair turbine components in Nepalese hydro power plants are presented in section 6.4.

Chapter 5

Erosion of hydraulic machinery

5.1 Introduction

Turbines and pumps are two broad categories of hydraulic machinery. In the case of turbines, the energy is available in the form of either potential or kinetic energy of water, which furthermore depend on the mass of water and available head. Contrary to this, mechanical energy should be expended to lift the water to higher elevation. The energy available in the water is converted into mechanical energy in the form of turbine rotation at the cost of reaction to the turbine structure. Similarly the physical movement of pump impeller exerts force on fluid. In doing so, any constituents present in the water exert force on turbine or pump, which the material has to resist. One of the very significant constituent of the water in such application is sand. The turbine and pump surface should be strong enough to sustain any forces due to solid particles against any deformation or failure. The deformation or dimensional change of turbine or pump surface is one form among several wear types. Various terms such as erosion, hydraulic abrasion, abrasion and hydro-abrasion are used in the literature for describing the process of gradual change in the shape and state of the surface due to the particles in the water. Among the terminologies in use, the term *Erosion* best describes this phenomenon.

The hydraulic machineries can be classified in several ways depending on nature of construction, principle and range of operation. Mutual dynamic action between the machine and fluid can be both rotary and reciprocating. The damage due to fluid born particles in the reciprocating machine is more of abrasive in nature and different than that appear in rotating machines. Only rotating type of hydraulic machinery, also known as hydrodynamic machines are considered for the discussion of erosion damage in this research. The hydrodynamic machine is subdivision of rotodynamic machines, in which rotor is an essential part. Thermal turbo machines are operating at high temperature with steam or gas as working fluid and steam droplets or fly ash as eroding particles. On the other hand oil or water is used in hydrodynamic machines with sediment or contaminants as eroding particles. The nature of erosion damage is similar in all the rotodynamic machines even if the working fluids, particles and operating conditions are different.

Water turbines are classified in to impulse and reaction turbines based on the principle of energy conversion. Francis, Kaplan and bulb turbine are reaction turbines. Similarly, Pelton and turgo are impulse turbines. The cross flow turbines are two stage impulse turbine used for smaller units.
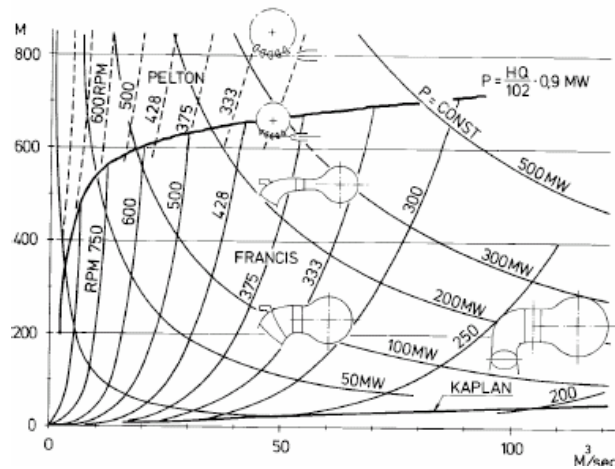
Figure 5.1.1 Range of operation for different types of turbines (Brekke, 2000)

For the purpose of sand erosion, hydraulic turbines can be divided in to following categories:

- impulse turbines
- high head reaction turbines (low specific speed Francis turbines)
- low head reaction turbines (high specific speed Francis, Kaplan and bulb turbines)

All these types of turbines are widely used in power plants built on Himalayan Rivers. Beside these, indigenous cross flow turbines are also extensively used. Figure 5.1.1 gives type and basic shape of turbine for the given range of operation of head, discharge and rotational speed. With the knowledge of relative velocity, discharge and concentration of sand, the erosion in particular type of turbine can be anticipated using the same figure.

It is difficult to distinguish the type of erosion on the hydraulic machinery in micro-level. Karelin et al. (2002) have classified erosion of hydraulic turbine according to visual appearance in six categories as shown in table 5.1.1. This classification could be useful for understanding the nature of erosion damage and could be helpful for maintenance planning. On the other hand Matsumura and Chen (2002) classified the erosion condition in hydraulic turbines in three categories as I, II and III, based on difference in flow velocity and impingement angle of particle (table 5.1.2). This classification was developed on the basis of erosion test of specimens located at different turbine components. The same component of turbine, for instance, the blade can have different type of erosion at leading and trailing edges; hence this classification can be confusing or misleading.

The erosion of hydraulic machinery due to sand laden water can be better classified based on the flow condition of particles and fluid suggested by Brekke (2002) as:

- Micro erosion
- Secondary flow vortex erosion
- Acceleration erosion

Micro erosion is found in the surface of turbine components where fine particles with grains size less than 60 μm are moving at very high velocity. High turbulence in the boundary layers gives high rotational motion to these particles causing several ripples in the direction of flow. The patterns with such erosion are also compared as fish scale or orange peel. Such type of erosion appears in guide vane and runner blade towards outlet and needle.

Secondary flow vortex erosion is caused by obstacles in the flow field or secondary flow in the corners of conduits. Any obstruction in the flow field causes secondary flow and horse shoe vortex is generated around the cylindrical obstacles like guide vane shafts. Similarly the needle of the Pelton wheel have vortex behind the ribs supporting needle and hence vortex erosion takes in the straight line behind the ribs. The vortices in the corner of conduits like guide vanes-facing plates and blades-band also cause this type of erosion. Such vortices and secondary flow are caused by combined effect of boundary layer and change in flow acceleration.

The acceleration of particles normal to the flow direction separates the particles from the flow direction and such accelerating particle strikes the surface causing collision in the water conduit surface. Large particles, for instance higher than 0.5 mm cause severe damage in the conduits in blades and in guide vanes of Francis turbine and Pelton bucket.

The hydraulic machines, working in the range of high Reynolds number such as 10^6-10^8 will normally be exposed to all three types of above mentioned types of erosion. The damage of specific components of main type of turbines is discussed in the following sections.

Table 5.1.1 Turbine erosion classification (Karelin et al., 2002)

Type	Description
1. Metallic luster	Shining surface with no traces of paint, scale or rust
2. Fine scaly erosion	Surface with rare, separately located and skin-deep minute scales
3. Scale erosion	Surface entirely covered with skin-deep fine scale
4. Large-sized scaly erosion	Surface entirely covered with deep and enlarged scales
5. In-depth erosion	Surface covered with deep and long channels
6. Through hole	Erosion of entire material

Table 5.1.2 Classification of erosion (Matsumura and Chen, 2002)

Type of erosion	Location	Flow velocity	Impingement angle
I	Spiral casing Draft tube	Low	Small
II	Runner blade Guide vane	High	Small
III	Wearing ring	High	Large due to vortex and turbulence

5.2 Impulse turbine

The most common type of impulse turbine is Pelton turbine, which operates at high head. Basic principle of Turgo-impulse turbine is similar to Pelton turbines, hence erosion characteristics are assumed similar and not discussed in this thesis. This is also due to unavailability of the erosion experience of this turbine. High velocity and acceleration of particles at the buckets are main reasons for the erosion of Pelton turbine. The Pelton turbine components can be classified in to four categories (i) inlet system (ii) nozzle and needle (iii) runner and bucket and (iv) wheel pit for the purpose of sand erosion.

Inlet system

The velocity at inlet system such as manifold, valve is normally maintained low. The water is slightly accelerated before it enters the valve and velocity is maintained slightly higher in the valve to reduce the size because of cost and weight. The velocity profile at the inlet system of the Pelton turbine up to nozzle is shown in figure 5.2.1 and magnitude of velocity is given by the following formulae (Brekke, 2002):

At inlet manifold, $C = k_i \sqrt{2gh}$ where $0.08 < k_i > 0.1$

At valve, $C = k_v \sqrt{2gh}$ where $0.095 < k_v > 0.12$

At nozzle, $C = k_n \sqrt{2gh}$ where $k_n > 0.99$

Kn=0.99
Kv=0.095-0.12
Ki=0.08-0.1

Velocity

$C = k_n \sqrt{2gh}$

$C = k_v \sqrt{2gh}$

$C = k_i \sqrt{2gh}$
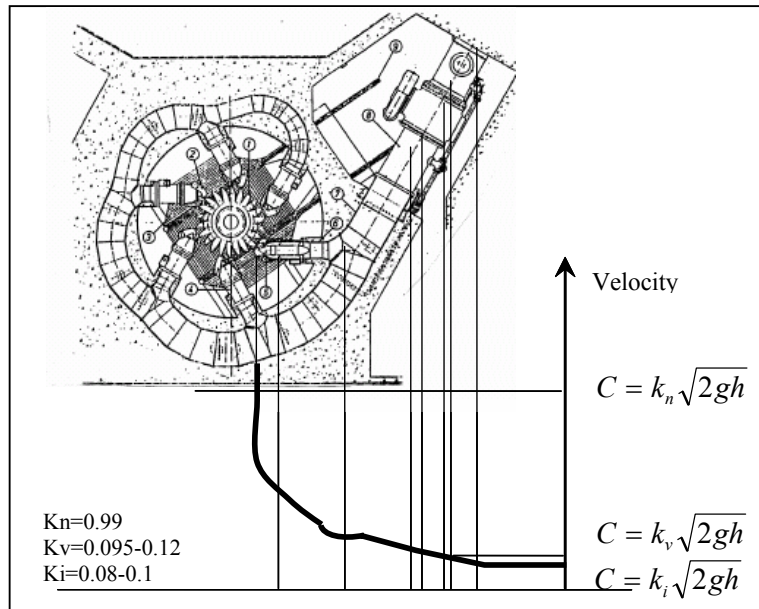
Figure 5.2.1 Velocity distribution in the inlet system of Pelton turbine

The turbine in the range of 600 m – 1500 m head will have velocity 10 m/s to 15 m/s at inlet. Low velocity is maintained at inlet system such that the concrete lining in the tunnel and waterways can also resist this velocity range.

The distributor is filled via bypass system before starting the turbine. Hence higher velocity (around 25 m/s) can be chosen for bypass flow. Regular inspection schedule should be planned because of sharp bends and valve in the bypass are more exposed to sand erosion.

The valve seals of both bypass and main valve face severe erosion. The bypass valve seal damage during closing period, whereas main valve seal damage during emergency closure when needles are open. The rubber seals can not withstand high pressure during emergency closing, whereas steel seals will have abrasion due to sand particles trapped between valve seal and housing. Leakages thorough damaged rubber seals or grooves in the steel seals cause combined effect of sand erosion and cavitation in case of leaking nozzle and turbine is not in operation. Because of the low operating velocity at the inlet, the piping will have only moderate effect of sand. Hence application of high erosion resistance rubber, epoxy based coating or paint may prevent erosion in such pipes. Slight erosion of this system does not affect the performance of the turbine by any mean, but severe erosion in bifurcation and bends may increase chances of rupture of pipe. The regular inspection and maintenance should be carried out to prevent any catastrophic effect.

Nozzle and needle

The water is accelerated in the nozzle and comes as a high velocity jet of magnitude close to $\sqrt{2gh}$. Pelton turbine installed with the head 1200 m can have jet velocity up to 150 m/s. Such extremely high velocity damage both nozzle and needle. The flow is accelerated from the outlet of fins supporting needles up to nozzle tip and all the energy available in the water is converted in to kinetic energy.

High velocity creates strong turbulence in the boundary layer close to needle tip. The fine particles bombarding due to turbulence strikes the needle surface several times and severe erosion can be seen in short time. The cavitation can follow in short duration and severe damage of needle can take place. Figure 5.2.2 shows Pelton needle after the severe erosion damage followed by cavitation. The nature of damage by 0.15 mm particle in needle can be seen in figure 6.3.5.

The nozzle tips are relatively sharp and contact between nozzle and needle are maintained only about 1 mm to reduce cavitation damage and to obtain highest possible efficiency. This makes the nozzle tip vulnerable to sand erosion. If nozzle diameter increases by 5% due to erosion at tip, the turbine will run at 10% load even if needle is at closed position. It may affect entire control system of the power plant. Figure 5.2.3 shows the erosion damage on nozzles of two jet horizontal Pelton turbine. The lower nozzle is more damaged due to large quantity of bigger particles passing through lower jet (Thapa and Brekke, 2004).

The protection of needle and nozzle surface by applying ceramic-metallic coatings may help to improve erosion resistance. Ceramic coating is not very effective in case of larger size particles. There is very little scope to improve the erosion resistance of needle and

nozzle by hydraulic design, but maintainability can be improved by designing replaceable nozzles tip.
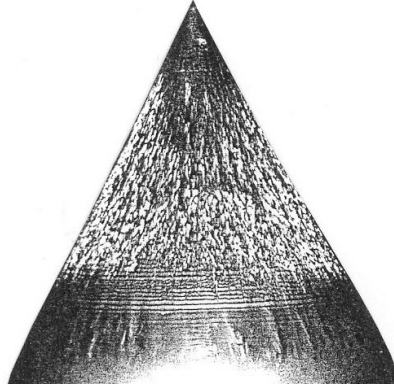
Figure 5.2.2 Eroded needle Mel power plant, Norway (P=52 MW, H=810 m) (Aunemo, 1992)
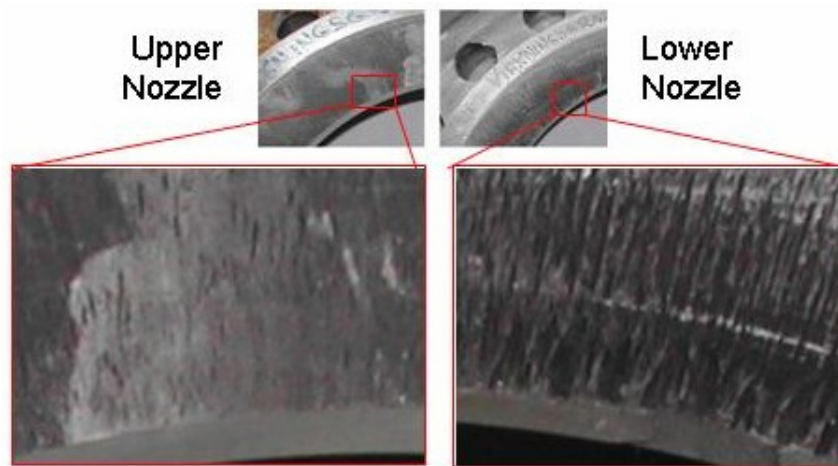
Figure 5.2.3 Upper and Lower nozzle of Skagen (Thapa and Brekke, 2004)

Runners and buckets

Sand erosion has impact on both performance and reliability of the Pelton runner. Bucket is the most affected part of the Pelton runner. The change of bucket profile alters the flow pattern causing loss of efficiency. Similarly loss of material weakens highly stressed parts increasing probability of fracture. Hydraulic analysis of flow in Pelton bucket is done by graphical and numerical methods (Hana, 1999). The acceleration of water particle in radial, axial and mutually perpendicular direction is plotted graphically assuming particles are always normal to the bucket surface (Brekke, 1994). The graphical analysis also revealed that maximum acceleration normal to the bucket surface can reach up to 50000 to 100000 m/s^2. Such a high acceleration separates the particles from streamline. The curvature of the Pelton bucket is very important because of very high acceleration.

The nature of damage of Pelton turbine erosion with fine or coarse sand is different. With coarse particles, most of the damages are in the area where the jet directly hits at the bucket inlet. Surface damage is not of the nature of cutting action by sharp edge, but is more like hammering. Long scars are also seen in the flow direction in each side of the splitter (figure 5.2.4) but no damage is observed at the root of the bucket. Splitter and entrance lip are most severely damaged portion of the buckets, because of direct hitting of particles.
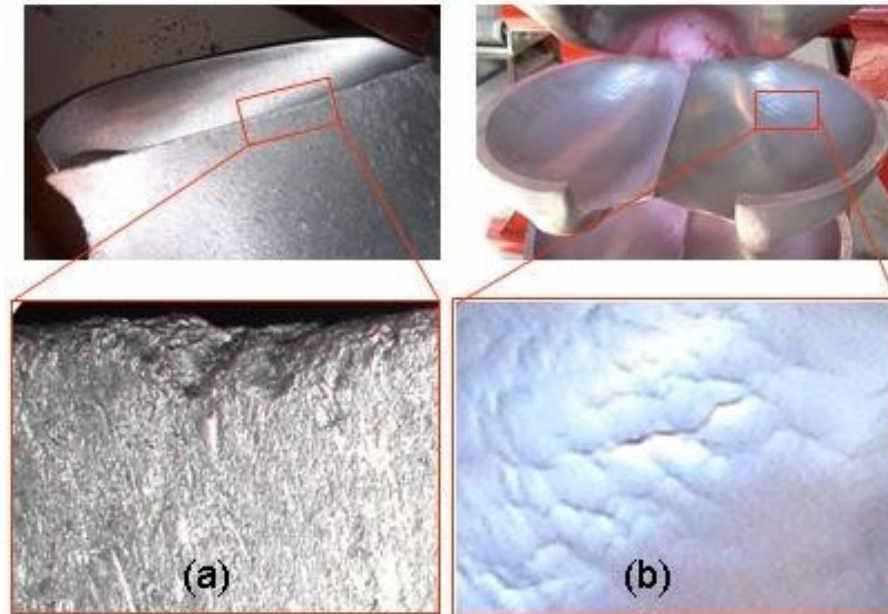
Figure 5.2.4 Eroded Pelton buckets (a) Skagen (b) Khimti (Thapa and Brekke, 2004)

Following conclusions can be drawn from erosion damage of Pelton turbines from hydropower plants- (i) Mel (Norway) with sand particles size equal and less than 0.06 mm, (ii) Khimti (Nepal) with particles size less than 0.15 mm and (iii) Fortun (Norway) with large particles (gravel hitting):

- If the particles are fine (silts), then there will be erosion on the needle but not much erosion in the buckets.
- If the particles are coarse (sand), then there will be erosion in the buckets and there is less erosion of needles.
- With medium size particles, both needle and bucket will be eroded.

Fine particles may glide along with water inside the bucket and strike the surface toward outlet edge, causing severe erosion around outlet. Due to distortion of bucket profiles near the outlet, but not at the edge where the acceleration is zero, the direction of flow changes bending inward and strike backside of following bucket with braking effect. This phenomenon is schematically explained in figure 5.2.5.

The damage of splitter of Pelton bucket can be seen in figure 5.2.4 (a) and 5.8.6 (c). The splitter may be damaged locally by stones causing local cavitation towards the bottom of bucket. Only negligible improvement in efficiency was observed after grinding splitter lip as sharp edge. However, welding and restoring shape of entrance lip improves efficiency. The damage of entrance lip causes bypassing of inlet jet as illustrated in figure 5.2.6 and this is a main cause of efficiency drop in Pelton turbine.

$$C = \sqrt{2gh}$$
$$U = 0.49\sqrt{2gh}$$

Larger particles (Stones)

Out flowing water due to erosion at edge

Water surface

R

Smaller particle (Silt)
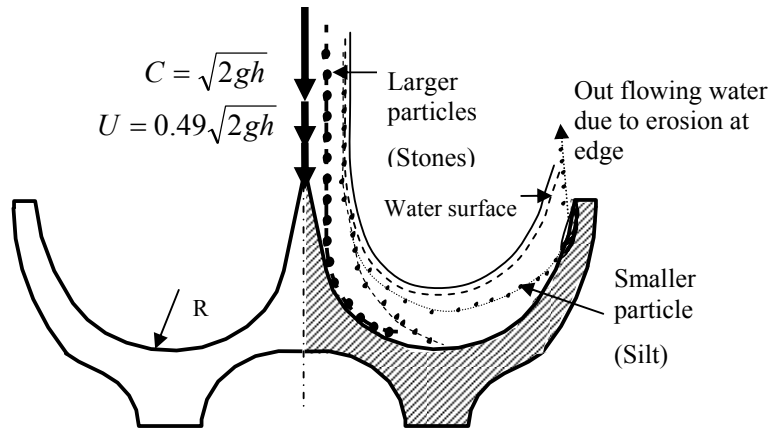
Figure 5.2.5 Illustration of particle separation at high acceleration (Thapa and Brekke, 2004)

Other parts

The jet directly hits the deflector, but because of short exposure time the erosion of deflector is not serious. Moreover it can be replaced easily; hence deflector erosion is not crucial. Similarly turbine pit liners can also be eroded with the deflected water. This can be considered minor because impact energy on liner is not very high. Normally there is no problem of sand erosion in runner disc, because water and particle does not strike the disc surface. But some sections of the disc can be eroded due to improper flow out of the bucket. The example of erosion of runner disc is shown in figure 5.2.7. When the groove due to erosion is small compared to thickness and size of disc, there is no danger of disc failure.

The needles, nozzles and buckets of Pelton turbines are normally protected by hard surface ceramic coatings (Khanna 1996, Aunemo 1992). In real life, such coatings have shown mixed response and have not performed well in the case of large particles. The deflector can also be coated with ceramic, but only soft coating or paint may help for reducing erosion in turbine pit liners.

There are three basic criteria for the design of Pelton turbine to minimize the effect of sand erosion. They are:

1. The curvature radius should be as large as possible at the location where flow direction changes
2. The number of jets should be as low as possible
3. The hydraulic radius of the bucket and nozzle size should be large. This brings minimum sand particles in contact with surface
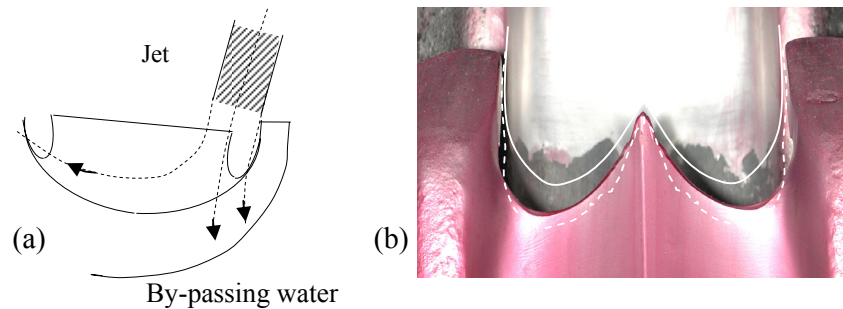
Figure 5.2.6 Illustration of (a) by-passing of water in a damaged entrance lip due to erosion (b) different entrance lip size before and after erosion (exaggerated) (Photo- Khimti turbine)
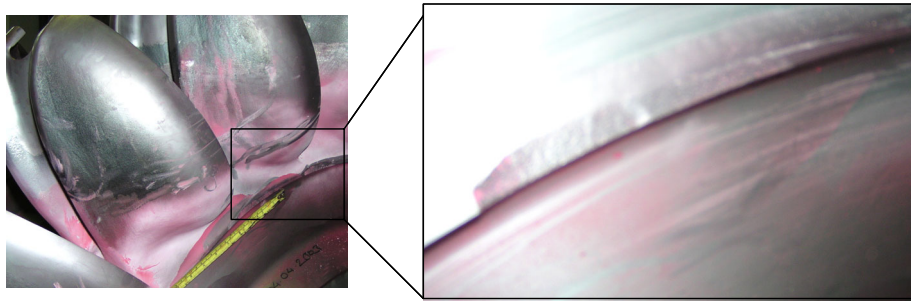
Figure 5.2.7 Erosion of runner disc at Khimti hydropower project

The maintainability of the eroded turbine mainly depends upon dismantling time of the runner. The design of power house to dismantle the runner without dismantling other adjacent components like bearings and generator is favored in the case of turbine erosion.

The horizontal turbine with 1 or 2 nozzles with wide bucket have less effect of sand erosion, but the price of turbine will be higher due to size. Hence vertical turbines with 4 nozzles can be suitable option in such case. Brekke (2002) has argued that the life of Pelton runner with 4 nozzles will have 2.5 times longer life compared to 6 nozzles in case of clean water operation. But this ratio of life increases up to 3.06 in the case of sand erosion. Hence from the point of view of turbine erosion, one or two units of bigger size are more favorable than many smaller units. For example, 3 units of 20 MW would have been better option for Khimti power plant in Nepal compared to 5 units of 12 MW. The difficulties of casting big runners and fatigue problems due to more defects in bigger units are some of the hurdles of having large units.

The buckets can be made up of additional 5-10 mm of thickness without large drop in efficiency where sand erosion can be expected. Regrinding to original profile should be preferred against heat applying processes like welding and thermal spray, which may

decrease fatigue strength. Similar to the nozzle and needles, ceramic coatings are applied at bucket surface to improve erosion resistance. Coating of bucket is also not successful and heating of runner is one of the limitations of its application. The brittleness of ceramic is also a drawback in the case of cyclic loading and impact with large particles.

5.3 Reaction turbine

5.3.1 Francis turbine

High head Francis turbines and reversible pump turbine are reaction turbines which are most affected by sand erosion. Kaplan and bulb turbines operating at very high sediment concentration with hard abrasive particles are also eroded. Since the nature of the erosion is same in most of the reaction turbines, the case of Francis turbine is discussed in detail. The velocity profile at different sections of the typical high head Francis turbine is presented in figure 5.3.1. The general design philosophy for high head Francis turbine is that, 50% of energy is converted in to kinetic energy at guide vane and remaining 50% is retained as potential energy. This could reach up to 65-70 m/s on high head turbines. Hence guide vane faces high absolute velocity. The runner outlet has highest relative velocity. The velocity at the runner outlet is normally selected around 40 m/s during design to ensure flow of water out of the turbine. In the case of pump it could go up to 55 m/s and high relative velocity can be found also in the pressure side of the runner in reversible pump turbine.

Apart from high velocity, high acceleration region in the turbine is also potential location for erosion. Together with high velocity, high acceleration can also be found in guide vane cascade and pressure side of the runner blades. In case of Francis turbine, effect of sand erosion can be discussed in following five categories: (i) inlet system (ii) guide vanes (iii) runners and labyrinth seals (iv) draft tubes (v) shaft seals.
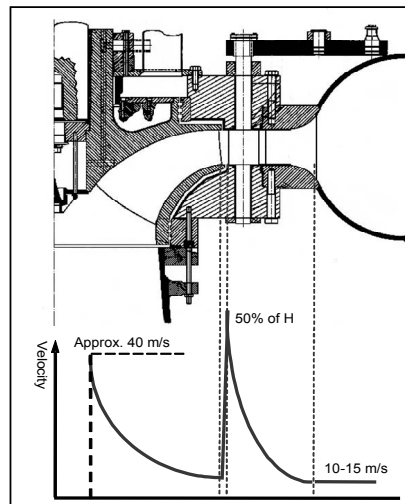
Figure 5.3.1 Typical velocity distribution in high head Francis turbine.

Inlet system

Inlet manifold, valves and bypass system of reaction turbines are similar to the inlet system of impulse turbine. Together with those components, spiral casing of reaction turbines can also be placed in inlet system. Compared to inlet valve of Pelton turbine, its inlet valve will face 50% less pressure during closing due to pressure created by spinning runner. Hence inlet valve of Francis turbine have rubber seat against movable steel seal, which has better erosion resistance. The lower pressure in the spiral casing before opening inlet valve damage main valve seal and bypass valve seat. Hence bypass system in the Francis turbine has to be stronger than Pelton turbine to create higher pressure in spiral casing. The starting pressure in the guide vane system gives indication of leakage due to sand erosion. Erosion damage of butterfly type bypass valve of Jhmruk hydropower plant (Francis turbine) is shown in figure 5.3.2.
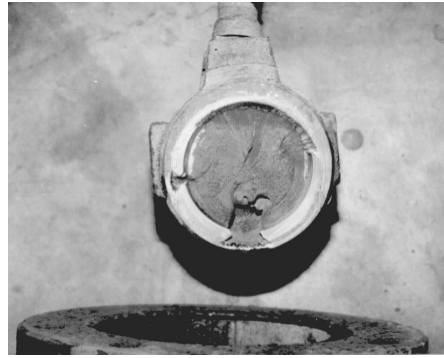
Figure 5.3.2 Erosion of bypass valve of Jhimruk hydropower plant in Nepal (Photo courtesy BPC)

The velocity at spiral casing is higher than Pelton turbine manifold because of shorter distance between inlet valve and guide vanes. The velocity at the inlet of the spiral casing is almost same as the meridional velocity at the runner outlet and inlet of valve. The secondary flow can take place in the spiral casing due to incorrect flow. Because of the secondary flow, incorrect flow angle in the top and bottom region of inlet of stay vanes in traditional design can cause turbulence erosion in high head turbines. The corrosion followed by removal of paint accelerates the erosion rate. However, modern parallel stay rings reduces incorrect flow and minimize erosion at stay vane inlet. Under normal condition, erosion resistant paints can be used in spiral casing and stay vane, but for high head turbines, stainless steel stay vanes can be used to reduce the effect of sand erosion.

Guide vane system

As seen from the figure 5.3.1, the guide vane system is highly affected by sand erosion due to highest absolute velocity and acceleration. For high head turbines, the relative velocity head $(C^2/2g)/H_n$ for guide vane increases from 10% at guide vane inlet to 50% at runner inlet. At normal speed, pressure drop across the guide vane will be approximately 40% of net head at full load and 50% at small opening, which is one of the reason for cross flow and hence erosion takes place at the junction of guide vanes and facing plates.

The erosion of guide vane due to sand laden water can be classified in following four categories (Brekke, 2002):

1. Turbulence erosion at the outlet region and facing plate due to high velocity of fine grain sand.
2. Secondary flow erosion in the corner between guide vane and facing plates due to fine and medium size particles, which makes horse shoe grooves in the facing plates following contours of guide vanes.
3. Leakage erosion at the clearance between guide vane and facing plate due to local separation and turbulence increases the horse shoe vortex in the suction side. The leakage also cause local separation and turbulence at the pressure side at inlet and suction side at outlet of guide vanes causing even a deep groove at the bottom and top of the guide vanes.
4. Acceleration erosion is caused by separation of large particles from the stream lines of main flow due to rotation of water in front of runner. This acceleration of particle is normal to streamline and strikes guide vane surface causing severe erosion. This acceleration also creates secondary flow causing erosion at the corner between guide vanes and facing plates by fine particles.

The acceleration erosion in the guide vane in reaction turbine can be reduced by designing the flow with smoothest possible acceleration. The stay vane outlet angle should be carefully chosen so that guide vane will be in neutral position in normal operation condition. Similarly reduction of clearance between guide vane and facing plate avoid cross flow and secondary flow. Rubber sealings are often used to reduce gap between guide vane and facing plates with the intention to improve efficiency, but this could be more destructive once damage of such seal commence. The turbulence and secondary flow create dangerous galling in facing plates. It destroys flow pattern and also reduces turbine efficiency. The guide vane clearance for new turbine is recommended roughly 0.5 mm in pressurized condition, which is dependent on deflection of head cover. Low initial dry clearance in the order of 0.05 to 0.1 mm may give low clearance in pressurized condition, but such a low dry clearance may cause abrasion and adhesion between guide vane and facing plates. The facing plates can be improved by cladding underneath the guide vanes, but the difference in hardness between guide vanes and facing plates should be maintained to avoid galling of surface. The hardness of 16Cr5Ni Guide vanes with 350-400 HB and facing plate with 17Cr1Ni with 300 HB is an example of appropriate combination which avoids galling and abrasion. The necessary tolerance and surface finish at the mating part of guide vane and facing plate should also be maintained to get rid of these problems. The maintainability of the facing plate is often improved by designing replaceable layer to save maintenance time and expensive bulk material.

Runner

The inlet region of the runner has highest absolute velocity and acceleration, but small relative velocity. Hence impact due to kinetic energy is small compared to force exerted by large accelerating particle. Contrary to this, the relative velocity is highest at the outlet of the runner blade. Hence turbulence erosion due to fine sand is always susceptible at the outlet edge of the blade. Because of the effect of centrifugal force, most of the particles will move towards outer diameter in the runner outlet and hence more effect of erosion is seen

there. Inlet region of the runner is sensitive to incorrect pressure distribution between pressure and suction side and any separation caused by this may cause severe local erosion at the inlet due to fine grain sand. The horse shoe vortex is created at the blade root by cross flow from hub to band due to incorrect blade leaning. This causes horse shoe grooves similar to the guide vanes at the inlet of the blade.

The improvement of blade leaning and correct blade loading at inlet may improve performance of Francis turbine against erosion. The splitter blades at the inlet of runner help to reduce danger of flow around inlet edge at off design operation, which ultimately improves the resistance to sand erosion and cavitation. Incorrect blade leaning may lead to cross flow between hub to band and such cross flow may intensify erosion effect together with other loss associated with it. The leaning of the blades can be improved by using X-blades and improvement in erosion resistance of such blade is expected in Three Gorges project in China.

Labyrinth seals

Labyrinth seals provide sealing for water in the runner utilizing series of pressure drops to reduce the leakage. Its performance depends on labyrinth gap and length of meandering path. Rings and grooves on the rotating and stationary part provide the basic labyrinth. Minimum three groves are used to provide sufficient sealing and clearances vary between 0.25 to 1.0 mm depending on runner speed and pressure. The efficiency of a labyrinth seal is inversely proportional to clearance gap. Hence gaps should be made smallest possible to have minimum leakage, but it has to be sufficiently large to avoid any direct contact between rotating and stationary part. The Norwegian solution with labyrinth seal for high head turbines that is running without water during operation has less erosion caused by water leakage during stand still of the runner.

The turbulence erosion due to fine sand is always susceptible in the labyrinth seal because of high velocity in its surrounding. For high head turbine, velocity in the labyrinth is in order of 45 m/s. Labyrinth seals having small clearance and working with coarse sand may also have erosion as well as abrasion effect. The rotating labyrinth seals are made up of steels to achieve longer life, while stationary seals are normally made of softer materials such as bronze. The replacement cost for the stationary seal is cheaper. But in the case with high sediment concentration, even the stationary seals can be made up of steel which has higher erosion resistance than softer material. For example, bronze sealing rings in the Jhimruk power plant in Nepal is changed to stainless steel ring to combat the erosion problem.

Draft tube

The draft tube section closer to runner will be exposed to highest velocity because of high absolute velocity of water coming out of runner. This section may get mild sand erosion and there is no erosion in the rest of draft tube. Hence draft tube section close to runner is made of stainless steel.

Shaft seal

Mechanical shaft seal will be damaged if the sand-laden water comes in contact with it. The damage could be due to more abrasion than erosion. Shaft seals are normally made up of carbon rings, bronze and steels with lower hardness compared to shaft material. Apart from selection of erosion and abrasion resistance material for seals, insertion of pressurized clean water in the shaft seal also avoids wear.

5.3.2 Kaplan Turbine

The design issues discussed for Francis turbine holds good for Kaplan turbines as well. Kaplan blade tips and region around trailing edge are highly exposed to sand erosion. Erosion damage may be reduced by making straight surfaces toward trailing edges. The thickness of the blade may also be increased toward trailing edge so that blade profile will not be changed by erosion very soon. Schneider and Kachele (1999) have considered the tip of the Kaplan blade as 'hot-spot' because of high velocity at the tip due to circumferential speed, additional hydraulic load due to gap flow and cavitation. In addition, sharp tip will always have discontinuities of coating, which makes such place vulnerable to erosion initiation. Such sharp edges may be changed to replaceable radii at the edge to get rid of excessive erosion effect at the blade trailing edge tip. The most affected area of Kaplan turbine blade is schematically illustrated in figure 5.3.3.
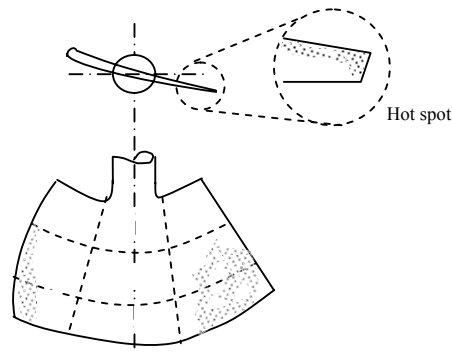
Figure 5.3.3 Illustration of erosion area in Kaplan turbine

5.4 Erosion of pumps

The pumps may also have to handle suspended solid particles or slurries. The solid particle erosion takes place in almost all the wetted surface of such pumps. The mechanisms of the erosion for rotary pumps are also similar to reaction turbines. Although Palgrave (1990) classified three types of erosion mechanisms in the case of pump as impact, grinding and turbulence, they are similar to the mechanisms discussed in case of reaction turbines. The rotational speed, impeller and casing geometry, flow velocity and material are the factors affecting erosion of pump components.

The erosion of pump impeller is analogous to the runner of reaction turbine. The velocity vectors of impeller blade are important in case of erosion of pumps. Relative velocity distribution, tip vortex together with the location of solid particle collection and strike in pump impeller are shown in figure 5.4.1. The nature of erosion at different part of impeller of centrifugal and mixed flow pumps are briefly discussed in this section.

Both side of the blade inlet are affected by erosion due to particle impact at high impingement angle. The erosion of leading edge is dependent on inlet velocity vector; hence it should be kept minimum to avoid erosion at inlet of the impeller blade. Solid particles tend to segregate and local concentration is created along the concave wall of blade due to difference in relative velocity. This may cause erosion in the concave wall of the blade due to impact of particles in smaller angles. Similarly there is a large gradient of relative velocity at the trailing edge of the blade causing high erosion rate. Erosion at the trailing edge is due to both low impingement angle and high turbulence. The tip vortex may cause erosion of blade tip at outlet. The hub surface will be eroded due to change in flow direction. Erosion of front and rare liner is because of low impact angle and these are very sensitive to performance of pump.

The fluid leaving the impeller blades causes erosion of casing volute tongue/cutwater due to high impingement angle. The clearance at the tongue also influences the efficiency of the pump. The erosion of labyrinth and shaft seal of pump are also similar to that of reaction turbine. Together with the loss of hydraulic efficiency, leakage through sealing causes volumetric loss.
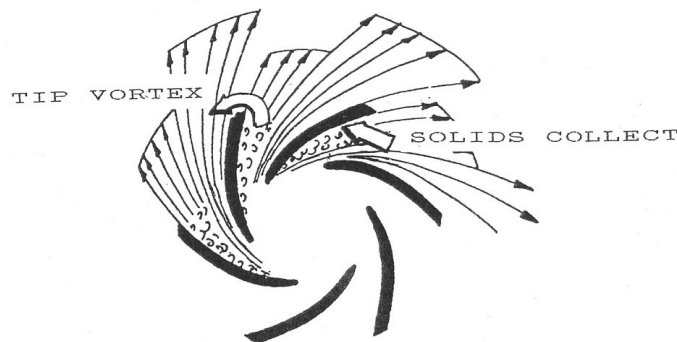
Figure 5.4.1 Relative velocity profile at pump impeller outlet (Palgrave, 1990)

5.5 Design of turbines against sand erosion

It is not possible to avoid sand erosion of turbine components by design alone. The means for reduction of sand erosion of turbine components can be hence divided in to three main activities as (i) Hydraulic and mechanical design (ii) Material selection and (iii) Design for maintainability. Some issues in the design of turbine in the view of sand erosion which are not touched in previous sections are discussed in the following section.

Turbine type

The turbine selection diagram (figure 5.1.1) is developed on the basis of hydraulic performance and mechanical strength of turbine unit. The general rule for turbine selection is to go for axial flow turbines for low head and high discharge flow conditions whereas Pelton turbine is preferred for high head and low discharge. In between extreme head and flow, there is possible overlap for different type of turbine and erosion aspect can be deciding factor for selection in such overlap region. In the overlap between Pelton and Francis, former should be selected because of lower replacement and maintenance time, despite of high initial investment for generator and civil structure. Time to change runner, needle and nozzle is much lower in Pelton turbine compared to replacement of guide vanes and runner of Francis turbine. Hence Pelton runner is preferred instead of high head Francis (400-450m) where sand erosion is expected. The regrinding of eroded bucket to regain profile is possible even without dismantling the runner from shaft in horizontal Pelton turbines. In addition, the accessibility to repair in Pelton turbine is much better compared to Francis. If the turbines have to operate in off design condition, Pelton turbine is preferred due to lesser drop in efficiency in part load. Kaplan turbine could be preferred to the Francis in the overlapping zone because of low relative velocity if sand erosion is expected, but cost of dual regulating system in Kaplan turbine can alter the decision.

Number of units

The number of turbine units on the hydropower project is decided by optimizing investment cost and availability in case of failure. Large turbine with lower number of units should be preferred where sand erosion is expected, because large curvature in bigger units will have lesser erosion. But other limitation like load carrying capacity of local road and bridges for transport of turbine, generator and transformer up to the site can also play decisive role for number of units even if that number is not optimum for the purpose of sand erosion. For instance, transport capacity was main deciding factor for five units at Khimti hydropower project, Nepal.

Speed

The turbine erosion is highly influenced by the particle velocity and also related to the rotational speed of runners. Hence lowest possible speed should be selected for the case where sand erosion is expected. The general guideline could be to select one or two step lower speed of rotation than synchronous speed selected for the clean water condition.

Other design issues

Apart from the main turbine components discussed above, the special attention should be given for designing following components in the case of sand laden water.

- The special packing should be provided in the guide vane bearings to prevent entry of water and provision should be made to replace packing without dismantling guide vanes.
- The top cover pressure may increase due to increased leakage from labyrinth. Hence there should be adequate pressure relieving arrangement.

- The drainage of leakage water from top cover is required either by providing a pump or providing inbuilt radial fins on the crown top for self pumping.
- Closed circuit cooling system with clean water can be used for cooling of bearings.
- Special power house arrangement to remove runner from bottom in vertical units.

5.6 Performance of eroded turbines

The removal of material from turbine component reduces mechanical strength of turbine and also causes the disturbance in the flow pattern. Any uneven material removal from the runner and damage of bearings may cause severe vibration of the system. Another important effect of turbine performance due to sand erosion is reduction in efficiency.

Takagi et al. (1987) have investigated performance of a model turbine in suspended solids. Around best efficiency point (BEP) the efficiency varied as the concentration increased up to maximum 8.8% by weight. They observed power output ratio is directly proportional to specific gravity ratio of mixture with clean water. This observation was made assuming change in turbine performance is similar to change in pump performance. The increase in hydraulic loss in sand water handling pump is due to friction loss and pressure loss, which is larger than other loss in higher concentration. They have derived empirical expression for the turbine BEP based on the observation that efficiency decreases in straight diagonal line with increase in concentration of particles. The ratio of efficiency with mixture to clean water is given by equation:

$$\frac{\eta_m}{\eta_w} = -0.085\ C_w + 1.0 \qquad\qquad 5.6.1$$

Here, C_w is the ratio of weight of solid to the weight of mixture, η is efficiency and subscript m and w represents mixture and clean water respectively.

The change in performance of turbine due to erosion is much more significant than the change in performance due to variation of sediment concentration in the water. Hence only reliability of turbine component in term of mechanical strength and drop in efficiency due to sand erosion are discussed in this section.

5.6.1 Efficiency

The drop in hydraulic efficiency in turbine is due to several reasons such as leakage of the water without doing useful work, secondary flow within the flow field or friction loss due to roughness of the surface. The nature of drop in efficiency in Francis and Pelton turbines due to sand erosion are different. In Francis turbine, highest drop in efficiency is at part load whereas in Pelton the highest loss is at BEP which is schematically demonstrated in figure 5.6.1. The causes of efficiency drop because of sand erosion in common hydraulic machinery are discussed in the flowing sections.
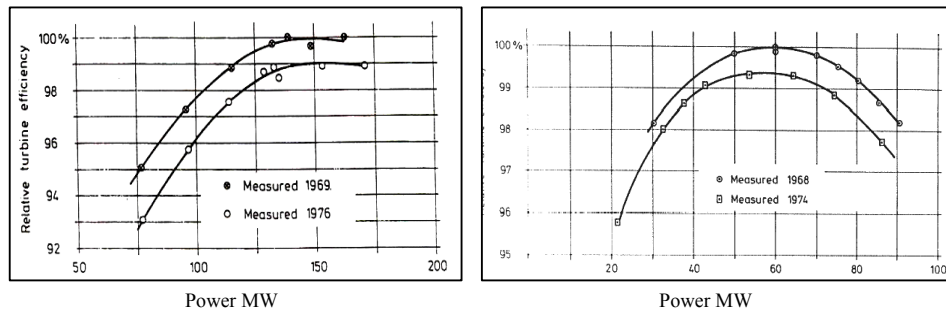
(a) Efficiency curve for 165 MW vertical Francis turbine before and after sand erosion, H_n= 430 m, N=375 rpm

(b) Efficiency curve for 81 MW vertical Pelton turbine before and after sand erosion, H_n= 645 m, N=500 rpm

Figure 5.6.1 Efficiency curve for normal and eroded turbines (Brekke, 1978)

Pelton turbine

Brekke (1978) has suggested thumb rule to estimate the drop in efficiency by measuring the thickness of splitter. The height of splitter gradually decreases due to erosion which is proportional to the erosion depth in the bucket. This thumb rule is stated as "When the thickness of the splitter increases to 1% of the bucket width, the drop in relative efficiency at full load is 1%". This condition is observed when needle is not damaged.

The loss of efficiency in eroded turbine is due to combined effect of following reasons:

1. Loss of water through eroded entrance lips.
2. Change of flow direction due to erosion at outlet edge of bucket and braking effect by back hitting

The entrance lip of Pelton bucket is bent towards jet to avoid water jet streaming out of the entrance instead of bucket sides. This is done to obtain highest possible efficiency, but it is very sensitive to both cavitation and sand erosion. The measure of the width of the splitter is only way to measure the erosion. The loss occurs at the entrance because of loss of outlet water by-passing the bucket.

Francis turbine

There are several reasons for loss of hydraulic efficiency of Francis turbine. These losses are illustrated in figure 5.6.2. The increase in clearance between guide vane and face plates, leakage through labyrinth seals and friction loss in eroded rough surface are main reasons for loss of efficiency in case of Francis turbine. With the experience from measurements at Norwegian hydropower plants, Brekke (1978) proposed the thumb rule for loss of efficiency of Francis turbine as "If the total clearance between covers and guide vanes have increased from 0.2% (new at full pressure) to 0.4% (after erosion), a loss of about 1% can be expected at best efficiency".
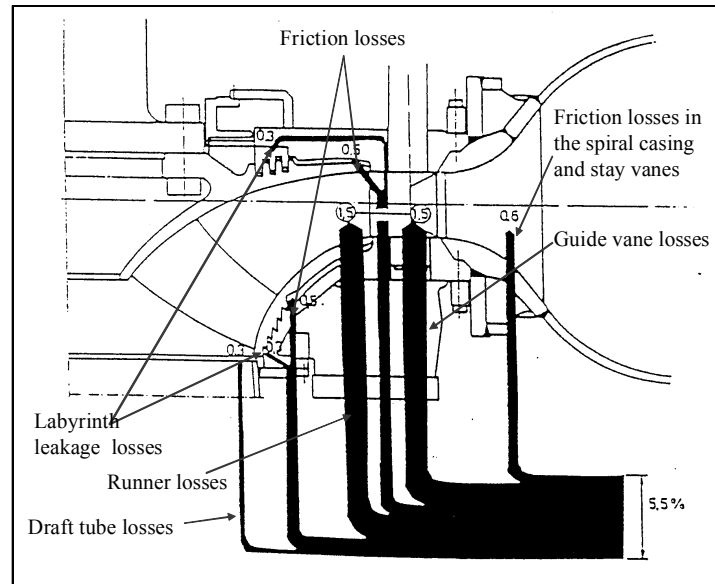
Figure 5.6.2 Energy losses in Francis turbine (Brekke, 2000)

The loss of efficiency in high head Francis turbines are due to three major reasons. They are:

1. increase in clearance between guide vane and face plates
2. friction loss due to roughening of surface of guide vane, top cover, blade surface
3. leakage through seal rings

Erosion of faceplate is very crucial for drop in the efficiency of Francis turbine because of increase in the clearance and disturbance in flow field. The effect of the faceplate erosion was investigated by Brekke (1988) in the Driva Power Plant (71.5 MW, H_n = 540 m, N=600 rpm) in Norway. The relative efficiency increased about 4% at Best Efficiency Point (BEP) after the repair of the faceplate. The improvement of efficiency at the points other than BEP was even more. Similarly, the effects of increase of gap between face plate and guide vanes were studied in two power plants in Norway by inserting seams to create artificial gap. The thermodynamic efficiency measurement at Kvilldal Power Plant (315 MW, Hn=520 m, n=333 rpm) and Lio (45 MW, Hn=335m, n=600rpm) revealed that for 1% increase in clearance, 3.9% drop in relative efficiency was observed at Kvilldal and 1.6% at Lio at BEP. This indicates the contribution of increment of clearance gap due to sand erosion in loss of turbine efficiency. The efficiency curve for before and after the effect of sand erosion shows that high losses occur at low guide vane openings due to following reasons:

1. Pressure gradient at two sides of guide vanes are higher at low guide vane opening causing high leakage.

2.   The guide vanes are positioned at eroded surface at low opening, hence contributing increase in gap and hence leakage. This also creates false direction of velocities and recirculation, which reduces efficiency.
3.   Small guide vane opening makes narrow channel with rough surface due to sand erosion, which causes high frictional losses at high velocities.
4.   The flow through the labyrinths increases at low guide vane opening causing more losses compared to large opening.

The observation of efficiency measurement severely erosive eroded Francis turbine of Jhimruk hydropower plant (JHP) Nepal is presented in section 6.7.

5.6.2 Reduction of thickness

Different sections of the turbine components are dimensioned corresponding to stresses in that section. The typical stress distribution in the Pelton bucket can be found in Brekke (1984), which indicates that the bucket root and splitter section close to the entrance lip are most important area from the stress point of view. The root section is normally thick compared to splitter. Brekke (1984) has also indicated critical stress zones for Francis and Kaplan turbines. From the point of view of mechanical strength, the thickness at the highly stressed zones may be slightly higher because of sand erosion. Examples of such area are Francis turbine runner blade outlet near the band, outlet edges of Kaplan turbine and entrance lips of Pelton turbine.

5.7 Operational strategy

Cavitation/submergence

The turbine submergence is basically decided on critical cavitation coefficient determined from laboratory model test on clean water for maximum output condition on rated and maximum head. However, cavitation nuclei formation in silt laden water is higher than in clean water and synergic effect of cavitation and sand erosion may appear. Hence deeper submergence is needed to avoid cavitation in the sand laden water and additional submergence depends on factors like concentration, size and particle composition.

Concentration cutoff

Higher the concentration, higher will be the possibility of large number of particles coming in contact with the surface. In the laboratory test, the erosion rate remains constant at higher level of concentration due to inter-collision of the incident and rebounding particles. This type of condition may prevail in slurry handling pumps, but such case will hardly appear in hydraulic turbine.

Though the technology to monitor instantaneous concentration in the river and decide operational strategy is still not developed, there is a general practice to shut down power plant after concentration passes cutoff point. Naidu (1996) has presented cutoff concentration for low and medium head turbines (< 150 m) as 200 PPM and for higher heads only 150 PPM for 0.2-0.25 mm particles. In actual practice, the concentration level in

the water passing through turbines of the power plant of Himalayan Rivers is quite higher than this cutoff level for most of the time.

Off design operation

The operation of turbine at off design may cause poor efficiency, increased turbulence and higher or lower relative velocity at the runner outlet than at best efficiency point operation. The secondary flow and vortices at part load causes to local erosion. Hence turbines should be operated at full load as far as possible to reduce erosion of guide vanes and runner inlet. However, the erosion at the runner outlet of Francis turbine will increase at high load caused by increased relative velocity. For Kaplan turbine the relative velocity at the blade outlet decreases due to more open blade channels.

Frequent start and shutdown causes instability in the flow system and mass oscillation may take place due to this. The particles in the tunnel floor can be carried out by such mass oscillation or during emptying of tunnel or canals and excessive sediment in water causes erosion of turbine components.

5.8 Appearance of eroded surface

The simplest way of identification of erosion is visual observation. Since cavitation, corrosion and sand erosion can appear simultaneously or independently, it is necessary to know the differences in the appearance of these damages. Basically the cases related to hydraulic machinery is discussed in this section, but general appearances of erosion pattern are similar in all the other applications as well.

The common appearance of cavitation is like pit holes and the damaged surface is spongy in appearance with several tiny holes. Different types of corrosion may take place especially in pumps, operating at corrosive environment. Even in hydraulic turbines, the junction of dissimilar material may have corrosion effect. The appearance of corrosion depends on its type, but in common, corrosion or rusts of different color can be clearly distinguished from the base material. In addition, the pits in combination with corrosion may also appear. On the other hand, the appearance of sand erosion surface is wavy or plane shining luster. The basic appearances of erosion is also similar to the classification of erosion of turbines (Table 5.1.1) proposed by Kareline et al. (2002). There is no difficulty in differentiating sand erosion and cavitation, still Professor Hermod Brekke suggests practical and reliable tip to distinguish between cavitation and sand erosion. He states "When finger is rubbed in the damaged surface, and if it is bleeding it is cavitation, otherwise it is sand erosion". Hence cavitation surface have sharp projections whereas sand eroded surface are smooth and with blunt edges. It is already discussed; there are cases where cavitation and sand erosion may exist together. But it is difficult to distinguish such combined damage. The hitting by sand may have dominating role in detaching the material from surface; hence in case of combined effect also, the appearance may be dominated by wavy surface. But it is interesting to observe, which appearance dominate at different operating condition depending upon cavitation strength and effect of sand at different concentration and velocity. Figure 5.8.1 illustrates the cavitation pitting in Francis turbine

blade, sand erosion in Pelton bucket and the corrosion in band and head cover can be seen in figure 6.5.2.

Figure 5.8.1 Pictures of severe cavitation damage in Francis runner (left) and damage of Pelton bucket due to sand erosion (right)

Eroded surfaces normally have ripple or wave pattern irrespective of erosion mechanism and eroding environment. Ripple formation in surface are also seen in other flow related cases such as (i) ripples and dunes of sand in desert due to wind, (ii) wavy pattern in snow surface due to wind (iii) ripples in rive beds due to water current and like that. The ripple pattern due to sand erosion in turbine component is also somewhat similar to the others mentioned above. Normal impingement of jet produces hill-and-valley (Peterson, 1995), whereas small angle produce ripples in the direction flow. The sizes of ripples are function of flow parameter and time of exposure to a certain limit, but they attain steady state after certain duration. Karimi and Schmid (1992) observed ripple patterns in between 0.2-0.3 mm to 0.7-0.8 mm even in the absence of solid particles in the flow, which indicates the importance of flow parameter in the formation of ripples. The reason for ripple formation in particle free flow is though not clear, but may be due to cavitation, liquid jet impact or turbulent bursting phenomenon in boundary layer.

Several models and hypothesis of ripple formation, for example Abrahamson (in 1961), Stringer and Wright (in 1987) and Yalin (in 1971) are discussed in Karimi and Schmid (1992). Correlating with sediment ripples and dunes may not be suitable for erosion of metal because of the difference in metallic bond strength. Abrahamson has proposed *Indentation Theory*, which is based on permanent periodic wave formation due to traveling jet. In this theory, local depression takes place under jet and surface will be raised elsewhere. Contrary to this, the model based on *Wear of Material* suggests that single craters overlap to generate surface of randomly distributed depressions and ridges. Stringer and Wright proposed a model considering flow properties rather than action of particles. The flow of impacting erodent displaces material and accumulation and coalescence of individual erosion craters form ripples. Yalin used analytic fluid dynamic approach considering effect of turbulence and eddies rotating on surface to describe ripple formation.

Based on experimental observation, Karimi and Schmid (1992) proposed descriptive model (figure 5.8.2) for ripple formation. This model is based on boundary layer flow, and it could be close to the case for erosion ripples of hydraulic machinery. Micro-roughness due to machining forms turbulent boundary layer in initial stage and eddies are formed. This initial roughness is then replaced or enlarged by individual erosion in intermediate stage causing larger eddies, which determines impingement angle and area of impact. Such change take place until steady state with constant wavelength and shape is achieved. If the flow is highly turbulent, deep ripples may form causing cavitation as shown in figure 5.8.2 d which shows region of cavitation (I) and region of large-angle impact and erosion (II and III) in case of extreme flow condition. Similarly, figure 5.8.3 explains the growth and shift of microripples schematically in the case of ceramic (Fang et al. 1998). Such condition may prevail in the case of erosion Pelton turbine needle and buckets together with other type of turbines. The observations of erosion of Pelton turbine splitter from Khimti hydropower project, Nepal are shown in figure 5.8.4, 5.8.5 and 5.8.6. These observation and photographs supports the models discussed above.

(a) Initial stage   (b) Intermediate stage

(c) Final stage   (d) Cavitation due to extreme ripple formation
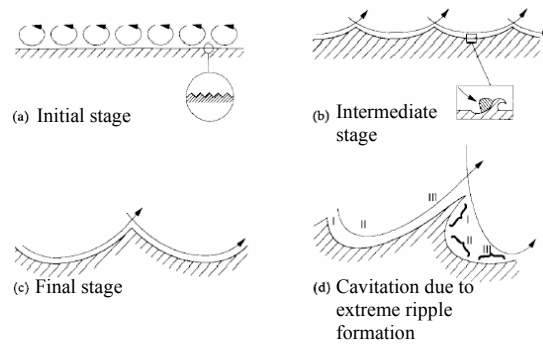
Figure 5.8.2 Ripple formation due to turbulence eddies and the influence between micro roughness and eddies size (Karimi and Schmid, 1992)

There may be slight differences in ripple pattern and dimension for different materials. Stainless steels develop larger and more pronounced ripple compared to ceramic and cermets. This difference of ripple size is partly due to fluid flow pattern in boundary layer (influenced by surface micro-roughness) and partly from higher erosion resistance of coatings. The eroded surface micro-roughness is characterized by the single scratch dimension in alloy, whereas size of spray particle in ceramics and carbide size and distribution in cermets.

Zu (in 1990) suggested an empirical description of ripple wavelength (λ) for ductile metals as shown in equation 5.8.1 (in Fang et al. 1998). The fracture toughness (K_c) is added in equation 5.8.1 by Fang et al. (1998) to incorporate higher hardness of brittle material. In case of brittle material, 'Brittleness factor' replaced the hardness in equation 5.8.2. These equations approximate the relationship between ripple characteristics based on material properties.

$$\lambda = \frac{kt^{1/2}}{H_v} \qquad\qquad 5.8.1$$

Here λ is ripple wavelength, k is an intrinsic constant for all ductile material, t is erosion time and H_v is hardness of metal target.

$$\lambda = \frac{kK_c t^{1/n}}{H_v} = \frac{kt^{1/n}}{B_s}$$ 5.8.2

Where K_c is fracture toughness and brittleness B_s is the ratio of (H_v/K_c).
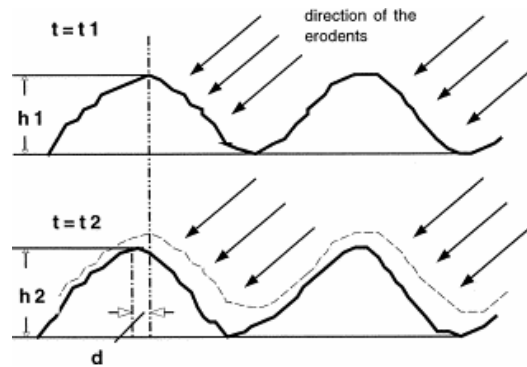
Fig 5.8.3 Schematic diagram illustrating the shadowing effect which is responsible for the growth of micro ripples on brittle materials (erosion time $t_2 > t_1$; ripple magnitude $h_2 > h_1$; d is the ripple peak change distance) (Fang et al., 1998)

The ripple wavelength was observed in between 10-50 μm in ceramics by 600-850 μm silica slurry in 8 hours. The ripple wavelength decreases as the brittleness of material increases and ranking of ripple wavelength was also found in the same order of B_s.

The ripples of Francis turbine blades and Pelton needles are normal to the flow direction. Both ripple length and amplitude decreases toward trailing edge. At the blade root the influence of supporting wall can be seen, which disturb wave pattern and increase the erosion locally. Ripple dimensions are related to local flow parameter, for instance ripple dimension increases with local velocity and turbulence. The ripples in the face of guide vane can be similar to the blade surfaces, but the ripple pattern in face plates are complex with the horseshoe shaped grooves. Vortices initiated by the slightly protruding circular base can be seen with increase in local ripple depth. Cavitation can also be observed on the lee sides of these waves due to separation. On the places without flow disturbances, smaller and more regular ripples can be observed.

The ripple dimension and shape can be direct reflection of the local erosive condition, which is a function of flow pattern and particle size, shape and concentration. Such information of ripple shape and size can be used as inspection indicator in the hydraulic turbines and decision of repair can be made once the ripples attain certain size.
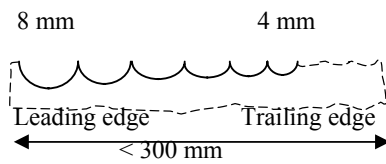
Figure 5.8.4: Wave pattern in the splitter of Pelton bucket.
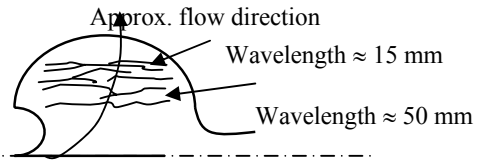
Figure 5.8.5: Wave pattern in the Pelton bucket half section.

(a) needle

(b) close to root of bucket

(c) Splitter tip
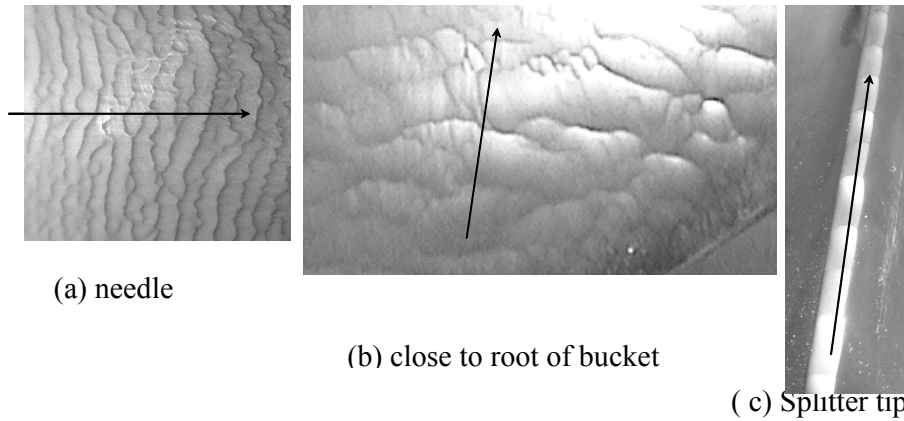
Figure 5.8.6 Ripple patterns in Pelton turbine components from Khimti hydropower project, Nepal (arrow indicate approximate flow direction)

5.9 Monitoring of turbine erosion

Monitoring of the turbine erosion is difficult task and as of the author's knowledge, there is no standard procedure for measuring the erosion effect in the turbine components. In laboratory tests, the specimens are small in size and they are of regular shape or flat plates. Hence it is easy to measure the effect of erosion in term of weight loss, volume loss, surface roughness or deformation dimension. Since the turbines in actual hydropower plants are big and the runner blades or buckets are not flat, it is difficult to measure the extent of erosion damage by above mentioned procedures.

In literature, the erosion damage of turbine is generally presented in term of reduction of thickness. There are several challenges in measuring decrease in average thickness. Some of them are:

- thickness is not uniform in the entire wetted surface

- due to the erosion ripples, measurement of local thickness is difficult
- the change of original edges (for example in Francis blade outlet and splitter in Pelton) makes it difficult to locate reference for comparison
- due to irregular curved surface, it is difficult to trace the profile of the surface
- due to the size of blades, it is difficult to use calipers at all locations
- surface roughness measurement is also difficult in several locations due to surface curvature

Even though the erosion measurement by conventional method is cumbersome, still it is widely in use. The difficulty of measuring erosion at the turbine and duration of shut down may be reduced by taking replica of eroded components by Plaster of Paris or other quick setting materials. This method may not be accurate in gravimetric method due to hygroscopic nature of such material, but it can give good replica for volumetric shape change. The best thing is, it gives minimum stoppage time and storing the physical geometry for successive measurements for comparison is possible.

Image processing technique can be used for comparison of eroded surface with original image and it may give exact loss of material at different location. Only challenge for this is to retain un-deformed reference location to take the image of the components.

Use of video probe to observe eroded component has certain benefits like inspection without major dismantling, less inspection time and images can be compared offline. This technique is seldom used in hydropower plants for inspection. Boroscope inspection was carried out at Jhimruk hydropower project for evaluation of different coatings on guide vanes and runner. Boroscope picture of eroded turbine gives the major damage like holes and cutoff (figure 5.9.1).

Figure 5.9.1 Boroscope picture of eroded turbine of JHP (Dahlhaug and Thapa, 2004)

Chapter 6

Hydropower development and problems in Nepal

6.1 Introduction

Nepal lies in south slope of Himalayas in between Gangetic plain in the south and the Tibetan Plateau in the north having east-west length approximately 885 km and north-south mean width 193 km with total land area 147181 km^2. The land system in Nepal is divided in to five distinct regions based on physiography which runs almost parallel east to west as shown in figure 6.1.1. The Tarai, 26-32 km wide belt in the south is fertile alluvial plane of and rest of the land is slopes land valleys where severe surface erosion takes place. Siwalik, middle mountains and high mountains are the major areas of Nepalese settlement. The Himalayas are high mountains with permanent snow and ice.

Nepal is a developing country with population of approximately 23.1 millions (SYB 2002) and majority lives in the rural areas. Nearly 90% of its energy demand is met by traditional sources, which is mainly used for cooking and lighting (Thapa et al. 2000). The electricity is serving only about 1.2% of total energy need and only 18% of the populations have access to the electricity (Shrestha, 2003). The electricity demand is increasing by 7.98% on average (NEA, 2002/03). It indicates large domestic market for the electricity in the country. Beside domestic markets, giant neighboring countries, India and China with very high energy demand, are potential customer of hydropower.

Nepal is gifted by nature in term of water resources with glaciers in the Himalayas and regular monsoon rains. Average precipitation in the country is 1503 mm and total annual runoff of is about 224 billion cubic meters (MWR, 2003). There is a spatial and temporal variation of rainfall throughout the country, which drains toward north to Ganges River in India through 6000 large and small river/rivulets. Considering rivers with catchments area larger than 300 km^2, Dr Hari Man Shrestha (in 1966) revealed that hydropower development capacity of Nepal is 83000 MW. He also roughly estimated total hydropower potential 126000 MW including smaller catchments (Parajuli, 2003). The overview of hydropower potential in different river basins is presented in Table 6.1.1 and that shows nearly 43000 MW can be economically exploitable.

Figure 6.1.1 Physiographic map of Nepal

Despite Nepal's enormous potential, only 580 MW is harnessed until 2004 and about 115 MW is under construction. Even though the first hydropower plant (500 kW Pharping project) was installed way back in 1911, the pace of development of hydropower is very slow and it took almost 3 decades to commission second (640 kW Sundarijal project). Successive hydropower projects were developed with the assistance of India, USSR, China and several development cooperation agencies. The global and regional economic liberalization trend led Nepalese government to formulate Hydro-power development policy (1992), which opened the door to national and foreign private sector investment. As a result of that several small and big hydropower projects are promoted jointly by Nepalese and foreign companies and some are under construction or in pipe line. Nepal's main challenge for hydropower development is financing, because both private and public sectors can not meet the huge investment required for hydropower.

Table 6.1.1 Hydropower capacity in different river basins in Nepal (MWR, 2003)

Main river basins	Small river (catchments area 300-1000 km^2)	Major river (catchments area>1000 km^2)	Total (GW)	Economically feasible Capacity (GW)
Sapta Kosi	3.6	18.75	22.35	10.86
Sapta Gandaki	2.7	16.95	20.65	5.27
Karnali and Mahakali	3.5	32.68	36.18	25.1
Southern rivers	1.04	3.07	4.11	0.88
Country Total	10.84	72.45	83.29	42.13

6.2 Sediment problems

The climatic and physical conditions are highly favorable for erosion and sedimentation in Himalayan Rivers. Out of 20 billion tones of earth's materials carried to sea annually, nearly 6 billion tones are in Indian sub-continent alone (Naidu, 1996). Likewise the specific sediment yield is very high in Nepal's Karnali River (4362 $t/km^2/yr$) compared to other large sediment producing watersheds for example Yellow river in China (2470 $t/km^2/yr$) (Galay et al., 2002). Such excessive sediment in the Himalayan River is due to presence of weak rocks, high monsoon rain and extreme relief in the region. Hence sediment management has become primary importance for the safety, reliability and longer life of infrastructures like hydropower, irrigation and drinking water projects.

The erosion of earth's surface and sedimentation is highly influenced by local geology. The rate of sediment production depend on the type of rock, uplift and the faulting of the rock together with the mass wasting along the mainstream valley walls. The local geology due to the process of formation of Himalayas greatly influences the rate and type of the sediment in the river, which can be seen in the N-S formation of the Himalayas with distinct rock composition (figure 6.2.1). Most of the sediment deposition zones are primarily running in middle mountain range where most of infrastructure development takes place.

On average 70-80% of annual rainfall occurs with in 4 months of monsoon period in Himalayan region. The intensity of the rainfall decreases towards west of the Himalayas whereas intensity and amount is normally higher in the lower portion of the Himalayas (Siwalik and middle mountains). The quantity and type of sediment can be estimated with the help of watershed classification of Nepalese Rivers (figure 6.2.2) and geology (figure 6.2.3) from which river is flowing. Together with these two figures (6.2.2 and 6.2.3) and surface erosion in the watershed, which can be estimated from intensity and duration of rainfall, the qualitative information of sediment properties in river can be obtained.

Higher and middle mountain regions are most prospective area for hydropower developments. The geology of Class II watershed (figure 6.2.2) contains rocks such as phyllite, limestone, quartzite and schist with relatively harder materials. Similarly rivers from Class III watersheds flow through area mainly consisting sandstones and conglomerate. The Himalayan rocks can be classified in to sedimentary, metamorphic and igneous rocks. Sedimentary rock consists of loose and easily erodable rocks like sandstone, mudstone, siltstone and conglomerates, which are found in the Siwalik belts of the sub-Himalayas, whereas stronger sedimentary rocks like black shale, limestone, sandstone and dolomite are found in the lesser Himalaya and higher Himalaya. The conglomerates are rocks which are composed of more than 30% rounded sediment particles larger than 2 mm. Mudstones are young type of rocks containing minerals like quartz, feldspar, clay minerals, mica, chlorite, calcite and dolomite. The sandstones are formed after lithification of sand fraction (0.06-2 mm) of sediments mainly consisting quarts and feldspar. Limestone, dolomite, marble and chalk are soluble rocks available in Himalayan region. Similarly slates, phyllite, schist, quartzite, marble gneiss are metamorphic rocks in the region. Quartzite is hard and abrasive but most of the constituents in phyllite and schist have low abrasiveness. Generally volcanic rocks are not available in the Himalayan region, but

granite is found in the higher Himalayan crystalline belt. The presence of different groups of rocks at different part of the country can be seen in figure 6.2.3.

The sediment data collection was started in Nepal since 1963 in Karnali river basin. Hydropower projects like Marsyangdi, Jhimruk and Khimti are monitoring sediment regularly. Still there is a lack of sufficient information of sediment quantity and property for scientific analysis for estimation of its effects.

Multidimensional approaches such as management of catchments area to reduce sediment yield, settling basin management to prevent particles to enter in to power plants and improving erosion resistance of equipment or material to minimize the effect of sediment are needed to tackle with the sediment problems in hydropower projects. In spite of overall sediment management system, several troubles are faced in the operation and maintenance of hydropower plants in Nepal. Together with turbine damage other major problems are:

- Frequent chocking of strainers or trash racks
- Damage of the cooling system
- Damage of drainage and dewatering system due to sediment settling in the sump
- Seating and sealing problem of intake and draft tube gates
- Damage of the liners in the sluiceways

6.3 Case study of erosion in Nepalese hydropower projects

Even though sediment measurement had started in Nepal since 4 decades, still there is no general agreement and standard about the methodology on measurement of suspended sediment which is passing through the turbines. Without a knowledge of sediment quantity and properties that is passing through turbines, it is difficult to assess erosion damage. In general, sediment are monitored only at the headwork or at the reservoir and that also merely in project period. Hence the sediment data are not available for the majority of earlier hydropower projects.

There are 19 power plants in Nepal with generating capacity higher than 2 MW. Among them, except Kulekhani hydropower project, all others are Run-off-River (ROR) projects and almost all of them have effect of sand erosion. The turbines of Kulekhani hydropower project is relatively less eroded. Even though there is sedimentation problem in Kulekhani reservoir, majority of coarser particles settle down before reaching intake. Francis turbines of old power plants such as Panauti, Trishuli and Sunkoshi hydropower projects were eroded frequently and mostly refurbished by welding and grinding. Marsyangdi hydropower project (MHP) and Jhimruk hydropower project (JHP) are the pioneers to realise the economic effect of erosion. Nepal Electricity Authority (NEA) with majority of the plants has about 19% technical and non-technical losses. Hence control of erosion may not be in their priority compared to reducing other losses. In spite of that Maintenance related to erosion has become part of regular activities in most of the projects. In addition, all the hydropower plants have extra standby runners ranging from 1 for each plant to 1 for each unit.

The activities of sediment monitoring in the Nepalese hydropower projects are increasing day by day. The experience of sediment monitoring together with nature and extent of damage of some of the turbines in Nepalese hydropower projects are presented in this section based on the author's field visits and literature study.
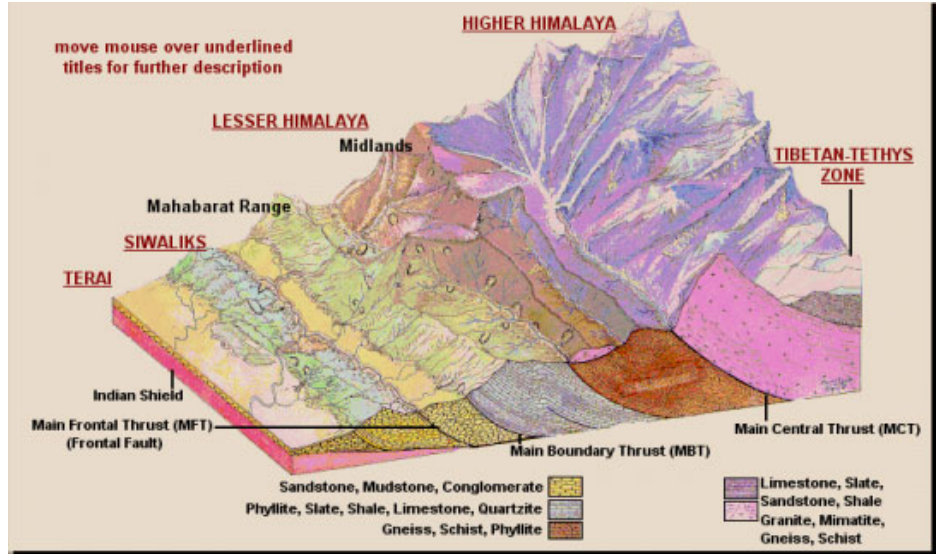
Figure 6.2.1 Geological formation of the Himalayas along North-South (Galay et al., 2002)
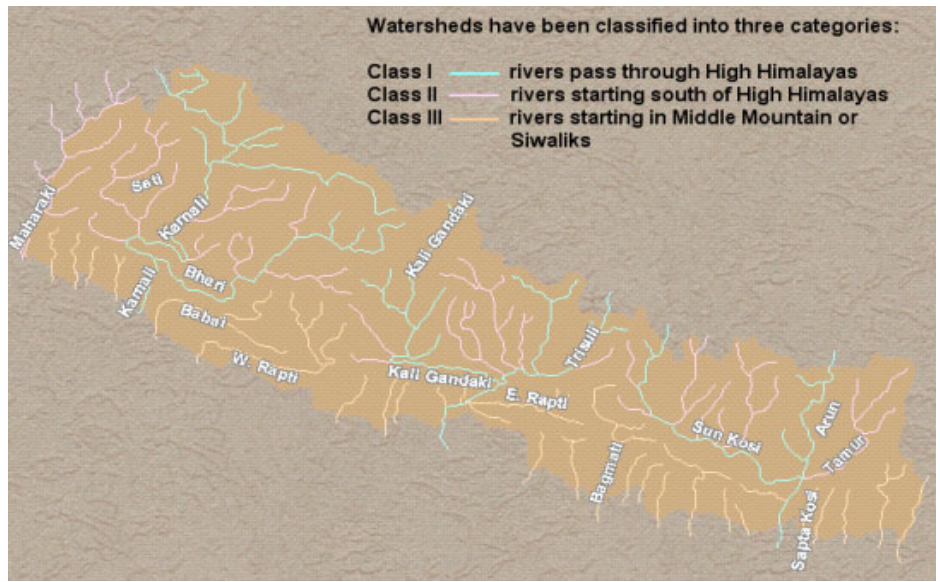
Figure 6.2.2 Watershed and river classification of Nepal (Galay et al., 2002)
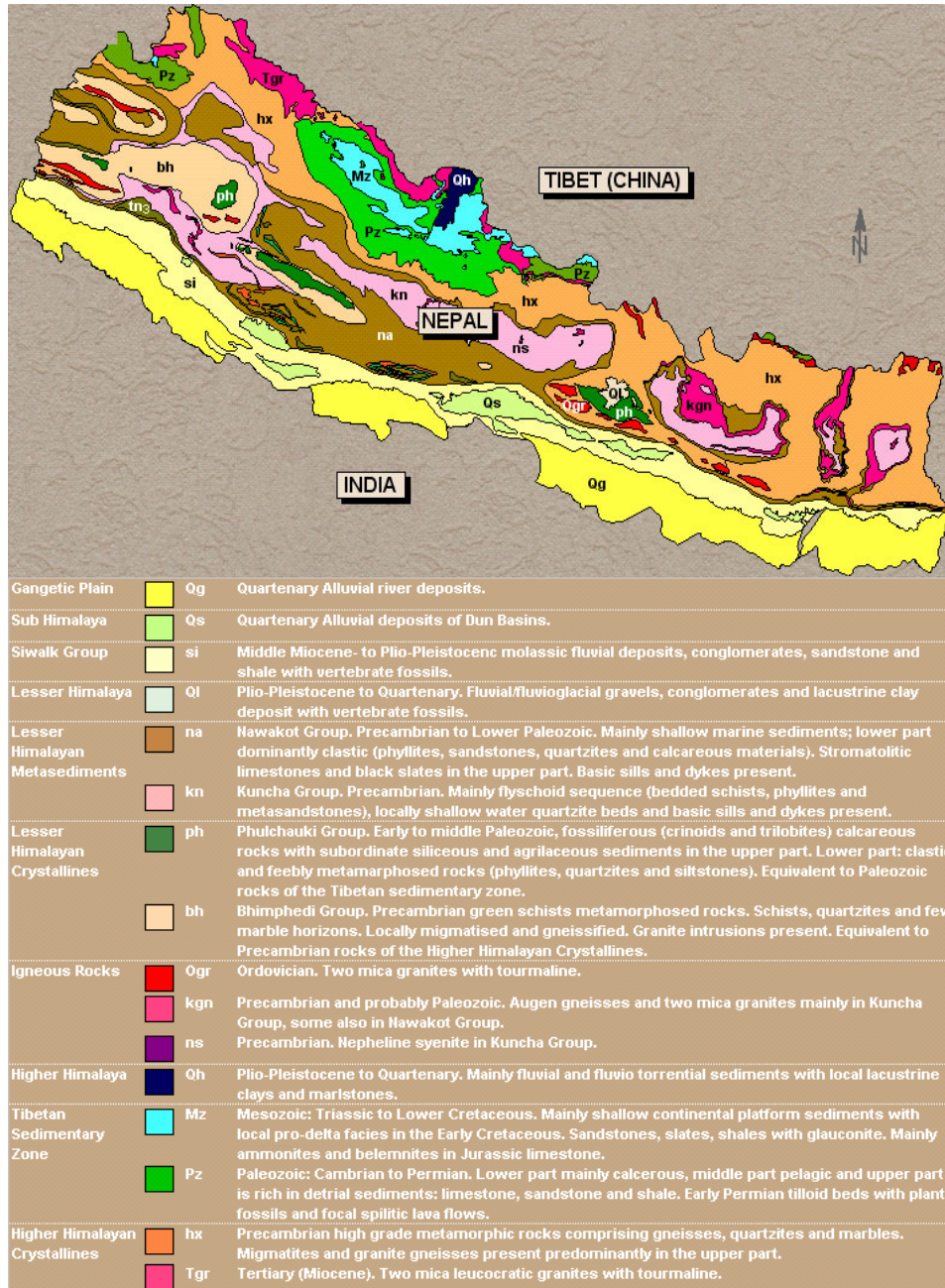
Figure 6.2.3 Geological formation along E-W of Nepal (Galay et al., 2002)

6.3.1 Marsyangdi hydropower project (MHP)

The 69 MW Marsyangdi Power project (MHP) is located in the middle of Nepal. It has 92 m gross head and is designed for annual production 462.5 GWh. This project is regularly measuring sediment concentration passing through headwork and turbines. Based on average daily discharge and concentration at sill I in the period of 1991-1998, approximately 16.7 million tons of suspended sediments are expected to flow through head works of MHP every year. Maximum suspended sediment load is recorded as 24.12 million tons in 1998 and highest concentration of 15164 mg/liter (PPM) is also recorded in the same year (Kayastha, 1996). The mineralogical content in of sediment in this project is 60 % Quartz, 30 % Feldspar 10 % Mica (Chaudhary, 1999).

This power plant has three Francis turbines each having 13 blades made up of 13Cr4Ni stainless steel (Nayak, 1996). In spite of proper functioning of settling basin according to design criteria, huge quantity of fine sand is passing through the turbine each year. These sediments are monitored by taking 3 samples of suspended sediment every day in the draft tube of Unit 1. Each unit had operated for approximately 70000 hours until 1999 since the commissioning at 1989 (Chaudhary, 1999). The particle size distribution (PSD) of sediment sample from the turbine showed that more than 80% of sediment was of less than 0.05 mm whereas particles greater than 0.125 mm are negligible. The annual average sediment concentration through turbine is almost about 5400 PPM and annual average sediment load passing through turbine is 1.83 million tons.

Runner blades, guide vanes, facing plates, labyrinth seal and shaft seals are most eroded components of turbines at this power plant. Erosion effect was most critical at 40 mm from the band at the outlet edge of the blade. In between 1990 to 1993, based on observations of 13 blades of unit 3, blade thickness was reduced to 6.8 mm from 10.8 mm giving 3 mm thickness loss. Similarly, unit 1 blade thickness was reduced to 5.1 mm loosing more than 50% thickness and unit 2 was severely eroded at the same duration. Upper labyrinth seal and head cover gap had increased from 2.6 mm to 4.15 mm, and similarly band and lower labyrinth seal gap was increased to 4.85 mm. The guide vane clearance was increased from 0.3 mm to 1.6 mm. The sediment load and its effect on turbine blade erosion is shown in figure 6.3.1.

6.3.2 Jhimruk hydropower project (JHP)

The Jhimruk hydropower project (JHP) with 3X4MW Francis turbine is located at mid-western part of Nepal. JHP is also monitoring sediment at three locations, at intake of river, end of settling basins and end of headrace tunnel. The highest sediment concentration was measured as 57094 PPM in July, 1996, but concentration in the winter season is normally low. The highest, lowest and average concentration of suspended sediment for monsoon season for the year 1994 to 1997 is presented in figure 6.3.2. Concentration above 5000 PPM is found only for less than 10% of period (Bishwakarma, 1999). Within one month of operation in July/August 1995, sediment deposits in between 20-30 cm were found in the tunnel (Basnyat, 1999). All such deposited sediment can pass through the turbines due to water flow oscillation in the tunnel and frequent start-stop situation, which was very likely situation due to operational pattern of the plant only in the peak hours as required by Nepal

71

Electricity Authority. The particle size distribution and mineralogical contents of the sample from deposits of headrace tunnel are presented in table 6.3.2.
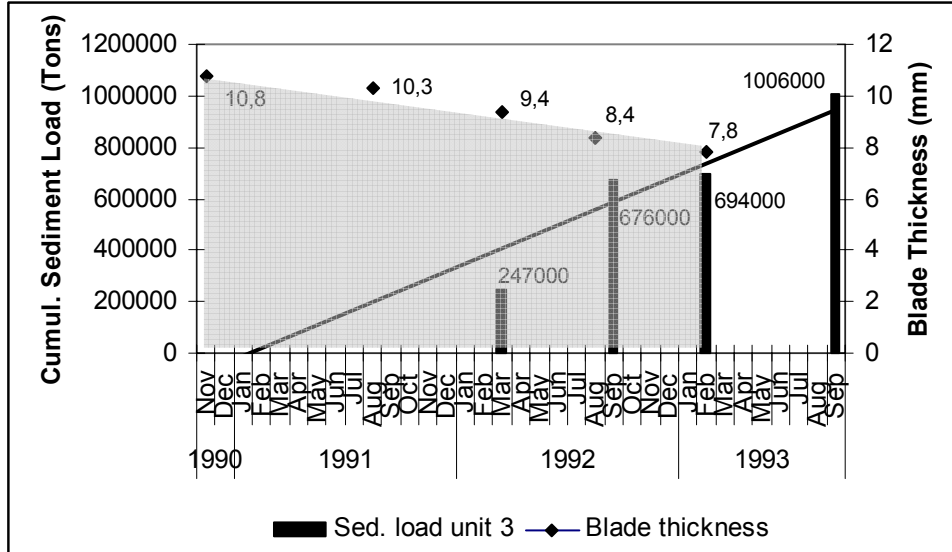
Figure 6.3.1 Sediment passed through turbine and corresponding turbine blade erosion (based on data of Kayastha, 1999)
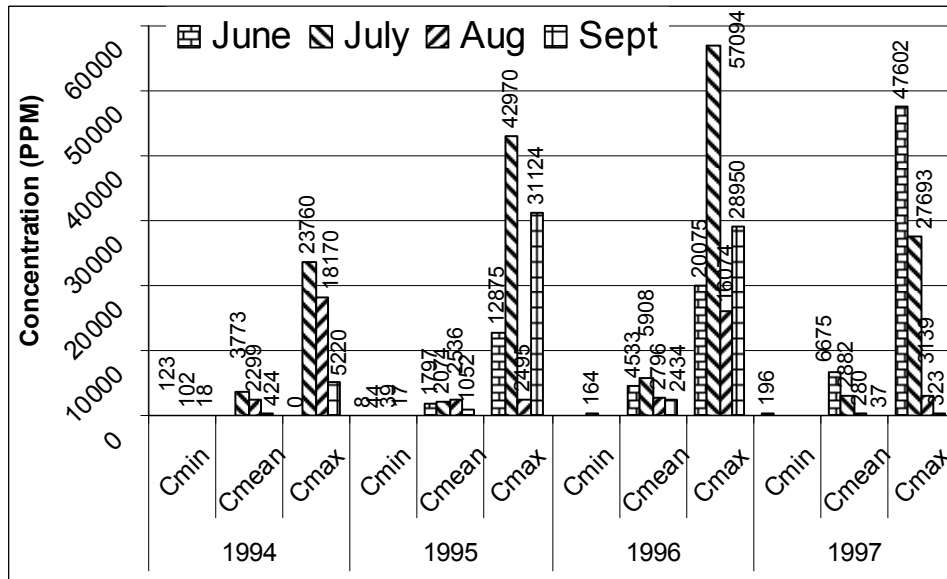
Figure 6.3.2 Suspended sediment concentration at Jhimruk power plant (JHP), Nepal (based on data from Bishwakarma, 1999)

After 5 months of first operation in 1994, turbine blades, guide vanes, facing plates and casing were severely eroded as shown in inspection record presented in table 6.3.2. The turbines were eroded almost in to un-repairable condition in about 4000 hours of operation, that also in only 25% of operation time in monsoon. The blade had erosion in all area and especially severe erosion towards the outlet of the blades. Small area had been completely removed at the outlet edge of the blade close to the band. Basnyat (1999) reported the average of 0.5 mm erosion of the blades with 1.5 mm maximum erosion at certain places. The guide vanes are damaged on both outlet edges and bottom with the grooves. Similarly lower facing plate had horse shoe grooves at different guide vane opening positions with maximum effect on neutral position of guide vanes. The bronze sealing ring was also severely damaged and later replaced by stainless steel sealing rings.

Table 6.3.1 Particle size distribution and mineralogical content of JHP (Basnyat, 1999)

Sieve size	Particle size	% Retained	% of mineral content (volume wise)		
Mm			Quartz	Feldspar	Mica group
0.5	> 0.5	0	-	-	-
0.2	0.5 - 0.2	0.15	15	< 2	77
0.09	0.2 - 0.09	16.85	57	< 2	41
< 0.09	< 0.09	83.0	85	< 1	14

Table 6.3.2 Running hours and condition of turbines at first inspection of JHP (Basnyat, 1999)

Turbine (Unit no)	Total hours	Monsoon hours	% of operation in monsoon hours	Remarks
3	3019	589	20	Damage by wear
2	4212	439	10	Damage by wear
1	4185	1101	26	Severe wear

The damaged turbines were inspected on July 2001 at Nepal hydro and electric (NHE) during repair. The height of the guide vane is 125 mm with 55 mm shaft diameter. Each runner has 22 blades with thickness about 12.2 mm at the inlet and 1.5-2 mm at the outlet edges. The hole, 2-4 mm wide and 10-12 mm long appeared in one of the turbine blade since first inspection and that hole is appearing every year even after repair of turbine by welding and coating. The horseshoe shape of erosion grooves at lower facing plate has depth of about 4 mm and 11.5 mm width. Out of the three grooves in the labyrinth seal, the outer one is most eroded. The photographs of the eroded turbine components of this power plant can be seen in figures 6.7.1.

The sediment analysis takes at least 1-2 hours to obtain rough information of concentration. By this time, high sediment concentration could almost pass through turbines. Hence online monitoring of sediment concentration is necessary to follow the strategy to shut down the power plant in the case of exceeding cutoff concentration level. For instance, time to travel the particles from headwork to power house are 24, 36 and 72 minutes respectively for 3, 2 or 1 units run in full load (Basnyat, 1999). JHP has tried

online monitoring of sediment by using the SMOOTH concept (Sediment Monitoring and Operation Tool for Hydro Projects), conceived and developed by Prof. Haakon Støle, NTNU. This concept is in further development stage and is very promising for optimization and automation of power plant operation.

6.3.3 Khimti I hydropower project (KHP-1)

The 5X12 MW Khimti I hydropower project (KHP-1) installed in 684 m gross head represents typical high head power plants in Himalayan Rivers. The horizontal Pelton turbines of KHP-1 have two jets with discharge 2.15 m^3/s. Khimti River of KHP is also example of rivers with high gradient, heavy monsoon flow and high sediment concentration of hard minerals. Less than 20% of Khimti Basin lies in High Himalayas, about 30% in Lesser Himalayas and 50% in the region of middle mountains, which is formed as a result of local tectonic movements, river down cutting and sedimentation. Hence the risk of rock falls and landslides are high and extensive deforestation has led to increased soil erosion. The average concentration of suspended sediment at Khimti River in 1994-95 monsoon seasons varied from 13 to 1244 PPM and maximum recorded concentration was 8536 PPM (Haakon, 1999). The higher concentration is expected in the flood situation and hence 20000 PPM suspended sediment is used as design value for sediment settling and flushing capacity. Two parallel sediment settling basins which were optimized with respect to erosion of turbine are dimensioned as 90m x 12m x 2m to exclude 85% of all particles with a fall diameter of 0.13 mm and 95% of all particles with a fall diameter 0.20 mm (Bishwakarma et al., 2003).

Significant amount of erosion had appeared in turbine bucket and needles in first year of operation (about 6000 hours). Even though the settling basin with Sediment Sluicing Serpent System (S4) is performing according to design criteria, large quantity of sediment (may be particles smaller than design size) pass through turbines especially during monsoon. Since this is a high head turbine, even 0.15 mm particle have high particle impact energy approximately 8.12 μJ that cause severe erosion of turbine components. The observations of the effect of the erosion on turbine component during inspection visit on July 2003 are presented in the following section.

The runner of this turbine is made up of steel 13Cr4Ni. The thickness of bucket close to the root is found 11 mm, whereas the thickness around centre and entrance lip is 12 mm. Hence it appears at least 1 mm thickness is already lost towards root. From the strength point of view, the thickness towards to the root should have been more. Runner outer diameter is 800 mm with 22 bucket. Distinct erosion is observed in the area towards root and outlet region of the bucket. But the area on both sides of splitter is smooth and appears as if there is no erosion. The erosion ripples at the centre of the bucket are smaller than those in the sides which are shown in figure 6.3.3. The shapes of entrance lips are also deformed slightly, which can be seen in figure 5.2.6 and damage is more toward splitter tip. Since original dimension was not available, the increase in size of cut-off could not be confirmed. Beside sand erosion, cavitation effect was also observed at the centre of inner surface of all the buckets only in runner number 9.

The back side of the turbine is not ground during manufacturing, even towards the root. Some casting defects can be seen in the back side in the form of pores and scratches. All the

surfaces in the back side was rough, but the area up to approximately 30 mm from the edge is ground and polished and further area about 25 mm from there, the effect of hitting of sand laden water coming out of the bucket can be observed.

The erosion pattern in splitter is unique in this turbine. The splitter is not straight or smooth curve, but it is in the form of waves or saw tooth as shown in figure 5.8.4 and 5.6.6. This waviness is not uniform throughout the splitter. The size of wave towards the root is small with approximate length 4 mm and toward cut-off, wave length is double than the root. The thickness of the splitter has also increased to 4 mm, which is approximately 1% of bucket width (figure 5.8.6 c). Considering Prof. Brekke's thumb rule, 1% loss of relative efficiency can be expected in this runner.

Normally the runner disc will not come in contact with the sand laden water and hence they will not erode. But the one of the disc (unit 4) at KHP, was found eroded as shown in figure 5.2.7. The erosion locations were corresponding to each bucket outlet edge but only in one side. The length of erosion effect is 70-80 mm. The erosion at the outlet at root of this runner was more compared to other units. This damage could be due to either misalignment of needle with respect to bucket centre or difference in bucket profile in this particular unit towards root. This amount of erosion may be tolerable both strength and hydraulic point of view, but if they grow, there could be serious problem for the reliability of the disc.

Both the nozzles and needles of KHP are eroded. The ripple pattern and damage of different location of needles are presented in figure 6.3.4. The inner side of nozzle tip have also pattern similar to the middle section of the needle. This ripple pattern is typical in the needle with the circular grooves when viewed in axial direction (figure 6.3.4 b). Two distinct grooves towards axial direction can be observed straight ahead of the two webs to support needle guide (figure 6.3.4 c). This could be due to Von-Kamran vortex formed at the trailing edge of such webs. These groves are approximately 70 mm length starting from the needle tip and are nearly 10 mm wide. Out of the 150 mm taper length, nearly 70 mm from tip is affected with relatively higher ripple wave length except at tip. The last 30 mm toward the bottom of taper is smooth and polished and the remaining portion with fine scales. There is no specific difference in the erosion of upper and lower needle in this turbine which is different from the observation in the Fortune power plant, Norway (Thapa and Skare, 2002) with large size particles.

The damage of turbine at this power plant is being closely monitored and efforts are made to minimize erosion effect by spraying hard ceramic-metallic coating (WC-Co-Cr), hardness 1350 HV) in the bucket and needle surface. But initial inspection of the coating has not shown promising performance. The damage in the coated bucket can be seen in figure 6.3.5.
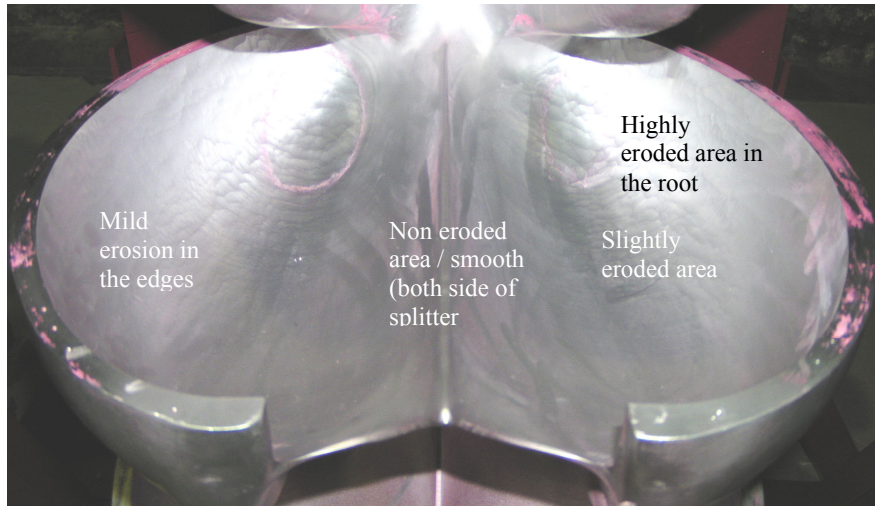
Figure 6.3.3 Erosion damage of Pelton bucket (KHP-1)
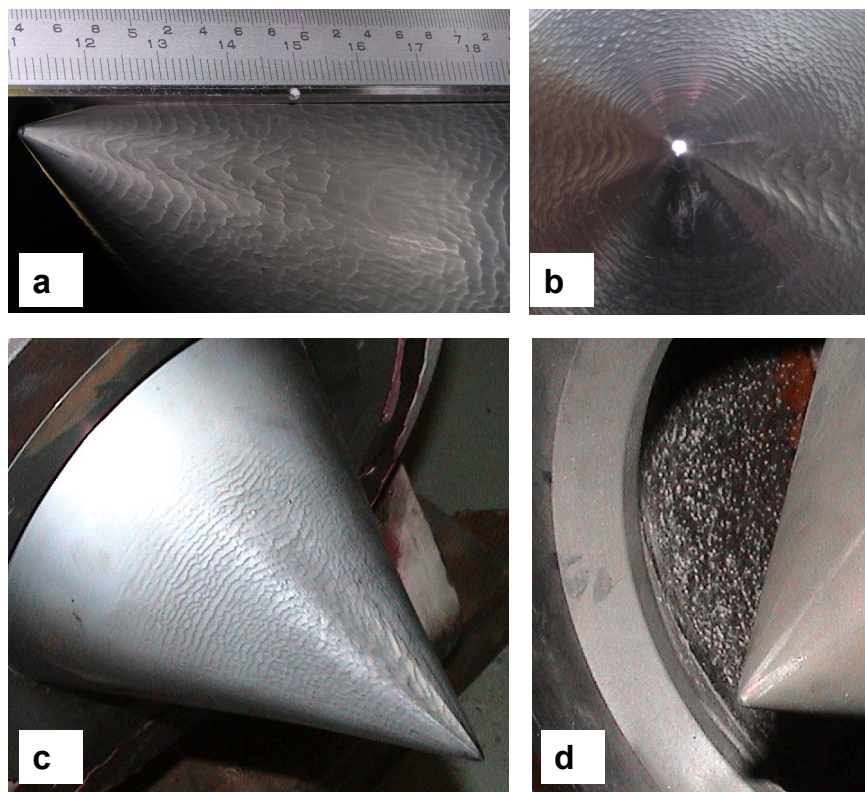
Figure 6.3.4 Pelton needle and nozzle of KHP-1 (a) Ripple pattern and size (b) groove corresponding to needle support web (c) eroded and non-eroded portion of needle and (d) the hitting inside the nozzle

Figure 6.3.5 Erosion damage on ceramic-metallic coating on KHP bucket (Photo courtesy HPL).

6.4 Repair of eroded turbine

Corrective maintenance with minimum intervention in production was general maintenance philosophy in the hydro power projects except some routine maintenance. The maintenance activities are well organized in MHP and has competent crew to repair eroded turbine by welding, regrinding to appropriate profile and thermal spraying. Nepal Hydro and Electric (NHE) was established to provide service to Andhikhola and Jhimruk hydropower projects. They are regularly refurbishing turbines of those two projects and gained competence to repair eroded turbines together with some other project (Adhikari, 1999).

Several erosion resistant welding and coatings are applied to MHP turbines to find suitable solution to increase turbine life. Erosion resistant coating materials ceramic pastes (CERAMIC - R) and ceramic paint (CERAMIC - S) were used to coat the turbine blade. Similarly ceramics in powder form (METACREAM 25050) was also used as high resistance to abrasion and corrosion. A cobalt base welding electrode (EUTROLOY 16606 G) was coated by TIG welding as a protective coating (Nayak, 1996). The problem of the erosion of shaft seal in the MHP was partially solved by supplying clean cooling water.

Turbine unit 1 of JHP was beyond repair after its first inspection hence that was replaced by a spare turbine treated with plasma nitriding. The nitrated surface is so thin which could not resist erosion for long time and that was so hard that subsequent repair welding was difficult. The guide vane was repaired by Citochrome 13/4 welding electrode and Citochrome 17/4 was used for runner, sealing rings and other accessories in 1997. In 1998/99, all runner, guide vanes and sealing rings were repaired by Terroweld DSI and OK 63.3 welding electrodes. Similarly in 1999/2000 Metacerem 25050, 52 BW and ultrabond-500 spray was applied in 15 guide vanes (each coating on 5 guide vanes), 1 runner and six facing plates. But these coatings have not lasted more than 1 season. It is observed from field visits that selection of coating material basically depends on recommendation of supplier. Brief description of the coating materials used in power plants in Nepal is presented in the following section.

Ceramic - R and Ceramic - S are the silicon steel alloy blended within high molecular weight reactive polymers and oligomers. These materials are applied in cold condition and can protect material from corrosion and erosion. Ceramic - R is in paste form; hence even thick layers can be applied in deep grooves and holes. Ceramic - S is in paint form and hence only thin layer can be applied. These products have better performance in stationary parts compared to rotating parts. Hence it can be applied to the casing and guide vanes. The stability of these products depends upon surface preparation and correct application.

Eutroloy 11606G is cobalt based TIG welding electrode with high resistance to corrosion and erosion. This kind of welding does not form slag, there is no oxidation and the welding is very smooth. Nayak (1996) has reported better performance of this material compared to base metal (13Cr/4Ni) at MHP. EutecDur 9080 also have similar properties as Eutroloy 11606G. The electrode deposit incorporates a cobalt-chrome-molybendum alloy which has high resistance to corrosion and oxidation and is recommended by manufacturer for hydraulic turbine parts. It has hardness of 30 RC (Rockwell Hardness Number).

Metacerum 25050 is chromium based, oxygen stabilized ceramic compound in powder form. It has specific grain size distribution and controlled morphology. It is applied on high temperature by spraying; hence very thin layer can be added to the surface. The effectiveness of this process and the bond with base metal depends upon surface preparation. Xuper Ultrabond 50000 is used to prepare surface of material.

6.5 Economy of turbine erosion

The operation and maintenance cost for hydropower plants increases over the period of time and the rate of increment is high in case of sand erosion. Maintenance cost includes the direct material, manpower and downtime cost. Repair of eroded turbine is labor-intensive work; hence cost of maintenance varies on different part of the world depending upon wages.

The output of hydropower plant gradually decreases as erosion of turbine increases. The output can be brought back to rated output and in some cases it can even be increased by rehabilitation or redesign of the system. One of the simple methods to improve efficiency and increase life of turbine is erosion resistant coating in the turbine components. Figure 6.5.1 is a schematic illustration of improvement of efficiency after application of such coatings. Halg and Krause (1996) also observed similar trend in Pradella hydropower plant in Swiss Alps. Of course, the efficiency of coated turbine also decreases over the period of time, but the rate of decrease in case of coating is much less. The nature of these curves depends on several factors like coating properties, particle properties and operating conditions. The gain in efficiency increases production benefit and together with that the repair interval will increase.
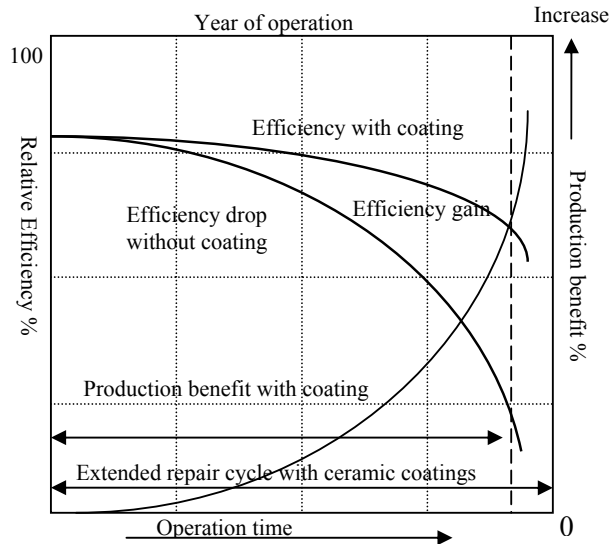
Figure 6.5.1 Illustration of efficiency gain and increase of life due to coating on turbine

The efficiency of the eroded turbine can be monitored over the period of time to investigate gain in efficiency. But normally there should be regular inspection to find repair cycle. The ratio of life cycle of steel to coating can be investigated from laboratory tests, but the laboratory results and actual erosion in the plants often show different result due to differences in operating conditions.

It is really difficult to judge the economic impact of erosion of turbines due to lack of appropriate data in Nepal and it is also not easy to segregate maintenance cost and loss in production due to this. Systematic rehabilitation of hydropower plants were started only after 1980's in Nepal. Only in late eighties, performances of existing power plants were critically reviewed and rehabilitation and refurbishment is thought of to meet the growing demand of electricity in short period of time (Thakur, 1996). Trishuli and Devighat hydropower projects were rehabilitated in early 90's as electro-mechanical equipment were close to their last stage of designed life. Similarly, the performances of Sunkoshi hydropower project turbines were deteriorated after 24 years of operation and they were rehabilitated. Figure 6.5.2 gives the condition of eroded turbine after 24 years of operation before discarding.

Basnyat (1999a) had estimated the turbine replacement cost for JHP as NRs 14.3 million. Since the maintenance cost is only less than 10% of replacement cost, the repair of turbines every year is preferred even if the efficiency of system is poor. Similarly based on cost presented by Kayastha (1999) for overhauling of turbine runner of Marsyangdi hydropower project, maintenance cost is only 15% of replacement cost at MHP. Compared to JHP the percentage of maintenance cost to replacement cost in this power plant is slightly high but with the 3 years repair cycle and good maintenance schedule, repair is preferred to replacement of new turbines. Khimti hydropower plant has started ceramic coating of

Pelton bucket, nozzle and needle at the cost of US$ 25000 for each unit. It is worthwhile to assess the improvement in efficiency and life after this investment. Beyond such limited economic information, it is difficult to carryout economic analysis of consequence of erosion damage due to lack of data.

Figure 6.5.2 Photographs of eroded turbine of Sunkoshi hydropower project (left – top cover, right – runner)

6.6. Ranking of erosivity of hydropower plant of Nepal

Even with 560 MW installed hydropower capacity in Nepal, the production is comparatively low due to frequent shutdown and poor performance of turbines. This is because of sand erosion of turbine components and sediment deposition at headwork. Although almost all the hydropower plants are facing sand erosion problem the degree of severity of erosion is different.

Together with general classification methods, hydropower plants can also be characterized and ranked based on effect of sediment deposition and sand erosion. This ranking can be used during design, operation and maintenance phase. The ranking of hydropower plants on this issue is not very common. SINTEF and NTNU have long experience of erosion of variety of materials and ranked them on the basis on erosion measurement at laboratory (Brekke et al., 1994). Apart from such comparison, the experience of existing power plants gives valuable information on erosion severity and plants can be classified in to different categories based on frequency of repair of eroded turbine and extent of damage. This gives qualitative ranking, but the major hurdle to prepare such ranking is lack of documentation of maintenance system.

One of the scientific method for ranking of erosion severity of hydropower plants is based on particle impact energy. The particle impact energy can be determined with relative velocity and size of particles striking the turbine. But it is difficult to correlate this ranking procedure with different types of turbine operating with different sediment properties. To correlate particle impact energy, following specification of turbine is essential together with operating head and discharge:

- Make of turbine (and hence profile of blade/vane/bucket)
- Turbine material
- Operating speed
- Dimension of turbine (blade/bucket radius & curvature, bucket size, number of bucket/blades/guide vanes and , guide vane-facing plate clearance and so on)

Pande et al. (1999) have ranked individual of component of power plants in India in term of "Erosion Severity Number" based on particle property and flow. Hydropower plants are classified in to three categories (A, B and C) based on vulnerability to erosion in India. There are differences in the definition of the periodicity of renovation for these categories. The definition by Naidu (1999) and Mann (2000) are shown in table 6.6.1. The classification according to periodicity of renovation can be developed only after the experience of erosion for several years. Hence it is reasonable to have some contradiction in this classification system. Turbines of Jhimruk hydropower project (JHP) are repaired every year, hence can be considered in category A whereas turbines of Marsyangdi hydropower project (MHP) may be in class B because they are repaired in every 3 years. The Pelton turbines of Khimti hydropower project (KHP-1) are also repaired in approximately 1 year (6000 hours) of operation, hence it can also be considered in category A. But this classification system could be misleading due to difference in plant utilization.

Another way of judging the severity of the erosion of turbines is by using particle impact energy as suggested by Mann (2000) (table 6.6.1). Wood et al. (1997) have also used particle kinetic energy to compare erosion rate in laboratory measurement. Assuming particles greater than 0.2 mm are trapped and excluded in the hydropower projects, almost all the Nepalese hydropower projects fall in to category C. The particle impact energy for hydropower plants of Nepal are presented in figure 6.6.1 and data of existing hydropower plants in Nepal is presented in table 6.6.2. Though JHP turbine has low particle impact energy and low plant capacity, the extent of erosion is very severe. Similarly other power plants with low particle impact energy are also severely eroded due to higher sediment concentration.

Table 6.6.1 Classification of hydropower plants based on erosion damage

Category	Extent of the damage	Periodicity of renovation effort		Particle impact energy (μJ) (Mann, 2000)
		Naidu (1996)	Mann (2000)	
A	Extensive /Very severe	Every year	Every 2 monsoon	> 10 μJ
B	Substantially high / Severe	Every 3 years	Every 3-4 monsoon	5 – 10 μJ
C	Considerable	15-20 years	Every 7-8 monsoon	< 5 μJ
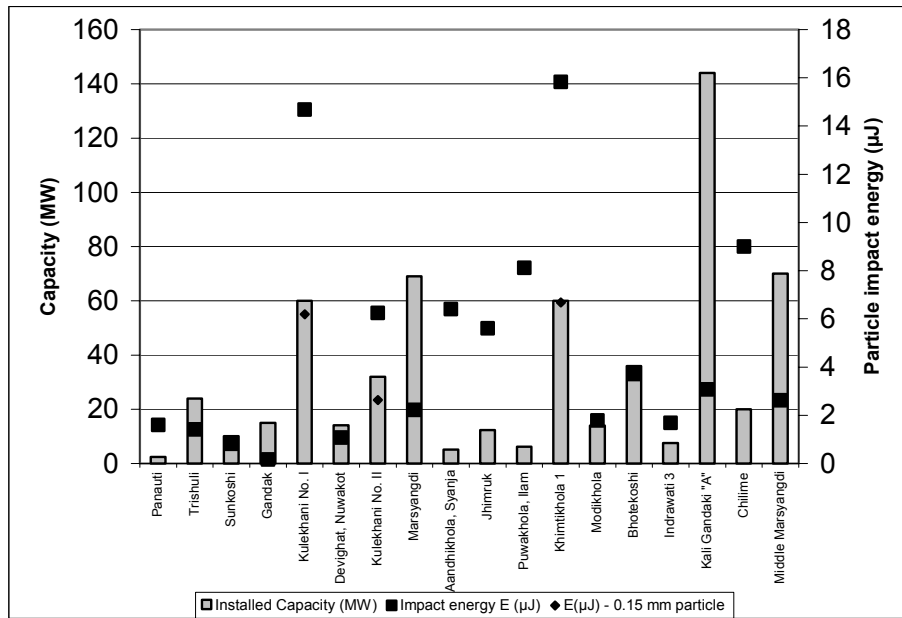
Figure 6.6.1 Generation capacity and particle impact energy for hydropower plants of Nepal

Table 6.6.2 Data of main hydropower plants in Nepal

Year of Commission	Plants Name	Installed Capacity (kW)	No of Unit	Head m	Discharge m3/s	Type of turbine
1965	Panauti	2400	3	60	3X1,61	F
1967/1996	Trishuli	24000	7	53	45,3	F
1972	Sunkoshi	10050	3	30,5	13,3	F
1979	Gandak	15000	3	6,09	300	K
1982	Kulekhani No. I	60000	2	550	13,1	P
1984	Devighat	14100	3	40	45,3	F
1986	Kulekhani No. II	32000	2	234	13,3	F
1989	Marsyangdi	69000	3	83	100	F
1990	Aandhikhola	5100	3	240	2,7	P
1994	Jhimruk	12300	3	210	7,05	F
1999	Puwakhola	6200	2	304	2,5	P
2000	Khimtikhola 1	60000	5	684	10,73	P
2000	Modikhola	14000	2	67	25	F
2000	Bhotekoshi	36000		139		
2002	Indrawati 3	7500		63		
2002	Kali Gandaki "A"	144000	3	115	141	F
2003	Chilime	20000	2	337	7,5	P
2003	Piluwakhola	3000	2	112,5	3,35	TI
Under const.	Upper Modi	14000				
Under const.	Middle-Marsyangdi	70000	2	98	80	F

P – Pelton   F – Francis   K – Kaplan   TI – Turgo-Impulse

82

Erosion measurements by actual river sand from several locations of Nepal were carried out to assess erosivity of these sediments to turbine components. The detail of this measurement is presented in section 8.14.

6.7 Efficiency measurement at the Jhimruk hydropower plant (JHP)

The damaged turbines of Jhimruk hydropower plant (JHP) were inspected at the workshop of Nepal Hydro & Electric (NHE) Butwal on June/July 2001 and 2002 (section 6.3) as part of PhD research field study. There was a curiosity on performance of such severely damaged turbines (figure 6.7.1). The efficiency of the turbines is normally not monitored in Nepalese hydropower plants except for performance guarantee and hence the information on effect of sand erosion on efficiency was not available at all. The thermodynamic and relative efficiency measurements were carried under the leadership of Associate Professor Ole Gunnar Dahlhaug, Waterpower Laboratory, NTNU. The results of thermodynamic and relative efficiency measurement at JHP are discussed in this section.

The thermodynamic efficiency measurement was carried out according to the IEC procedure described in IEC Publication 41, Third Edition 1991-11 *"Field acceptance tests to determine the hydraulic performance of hydraulic turbines, storage pumps and pump-turbines"*. The temperature of water, pressure, power output and flow rate were measured for the purpose of thermodynamic efficiency. The thermodynamic efficiency measurements were carried out on unit 3 of JHP on 1st September and 11th November 2003. The results of thermodynamic efficiency measurement have shown 4 % loss at BEP and 8 % loss at 25 % load in this period (figure 6.7.2). The sediment monitoring in the same period have indicated that approximately 6900 ton of sediment has passed through this unit during test period.

It is difficult to determine contribution of each of the component on efficiency drop. The overall efficiency can be seen in figure 6.7.2, which incorporates all the factors associated with hydraulic loss. The leakage flow between the lower labyrinth and the runner is not possible because that flows into the draft tube. But the leakage between upper cover and the runner can be measured and shown in Figure 6.7.3. The flow rate through upper labyrinth seal has increased significantly in the period between the two efficiency measurements. This indicates heavy erosion of labyrinth seals and it can be assumed that approximately same quantity of leakage takes place from lower labyrinth seals as well.

The efficiency loss due to the leakage flow in the upper sealing ring is given in figure 6.7.4. This loss can be divided in two types of losses:

1. Firstly, the loss due to the flow that is passing through the sealing ring without doing useful work. This loss can be calculated based on the leakage flow rate.
2. Secondly, the loss due to the fluid friction due to spinning of fluid in between runner hub and the head cover. This loss can be calculated based on temperature rise of the leakage flow.
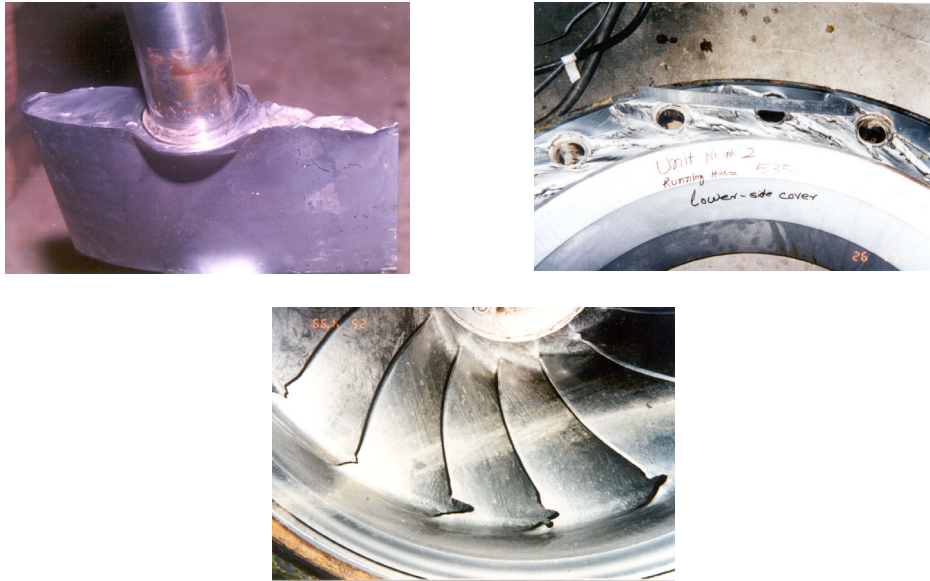
Figure 6.7.1 Photographs of eroded (a) guide vane (b) face plate and (c) runner of JHP (Photo courtesy: BPC)
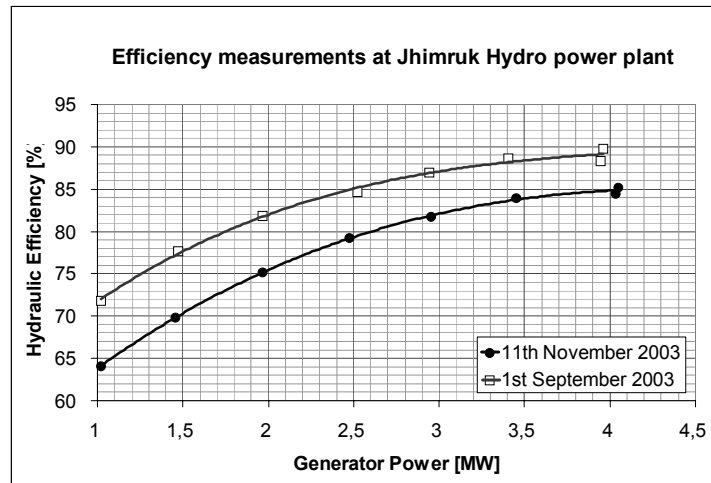
Figure 6.7.2 Results from the thermodynamic efficiency measurements (Dahlhaug and Thapa, 2004)
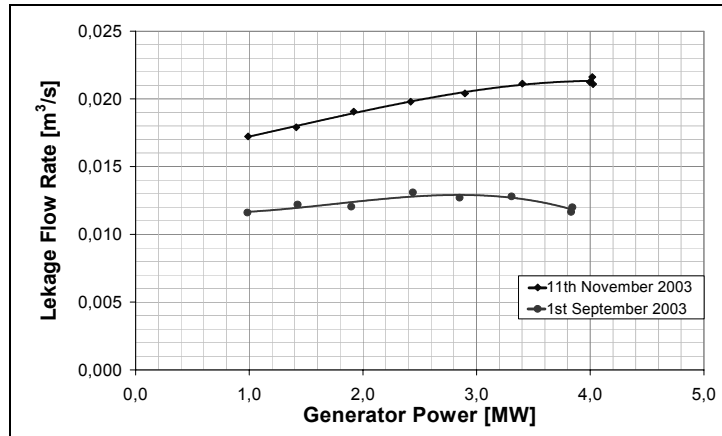
Figure 6.7.3 Leakage flow rate in upper sealing ring (Dahlhaug and Thapa, 2004)

There is approximately 0.5% difference in loss due to flow through seals in between two measurements in almost all generator outputs. Assuming similar trend in the lower labyrinth as well, total of 1% efficiency loss can be expected due to erosion of labyrinth sealing rings. The friction is also of same magnitude of flow loss for all generator outputs. Assuming similar trend of friction loss in the first measurement too, 1% of efficiency loss can be considered from the friction loss. This gives 2% increase in efficiency loss in total due to the leakage of water through seals because of the erosion of sealing rings in the period between the two efficiency measurements. Since the figure 6.7.4 shows the total leakage loss only for upper labyrinth, both sealing rings give 8.2% loss at 1 MW generator output and 4.2 % at 4 MW output.
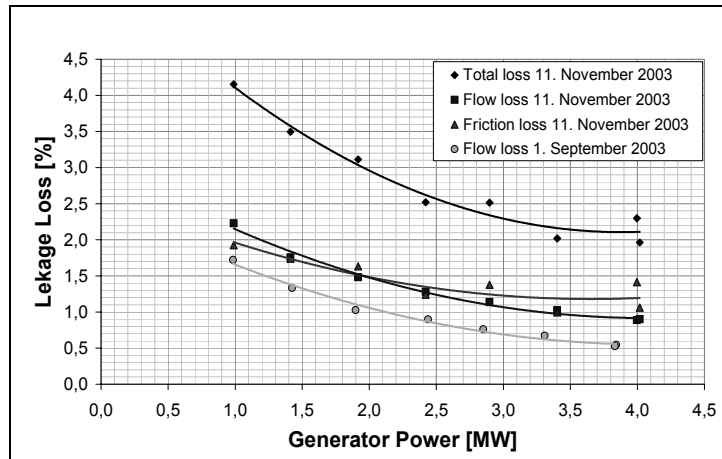
Figure 6.7.4 Efficiency loss from the upper sealing ring leakage flow (Pradhan et al., 2004)

The increase in leakage loss due to sand erosion of labyrinth against repaired one was observed only about 0.5% of total loss (10% of relative efficiency loss) at the BEP at Driva

power plant, Norway (P = 71.5 MW, Hn = 540 m and n = 600 rpm) (Brekke, 1988). On contrary, the leakage flow loss in JHP turbine is high. The clearance of this turbine was increased compared to design value to avoid possible contact because of replacement of bronze seals by steel seals. It could have also contributed to increase leakage loss from the gap. The loss due to leakage contributes about 50% of the total loss in this case (Dahlhaug and Thapa, 2004) and there could be possibility to minimize this loss. One of the probable solution is to insert pressurized clean water through the upper and lower sealing rings to prevent sand laden water to pass though narrow gap seals and avoid erosion. By such modification the efficiency will increase due to smaller gaps in the sealing rings and prevent 2 % efficiency loss during the monsoon period.

The relative efficiency measurements was also carried out at JHP during same period using Winter Kennedy flow measurements and inlet pressure, outlet water level and generator power output were logged in 10 minutes intervals. Unfortunately, the Winter Kennedy measurements gave mostly bad results due to sediments that blocked the pressure taps. A flushing devise were installed and flushing was carried out every day. The reliable data could not be obtained by this modification as well. However, few efficiency gradients from the vast amounts of data can be considered as just a trend or indication. An efficiency loss from 0.4 % to 0.7 % in 3 – 5 hours was recorded when sediment concentration was only in between 800 and 3000 PPM (Dahlhaug and Thapa, 2004). This efficiency drop rate per unit time does not match with overall efficiency drop in test period. The conclusion of this observation is that the taps for pressure sensors should be redesigned to avoid clogging and erosion of sensor.

Chapter 7

High velocity jet erosion test rig: Experimental

7.1 Introduction

The experimental research and study of erosion are done in two ways:

1. Field testing at actual operating conditions
2. Simulating erosion in the laboratory

It may take long period of time for the erosion effect to appear distinctly in actual working station. Hence there could be problem for quick decision making for erosion performance of base materials and coatings. The findings from field tests are often qualitative because of difficulty in changing the variables affecting erosion and hence could be difficult to develop models for erosion.

More specific object of different tests carried out in this research is mentioned in respective sections in chapter 8. Some of the general objectives of erosion experiments in the laboratory are as follows:

1. To study the mechanism of erosion
2. To understand the erosion behaviour of particular family of materials
3. To study if it is possible to determine or simulate erosion of materials by experimental test rig
4. To find the possibility of accelerated erosion testing
5. To compare erosion resistance of :
   - Different base materials (for optimal selection and screening)
   - Coating materials (i.e. welding electrodes and coating materials) used for improving wear resistance
   - Methods used to improve erosive erosion resistance (surface hardening and heat treatment) of material
6. To study the effect of variables influencing the erosion rate in terms of erosion mode, process and magnitude.
7. To support the development of predictive or descriptive models for erosion
8. Estimation of service life of material

The experiments on this research are based on the theoretical background presented in chapter 3 and 4. The effects of all three factors affecting the erosion, in particular, operating condition (impingement angle and velocity), particles properties and target materials are

studied experimentally in this research and attempt have been made for practical use of the experimental observation.

7.2 Selection of test equipment

The erosion studies by experiment had already started from the middle of 20th century. The literature survey presented in Appendix A has shown wide variety of test rigs which are in use for erosion measurement in the academic or research centres around the world (Clark et al., 2001, Wood et al., 1999, Field et al., 1995 and so on). This author has classified the erosion test rigs in to 21 different types according to 6 typical basis for classification in this literature survey review. In most generalise way, three typical erosion test rig types can be considered on the basis of relative motion between mixture and specimen. They are: (i) jet/nozzle type (ii) rotating disc/arm type, and (iii) centrifugal accelerator type. NTNU and SINTEF have long experience in the erosion test and several materials/coatings have been tested in rotating disc and rotating cylinder test rigs (Bjordal 1996, Berget 1999). The jet type of the test rig was developed in the SINTEF erosion/corrosion laboratory for carrying out test in high velocity region in erosion-corrosion environment. Few tests were carried out in this test rig in the past to study erosion of materials (Frantzen and Haldogård, 2000) together with the computational fluid dynamics (CFD) simulation of the rig (Svensson, 1989). But detailed investigation of performance of this test rig and investigation of erosion of material are to a large extent not carried out so far.

Jet type of test rig is selected for experimental investigation of erosion in this research to enhance the knowledge of the erosion mechanism, compare the results of this test rig with other type of rigs available in SINTEF and to supplement the work of author during his thesis work for Master of Engineering at Kathmandu University (KU) in similar test rig (Thapa, 1999).

The reasons of selecting jet type of test rig compared to other rotating equipments and its advantages are:

1. Test cycle time in jet type of test rig is low.
2. The erosion of material for different impingement angles is possible.
3. Control of variables like velocity and concentration is easy and several test points are possible.
4. Very high velocities can be achieved compared to other available test rigs.
5. This is very much similar to the practical situation of Pelton turbine and low impact angle tests also resemble flow in reaction turbine components.

Though such tests can be used to compare the erosion resistance of different materials, they can not be graded as good or bad in term of erosion resistance without knowing the actual operating environment. Extrapolating and using the results from these experiments for different applications is difficult, complex and still a more challenging task.

7.3 Description of test rig

The erosion measurements at the laboratory were carried out at two different experiment setups:

1. High velocity jet test rig at erosion-corrosion laboratory, NTNU/SINTEF, Trondheim
2. Jet type test rig at Department of Mechanical Engineering, KU, Kathmandu

The majority of the experimental works on different materials and operating variables were carried out at NTNU/SINTEF, Trondheim. Some of the tests were carried out at Kathmandu University, Kathmandu. Both test rigs are jet type and work on similar principle, but at KU, the jet strike specimen as free jet, whereas at NTNU/SINTEF, it is submerged jet. The test rig at KU is a development of older version of test rig used by the author during his Master degree thesis (Thapa, 1999). The test rig at KU was used for erosion measurement with sands from Nepalese rivers. The development of sand erosion test rig at KU means a start in developing research capability at KU and is also a foundation for the development of turbine testing laboratory at Kathmandu.

NTNU/SINTEF Jet type erosion test rig

The test rig at NTNU/SINTEF (Figure 7.3.1) consists of high pressure pump, tank, sand mixing unit, nozzle, specimen holder and flow measuring device. A reciprocating pump (make Pratissoli-Itali) with 3 cylinders is driven by 37 KW, 1475 rpm electrical motor. The pump has a capacity of maximum pressure 125 bars and discharge 316 l/min with crank speed 745 rpm. Water is sucked through 63 mm PVC pipe from tank and delivered to nozzle through the high pressure hose pipe with 25 mm diameter. The water is re-circulated during the test. Small amount of water leakage from pump is compensated by supply of fresh water, which also ensures the constant temperature of water within the system against the heating of water by mechanical action of pump. The flow rate of water is controlled with the help of bypass regulator valve between suction and pressure side of the pump. A pressure gauge installed at the pump head gives working pressure of water. The tank (1m x 1m x 2.4m) is made up of fibreglass such that it can also contain corrosive liquid. The tank is separated into 3 equal compartments longitudinally with baffle on upper side of middle one to retard the flow and facilitate settling of sand particles after strike. The jet strikes the specimen at first compartment and water is sucked for recirculation from third compartment. High pressure water coming from the pump is converted into high velocity as it passes through converging section and finally comes out from 100 mm long and 8 mm diameter nozzle. Just before the converging section, six holes are made on 50 mm cylindrical disc that is provided to ensure straight flow of water and minimize the swirl. Sand particles are added in the jet slightly away from converging section and accelerated through straight portion of nozzle.

A conical hopper is connected with the middle compartment of the tank through 16 mm diameter plastic pipe and always maintains the level of water same as in the main tank. Flexible pipe of 5 mm diameter is connected in between bottom of this hopper and steel pipe with 2 mm bore, which leads to the nozzle just after converging section and is

concentric to the nozzle. The sand concentration is controlled by allowing the sand to flow freely from upper conical hopper with small opening ranging between 3 mm to 5 mm and mixing with water in the lower conical hopper. The water mixture is sucked at the nozzle by suction pressure due to converging section. This suction pressure depends on the flow rate of water. The distance between nozzle exit and specimen can be adjusted between 60 mm to 145 mm. The nozzle and jet are completely inside the water pool about 400 mm below the water level during the test. After strike, sand mixture flow through the top of compartment walls and settle down in the tank. Most of the sand settle down at middle compartment, very less are settled at 1st compartment due to high turbulence, where jet hits the specimen. Small amounts of fine sand also settle down at 3rd compartment, which is expected to be clean for recirculation of water to pump. The filter is provided before suction side of pump to trap unsettled sands and prevent sand from entering the pump. The flow meter (Rotor-X paddlewheel Flow Sensor) with digital display is fitted at the suction side of the pump. Flow meter is also counter calibrated by measuring the volume of water pumped in known time. There is an accumulator at the delivery side of the pump to damp the pressure pulsation. The specimen can be clamped at the desired angle during tests. Besides, there is a provision for electrochemical potential measurement at the specimen holder (figure 7.3.2 a) for erosion and corrosion measurement, which is not used in this study. New clamp (figure 7.3.2 b) was developed in this research for 4 point bend pre-stress erosion test.

Kathmandu University Jet type erosion test rig

A simple hydraulic circuit as shown in figure 7.3.3 is used at Kathmandu University (KU) to investigate the erosion effect of river sand on turbine steel. The circuit has 5.5 kW mono-block centrifugal pump (head 45 m and discharge 6 l/sec). Valves control the flow of water and particles. Bypass circuit is used to control the flow of water through nozzle. The sand is weighed and filled in to the 1 m height hopper ahead of nozzle. Once the pump is started, valve of sand hopper is slowly opened. The water creates disturbances inside the hopper and sands fall down in the horizontal pipe because of gravity. The sand is then accelerated by the water and strike the specimen 100 mm away from nozzle exit. The test is continued until all sand pass through the nozzle. This duration depends on several parameters like size of particles, velocity of water and opening of the valve. For the tests in this research, for 1 kg of sand, the test duration is 15 minutes, which is decided by past experience and hit and trial.

7.4 Test procedure

Most of the activities in the erosion test in high velocity jet experiment are manual. All observations of the experiments are recorded manually. Briefly, the sequence of the test procedure is as follows:

1. Cleaning the specimen with acetone in ultrasonic bath
2. Drying the specimen in oven
3. Weighing the specimen
4. Clamping the specimen in the test rig
5. Starting the pump and checking the level of water in the particle mixture hopper

6. Pouring the particles in the dry hopper
7. Recording particle flow time
8. Recording flow rate and volume of water pumped in the test duration
9. Running the pump until the particle in the dry hopper is finished and mixture is sucked from the mixture hopper
10. Removing the specimen from the clamp and rig
11. Cleaning and drying the specimen (repeating step 1 and 2)
12. Weighing the specimen after erosion
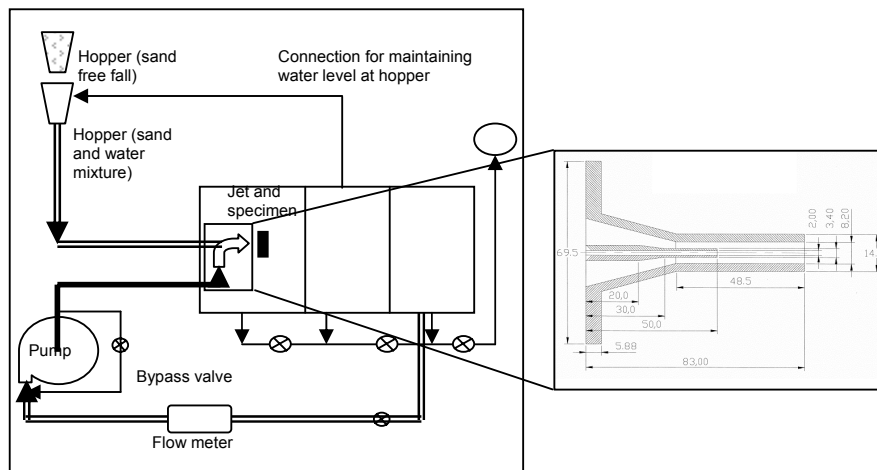
Figure 7.3.1 Schematic layout of erosion test rig at NTNU/SINTEF

The specimen holder shown in figure 7.3.2 (clamp a) of holder is designed for both individual and combined erosion and corrosion test and hence the specimen can be electrically separated by using insulator. This holder clamps the specimen from sides and clamping force is applied by screw bolt along axial direction of holder. By holding specimen like this, part of the back side of specimen is covered by holder itself and part of specimen is exposed to slurry in the tank. Other type of clamp used is similar to four point bending test equipment (figure 7.3.2 clamp b). The two edges of the specimen are supported in the body of the clamp and clamping force is applied through the screw bolt with the help of thick base plate to avoid any bending effect of specimen. The former specimen holder has to be removed each time from the test rig for clamping the specimen, whereas on latter specimen can be clamped while the holder is within the rig. Hence the cycle time with the first type of rig is high and it has exposure in the back side of specimen. On contrary, in latter type of holder, the cycle time is low and it can also cover the back side of the specimen. But there are edge effects at both ends of body support and there could also be effects of bending of specimen if clamping force is too high. If sand particles are trapped or enter in between the specimen and base plate, three body abrasion effects may appear on the specimen, which increases the overall weight loss.

Figure 7.3.2 Vertical section of test rig with nozzle and clamps
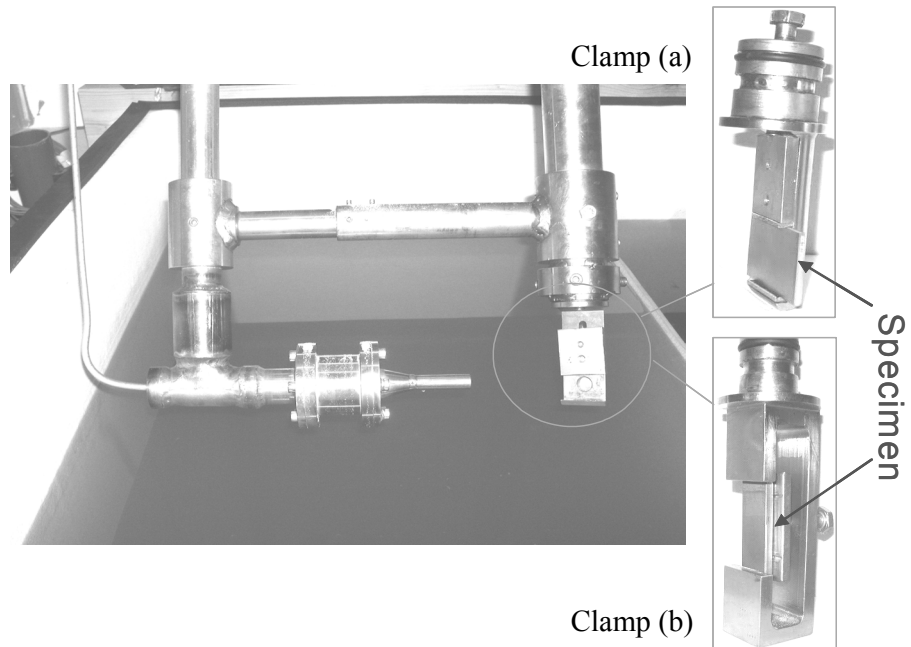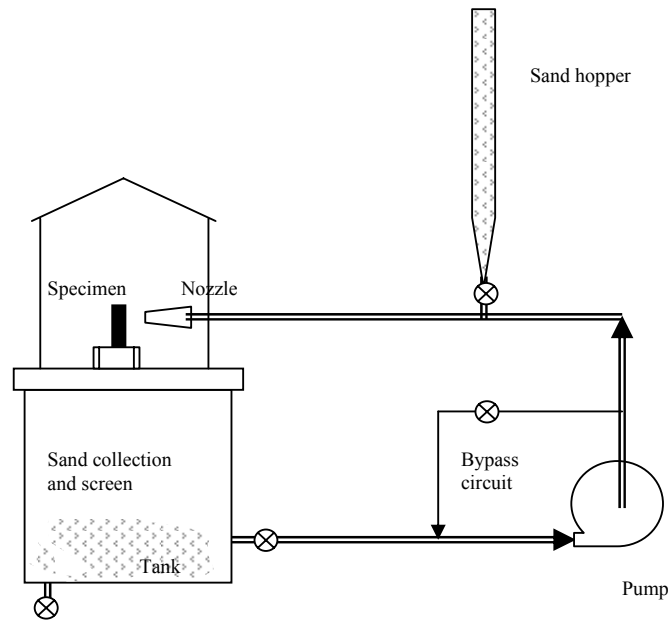

Figure 7.3.3 Schematic sketch of jet type of test rig for erosion measurement at Kathmandu University

The test is carried out until all the sand from the dry hopper drops in the mixture hopper and is passes through the nozzle. The completion of the flow of mixture can be seen through transparent plastic pipe. The quantity of the sand used for the tests are either 1500 gm or 750 gm based on the previous experience which gives the erosion quantity measurable in electronic balance with 200 and 400 gm capacity with 0.1 mg precision. Normally for the tests on aluminum specimens, lower quantity of particles (750 gm) is used. Depending upon the opening in the particle hopper; the flow time for 1500 gm of particles ranges from 8 to 24 minutes, whereas for 750 gm particles, it is on average 4.25 minutes. The minimum duration for the test is about 3 minutes for 750 gm garnet particles.

The eroded metallic and ceramic-metallic specimens are first cleaned with clean water, then immersed in the acetone and placed in the ultrasonic bath for about 20 minutes for removing any impurities. But elastomer coatings are cleaned only with distilled water, because these types of coatings are not resistant to acetone. The cleaned specimens are also dried in the oven before weighing.

Several parameters are varied in the experiments to investigate their effect in erosion of material. The variable parameters are selected to obtain the realistic relation between erosion rate and these parameters as discussed in section 3.3 with special interest to erosion of hydraulic machinery components. The variables used in this research are discussed in the following section.

7.5 Test variables

The test variables for measurements on high velocity jet erosion test rig at NTNU/SINTEF are reported in this section.

7.5.1 Particles

The sand is used as erosive particle in this test rig because they are the one causing erosion of turbine components. River sands are composed mixture of several organic components and minerals, which vary quite a lot in terms of their shape and size. Erosion tests of different turbine materials at different operating conditions have to be carried out with the uniform particles with known characteristics in order to obtain consistent results. Hence Baskarp-15, foundry sand is used as erosive particles in the tests because of uniform shape, size and moreover it's better flowability through the particle hopper opening in this test rig.

Baskarp-15 is quarry sand from Baskarp, Sweden which is red brown in colour and circular in shape but still have sharp edges. This is silica rich sand with high free quartz content. The mean particle size of Baskarp-15 is 0.15 mm, this sand is more graded compared to river sand, but it is assumed that this sand represents erosion behaviour of river sand. The particle size distribution of Baskarp-15 is shown in figure 7.5.1 and composition is as shown in table 7.5.1. Beside Baskarp-15, other particles used to study the effect of particles are presented in table 7.5.2 (a) and (b).
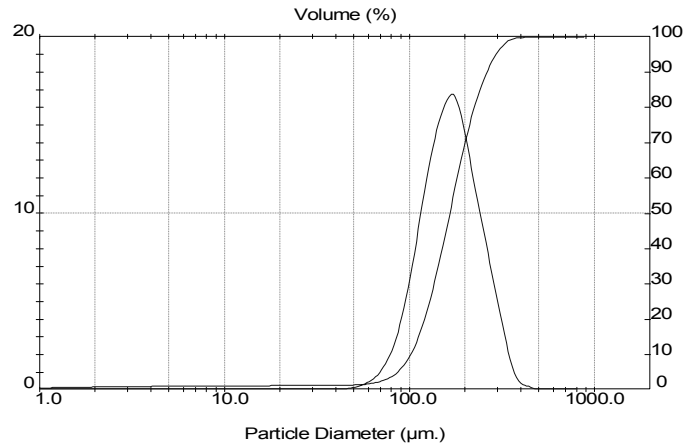
Figure 7.5.1 Particle size distribution of Baskarp-15 sand (courtesy-Tore Castberg).

Table 7.5.1 Chemical composition of Baskarp-15 sand

Composition	SiO_2	Al_2O_3	Fe_2O_3	CaO	MgO	Na_2O	K_2O	Free Quartz
%Weight	88.4	6.4	0.63	0.61	0.1	1.4	2.6	67

(Courtesy: Baskarp AS, Sweden).

Table 7.5.2 (a) Particles used in erosion test and their properties

Particle	Color	Average Size	Hardness[*]	Density g/cm^{3*}	Flow rate $gm/min^{\#}$
Artificial silica sand (Sand-25)	Grayish	250 micron	7	Nearly 2.65	157.89
Garnet	Brownish	30/60 mesh	6.5-7.5	3.5-4.3	252.8
Aluminum oxide	Blackish		1100 kg/mm^2	3.69-3.89	233.16
Baskarp 15	red brown	150 micron	7	Nearly 2.65	182.92

% visual observation   * various sources on internet
# measurement (from 4.5 mm hopper opening)

Table 7.5.2 (b) Particles size distribution

	Particles retained in sieve (%)				
Particle	0.5 mm	0.25 mm	0.125 mm	0.063 mm	< 0.063 mm
Silica sand (Sand-25)	12.6	63.2	22.5	1.2	0
Garnet	5.1	71.6	20.3	2.5	0
Aluminum oxide	0	0.2	99.3	0.6	0
Baskarp 15	0	5.8	70.3	24.0	0

7.5.2 Concentration

The concentration of the particles in the NTNU/SINTEF test rig can be controlled and calculated with the help of particle and water flow rate. The flow of particles from the hopper can be controlled by changing the size of opening in the dry hopper, which also depends upon the shape and size of the particles. More irregular shape of particles tends to interlock each other and reduces the flow rate, whereas rounded particles smoothly flow from opening. Wet sands have very poor flowability due to cohesion and they will be packed into the hopper tightly. Six different hopper openings ranging between 2.9 mm to 5.0 mm are used for changing the particle flow rate. The average particle flow rate for Baskarp-15 sand is given in table 7.5.3.

The particle flow rate from the dry hopper opening is found almost linearly proportional to the area of the opening as shown in figure 7.5.2. On the other hand, the flow rate of different particles from the same size opening found varying as shown in figure 7.5.3. The ranking to the flow rate is almost in the same rank of density of particles.

Table 7.5.3 Particle Flow rate for Baskarp-15 sand

Opening (mm)	5	4.5	4.3	4.0	3.6	2.9
Flow rate (gm/min)	227.85	182.19	156.79	126.76	93.75	62.5
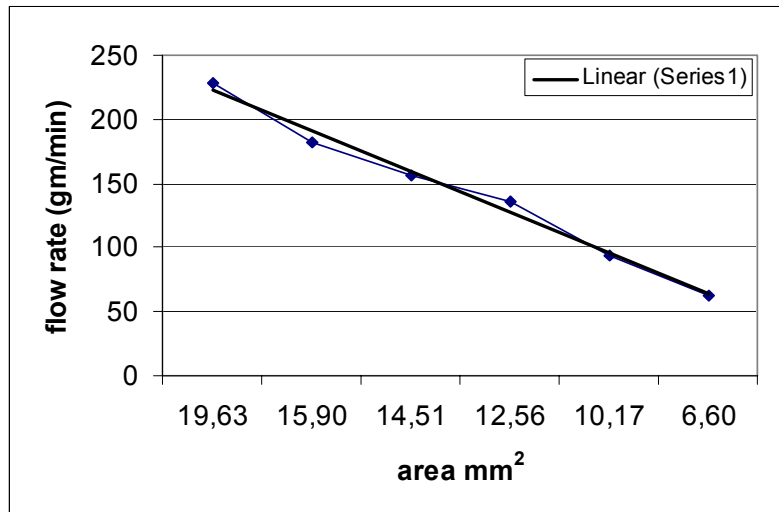
Figure 7.5.2 Particle flow rate from different openings of the dry hopper

Flow rate of particles from 4.5 mm opening
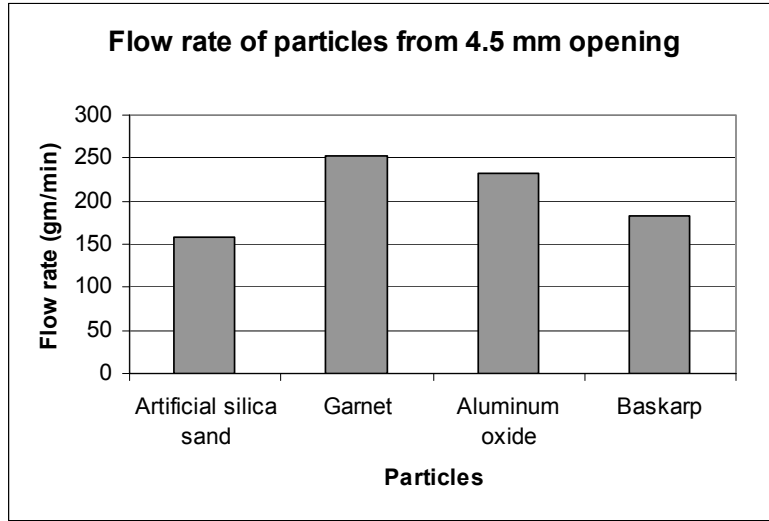
Figure 7.5.3 Flow rate for different particles

The maximum concentration of particles can reach up to 0.38% when flow rate is around 20 m/s and particle are falling with the largest hopper opening (5 mm diameter). Similarly, minimum concentration can be observed at the highest flow rate nearly around 80 m/s with smallest hopper opening (2.9 mm diameter). For Baskarp-15 particles flow from 5 mm hopper opening gives the curve as shown figure 7.5.4 against different flow rates from the nozzle.
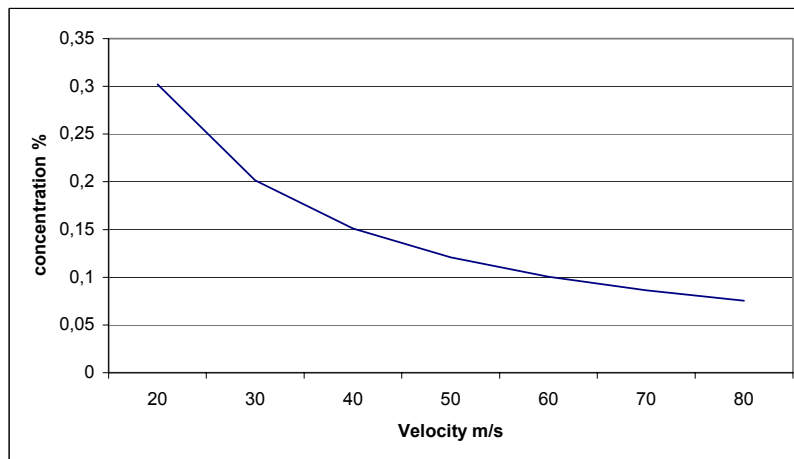
Figure 7.5.4 Variation of concentration as a function of change in jet velocity

This concentration is the one, which is coming out of the nozzle. It is difficult to say if all of these particles are striking the specimen, because some of the particles may deviate and escape the specimen without striking. On the other hand, the finer particles which are recirculated along with the water inside the tank are not taken in to account. Similarly the

effect of jet suction and secondary flow are also not considered for estimating concentration.

7.5.3 Flow

As mentioned in the description of test rig, the flow in the system is changed by adjusting the flow through the bypass valve. The flow in the suction side is measured by flow meter and velocity of the jet through the nozzle is calculated based on continuity. Flow meter is also counter calibrated by measuring the volume of the water pumped at a given time. Based on rated flow of the pump and the nozzle diameter, theoretically velocity up to 100 m/s can be achieved in this test rig, but in actual practice, tests were possible only in the velocity range in between 20 m/s to 80 m/s. The velocity region below 20 m/s is not sensed by sensor and not displayed, whereas velocity region above 80 m/s is difficult to achieve in this system due to vibration of the test rig, noise level and leakage. It is difficult to achieve exact operating point after changing bypass valve position, but very close condition can be traced. The velocity of particle is considered equal to the velocity of water jet, which is different in actual practice.

The monitor of flow measurement system +GF+ SIGNET 5500 is set to display the flow in term of liters per minute. The velocity of jet through nozzle is calculated considering 8.2 mm nozzle diameter, which gives the multiplying factor 0.3155 for flow rate reading displayed at monitor. Besides, total discharge in liters can also be recorded in the monitor. There is considerable fluctuation in the reading of flow rate; hence average flow rate is computed based on total volume pumped in a given time. The flow meter is counter calibrated by measuring the volume of water pumped at given a period of time. Based on that, the combined correction and multiplying factor for calculating jet velocity with respect to flow rate in liters per minute is taken as 0.58 with previous experience on this test rig (Castberg 2002 and Kjell 2002).

7.5.4 Test materials

Several materials are tested in the test rig with different objectives. The aluminum specimens are used to get quick result of erosion at moderate operating conditions, where as different types of stainless steels are used to study the effect of different operating conditions. Among the stainless steels, some are general purpose steels and some are turbine material steels.

The materials used for tests are as follows:

Stainless steels

Duplex steel SAF 2304	Austenitic steel AISI SS 316
Austenitic steel 18Cr9Ni	Martensitic steel 13Cr1Ni
Martensitic with 25% austenite 16Cr5Ni	Martensitic with 20% austenite 13Cr4Ni

These stainless steels were received from leading turbine manufacturer and steel producer. Detail properties of these steels were not provided, but whenever allowed, the information is presented.

Coating materials

HVOF sprayed coatings M1, M2 and M3 of following composition applied on duplex steel from two different coating companies (PP 1 and PP 9) are used for erosion tests. These coatings are ground and polished to mirror like surface.

M1   86WC-10Co-4Cr
M2   86WC-6Co-8Cr
M3 $75Cr_3C_2$-25(80Ni20Cr)

Five other ceramic-metallic coatings supplied by one of the leading turbine manufacturer are used for tests in as received condition (without grinding and polishing). These are:

GEC   86WC-10Co-4Cr (HVOF sprayed)

GES 1, GES 2, GES 4, GES 10 are thermal spray WC-Co-Cr coatings which are different with respect to microstructures and carbide size. Soft coating material (Elastomer) with different composition EL1 and EL2 are also tested for erosion. Details of these coatings are not disclosed by the supplier.

Both WC coatings and elastomers are applied on stainless steel base of dimension 75 mm x 25 mm x 5 mm. All of these base materials are not of same chemical composition and one has hole made at one end for clamping the specimen during spraying. The coating thicknesses are relatively high compared to coatings supplied by coating companies PP 1 and PP 9. Among these materials, coatings M1, M2 and M3 are tested for erosion and corrosion by SINTEF under a separate project. The coatings GEC and GES are also tested in several test rigs including ring and pin type test rig at SINTEF and field tests at one of the power plant in Nepal, under a separate project. The information of ceramic-metallic coatings and stainless steels are given in table 7.5.4 and table 7.5.5 respectively. All the stainless steels are not of same surface area and thickness. The specimen sizes for these stainless steels are given in table 7.5.6.

Table 7.5.4 Description of ceramic-metallic coatings

Description	Coating 1 (GEC)	Coating 2 (M1)	Coating 3 (M2)	Coating 4 (M3)
Chemistry	86WC-10Co-4Cr (weight %).	86WC-10Co-4Cr	86 WC-6Co-8Cr	$75Cr_3C_2$-25{80Ni20Cr}
Spray by	SM	PP1, PP9	PP1, PP9	PP1, PP9
Spray method	HVOF	HVOF	HVOF	HVOF
Density gm/cm3	13 (approx)	13,97	13,77	7,06
Specimen size (mm)	65X35X3	25X50X10	25X50X10	25X50X10
Coating Thickness	As sprayed	Ground	Ground	Ground
Base material	16Cr5Ni	Duplex SS	Duplex SS	Duplex SS

Table 7.5.5 The composition and properties of stainless steels

Steel	C	Si	Mn	P	S	Cr	Ni	Mo	N	Cu	Ti
SS 18-8	0.041	0.63	1.48	0.031	0.001	18	9.7	0.51	0.043	0.21	0.01
SAF2304	0.02	0.39	1.33	0.025	0.0006	23	4.78	0.33	0.087	0.29	0.016

(Courtesy- manufacturer)

Table 7.5.6 Specimen size of stainless steels

Stainless Steels	SS 18-9	SAF2304	13Cr4Ni	13Cr1Ni
Thickness mm	2	3	3	5
Specimen area (mm^2)	25 x 60	60 x 30	30 x 65	30 x 50

The effects of particles of different size were studied on curved specimens. Together with the weight loss of specimens, the erosion damages were also assessed by measurement of surface roughness in the exposed area. The specimens with different curvatures were prepared from the aluminum blocks of 40 mm wide in milling machine. Three specimens were prepared with regular curvature of radius 10 mm, 15 mm and 20 mm (figures 7.5.5 a). Other two non-symmetric curvatures are prepared as shown in figures 7.5.5 b and c.
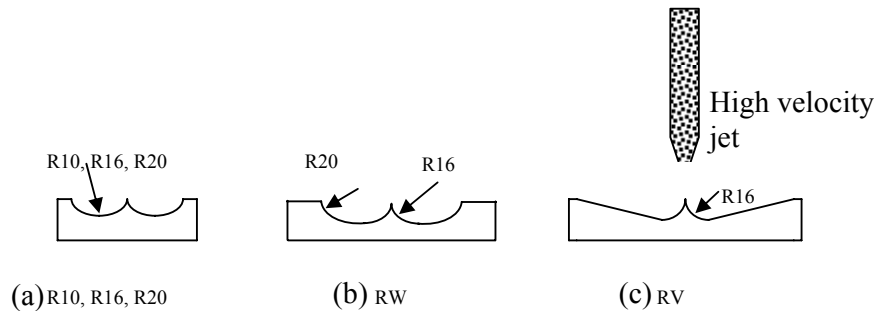

Figure 7.5.5 Specimen curvature and identification code

7.5.5 Impingement angle

The impingement angle of jet can be changed in between 0° to 90°. This angle of impingement influences the effect of particle impact on specimen. The circular shaft specimen holder is inserted in to the tube, which is supported at the cover of the tank and will be in normal to the jet in closed positing of cover. The specimen holder can be rotated in any angle with respect to jet axis and fixed with the help of set screws.

The template with different angels is used to fix the angle of impact with reference to nozzle axis. Normally the angles at the interval of 15° are used for the measurements, but there are many uncertainties around 15° and below. Depending upon the specimen dimension and orientation, there is variation of effective particles impact, which is also discussed in the discussion on performance on equipment on section 8.12.

7.6 Variables for erosion test at KU

Main aim of test erosion test at jet type erosion test rig at Kathmandu University (KU) is to investigate erosivity of Nepalese river sands.

The erosion tests were carried out on turbine material 16Cr5Ni stainless steel. The test condition is maintained at the velocity approximately 50 m/s and the concentration about 280 PPM. All the tests are carried out at 90° impingement angle. Rest of the test procedure is similar to the one described in section 7.4.

Sediment samples

The erosion measurement of turbine material is carried out with the actual river sand to investigate the erosion rate and ranking of aggressiveness of sand from different rivers of Nepal. The sampling locations are tentatively shown in figure 7.6.1. The sediment samples were collected during June/July, 2003 from different parts of country covering 7 major river basins of Nepal. Several tributaries of some of the main rivers are also included in the sample. For example, all the samples in the Koshi basin are from tributaries of Saptakoshi River and several of tributaries of Rapti River are also considered. The sediment was collected from headwork and settling basins of Jhimruk, Andhikhola and Modi hydropower project, whereas samples from Tinau, Pokhara, Sunkoshi and Indrawati are from downstream of existing power plants. West Seti and Saptakoshi are the proposed location for hydropower projects. These samples are believed to represent sediment in Nepalese river system and hydropower projects. The sand sample for Bagmati includes close to the origin of river at Gokarna and bordering point with India in plane land at Gaur. In between these two points, main tributaries of Bagmati River inside Kathmandu Valley are also included in the sample. For Khimti hydropower project, the samples are collected from Khimti River slightly upstream of confluence with Tamakoshi River. The sample from the tunnel is collected upstream of pressure shaft by flushing them from slotted pipe sediment sluicer (SPSS) at adit-4. The erosion tests by suspended sediment sample are economically not feasible. Hence fine bed materials are collected as sample for laboratory tests and it is assumed that the finer fraction of these sample represent particle size distribution, mineral content and corresponding erosion rate of sediment passing through turbine.

About 20-30 kg sand is brought to Kathmandu from each sampling location. All the sediment are first screened with the window wire mesh to remove particles coarser than 1 mm. The sediment was then sieved into six fractions: <90 μm, 90-212 μm, 212-300 μm, 300-425 μm and 425 -500 μm and >500 μm. The quantity of sand in some size, for example, less than 90 μm was very small and not enough to carry out test by that. As long as available, the erosion tests are carried out by samples of all these fractions.
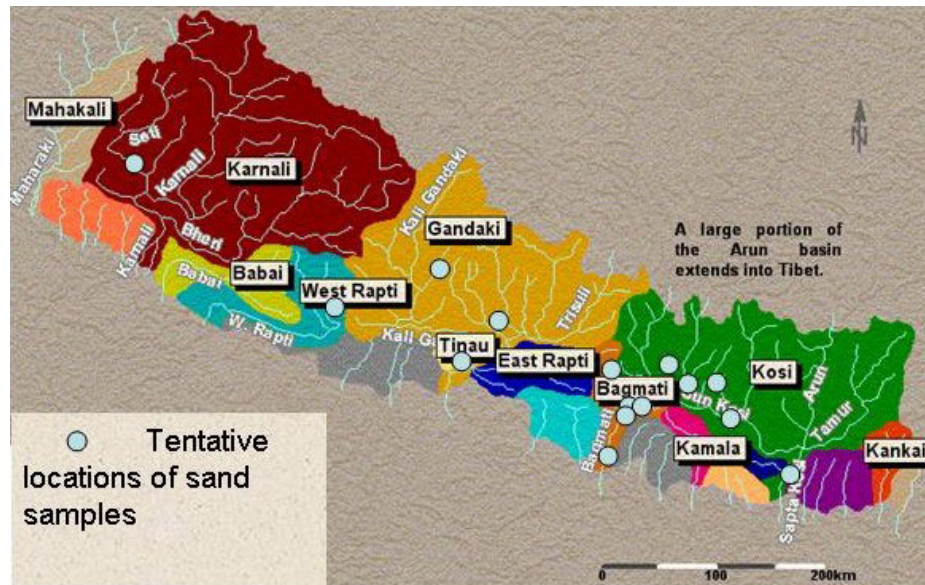
Figure 7.6.1 Nepalese major rivers with basins and locations of collection of sand samples (Background map Galay et al., 2002)

Sediment analysis

Particle size distribution (PSD) analysis of sediments was carried out in Vacuum Accumulation Tube (VA Tube) at Hydro Lab Pvt. Ltd. Nepal. Mineralogical analysis was done with high magnification binocular microscope at Department of Mines and Geology, Nepal. An average of counting of five samples is presented in term of percentage volume of mineral present in the sediment sample. Together with the mineral content, basic shape of particle is also observed.

7.7 Test results

Most of the test results from the erosion experiment presented in chapter 8 are represented in term of weight loss of specimen before and after erosion. Based on weight loss of specimen, erosion rates are presented either as a ratio of weight loss of material to weight of striking particles or volume loss of specimen to weight of striking particles. Normally erosion rate of coatings are presented in term of ratio of volume loss to weight of particles. Beside erosion rate, the surface roughness of the area affected by erosion is also measured in term of centre line average roughness value.

Chapter 8

High velocity jet erosion test: Results and discussion

The results of the experiment discussed in chapter 7 are presented in this chapter together with the discussion on each of parameters used for the test. The critical discussion on the performance of high velocity jet erosion test rig and thoughts to improve test is also discussed. The application of finding of erosion experiment on high velocity jet erosion test rig is also presented in this chapter. The findings of the erosion test carried out with sand samples from Nepal are presented at the end of chapter in separate section.

8.1 Erosion and impingement angle

The effect of variation of erosion rate with respect to impingement angle is studied with the following two prime objectives:

- to verify the performance of high velocity jet type of test rig and compare the observation with other established model of erosion rate versus angle (for example Finnie, 1960 and Bitter, 1962)
- to study the erosion rate of turbine material and coatings at different impingement angles

It is already discussed in section 3.3.1; erosion rate is a function of impingement angle of particles. Hydraulic machinery components are subjected to wide range of impingement angels at different locations. Hence, the investigation of the erosion rate at different angle gives idea of maximum erosion rate that may occur in particular test condition. These tests also indicate mode of erosion (ductile or brittle mode as shown in figure 3.3.1) for specific operating condition.

In general, it is believed that, the impingement angle of particles in the hydraulic machinery is small. Even though actual data for impingement angle are not available so far, it can be considered as spectrum of low impingement angles when the water is flowing almost parallel to the surface. At very high velocity the impingement can be almost normal to the surface due to turbulence as illustrated in figure 3.3.4. The jet striking the plain surface will also have spectrum of impingement angles, but at least in this type of test rig, jet angle with respect to specimen surface can be considered as reference impingement angle of particles.

All specimen materials discussed in section 7.5.4 are tested for the effect of impingement angles. These specimens are actual turbine materials received from industries; hence they are neither pure ductile nor pure brittle materials. In addition, the properties of these

specimens may not be uniform along the thickness and surface of the specimens. Pure metallic specimens are mechanically ductile whereas pure ceramic coatings are brittle. Even if pure metals are generally ductile, the forming and surface treatment process may alter the property at and close to the surface. The specimen of commercial aluminum sheet is tested to verify the ductile mode of erosion, whereas rests of the specimen are actual stainless steels and coatings used in hydropower industry.

All the tests are carried out by 1500 gm Baskarp-15 sand particles except for aluminum specimens, which are tested with only 750 gm sand particles. The series number in the charts represents the successive measurement on the same specimen or duplicate measurement at similar operating condition on another specimen of same material.

Aluminum

As discussed in the section 3.3.1, normally ductile material shows the highest erosion rate towards lower impingement angles around 20°-30°. However the aluminum specimen have shown maximum erosion rate away from 45° as shown in figure 8.1.1. This may be due to harder outer surface because of corrosion scales or stress hardening during rolling. The reason for higher erosion rate at normal impingement could also be due to brittle layer at outer surface of specimens. The erosion rate at 90° is higher than that at 15°, which is in line with general trend for ductile mode of erosion. The spread of data points at 45° could be due to variation of discharge during these test points and non-uniformity of material. Normally, the erosion rate should have decreased uniformly after the maximum erosion rate, but due to some reason the erosion rate at 75° is lower than the erosion rate at 90°. But more data points at this test condition may give values closer to that of normal impingement. The highest value of erosion rate is nearly double than the lowest one in figure 8.1.1, which is not so high compared to the relative values for ductile material seen in figure 3.3.1 and 3.5.1.
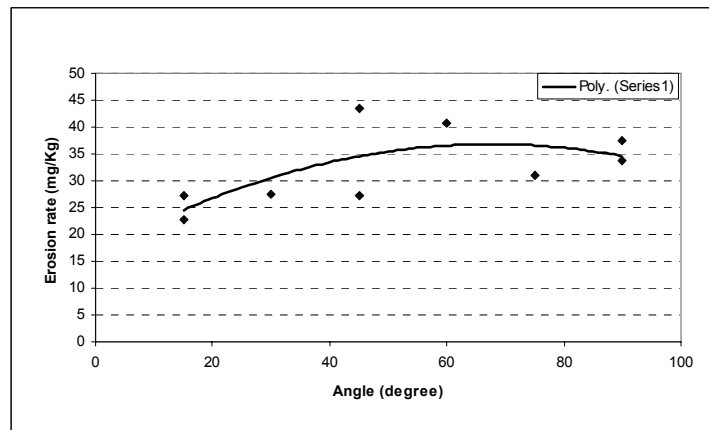

Figure 8.1.1 Effect of impingement angle on erosion rate for aluminum specimen at 60 m/s jet velocity

Austenitic steel

Austenitic steel AISI 316 is also mechanically ductile metal. The plots of erosion versus impingement angle in velocity 51 m/s and 22 m/s as shown in figure 8.1.2 and 8.1.3 respectively are similar to ductile mode of erosion. Data series 1 is erosion rate for the fresh specimen, whereas other series are repeated erosion tests normally on the same specimen. The plots are not exactly similar to generally accepted ductile mode of erosion as discussed in figure 3.5.1, but maximum erosion rate towards low angle is indication of ductile mode of erosion. Except for erosion rate at 60° for 22 m/s (figure 8.1.3) the curve is comparatively smooth. The magnitude of erosion rate at 22 m/s velocity is low compared to the precision of the weighing balance. Hence, even though differences appear on values above 60°; it could be considered as similar. The ratio of erosion rate for two velocity condition ranges between approximately 12 for low impingement angle to as high as 24 in normal impingement angels. The relative difference of erosion rate is more pronounced in lower impingement angles compared to higher impingement angles. This is in accordance with the assumption that cutting action as shown in figure 3.2.2 is predominant in ductile mode of erosion in lower impingement angles.
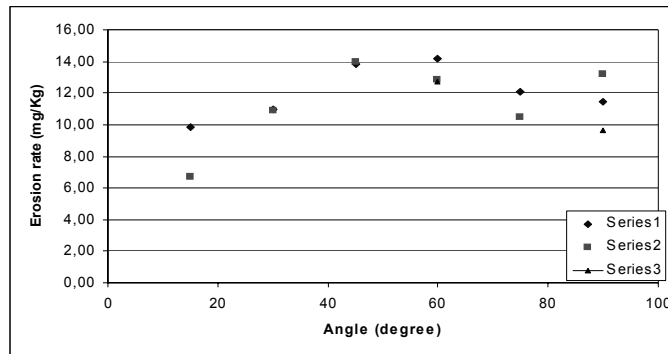

Figure 8.1.2 Effect of impingement angle on erosion rate for austenitic steel-316 at 51 m/s jet velocity
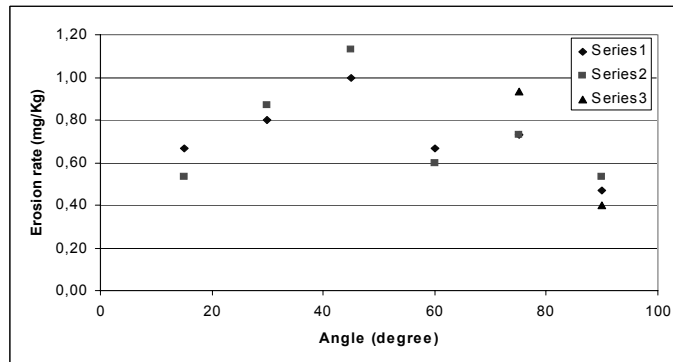

Figure 8.1.3 Effect of impingement angle on erosion rate for austenitic steel-316 at 22 m/s jet velocity

Martensitic and martensitic-austenitic steels

Martensitic-austenitic steel 16Cr5Ni is tested at three different jet velocities 22 m/s, 60 m/s and 75 m/s. In these velocity ranges, the brittle mode of erosion is observed. Erosion rate for 75 m/s (figure 8.1.4) and 60 m/s (figure 8.1.5) are increasing corresponding to increase in impingement angle. Highest erosion rate is observed at normal impingement angle, which is in line with the theory of brittle mode of erosion. Since the specimens for these steels are made from rolled plates their surface could have brittle behavior with respect to erosion. Martensitic steels are more brittle than the austenitic steels in general. Erosion rate for the case at 22 m/s also appear to be increasing (figure 8.1.6), but compared to magnitude of erosion rate in other velocity ranges, it can be considered as almost constant (figure 8.1.7). Since these tests are performed inside the water pool, at lower velocity, the energy of the particles may have lost due to fluid friction in the water pool. The effective striking velocity depends upon the secondary flow inside the pool in such cases.

The erosion rate for 60 m/s velocity is almost 20 times that of 22 m/s, whereas that at 75 m/s is as high as about 40 times. Hence it indicates that the effect of the erosion is higher at high head turbines compared to low head turbines. Even for the same velocity range, maximum erosion rate at higher impingement angles are almost double the minimum erosion rate at low impingement angles.
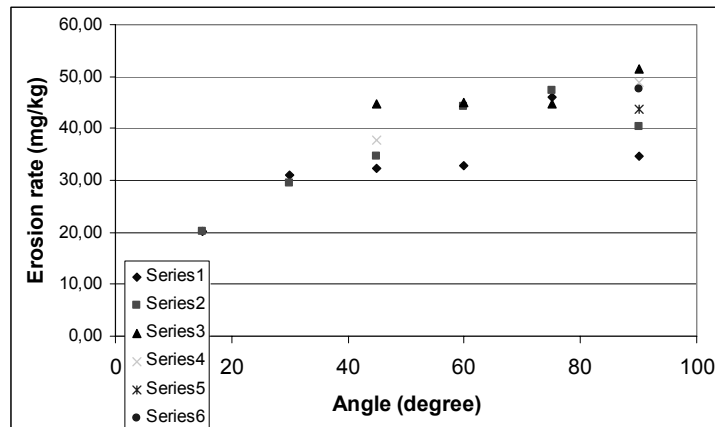

Figure 8.1.4 Effect of impingement angle on erosion rate for martensitic-austenitic steel 16Cr5Ni specimen at 75 m/s jet velocity

Martensitic-austenitic steels 13Cr4Ni (figure 8.1.8) and martensitic steel 13Cr1Ni (figure 8.1.9) have also shown maximum erosion rate toward higher impingement angles. Both of these specimens are prepared by cutting the specimen size from thick plate by power saw and ground by sand paper. Contrary to martensitic-austenitic steel 16Cr5Ni, the erosion rate at normal impingement is considerably lower than the maximum erosion rate. Besides, in both specimens, the curve is not smooth as in 16Cr5Ni. Specimen 13Cr4Ni has shown lower erosion rate at 45° than 30° and 60°. Similarly for 13Cr1Ni, erosion rate at 60° and 75° have dropped compared to 45° and 90°. There is significant variation of data mostly at normal impingement angle compared to other angles. Most of the observations for 90° are

taken on fresh specimens and it seems the brittle erosion is very much dependent on properties of materials close to the surface. At normal impingement, the effect of fatigue action may also be predominant, and material can fail suddenly after fatigue limit due to repeated tests on same specimen. This may be the reason for non-uniform behavior in consecutive tests.
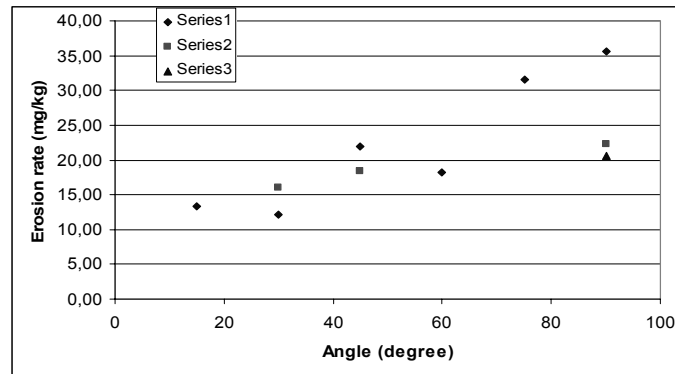

Figure 8.1.5 Effect of impingement angle on erosion rate for martensitic-austenitic steel 16Cr5Ni specimen at 60 m/s jet velocity
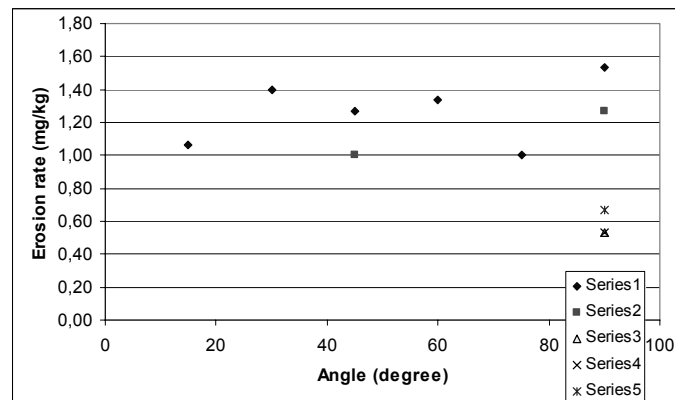

Figure 8.1.6 Effect of impingement angle on erosion rate for Martensitic-austenitic steel 16Cr5Ni specimen at 22 m/s jet velocity
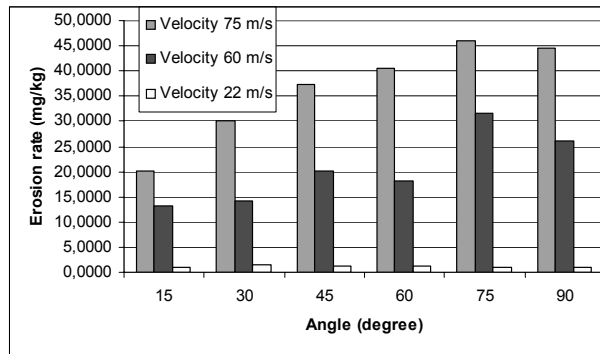
Figure 8.1.7 Comparison of erosion rate of martensitic-austenitic steel 16Cr5Ni at different jet velocity
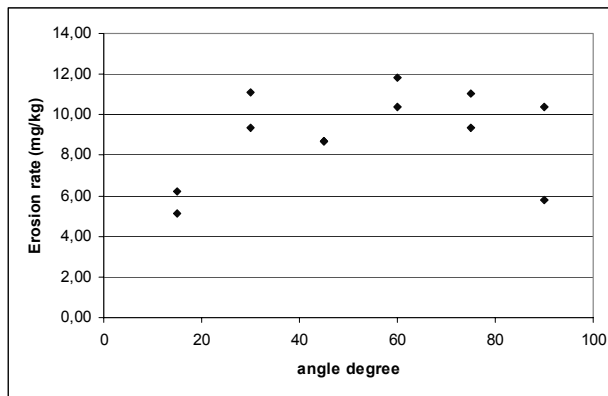

Figure 8.1.8 Effect of impingement angle on erosion rate for martensitic-austenitic steel 13Cr4Ni specimen at 53 m/s jet velocity
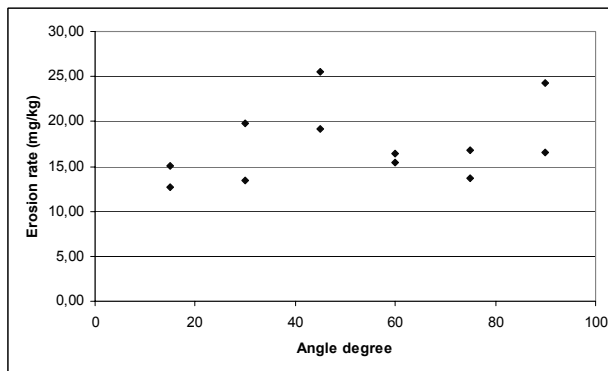

Figure 8.1.9 Effect of impingement angle on erosion rate for martensitic steel 13Cr1Ni specimen at 53 m/s jet velocity

Other steels

The austenitic steel 18Cr9Ni has shown erosion mode in between ductile and brittle (figure 8.1.10) with highest erosion rate around 60°. But the trend of the curve is very clear in this case and their difference in the minimum and maximum erosion rates is not as high as in other cases of martensitic and austenitic steels. The erosion rate at different impingement angles for duplex steel is almost same except for normal impingement (figure 8.1.11). Both 18Cr9Ni and duplex steel are thin rolled plates and surface of these plates are smoother and uniform compared to the specimens prepared from thick plates.
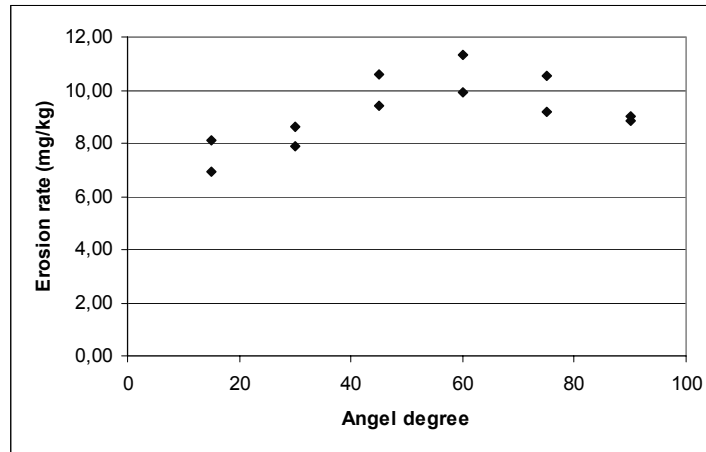
Figure 8.1.10 Effect of impingement angle on erosion rate for austenite SS 18-9 specimen at 55 m/s jet velocity
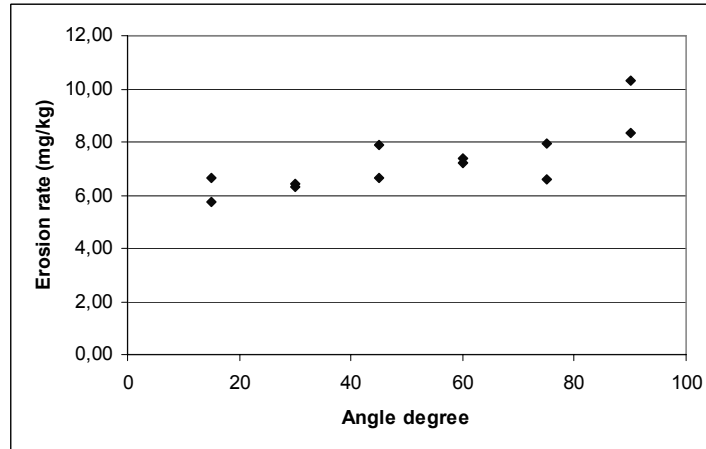
Figure 8.1.11 Effect of impingement angle on erosion rate for duplex steel specimen at 55 m/s jet velocity

Ceramic-metallic coatings have also shown mixed mode of erosion. In some cases, maximum erosion appeared at normal impingement and in other cases it has appeared slightly below the normal impingement. Normally ceramic-metallic coatings are believed to behave like brittle mode of erosion, which may depend upon the metal matrix and carbide. Though metal matrix is expected to be removed by cutting action of particles in low impingement angles, brittle mode of erosion could have significant effect because the particles size is as high as 10 times the carbide particles and metal matrix gaps. Detailed results of variation of erosion rate for different coatings are presented in separate section 8.6.

The low velocity range test on free jet test rig at KU (Thapa, 1999) and rotating disc apparatus (RDA) (Berget, 1999) have given measurable magnitude of erosion rate. But most of the data in low velocity (around 22 m/s) in this test rig is bad because of submerged jet. Hence, it is not recommended to carry out erosion test at low velocity range because of low particle impact energy in submerged jet test rigs.

Several test results have shown higher spread of erosion rate data towards higher impingement angle. In this particular test rig, the effect of recirculation may have played significant role. The effect of secondary flow should have been nominal in normal impingement. Hence the difference of data may be explained by effect to fatigue failure at normal impingement. The removal of material by cutting action can be more uniform compared to fatigue. The relation of erosion rate versus impingement angle found in this study is not exactly similar to curves given by models of Finnie (1960) and Bitter (1962). Large number of repetitive tests may give statistical trend or strike with relatively large quantity of particles compared to precision of weighing balance may give curves similar to the one found in the literature. Similar trend of the fluctuation between velocity and impingement angle obtained from experiment by Prof. Hojo can also be seen in Duan and Karelin (2002). They have also found different curve for erosion rate versus impact angle for different test velocities. Generally same material have shown similar behavior, but their findings for polymer materials are not in line with the results of general metals and results presented in this thesis. Wood et al. (1997) also found the polynomial curves similar to this research for WC-Co-Cr coatings against the general trend of brittle mode of erosion behavior for ceramic-metallic coatings.

The polynomial equations describing relation between erosion rate and impingement angle are not proposed in this research. Instead, this author proposes to carry out tests or consider the data of 45° impingement angle for erosion model. This gives conservative value with minimum disparity with lowest and highest value.

8.2 Erosion and velocity

Erosion tests were carried out at different velocities with all other parameters constant to develop the relation between erosion rate and velocity, which can be used to predict erosion of material operating at similar condition. The trend line for most of the experimental results of erosion rate versus velocity of particle fit well within the power law curve (Bjordal, 1995, Feng and Ball 1999). Similar observation was obtained in this research too. Hence exponent of velocity for such relation is obtained with the power law curve fitting

using Microsoft Excel tool. The relation between erosion versus velocity for aluminum specimens at 45° impact angle is shown in figure 8.2.1, which shows the value for velocity exponent close to 3.5. Similarly, martensitic-austenitic steel 16Cr5Ni (figure 8.2.2) shows exponent value slightly above 3 for the test condition both at 45° and 90° impingement angles with R-squared value (R^2) more than 90%. Few cases like austenitic steel AISI 316 at 90° (figure 8.2.3) and 18Cr9Ni at 45° impact angle (figure 8.2.4) have shown exponent value higher than 4, but on average majority of the values of exponent in all the operating conditions are less than 4. Some of the higher range exponents could be due to spread of data due to less number of data points in the test.
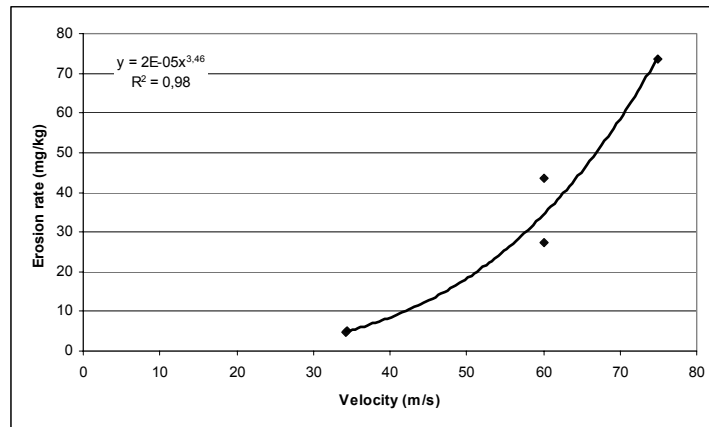
Figure 8.2.1 Relationship between erosion rate and velocity for aluminum (test condition 45° impact angle, 750 gm of Baskarp-15 particles)

Figure 8.2.2 Relationship between erosion rate and velocity for martensitic-austenitic steel 16Cr5Ni (test condition 1500 gm of Baskarp-15 particles)

The impact energy of the particle increases along with the velocity and because of this, the ability of particle to deform or damage the material also increases. The study of erosion

versus velocity was difficult in Rotating Disc Apparatus (RDA) and Rotating Cylinder Apparatus (RCA) because of limitation of rotational speed in the given set up and speed ratio depends upon available gear ratio. Jet type of test rig has advantage of changing the flow by changing bypass water and achieves different jet velocities. Bjordal (1995) has reported the difference in erosion rates of different rings depending on its position on RCA. Even though there is a wide range of impingement angles in RDA difference of exponent value are not very large. Hence data from jet type of equipment can also be used for developing generalized relation between erosion rates versus velocity for variety of applications.
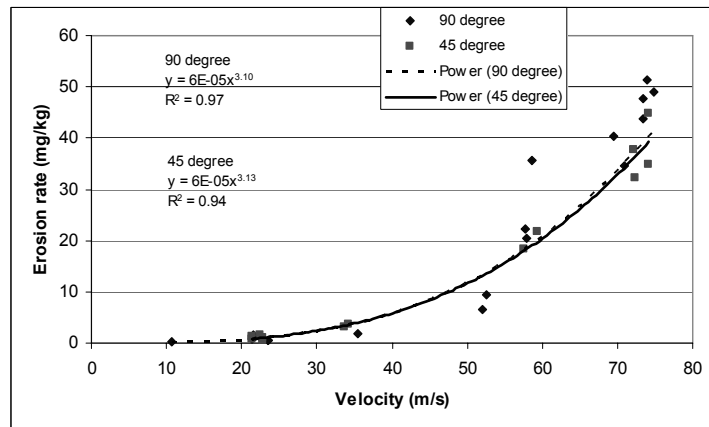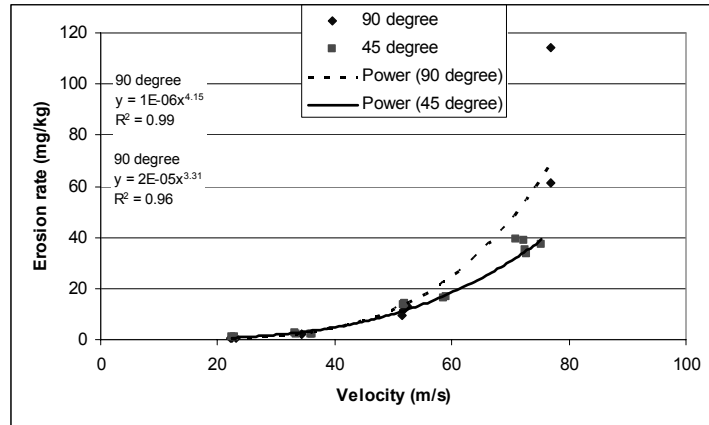

Figure 8.2.3 Relationship between erosion rate and velocity for austenitic steel AISI 316 (test condition 1500 gm of Baskarp-15 particles)
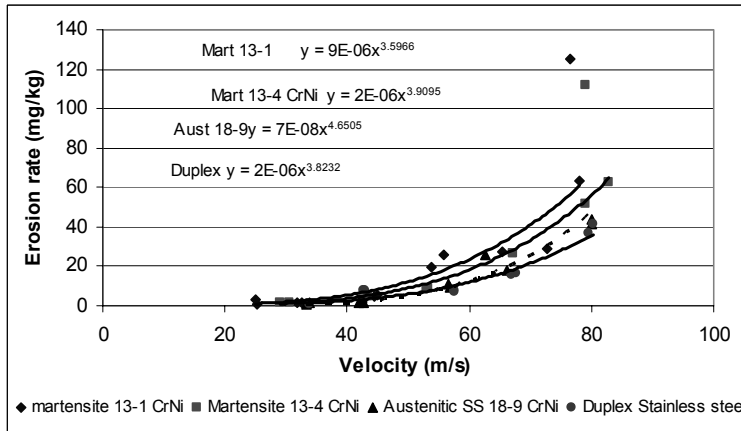

Figure 8.2.4 Comparison of relationship between erosion rate and velocity for different stainless steels (test condition 45° impact angle, 750 gm of Baskarp-15 particles)

Evidently, the slight change in velocity gives large change in erosion rate, but approximation of velocity exponent in between 3 to 4 gives conservative approximation for prediction of erosion rate with respect to increasing head for turbine operating at similar environment. Krause and Grein of Sulzer Hydro used the value of the exponent n as 3.4 for 13Cr4Ni stainless steel Pelton turbine for estimation and comparison of erosion rates between actual turbine and computer simulation (in Nanda, 1999). Despite the fact that theoretically erosion rate is proportional to the power of 3 of velocity based on kinetic energy of particles, several researchers have reported this value in between 2-5 (refer section 3.3.1). Based on this research, the exponent value in between 3-4 is recommended specially for the purpose of hydraulic machinery. The equations obtained from power law curve fitting (shown in respective charts) can be used for estimation of weight loss due to sand erosion and optimization of the size of turbine and sediment settling basins for new hydropower plants. The application of equation obtained from this test is discussed in section 8.13.

8.3 Effect of particle material

Several properties of particles that effect erosion are discussed on section 3.3.2. It is well accepted that erosion rate depends upon properties of particles for instance density, hardness and shape or sharpness of edges. The tests with different particles were carried out to find the difference in magnitude of erosion rate. The relation between erosion rate and velocity were expected to follow similar trend line with same exponent value. However, different particles showed different erosion behavior with respect to velocity. The observations of the experiment for erosion with different particles (on martensitic-austenitic steel 16Cr5Ni at 45° impingement angle as shown in figure 8.3.1) also fits well with the power law relationship. All the trend line curves have R-squared value (R^2) more than 95%, which is an indication of good curve fitting. If particle impact energy would have the only reason for erosion of material, the exponent of velocity should have been 3, but the value of exponent varies in between 3.26 to 3.76 for different particles. The value of velocity exponent is almost in the same order of density and hardness of particles. The particles with higher density and hardness have shown higher exponent value compared to lower density and hardness. The difference of erosion in low velocity region is nominal compared to high velocity region. This indicates the need of thorough analysis of sediment particles for high head turbines.

The increase of erosion rate at high velocity could also due to fracture of particles at high impact energy. When particles hit the target, stresses will induce in the grains as well. In such case there is even a probability of grains getting fractured. Together with general material properties, the probability of grain fracture also depends upon impact velocity, impact angle and size of the particles. Yashima et al. (in 1987) studied the relationship between critical impact velocity and particle size for fragmentation of abrasive particles and they have found critical impact velocity linearly decreases with the increase of particle diameter. For example, approximate critical impact velocity is 65 m/s for 0.1 mm diameter quartz particle and 25 m/s for 0.5 mm diameter particles. Harder materials like quartz have higher ability to retain their shape after impact compared to other abundantly present minerals in the river sediments.

Feng and Ball (1999) found the value of velocity exponent slightly higher than 2 for silica, alumina, WC, SiC and diamond particles and the erosion rates are found almost in the same order of hardness and angularity of the particles. For brittle materials, the erosion rate is dependent on kinetic energy of particle (thus density) together with size, relative hardness and toughness of erodent particles. On the other hand, for ductile materials kinetic energy and shape of erodent have more significance with only little or no effect of toughness or hardness of erodent.
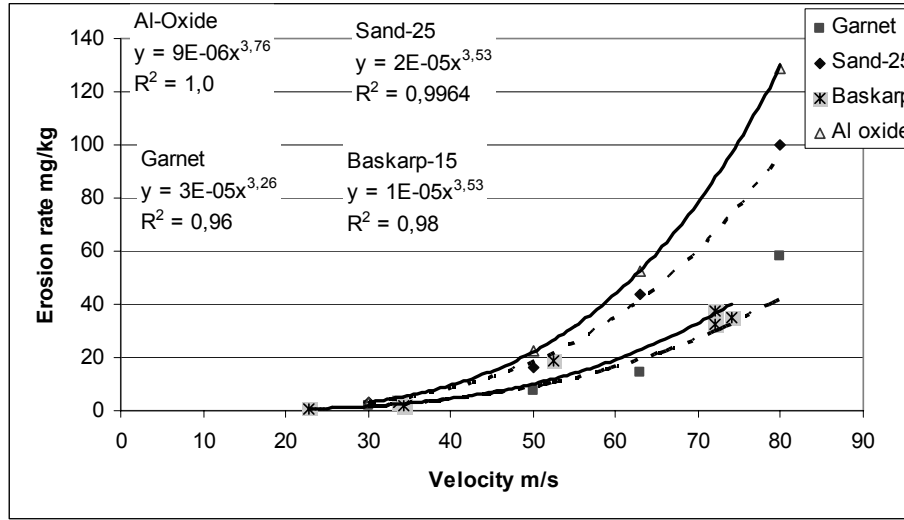

Figure 8.3.1 Relationship between erosion rate and velocity for different particles

8.4 Effect of particle flow

Concentration

As explained in the section 7.5.2, six different concentrations can be achieved for the same velocity in the system by changing the hopper nozzles with different opening. For each opening, the flow rate of particle is constant, but the flow rate of water can be changed with the bypass valve, hence wide range of concentrations can be achieved. Even though Himalayan Rivers can have concentration higher than 0.2% (2000 PPM) in monsoon season, the tests at high concentration for instance approximately 0.27% have often problem of blocking of pipe between nozzle and mixture hopper. However, since the erosion rate is presented as weight loss of specimen per unit mass of striking particles, no significant difference in erosion rate is expected in the concentration range between 0.06 to 0.27%. But as the test duration for different concentrations varies, the erosion rates per unit time for different concentration level will be different.

Figure 8.4.1 shows the erosion rate of martensitic-austenitic steel 16Cr5Ni caused by Baskarp-15 sand particles tested at approximately 55 m/s jet velocity. The average erosion rate at different concentration levels indicated by bars (figure 8.4.1) is about 13 mg/kg. Since almost same amount of the erosion effect appears earlier in higher concentration

level, the erosion rate is converted in to same unit to see its effect over the period of time. Even if the erosion rate in term of weight loss of specimen per unit particle weight appears to be higher in low concentration, it will reverse if we consider the erosion rate in term of weight loss per unit particle weight per unit time. Although it is believed that, the effect of concentration above certain limit does not have increasing erosion effect due to collision of rebounding particles, this test showed increasing erosion rate in term of time.
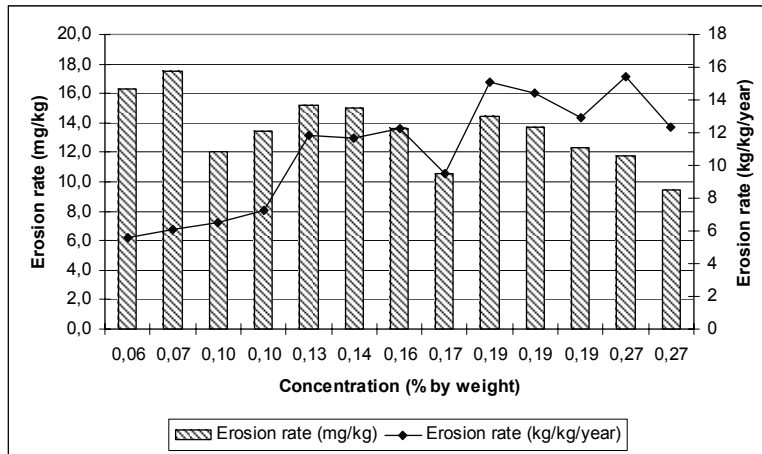

Figure 8.4.1 Effect of concentration on erosion rate with respect to weight of striking particles and time of exposure on high velocity jet test rig

Cumulative weight loss

The variation in the erosion in successive tests on same specimen is expected. Some sort of start up effect can be expected at the earlier stage such that the material becomes weak and later removed by successive hitting. On the other hand, the erosion at earlier stage could be higher due to imperfection and weak surfaces at outer layer. The start up effect of higher erosion rate is predominant in coatings compared to pure metals. The weight loss after first set of test is almost constant in all the metallic specimens at all angles (figure 8.4.2). Contrary to pure metallic specimen, there is large drop in weight loss after first test in ceramic-metallic coating (figure 8.4.3). Outer layer of the ceramic-metallic coatings can be weak and very much dependent on spraying parameters and that of pure metal is more uniform and stable. The cumulative erosion of pure martensitic-austenitic steel after 4 sets of test with 1500 gm of Baskarp-15 sand in each test is almost double (in term of weight) than the ceramic-metallic coatings GEC. The significance of difference of erosion rate in term of weight loss and volume loss for ceramic and ceramic-metallic materials is discussed in section 8.6.

Though erosion rate in successive measurements with equal amount of particles (in similar operating condition) is almost equal, the results obtained from successive tests carried out by increasing different quantity of particles in each test have shown different result (figure 8.4.4). No significant pattern or trend for the variation of particle weight is observed. The rates of particles flow are slightly different in these cases, but rather than effect of

difference in concentration due to difference in particle flow rate, other factors like secondary flow and effect at the back side of specimen may have greater influence.

The velocity of the water coming out of free nozzle at atmospheric pressure depends on the height of the water in the column. Hence the different discharge can be expected from free nozzle according to water head of fluid. But it is difficult to conclude whether this phenomenon is true in the case of solid particles freely falling from nozzle or not. Other factors like shape, size of particles, cohesive property of particles and adhesion between particles and cylinder wall may affect the particle flow rate more than the height of the particle in the hopper.
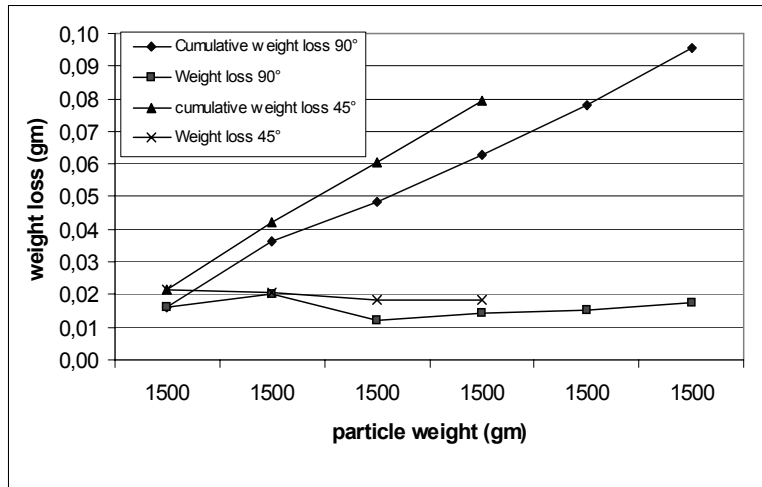
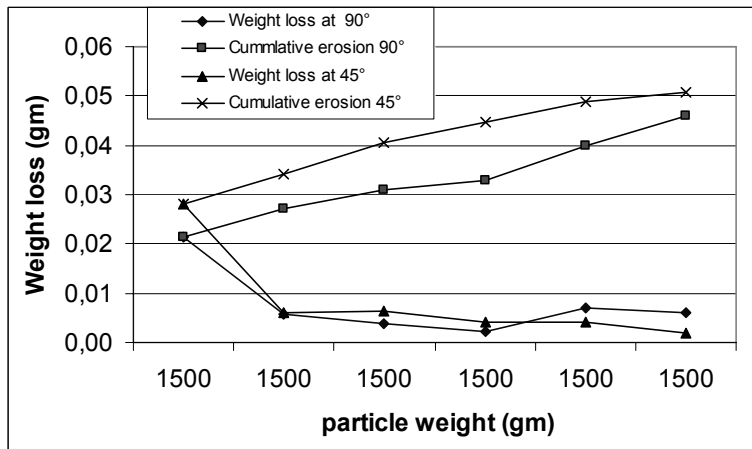Figure 8.4.2 Cumulative erosion and weight loss at each test for martensitic-austenitic steel 16Cr5Ni

Figure 8.4.3 Cumulative weight loss GEC ceramic-metallic coatings

115

There is no doubt that the erosion of actual hydro power turbine increases with increase in concentration of sediment, but the relationship between concentration and corresponding increase in erosion rate is very complex. The erosion rate increases in higher concentration because of higher number of particles strike the surface in such condition. Similar results can be observed in the rotating disc apparatus (RDA), where particles are placed inside the tank and whirling of arm or swirl of fluid brings the particle in contact with surface. In the jet type of equipment, most of the particles are assumed to strike the specimen surface and hence change in concentration may not have significant effect in erosion rate.
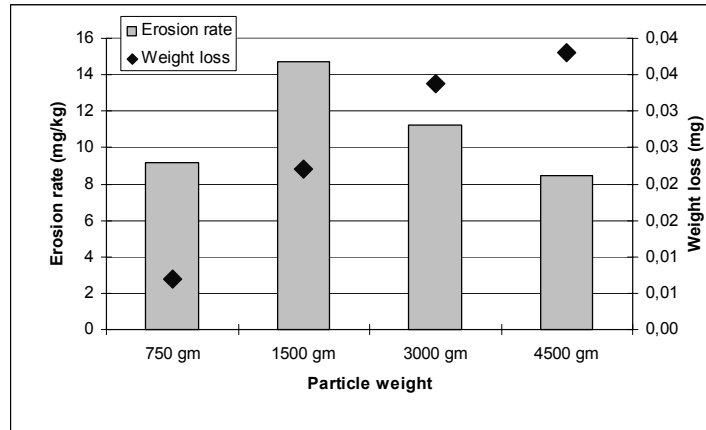

Figure 8.4.4 Effect of particle weight martensitic-austenitic steel at 45° and 55 m/s

8.5 Erosion of turbine materials

Three different turbine steels 13Cr1Ni, 13Cr4Ni and 16Cr5Ni are tested for sand erosion at different operating conditions. General purpose stainless steel austenitic steel AISI 316 and duplex steel used in oil industry are tested for comparison. Similarly stainless steel 18Cr9Ni supplied by one of the leading steel manufacturer is used as close substitute for 18Cr8Ni for the erosion test at jet type of test rig at NTNU/SINTEF.

The erosion rates for different stainless steels tested at 55 m/s jet velocity with 1500 gm Baskarp-15 sand particles are presented in figure 8.5.1. The erosion rate for 16Cr5Ni is not compared in same chart because the jet velocity for this specimen was little higher than others. Closest velocity tested for 16Cr5Ni is 60 m/s, which is about 10% higher than others and even if we consider the value of velocity exponent n as 3, the difference in erosion rate will be about 30%. The 13Cr1Ni has shown poorest erosion resistance, whereas 13Cr4Ni and duplex steel have shown relatively good erosion resistance. Though there is slight difference in the exposure area in these specimens because of size difference, the effect due to this is neglected.

Generally it is believed that 16Cr5Ni has the best erosion resistance among turbine materials. But the interpolation of erosion rate from the relation between erosion rate and impingement angle gives erosion rate about 16 mg/kg and 14 mg/kg respectively for 45°

and 90° impact angles respectively. This is higher than all other steels tested except 13Cr1Ni.
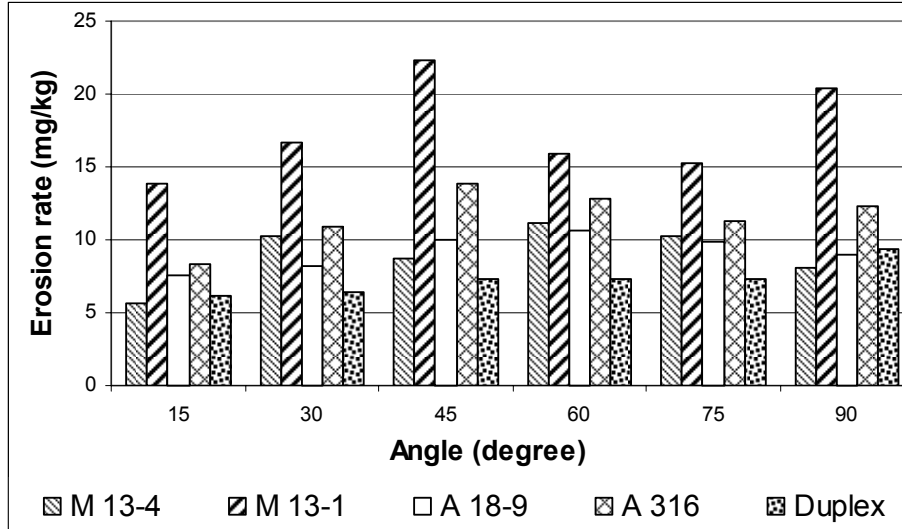

Figure 8.5.1 Comparison of erosion rate of different stainless steels tested at approximately 55 m/s by Baskarp-15 particles

8.6 Erosion of ceramic-metallic coatings

Several erosion resistant ceramic-metallic coatings are tested with the following aims

- to investigate erosion resistance of ceramic-metallic coatings
- to compare performance of different coatings and study their ranking on erosion resistance
- to investigate the effect of impingement angle on erosion rate for ceramic-metallic coatings
- to compare the erosion resistance of coatings with pure metals

The coating specimens used for the tests are discussed in section 7.5.4. There are basically following three variations in the specimens.

- Different compositions of tungsten carbide and chromium carbide coatings
- Same coating with two different coating companies
- Surface condition ground/polished and as sprayed (unpolished)

Each coating is tested with at least two specimens such that any abnormal measurement due to other failure can be traced and uncertainties can be minimised. Besides other measurement uncertainties, significant effects of the quality of coating and coating bond at edges have been observed. Similar to the tests for pure metallic specimen, the erosion of the coating is measured in term of weight loss of specimen. But the ranking of erosion resistance of coating based on weight loss and volume loss are completely different due to

difference in density of coatings. Hence, presentation of erosion rate in term of volume loss or reduction in thickness is very important. Even in actual practice, loss of thickness is more important in the turbine compared to loss of weight because it is almost impossible to find out weight loss of big turbines by weighing. The difference in ranking of erosion rate based on weight loss or volume loss can be illustrated in figure 8.6.1. Because of low density of $75Cr_3C_2-25NiCr$ even if it has lowest the erosion rate in term weight loss, shows maximum erosion rate in term of loss of volume (figure 8.6.1 b).
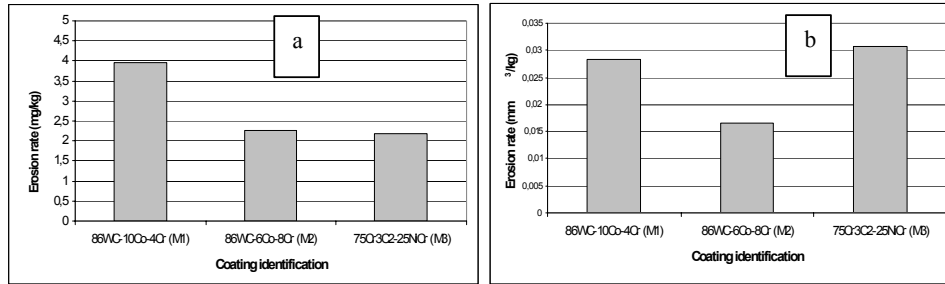

Figure 8.6.1 Erosion rate of Ceramic-metallic coatings in term of (a) weight loss and (b) volume loss (test condition: 45° impact angle, Baskarp-15 sand and approximately 55 m/s jet velocity)

The effective shape of jet before strike on different position of specimen from nozzle exit, their effect in the test area and non-coated area (edges) are discussed in section 8.12. Some sign of erosion in the non-coated edges were also observed. The ceramic-metallic coatings 86WC-10Co-4Cr, 86WC-6Co-8Cr and $75Cr_3C_2-25NiCr$ are coated in 10 mm thick duplex stainless steel substrates. The edge effects were found considerable in these specimens and this effect is more pronounced in the lower impingement angles. Since these tests are performed in the water pool, the swirling of mixture after direct hitting on the target surface also causes minor erosion in the edge of specimens. The specimens were prepared from the 100 x 50 mm duplex steel plate coated with the protective erosion resistant coating only on one face and later cut in to the 50 x 25 mm pieces by diamond cutting wheel. Even though the edges were ground in the sand paper to remove burr, some coatings had remained in the sides. The difference in erosion rate due to edge condition were realised only after the tests on impact angles 90° and 45°. After those tests, long edges were protected by shield in the further tests for 60° and 15°, which restricted the damage of edge to certain extent. In some cases, large area of coating is removed due to weak bond of coating. Other possible source of error is chipping off of coatings at the edge because of brittle nature of ceramic coatings. However main difference in performance of ceramic-metallic coatings is due to powder and spraying process properties. The explanation of differences in the performance of coatings can be better explained by the Scanning Electron Microscope (SEM) images. The SEM images for sectional view of three coatings M1, M2 and M3 are shown in figure 8.6.2 (a-c). Tungsten carbide (WC) particles appear as bright area in SEM images in figure 8.6.2 a and b, whereas chromium carbide (Cr_3C_2) particles appear as dark spots in figure 8.6.2 c. The WC and Cr_3C_2 particles in figure 8.6.2 a and c are coarser than WC particle in figure 8.6.2 b.

118

(a) 86WC-10Co-4Cr (M1)   (b) 86WC-6Co-8Cr (M2)   (c) 75Cr$_3$C$_2$-25NiCr (M3)
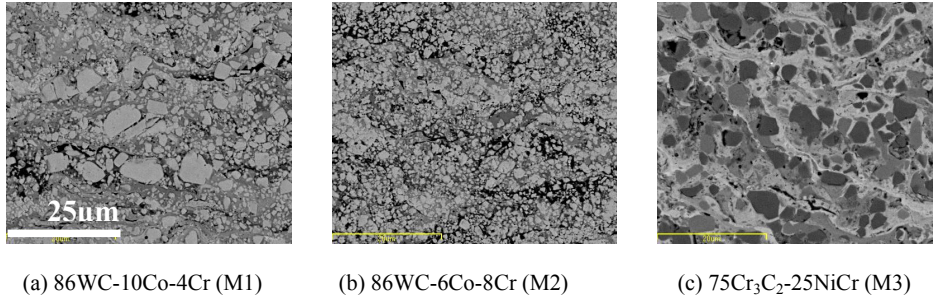
Figure 8.6.2 Scanning electron microscope (SEM) images of ceramic-metallic coatings (photo courtesy John Berget)

Comparison of ceramic-metallic coatings

Polished coatings

Separate comparisons are made for different categories to study relative erosion resistance. First, only the polished specimens are compared among themselves. Secondly, the polished specimens are compared with the one of the unpolished (as received) and thirdly, the unpolished coatings are compared among themselves.

Generally the coating M2 (86WC-6Co-8Cr) is found better than other two coatings in all impact angles tested, except at 15°. The fine WC particles in the matrix as shown in figure 8.6.2 (b) could be possible reason for better erosion performance of this coating. Similar observations were also obtained by (Berget 1999, Berget and Rogne 2004). The erosion rate ranking for these three coatings from high to low are 75Cr$_3$C$_2$-25NiCr > 86WC-10Co-4Cr > 86WC-6Co-8Cr (M3>M1>M2), except for 45° impact angle. Relative ranking is prepared for these coatings on the basis of lowest erosion rate observed on the test. Table 8.6.1 shows ratio of erosion rate of coating with respect to lowest erosion rate, which is found for M2 (sprayed by PP9) at 45° impact angle and indicated by M2*. The largest ratio of erosion rate is found as high as 7 times for M1 at 45° impingement angle.

Table 8.6.1 Comparison of erosion rate of polished coatings in term of volume loss (in mm^3/kg)

Ratio of erosion rate	PP1 90°	PP1 45°	PP9 90°	PP9 45°
M1/M2*	2.27	2.39	5.71	7.28
M2/M2*	1.29	1.39	2.33	1.00
M3/M2*	2.91	2.59	2.95	5.25

Apart from properties of coating powders, spray process parameters will also have significant effect on the quality and performance of coatings. Coatings of same powders, which are sprayed by two different companies, have shown different performance (figure 8.6.3). The coatings made by Company 1 (PP1) are found better than that by Company 9 (PP9). The factors affecting thermal spray coating properties are discussed in section 4.4 and details of effect of spray process parameters on the erosion and erosion-corrosion performance of coating can also be found in Berget (1999). The investigation of the cause

of difference in erosion rate due to difference in spray process parameter is not in the scope of this thesis, but jet type of test rig also confirmed the observation in other test rigs and real life experience. There is not much variation in the erosion rates for the coating M2 compared to other coatings by both the spray company. On the other hand, there is almost twice the difference in erosion rate for coating M1 between two partners.
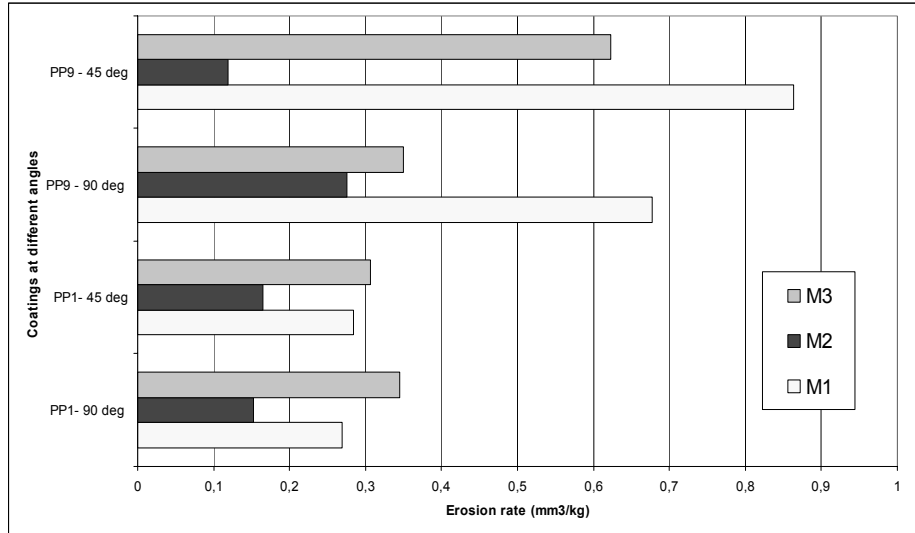

Figure 8.6.3 Comparison of erosion rate of coatings 86WC-10Co-4Cr (M1), 86WC-6Co-8Cr (M2) and $75Cr_3C_2$-25NiCr (M3) made by different companies (test condition: jet velocity 55 m/s, Baskarp-15 sand particles).

Polished and unpolished coatings

The coating GEC (86WC-10Co-4Cr) is as sprayed and erosion rate of this coating will not have same comparative index with coatings M1, M2 and M3. This is because of different surface condition of the specimen. The erosion rate for unpolished coating is found much higher than other ground or polished surface. GEC coating has about 10 times higher erosion rate than M2 at 60°. Large differences in erosion rates are found in higher angles of impact compared to lower ones. This may be because, particles in the rough surface may have detached easily at higher angles compared to lower angles, due to fracture at high impact angle. GEC coatings have less edge effect compared to other coatings. Hence, the actual differences in erosion rate between them could be even higher than that presented in table 8.6.2.

With these results, it can be believed that, thermal spray coatings can be machined to improve erosion resistance. Even though GEC and M1 are tungsten carbide coatings of same composition, there could be difference in erosion rate in these two because of difference in spray powder properties and spray parameter of two different companies. The difference between polished and as sprayed coatings can be studied for the same coating from same spraying company, which is not done in this study, but difference of erosion rate for polished and as sprayed coatings have also been observed at SINTEF (Berget, 2004).

Table 8.6.2 Comparison of erosion rate of as sprayed (GEC) and polished coatings made by company 1 (PP1) in term of in term of volume loss (mm^3/kg)

Ratio of erosion rate	90°	60°	45°	15°
GEC/M1	4.5	6.0	2.2	3.4
GEC/M2	8.1	9.8	3.8	1.6
GEC/M3	7.4	7.0	4.0	6.2

Comparison of unpolished coatings

The WC coatings of different composition and microstructure, provided by one of the leading turbine manufacturer are compared with each other for their erosion resistance in jet type of test rig. These coatings are believed to be suitable for the hydraulic turbines and among these, one is a new formulation. The composition and detail properties of these coatings were not provided by specimen supplier. Main aim of erosion test of these coatings in this study is to compare these coatings with turbine material and to compare the ranking of erosion resistance obtained on jet type of test rig with other equipment. All the coatings are compared with respect to GEC because the composition of GEC is known and its comparison with polished coatings (M1, M2 and M3) is possible in terms of volume loss. Since the densities of the unpolished coatings are also unavailable, the erosion rates for these coatings are presented in term of weight loss.

The bar chart with erosion rate of all as sprayed coatings shows that GES#4 is the best among these in all range of impingement angles (figure 8.6.4). At 45° impingement angle, all coatings have similar performance except GES#1. The erosion rates of GES#1 are still higher in angles lower than 45°, hence there could be more edge effect at lower angles, particularly for this coating. At normal impingement angle the erosion rate has increased almost linearly for coatings GES#4<GES#10<GES#2<GES#1<GEC. At 60° impingement angle, GES#2 has shown maximum erosion rate, whereas others have shown same order of ranking. The variations of erosion rate for different coatings are lowest at 45° impingement angle except for GES#1, which could be due to some unidentified abnormal test condition. In general, 45° impact angle may have minimum uncertainties and hence observation from tests at this angle can be used for ranking the erosion resistance of coatings. GEC has shown higher erosion rate in most of the cases, but the difference in ratio are less than that with the polished coatings. The relative ranking of ratio of erosion rate can be seen in table 8.6.3. GEC and GES specimens were tested using different holding device as shown in figure 7.3.2 and it is assumed there is no significant difference in erosion rate due to this.
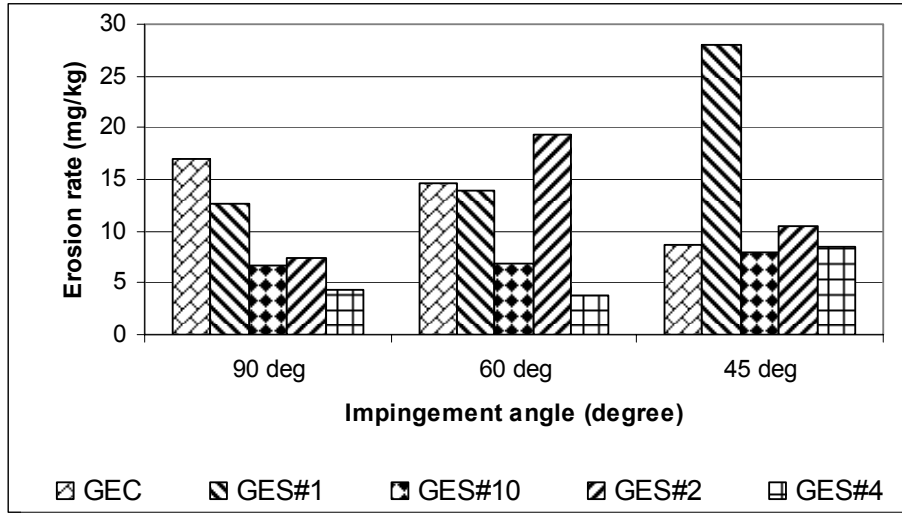
Figure 8.6.4 Comparison of unpolished coatings

Erosion rate versus impingement angle

The carbide coatings with metallic binders are expected to show erosion behaviour in between brittle and ductile material. But experimental results of all the coatings do not show similar behavior. Coatings GEC and M1 are same composition 86WC-10Co-4Cr from two companies and different surface condition. The profile of curves for M1 (figure 8.6.5 a and b) are neither ductile mode nor brittle mode, but GEG have shown somewhat brittle mode of erosion (8.6.7a). Coating M3 is reach in metal with 25%NiCr in the matrix. The highest erosion rate is observed around 45° in this coating, which is an indication of somewhat ductile erosion behavior, but there is not much difference in erosion rate in 45° and 90°. At these angles they show somewhat similar trend with maximum erosion around 90° impingement angle.

Table 8.6.3 Comparison of GE coatings in term of mass loss (mg/kg)

Ratio of erosion rate	90°	60°	45°
GEC/GES#1	1.35	1.05	0.31
GEC/GES#10	2.55	2.11	1.10
GEC/GES#2	2.32	0.76	0.83
GEC/GES#4	3.86	3.82	1.03

Coating M2 shows completely different behaviour. It also shows neither ductile nor brittle behaviour. Maximum erosion rate is observed at 15° and the erosion is decreasing towards higher angles for coating sprayed by company PP1 (figure 8.6.5 d). In some cases, carbide particles can be pulled out during grinding and the outer surface of such coating can have more metallic phase showing ductile behaviour. But it is difficult to make this conclusion because both M1 and M2 are also polished in the similar condition, but do not show similar behaviour. If the data for 15° is neglected because of uncertainty in edge effect, erosion rate for rest of the impingement angles can be considered almost constant. Similarly, coating M3 from coating company PP1 has also more or less uniform erosion rate for all the angles (figure 8.6.5 f).

Even though there is certain repetitive trends between successive series of tests, the specific trend of ductile or brittle material are not found and the spread of the data point are also very high for most of the GES coatings (figure 8.6.7). The erosion rate for coatings decreases considerably at early stage in successive tests in same specimen as shown in figure 8.4.3. Hence either separate specimens with similar properties should be used for comparison or data should be considered only after the elimination of start up effect.

There is a large spread of test results in the GES specimens compared to other polished specimens and GEC (unpolished). Series 1 data for coating GES#1 and GES#2 are from tests on as received specimen (figures 8.6.7 c and e). Start up effect with higher erosion rate was observed in first series of data sets due to weak coating at outer surface and chipping of coatings from edges. Rest of the specimens were slightly ground on the belt grinder to remove weak outer surface and some of the weak coatings from the edges. Beside these uncertainties, the leakage from pump had increased in these tests due to wear of piston/cylinder of pump during these tests. Even though this leakage is less than 5%, its effect in erosion could be considerable.

The qualities of the coating on GES specimens are not uniform, which can be very easily observed by the thickness of the coatings applied, the holding arrangement during coating and the base material. One of the specimen had a hole, may be used to hold the specimen during spraying and effect of corrosion was significant in the in most of the GES#4.

Erosion rate versus velocity

The relationship between erosion rate and velocity in case of ceramic-metallic coatings also follows power law. Compared to pure metallic specimens, there is a large variation of the values of exponent of velocity in case of ceramic-metallic specimen. This variation is in between 1.11-5.46 for polished specimen and 2.25-4.58 for unpolished specimen. Same coatings with different spray companies have also shown quite different values of exponents as shown in figure 8.6.6. All the curves with high velocity exponent (more than 3) have R-squared value (R^2)greater than 0.9, but in case of low exponent vales 1.11 for PP1 – M2 (figure 8.6.6 c) is very low, which is only 0.18, indicating extremely poor curve fitting. The R^2 values for unpolished specimens are also normally low. This may be due to less number of data points and more than that may be due to irregular pattern of material failure in some of the coatings because of poor coating quality. In case of these coatings, the values of exponent for coating materials are found approximately in between 4.6 to 4.96, which are slightly higher than that for pure metallic specimens as discussed in section

8.2. However both the coatings with similar composition M1 and GEC have higher values. With these observations, it can be concluded that, erosion rate follows power law with velocity, but the exponent depends on material or coating. Compared to pure metals, coatings have more erosion rate at higher velocity range. In other words, coatings can perform better in lower velocity range or low head turbines. In some cases, such as in PP9 M2, this exponent value is less than 2. This could be due to low weight loss of specimen compared to precision of weighing scale. Since velocity can not be increased from certain limit in this test rig, higher magnitude of weight loss can be obtained by increasing weight of striking particles and minimizing uncertainties of weight measurement.

The overall values of erosion rates for ceramic-metallic coatings are quite low compared to stainless steel. The erosion resistances of these coatings are better in lower velocity range. The erosion of coatings accelerates once damage initiates. The ceramics are showing higher exponent value of velocity for erosion rate compared to stainless steels. Among tested coating, tungsten carbide coating is better than chromium carbide coating with respect sand erosion. This difference could be because Cr3C2-based coatings are not as hard as WC-based coatings. There is also large area rich in metal phase which reduces erosion rate. The coatings with smaller particles size give better erosion resistance. Berget (2000) also observed similar trend in rotating disc and rotating cylinder apparatus. The polished or ground ceramic-metallic coatings have better erosion resistance than as sprayed coatings but polishing the coated component in hydraulic turbine is expensive.
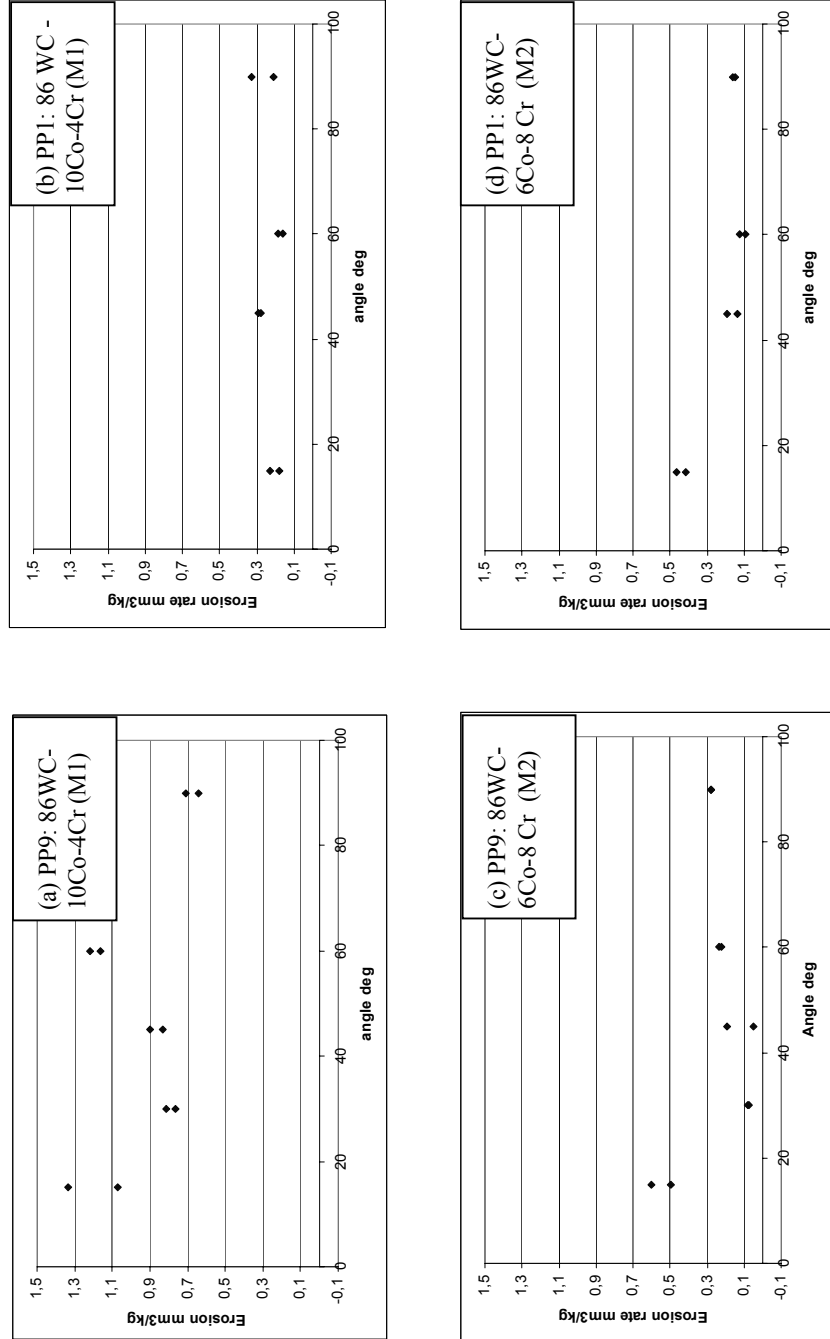
Figure 8.6.5 Continued

(f) PP1: 75Cr_3C_2-25NiCr (M3)
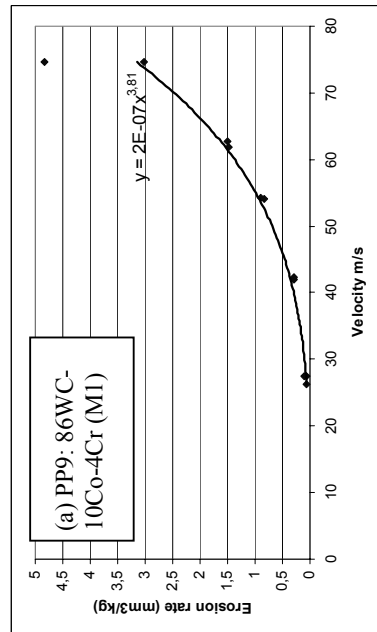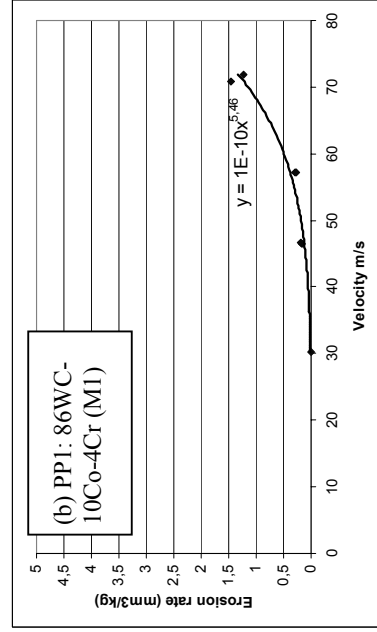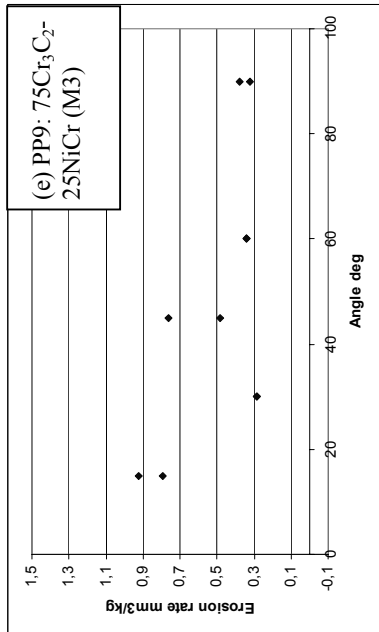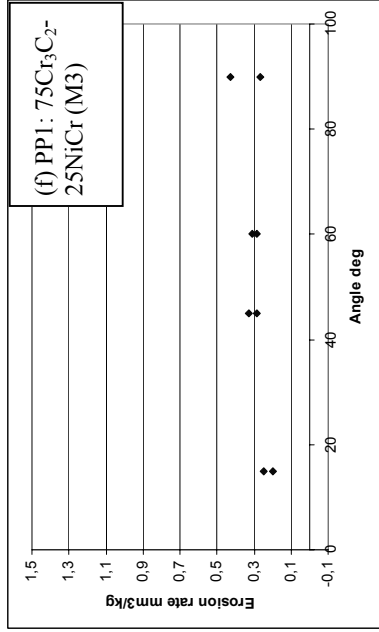
(e) PP9: 75Cr_3C_2-25NiCr (M3)

Figure 8.6.5 (a-f) Relationship between erosion rate and impingement angle for ceramic metallic coatings by different coating companies (PP1 and PP9) tested with Baskarp-15 sand at 55 m/s jet velocity

(b) PP1: 86WC-10Co-4Cr (M1)

$y = 1E\text{-}10x^{5.46}$

(a) PP9: 86WC-10Co-4Cr (M1)

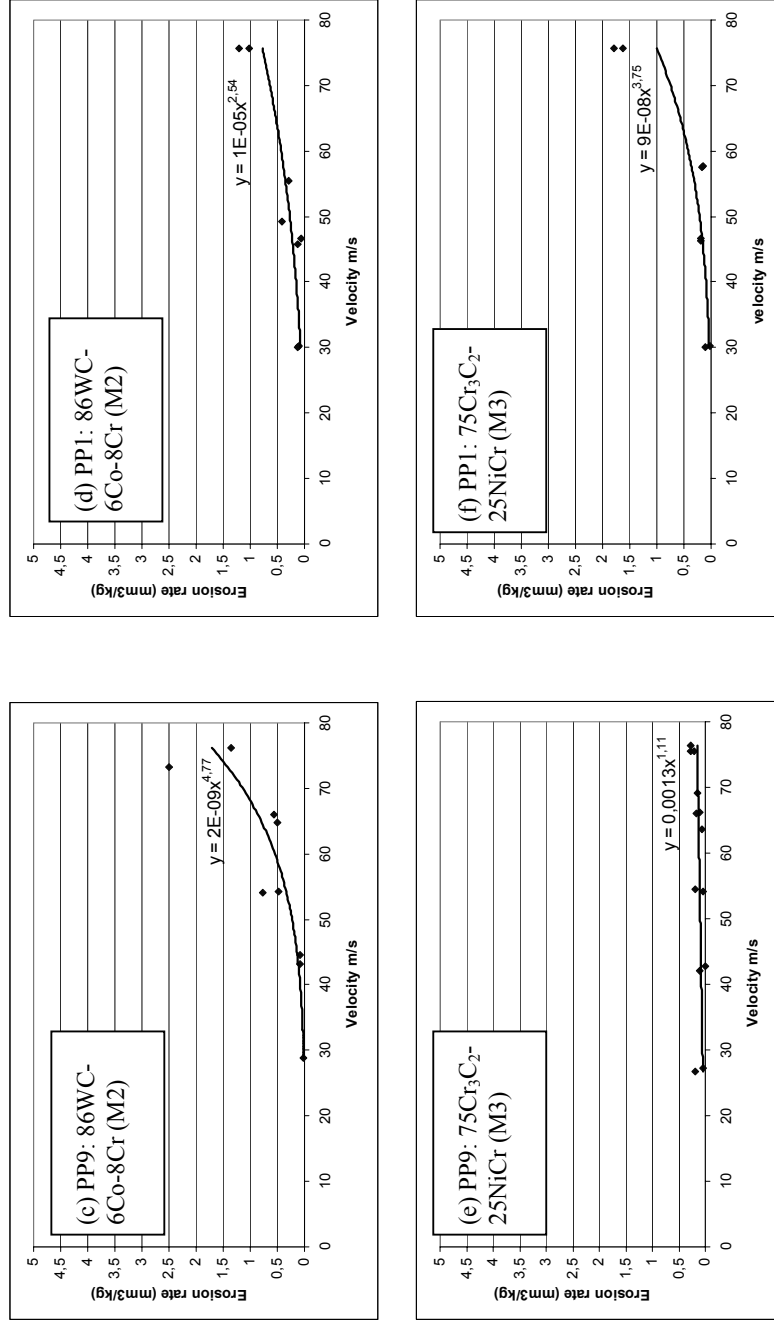$y = 2E\text{-}07x^{3.81}$

Figure 8.6.6 Continued

Figure 8.6.6 (a-f) Relationship between erosion rate and velocity for ceramic metallic coatings by different coating companies (PP1 and PP9) tested with Baskarp-15 sand at 45° impingement angle

Figure 8.6.7 (Continued)

(e) GES#2

$y = 0,001x^{2,25}$
$R^2 = 0,35$

(h) GES#4

$y = 0,0001x^{2,70}$
$R^2 = 0,78$

(e) GES#2

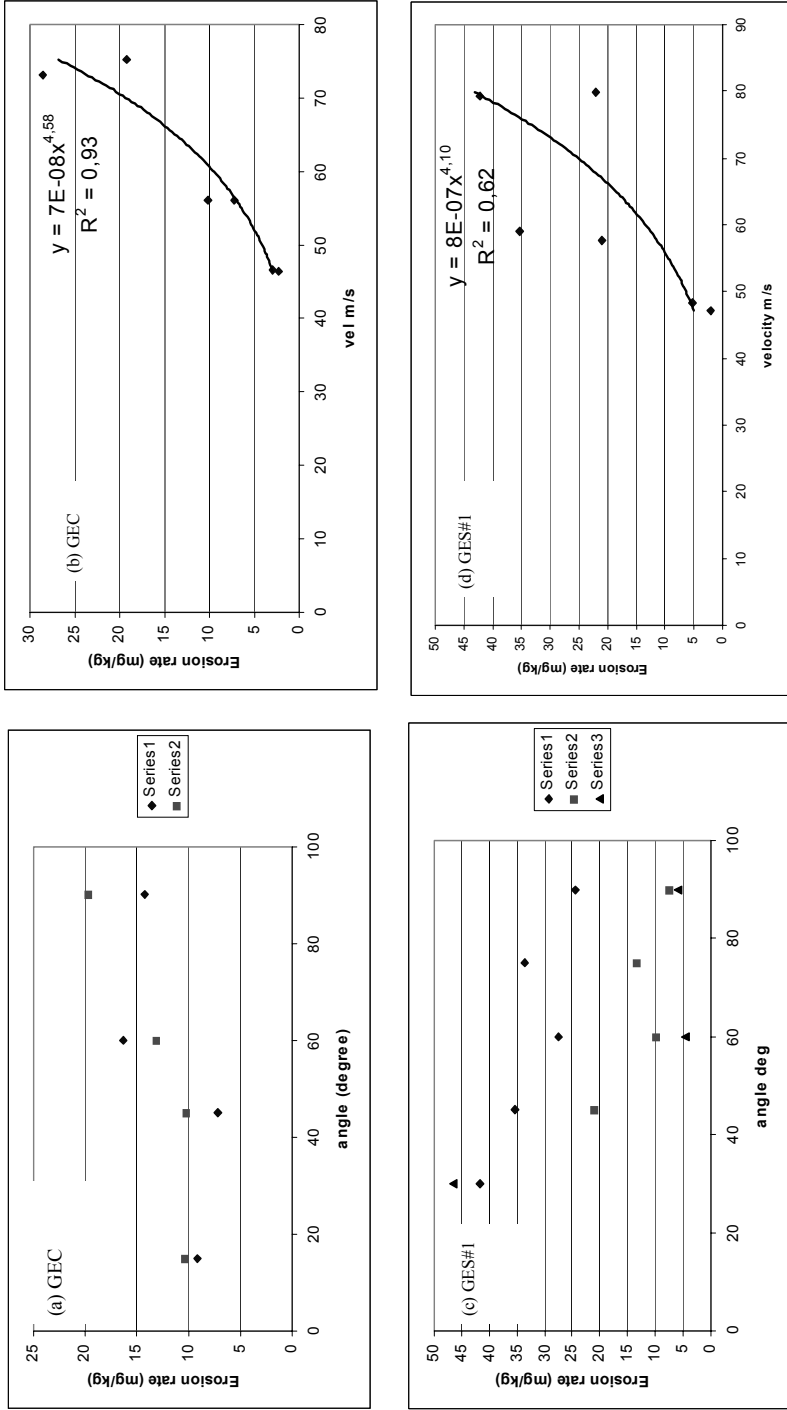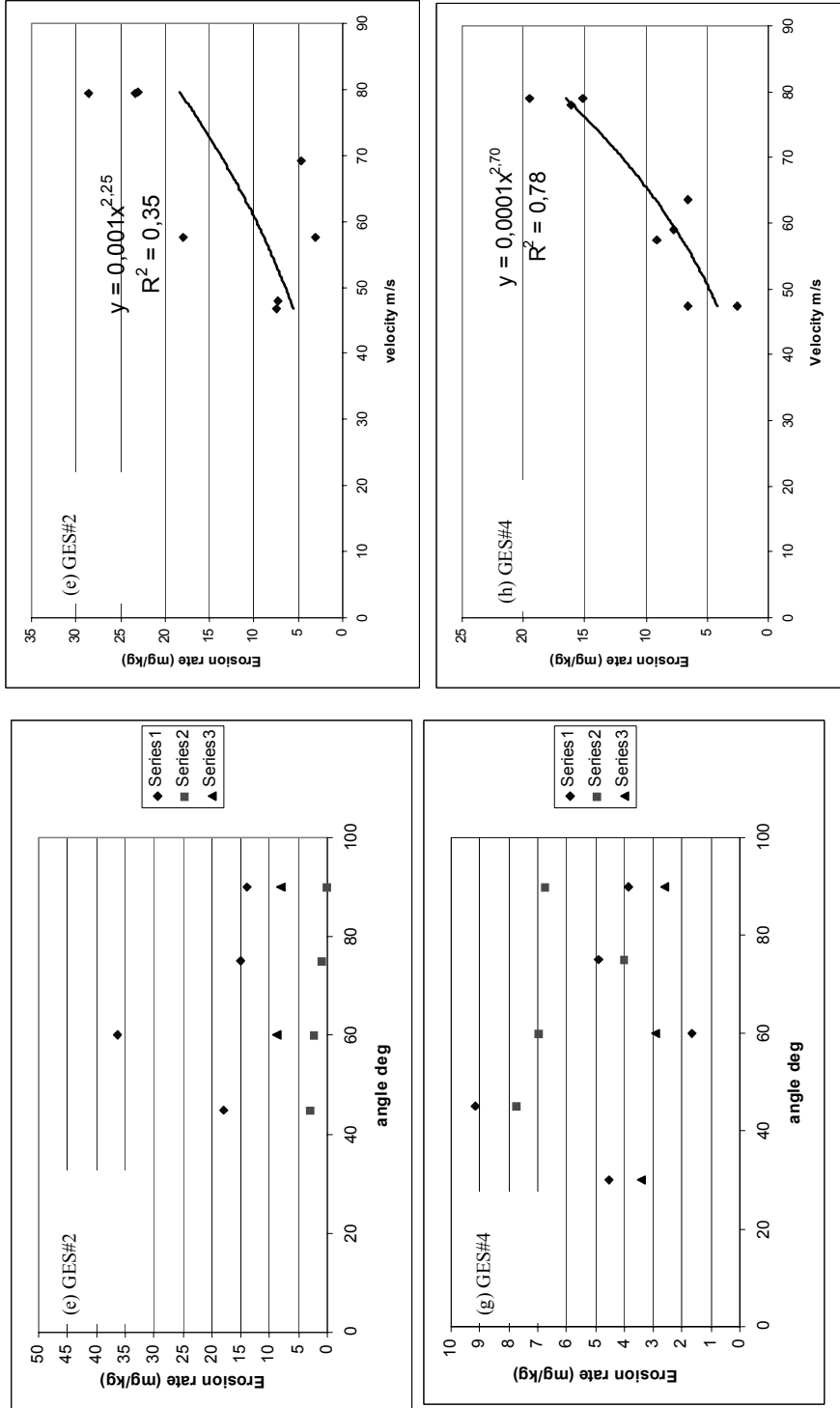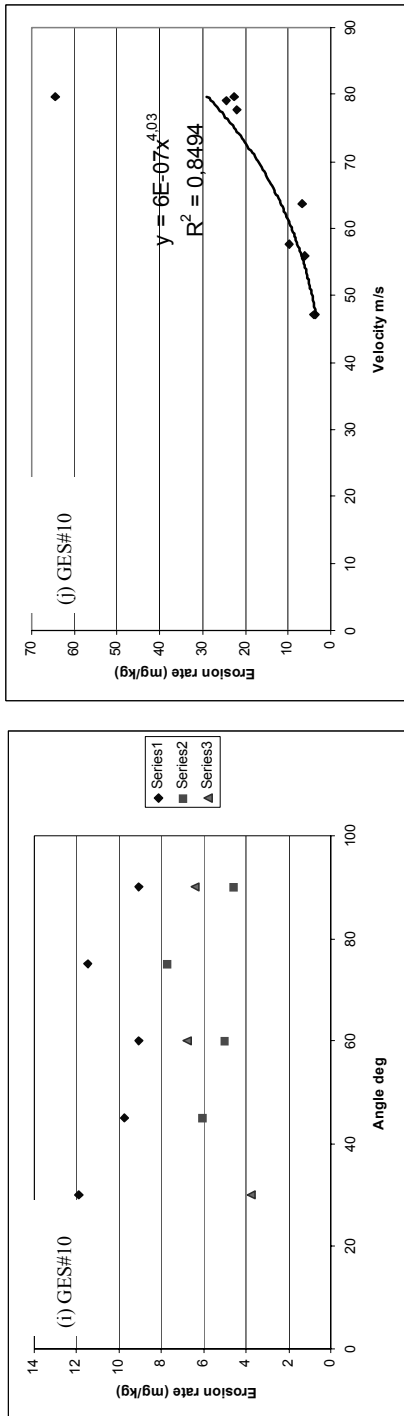(g) GES#4

Figure 8.6.7 (Continued)

Figure 8.6.7 Erosion rate of unpolished coatings (Effect of impact angles on 57 m/s and effect of velocity at 45 degree)

8.7 Erosion of elastomer coatings

The elastomer coatings with high ductility are believed to show better erosion resistance because of their ability to absorb particle impact energy. With this assumption two elastomer coatings supplied by one of the leading turbine manufacturer were tested. The specimens are tested at jet velocity 50 m/s with 1500 gm of Baskarp-15 sand particles at 90° and 45°impingement angles. On contrary to the original assumption, both the coating have performed very poor. The extent of damage is so high that it is not possible to report the erosion rate. The damaged elastomer specimens are shown in figure 8.7.1.
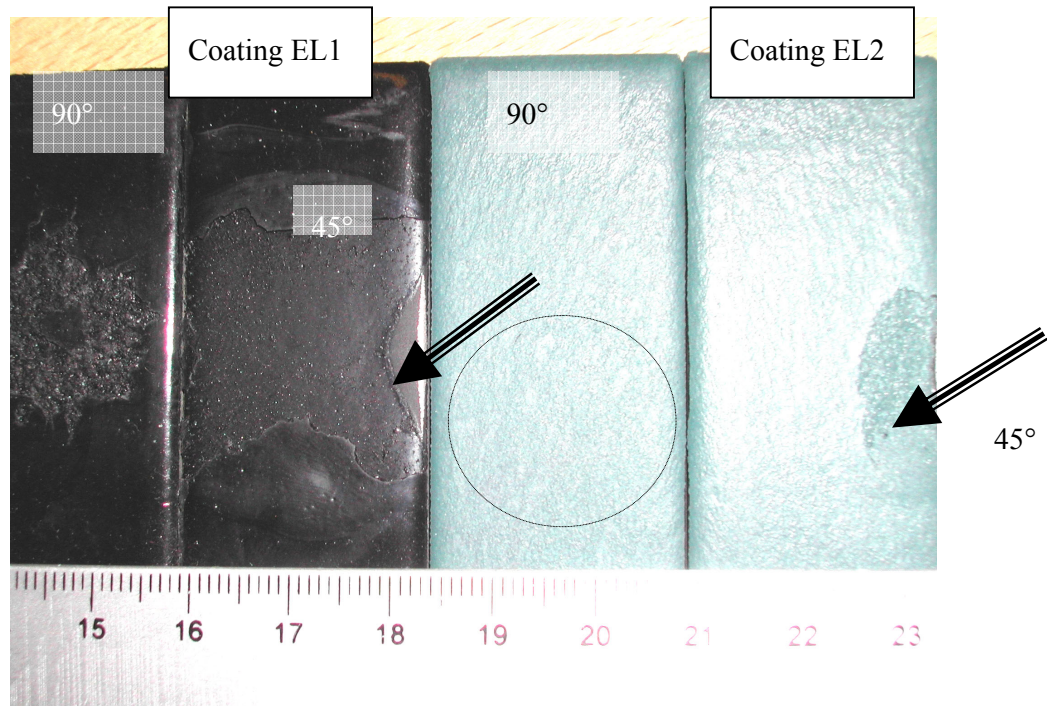

Figure 8.7.1 Damage of elastomer coating by high velocity jet of water and sand particles

The coating EL2 have shown better performance compared to EL1. But with the extent of the damage observed in this research, these types of elastomer coatings are not recommended for the operating conditions like hydraulic turbines. Because actual operating conditions at hydraulic machinery are much more complex than the laboratory test.

However, both types of coatings have shown slightly better erosion resistance at normal impingement. This is a indication of some sort of cushioning ability for striking particles. On the other hand, both the elastomer have shown very low tearing strength as observed in tests at 45° impact angle. The exposed area in black specimen (EL1) at 45° reveals different erosion properties at different layers (Figure 8.7.1). The outer layer of coating is separated from the inner layer up to large area. The appearance of eroded area of black specimen at

normal impingement is like pitting or failure by fatigue. Rather than getting erosion rate on these elastomer coatings, the observation from these tests can be used to explain the profile and nature of damage.

At low impingement angle, the removal of polymer coating is in the form of elongated-type craters or cavities, whereas for higher angles it is more like fatigue effect. Arnold and Hutchings (1990) have also observed failure of rubber specimens by fatigue process in their study. Zahavi et al. (1981) found decrease in erosion rate with increasing impingement angle for hard polyurethane, elastomeric polyurethane and fluorocarbon, but the erosion rate was almost independent of mass of striking particles. Although these coatings have shown ductile mode of erosion with maximum value at $30°$ and minimum at normal impingement, the values lower than $30°$ are not available. At lower impingement angle, the coatings can easily tear away or bonding with substrate will breakup easily if jet reaches interface. Zahavi et al. (1981) further described the erosion of polymer coatings in following stages:

1. the formation of local micro cracks
2. progression and intersection of micro cracks resulting the formation of fragments of coatings
3. detachment of these coatings from substrates
4. final removal of fragments from locally eroded area

The erosion test on polymer coatings some time even show gain in weight due to embedding of particles in the target surface. Hence actual measurement of weight loss is challenging in the case of soft coatings.

8.8 Erosion of curved surface

The erosion tests on curved surfaces were carried out to simulate the erosion on Pelton bucket and to study the effect of particle separation because of acceleration of particles normal to the surface.

The results from erosion tests on curved surfaces are presented in the form of erosion rate for different profiles and surface roughness at different locations. Together with weight measurement, surface roughness is measured by Mitutoyo surface roughness tester. The shape, profile and identification code for specimen are shown in figure 7.5.5.

The visual observation of the eroded specimen revealed that most of the coarse grains (Sand-25) strike close to the splitter. The effect of fine sand (Baskarp-15) is observed up to far away from splitter. The extent of deformation at splitter is observed more by coarse particles compared to fine ones. The erosion rate in term of weight loss per unit striking particle is found smaller with fine particles. This may be because, some of the fine particles are expected to escape without striking the specimen.

The nature of damage by different size particles are illustrated by monitoring the roughness at different locations in the curved surface of specimens. The plot of roughness over curved surface shows that coarser particles will have more effect close to the area of strike. The roughness produced in the specimens of different curvature size by small particles

(Baskarp-15) and bigger particles (Sand-25) are presented in figures 8.8.1 and 8.8.2. In figures 8.8.1 (a) and 8.8.2 (a), single peak is observed at the centre of the specimen (splitter) due to bigger particles (Sand-25). Smaller particle (Baskarp-15) have shown two peaks in specimen R20 (figure 8.8.2c), but for specimen R15, the roughness is skewed (figure 8.8.1c) due to misalignment of specimen with respect to jet. The damage by fine sand has shown more damage on bottom of each curvature. This observation is in line with the study of Lynn (1991) on collision efficiency and Tabakoff (1992) on erosion of steam turbine of different size fly ash. They have also observed that smaller particles will glide and follow streamlines.

The roughness measurements for the specimens with larger curvature and other non-symmetric profile (RW and RV) have shown different results compared to symmetric radius curvature (figure 8.8.3). The roughness of all the specimens has increased close to the area of strike, but the roughness of area far away from point of direct strike have not increased much compared to smaller curvature. There are no distinct two peaks even with finer sand (figure 8.8.3 b and h). But overall roughness is less in all cases compared to specimen with uniform radius. This could be due to gliding of the particles following the surface of larger curvature.
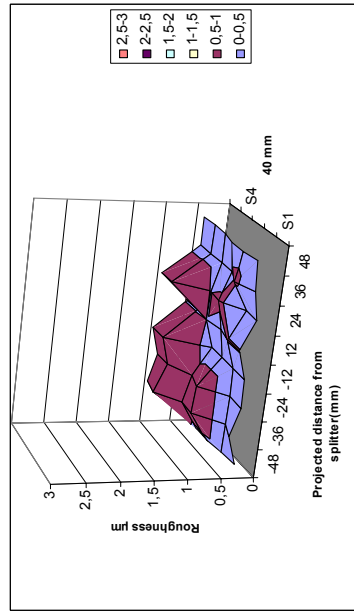
(b) R15 – before test
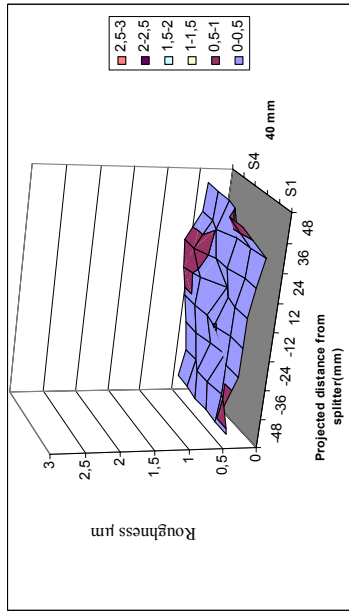
(d) R15 – before test
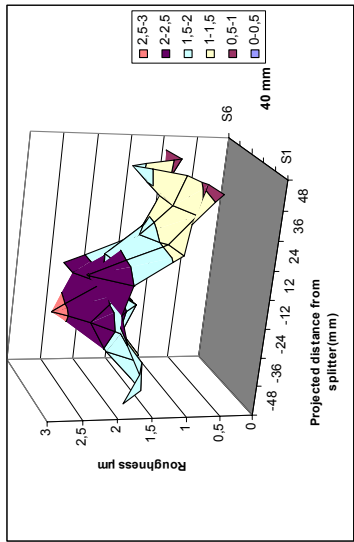
(a) R15 – after test by Sand-25
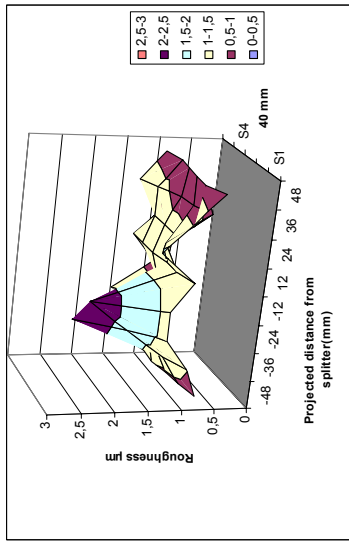
(c) R15 – after test Baskarp-15

Figure 8.8.1 Roughness created by particles in curved aluminum surface R15, by 750 gm particles at approximately 55 m/s jet velocity
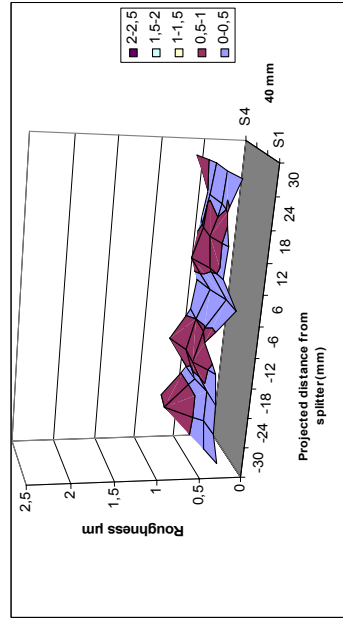
(a) R20 – after test by Sand-25

(b) R20 – before test

(c) R20 – after test by Baskarp-15
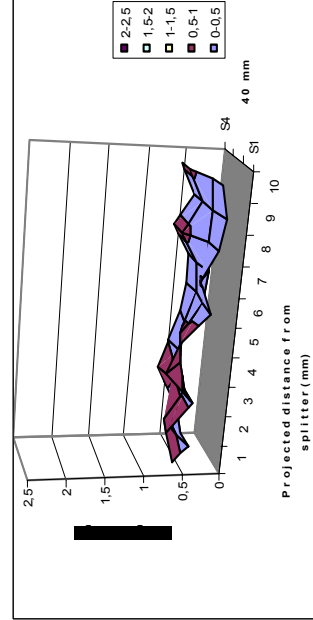
(d) R20 – before test

Figure 8.8.2 Roughness created by particles in curved aluminum surface R20, by 750 gm particles at approximately 55 m/s jet velocity
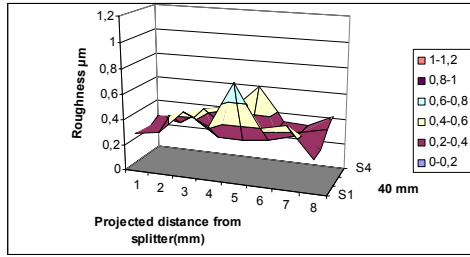
(a) RV – before test
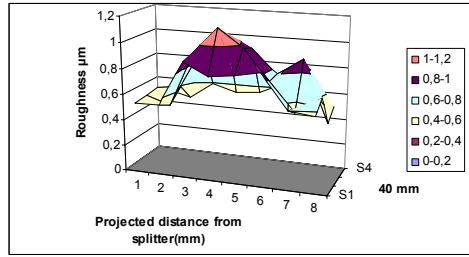
(b) RV – after test by Baskarp-15
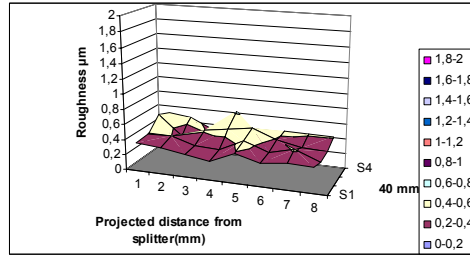
(c) RV – before test
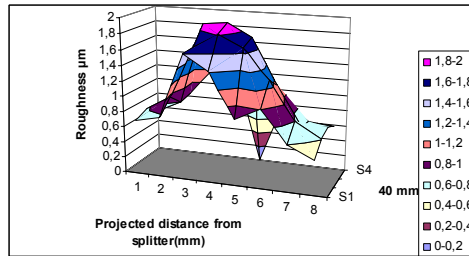
(d) RV – after test by Sand-25
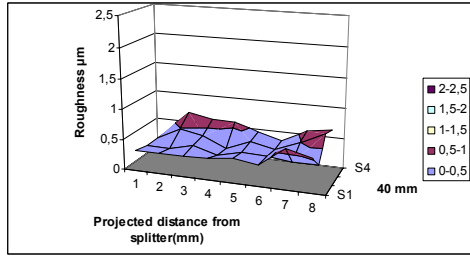
(e) RW – before test
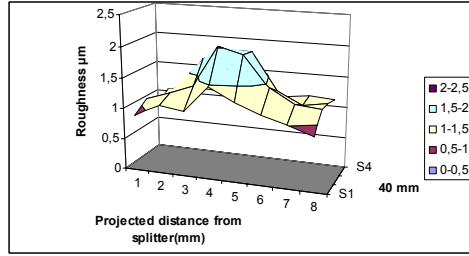
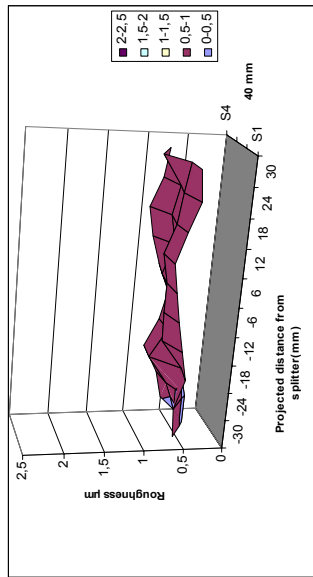(f) RW – after test by Sand-25
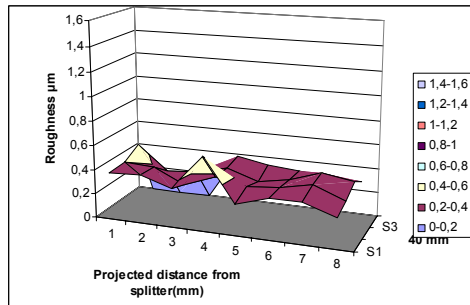
(g) RW – before test
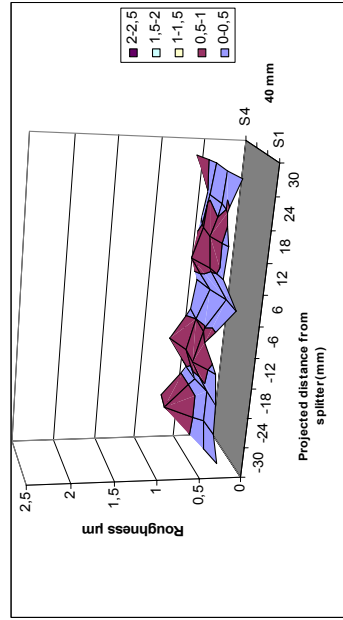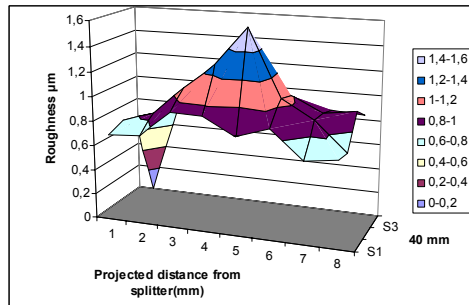
(h) RW – after test by Baskarp-15

Figure 8..8.3 Roughness created by particles in irregular curved aluminum surface
RV and RW, by 750 gm particles at approximately 55 m/s jet velocity

The average roughness of the curved specimens in the direction of flow at the location of jet strike is shown in figure 8.8.4 and 8.8.5. Highest roughness is at the centre or location of direct strike and roughness magnitude decreases away from the point of strike. Compared to bigger particles, the roughness made by smaller particles are almost uniform all along the exposed length (figure 8.8.4). In most of the cases the ratio of lowest roughness magnitude to highest magnitude is almost double. Specimens tested with bigger particles (Sand-25) have highest roughness ratio compared to specimen tested with fine sand (Baskarp-15).
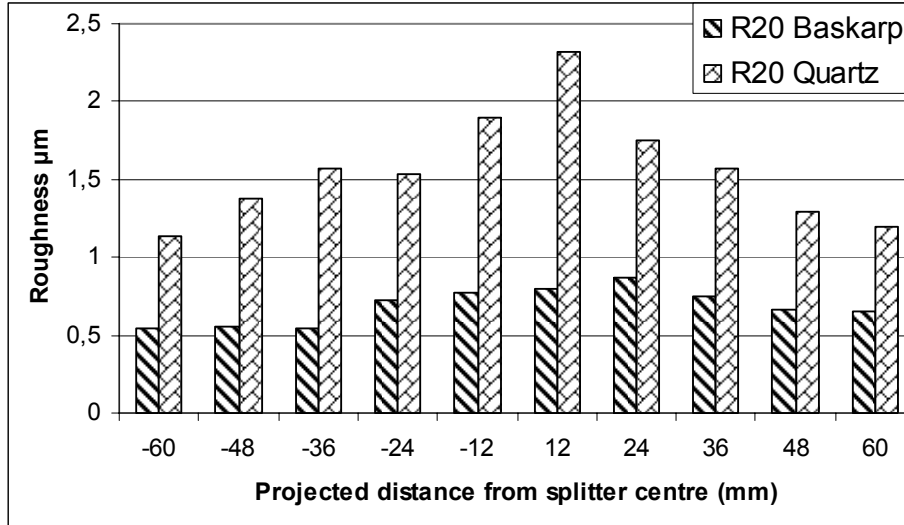
Figure 8.8.4 Roughness along the flow direction in regular curvatures (R20) at approximately 55 m/s jet velocity
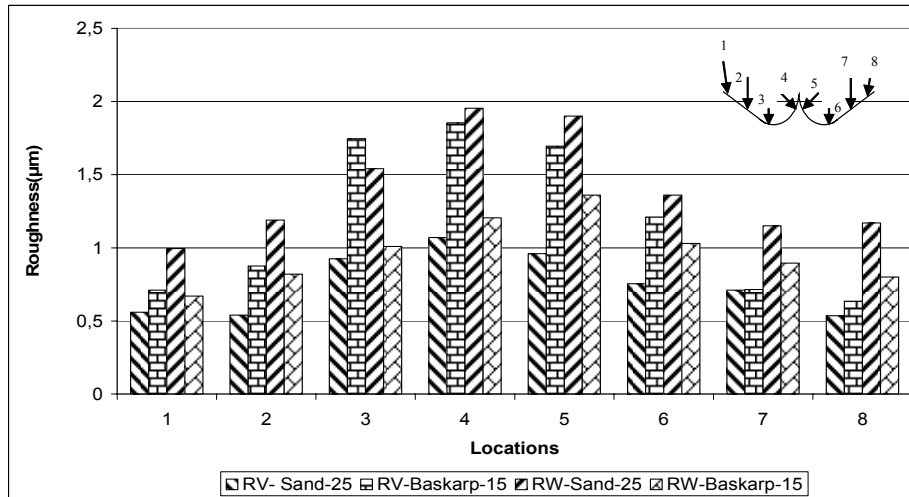
Figure 8.8.5 Roughness along the flow direction in irregular curvatures (RV, RW) at approximately 55 m/s jet velocity

Figure 8.8.6 shows the erosion rate of regular curved specimens. Erosion rate in term of mg/kg is found to increase with increase in radius of curvature. This observation is opposite to the general experience and belief, that larger the curvature less will be the erosion (Brekke, 2002). This may be because the area of exposure in specimen with larger radius is higher than smaller curvature. Hence probability of particles repeatedly striking or sliding in the same specimen is more in larger radius specimen. The ranking of erosion rate changes if erosion rate is presented taking exposed length in to account. Figure 8.8.6 (b) shows erosion rate in terms of exposed length (mg/kg/mm). But this form of presentation does not show exactly opposite trend or logical trend according to radius dimension. This observation has practical significance; otherwise flat surface would have shown no erosion even if we observe erosion in actual practice.
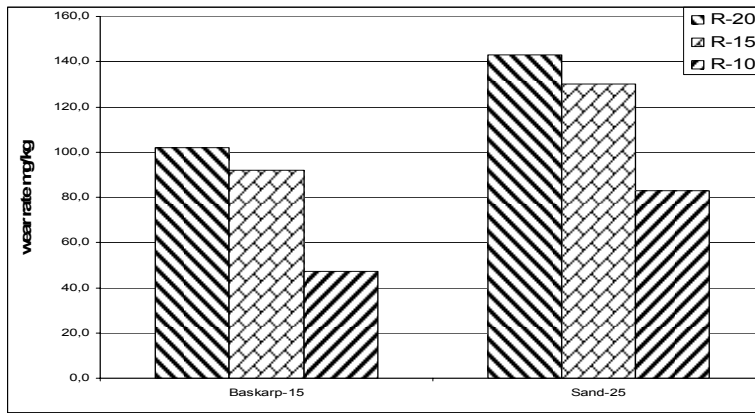
(a) Erosion rate of curved specimen in terms of mg/kg
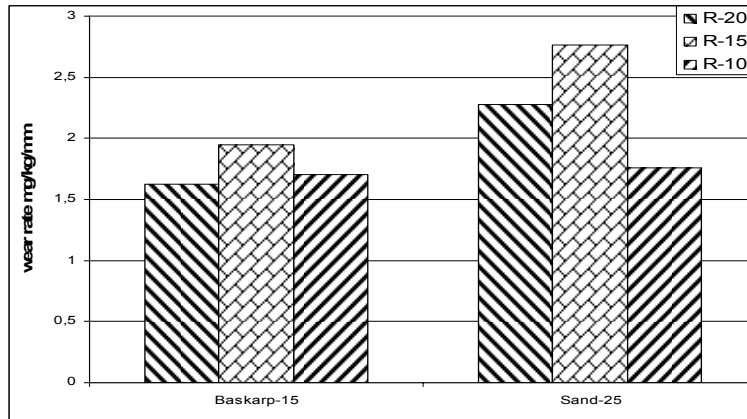
(b) Erosion rate of curved specimen in terms of mg/kg/mm

Figure 8.8.6 Difference in ranking of erosion rate of different curvature specimen with and without considering exposure length (750 mg Baskarp-15 sand and approximately 55 m/s jet velocity)

138

8.9 Erosion and surface roughness

The roughness of the specimens is related in two ways with respect to sand erosion. Firstly, surface roughness of the specimen changes due to erosion. The specimen surface becomes smoother due to sand erosion in macro level, while polished surfaces will become rougher in micro level. Hence there can be optimum level of surface finish in the case of hydraulic machinery operating in sand laden water. If the surface is highly polished to reduce the friction loss, the surface will damaged and become rough after a while. On the other hand, if certain level of surface roughness is allowed during machining, the erosion due to sand may maintain the optimum surface condition, which may save the manufacturing or finishing cost of the components. Secondly, the erosion rate of the specimen may change at different roughness level. At micro level, the impingement angle of the striking particles could be different than the one we observe due to asperities and orientation of surface. The resistance to deformation or material removal may also change due to difference in effective sections which are likely to fail. Such rough area may act as cavitation inducer in the high velocity region. The orientation of roughness layout could also have some effect in both hydraulic performance and material strength. The resistance to flow is expected in the fluid flow through rough surface, but Karimi and Schmid (1992) did not find any significant temperature rise when fluid is flowing through surface with erosion ripples.

The inter-relationship between erosion and surface roughness are discussed in the following sections.

Erosion rate based on surface condition

The study of the interaction between surface roughness and sand erosion are studied on aluminum specimens because of smaller test duration and their added effect on each other. The specimens with different roughness are prepared with the help of sand paper. Majority of the tests for this purpose are carried out at approximately 60 m/s jet velocity by 750 gm of Baskarp-15 sand particles.

The variation of erosion rate with respect to angle of impingement for roughness orientation parallel and perpendicular with respect to jet are shown in figure 8.9.1 a and b. The curve for perpendicular orientation (figure 8.9.1 b) is almost similar to that with the curve of smooth surface as shown in figure 8.1.1. Although the plots for erosion versus angle in the case of jet parallel to roughness orientation shows slightly different behavior, with the uncertainties that may come across in these tests, it can be concluded that there is no significant difference in erosion on rough and smooth surfaces.
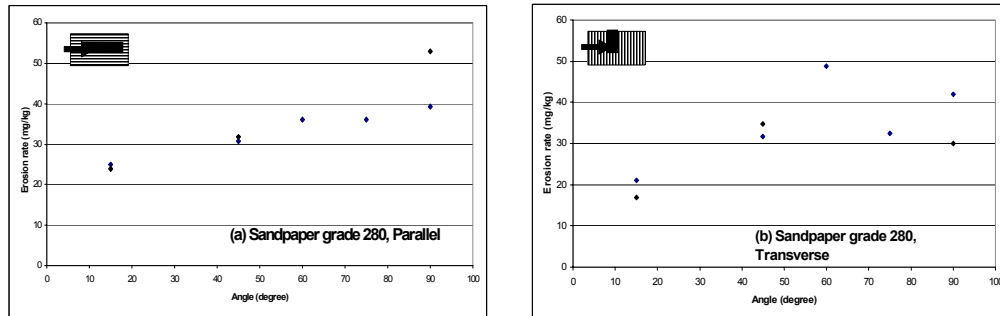
Figure 8.9.1 Erosion rate vs angle 280 grade (a) parallel (b) perpendicular

Figures 8.9.2 (a-f) shows the relationship between erosion rate for specimen of different roughness created by different grade sand papers in parallel and perpendicular orientations. There is no significant difference in experimental results for different operating condition compared to the uncertainties present in the tests on aluminum specimens. The uncertainties in these tests are the non-uniformities of the specimens in term of surface quality. Apart from this, the effect of secondary flow and probable cavitation pitting on the back side of specimen may have significant effect on spread of data.

There is not a large difference in erosion rate for the tests at 45° and 15° impact angles with roughness grooves in parallel or normal to the direction of jet (figure 8.9.2 e,f). For normal impingement condition, the orientation of roughness should not have any effect on erosion rate, but slight variations of the erosion rate are observed. This also shows that, more than effect of roughness, other parameters of uncertainties are playing a role on these tests.

There will definitely be some effect on erosion rate of surfaces with different roughness, but to discover the actual effect of roughness on erosion, the uncertainties on specimen material property and other effects like cavitation should be avoided and surface roughness should be prepared with uniform magnitude. The machine grinding with different size grinder on steel specimens may avoid such uncertainties.

Surface roughness of the eroded surface

The surface roughness of the specimen was measured to find out the effect of the hitting of particles on surface. As mentioned above, eroded surface are rougher at micro level and this increase in roughness may increase the erosion rate. The roughness of specimen due to erosion is dependent on hardness of particle and substrate together with the shape and size of particles.

The roughness of the surface at the point of hitting by 45° impact angle jet (figure 8.9.3) has increased up to 5 to 7 times for 16Cr5Ni specimens. Similar trend can be seen in other operating conditions as well. The roughness of specimens ground with the sand paper of 280 grit size before test was measured about 0.2 micrometer. The roughness created by large particles (Sand-25) is greater than that with smaller particles (Al oxide) as shown in figure 8.9.4.   The increase in roughness intensity is higher around the area of strike

compared to remote distance. But the overall roughness is found to increase in all the exposed area. The higher roughness intensity is localized to the area close to the striking point at 90° impingement angle, whereas for 45°; it spreads to larger area (Figure 8.9.5). Figure 8.9.3 (a) also indicates the annular ring around the point of strike similar to figure 8.7.1 at normal impact. Similarly, the intensity of roughness is localized in the case of particles with bigger size compared to small size particles as in case of graph of sand-25 and aluminum oxide as seen in figure 8.9.4. On the other hand, the highest value of roughness due to erosion with same particles is almost same for 45° and 90° impingement angles as seen in figures 8.9.5, 8.9.6 and 8.9.7.
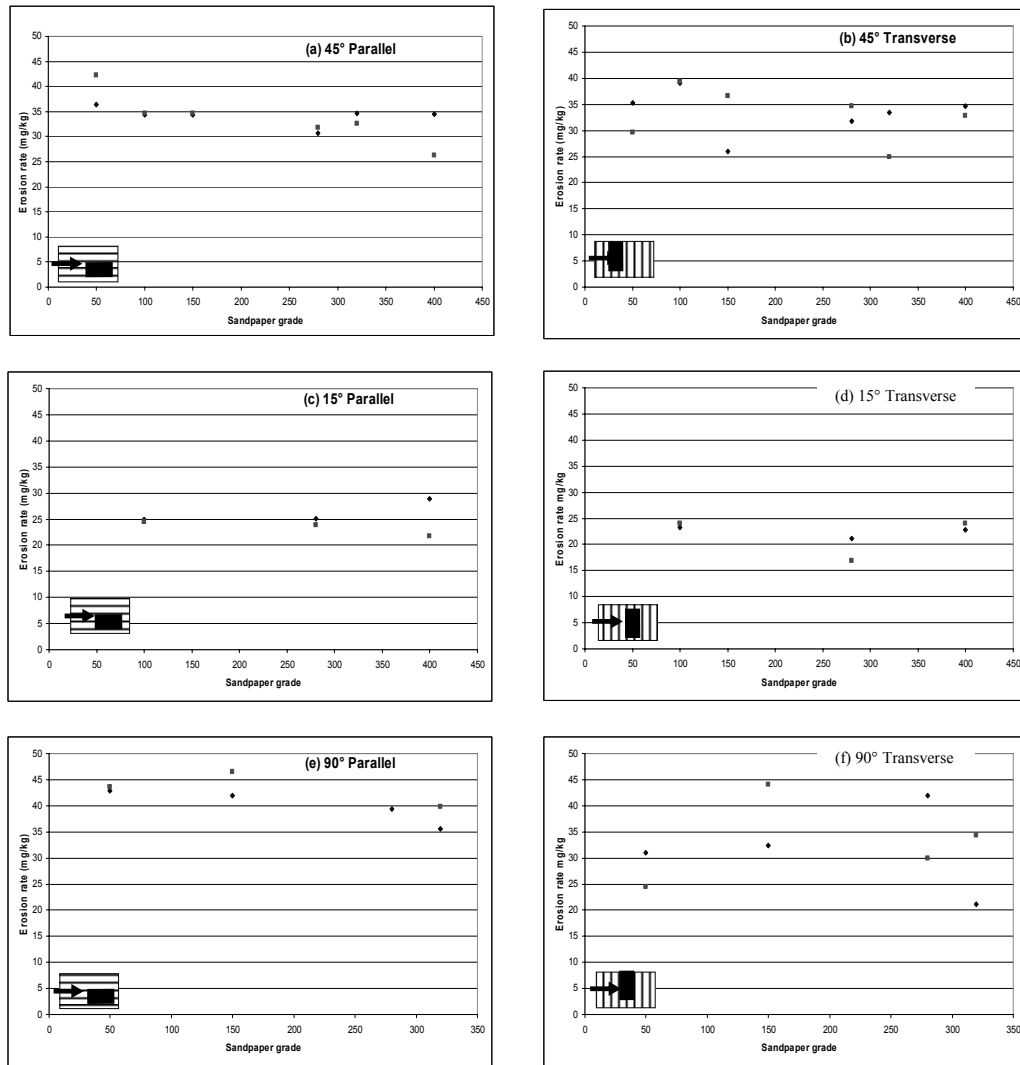
Figure 8.9.2 Effect of roughness in erosion rate at different operating conditions

Aluminum specimens have shown almost double roughness intensity compared to 16Cr5Ni at similar operating conditions. Hence, it can be concluded that the roughness as well as erosion rate depends on the hardness and ductility of the material. Similarly the roughness due to the larger particles (Sand-25) is higher compared smaller particle (Baskarp-15) as shown in figure 8.9.6 and 8.9.7.

Normally, the tungsten carbide coatings are not ground in the turbine components after they are sprayed. There may be higher friction loss in case of coated surface compared to ground surface. The roughness of the coatings depends on powder properties and spray parameters such as particle size, temperature and velocity of spray. There could be more of plowing effect in the WC coatings compared to cutting effect because of the rougher surface. The unpolished WC coating (GEC) used in this test have shown very high surface roughness(figure 8.9.8 a), almost about 10 times compared to polished coatings PP 9 M2 after the test (figure 8.9.8 b) which has shown the behavior somewhat similar to 16Cr5Ni steels (figure 8.9.5 a).

At low impact angles, Zahavi and Schmitt (1981) found higher surface roughness value for polymer coatings together with high erosion rate. They also revealed through microscopic observation that high erosion rate in higher roughness is due to local removal of material and detachment of pieces of coatings. They also found the low surface roughness and low erosion rate at higher impingement angle.

The measurements on eroded Pelton bucket have shown large variation of roughness such as 24 μm to 72 μm at the back side near to the outlet edge. The roughness in the eroded areas of splitter was about 32 μm to 37 μm and at the middle of the inner surface of bucket was about 51 μm to 56 μm, whereas non-eroded surface toward inner surface of outlet edge is about 16 μm to 21 μm. The heavily eroded surface of needle and surface with cavitation were so rough that, the roughness magnitude was out of the range of instrument (Thapa and Skåre, 2002). In the laboratory tests, the magnitude of the roughness is not high as compared to actual turbine erosion, which may be due to larger size of particles in this particular power plant and may be even due to large quantity of the particles hitting the surface. Moreover, the difference in roughness level in the area of strike and surrounding area reveal the importance of roughness level for monitoring the extent of erosion damage in the turbine.
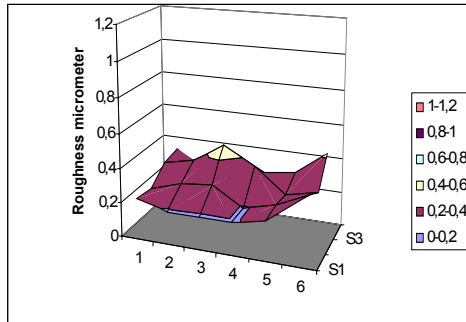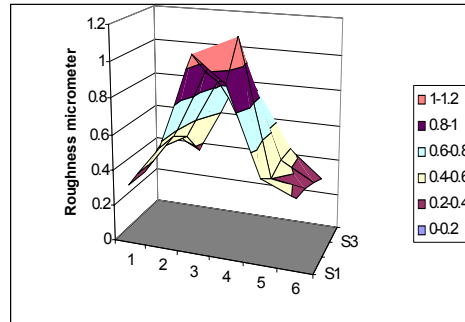
(a) Before test   (a) After test

Figure 8.9.3 The 16Cr5Ni steel specimen tested by Sand-25 particles at 90° impact angle and 50 m/s jet velocity
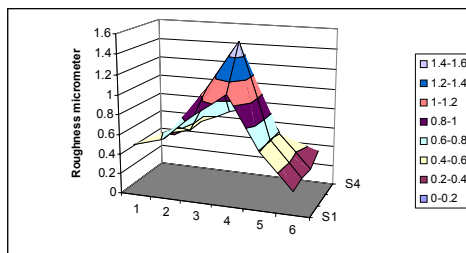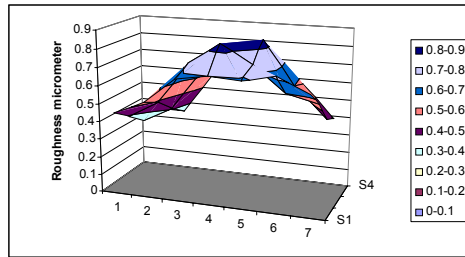
(a) Sand-25 particle   (b) Aluminum oxide particles

Figure 8.9.4 The 16Cr5Ni steel specimen after test by (a) sand-25 and (b) aluminum oxide particles at 45° impact angle and 50 m/s jet velocity
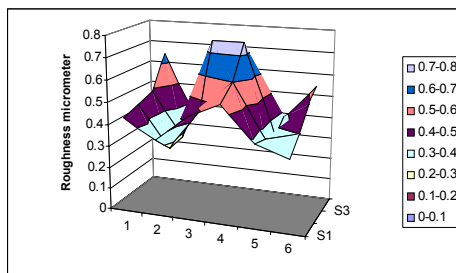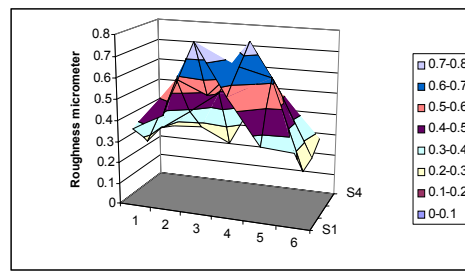
(a) 90° Impingement   (b) 45° Impingement

Figure 8.9.5 The 16Cr5Ni steel specimen after test by Baskarp-15 sand particles at 90° and 45° and 50 m/s jet velocity
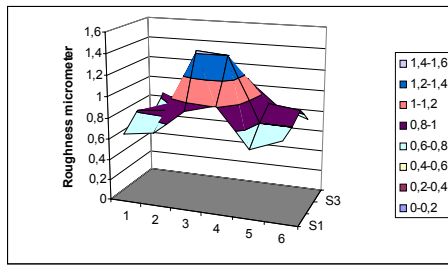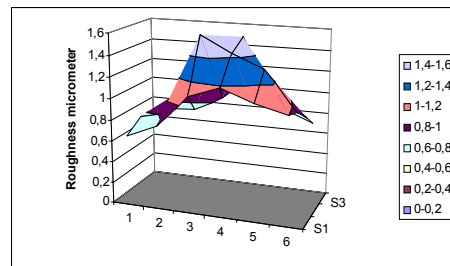
(a) 90° Impingement angle   (b) 45°Impingement angle

Figure 8.9.6 Aluminum specimen after test by Baskarp 15 sand particles at 90° and 45° and 50 m/s jet velocity
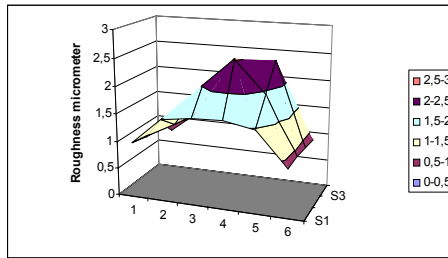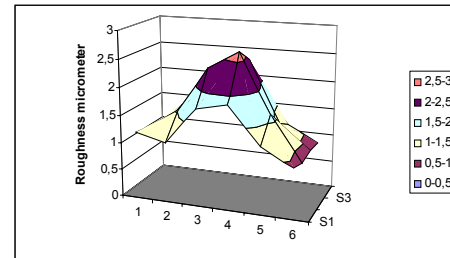
(a) 90° Impingement angle   (b) 45°Impingement angle

Figure 8.9.7 Aluminum specimen after test by Sand-25 particles at 90° and 45° and 50 m/s jet velocity
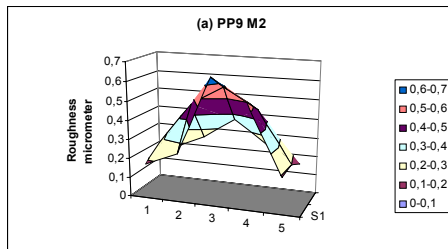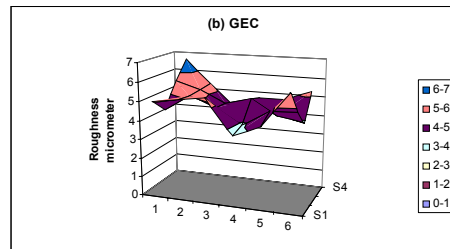
Figure 8.9.8 Coating tests with Baskarp-15 sand at 45° and 50 m/s jet velocity

8.10 Erosion on pre-stressed surface

The failure of material depends upon the stresses induced due to force. Therefore flow driven erosion of material could also depend on pre-stressing of material because the failure mechanism of erosion is also due to elastic or plastic deformation as described in section 3.2. Hydraulic machinery components, such as Francis runners, guide vanes, spiral casing;

Pelton buckets, manifold and deflectors are highly stressed and affected by sand erosion. The main source of high stresses in the turbine components are operating condition for instance high pressure and high rotational speed. On the other hand, stresses can also be residuals from production process, welding repairs and other similar activities. The reliability of the component and human safety can be greatly influenced by the erosion of the component, besides its effect on performance. When engineering practices demand higher stress levels in the machinery in order to reduce production costs or optimization of hydraulic performance, increased erosion susceptibility might be one of effective limitations for such a philosophy, which is not investigated to a great extent.

The clamping system of the high velocity erosion test rig is redesigned to have four point bending effect in the specimen and tests were carried out with the primary hypothesis that pre-stressing simply reduces threshold limit for which impacting particles have a damaging effect. But after few preliminary tests, no significant and logical effect was observed in the erosion test of specimens with pre-stressing. The results of erosion tests at velocity 55 m/s with 1500 gm of particles carried out on aluminum and austenitic steel AISI 316 stressed in 4 point bending clamp are presented in figure 8.10.1. The reduction in erosion rate was observed for stressed samples for both 45° and 90° impingement angles for austenitic steel samples, whereas for aluminum samples no uniform trend was observed. The difference in the erosion rate for aluminum for stressed and unstressed condition at 90° is negligible, where as in other cases these differences are slightly large.

On contrary to the initial belief, most of the tests showed decrease in erosion rate for stressed specimen compared to unstressed as shown in figure 8.10.1. The reason for decreasing the erosion rate on stressed specimens could be due to self hardening of surface layer during bending. Apart from this, the actual stress induced in the specimen at four point bending clamp also depends on the pre-stressing of the specimen during rolling of the plates. Both the aluminum and austenitic steel specimens are rolled plates and during rolling, the plates will have residual stresses such as compressive residual stress on the surface and tensile residual stress in the middle of the plate. Hence, all the erosion experiments carried out on rolled plate specimen may have initial compressive stress up to the certain thickness and instead, four points bending of the specimen may have neutralized this pre-stressing. The residual stresses are also caused by production and maintenance process such as surface grinding and welding. The weld pool contracts during welding and this contraction is restricted by rest of the plates which are not melted. As a result, tensile stress is generated in the weld and this is balanced by compressive stress in the parent material. The rolling and grinding may have similar residual stresses. Typical stress distributions for welding and grinding processes are shown in figures 8.10.2 (a) and (b). Such residual stress may effect in cracking of brittle material and may not have significant effect in ductile material.

No specific conclusion can be drawn from these tests on 4 point bend specimen on high velocity jet erosion test rig. But erosion test on specimen surface pre-stressed with shot peen or electrical spark may give some indication on effect of erosion on pre-stress or residual stress.
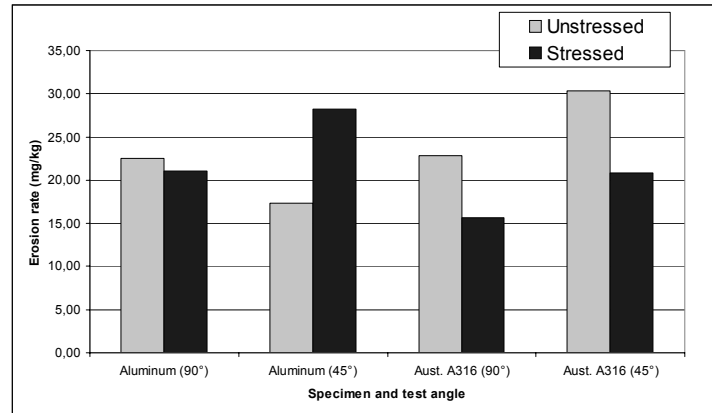
Figure 8.10.1 Erosion rate for stressed and unstressed materials

Even though the stresses on the components have not shown any significant effect on the erosion in laboratory test, it may have some relation with fracture mechanics. It is already discussed in previous section; erosion of brittle material is mainly due to cracking and fracture. The type or shape of the crack formed may depend on the shape of the striking particles. Chen and Li (2003) observed nature of erosion cracks by computer simulation of solid particle erosion of SiC target by sharp and round particles. Cracks were observed in both along and normal to the direction of load by triangular particles, among which crack prorogation in the direction of load is much higher. Radial cracks are observed by the erosion of spherical particle and they spread outwards from the periphery of the crack. The coalescence and merger of these cracks form lateral crack which propagates almost parallel to the surface. On contrary to the cracks by sharp particles, the median vertical crack propagation was very limited in round particles. The effect of crack and fracture mechanics in the design of hydraulic turbine is already discussed in section 4.2. Even though orientation of crack due to erosion is studied by Chen and Li (2003), the magnitude of the crack due to erosion is not found so far. Hence relationship between fracture mechanics and solid particle erosion has to be still investigated.
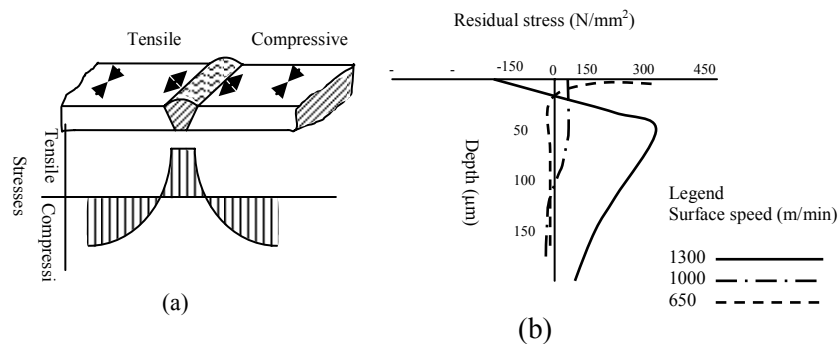
Figures 8.10.2 (a) Stress distribution in plate weld and (b) Residual stress after surface grinding (according to Ghosh and Mallik, 1986)

146

8.11 Effect of specimen and nozzle distance

The effect of distance between the nozzle exit and specimen is studied on austenitic steel AISI 316 with 1500 gm of Baskarp-15 particles at about 50 m/s jet velocity. It is expected that the jet velocity will be maximum at the nozzle exit and slowly reduces as it travel away from the nozzle due to fluid friction in the water pool and gravity. The tests were carried out at the interval of 15 mm in between distance 70 mm and 145 mm. The tests beyond 70 mm and 145 mm is not possible at existing setup due to restriction in sliding groove and interference of nozzle outer diameter with specimen at low impact angle. The erosion rate is presented for normalized positions (l/d), the ratio of length (l) to nozzle diameter (d). As expected, highest erosion rate is at minimum l/d=8.5 and lowest at maximum l/d=18. The erosion rate is found almost constant and equal in both 90° and 45° impingement angles in between l/d ratio 10 to 16. The erosion rate for 45° impingement angle is slightly higher compared to normal impingement in most of the cases. The difference in erosion rates for these two different impingement angles are more influential in lower l/d ratio compared to higher l/d ratio. At normal impingement, symmetric secondary flow can be expected in the water pool after the jet strikes the specimen whereas the secondary flow due to impingement in acute angle is skewed in one side of direction of jet.

The submerged water jet may create suction around the jet due to secondary flow and hence suspended particles may be pulled towards the jet and strike specimen. On the other hand, the skewed secondary flow in one side of the pool may destroy the jet strength. This could be the reason for up to 50% variation in erosion at l/d ratio 10.4 and 14. With the previous experience in this setup, most of the tests are carried out at l/d ratio 12.2, which is also a convenient distance for adjusting different impingement angles. Test at this position has shown only small variation of result in all impact angles.
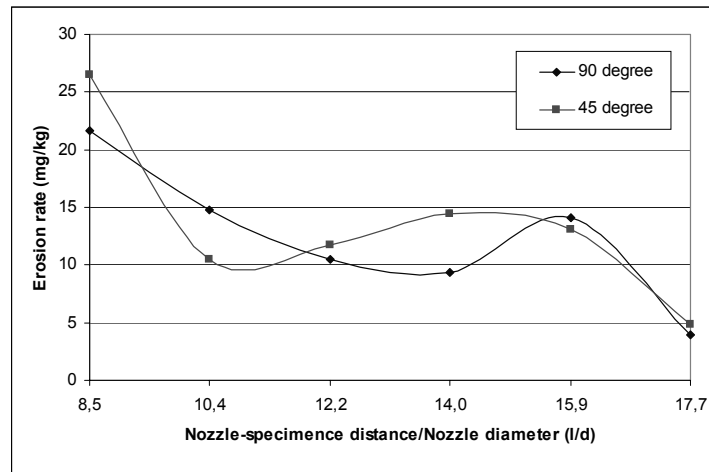
Figure 8.11.1 Erosion rate at different distance between nozzle exit and specimen

8.12 Discussion of test rig and its performance

The jet type of test rig used for this study was designed by SINTEF erosion-corrosion department and this author had no authority for modification of the rig. The details of the test rig are already discussed in the section 7.3. In this section, the test rig and its performance will be critically discussed together with the uncertainty in measurements so that further development can be made in such test system.

Shape of jet and secondary flow

The velocity and impingement angle of particles depend on shape and size of jet. It is discussed in Appendix A1, that majority of the erosion tests are performed by using air or gas as particle carrier and this author has not found the erosion test by high velocity in submerged jet. There are few studies on quality and performance of jet (Chevallier and Vannes 1995, Dosanjh and Humphery 1985, Wu et al. 2003), which shows the importance of jet quality, shape and positioning of specimen with respect of jet and nozzle. Chevallier and Vannes (1995) carried out the study of turbulent stream of air coming out of cylindrical nozzle with diameter d. According to them, the jet is diverging cone with apex angle in between 25°- 30°. Such divergent cone for free jet can be divided in to four distinct zones as follows:

- First zone (0<x<6.2d) – potential core where velocity field is uniform and equal to air flow in to the nozzle
- Second zone (6.2d<x<8d) – transition zone
- Third zone (8d<x<100d) – zone where flow is fully established
- Last zone (x>100d) – zone where velocity decreases rapidly in divergent cone following exponential law and moves quickly to zero

These four zones can be visualized from figure 8.12.1. Large x/d or l/d ratio gives the large impact surface so that large specimen and many erosive particles are needed to obtain minimum erosion. There are additional drawback at low impact angles, for instance the distance between specimen extremities are different and difference in impact angle are also significant in such cases. Chevallier and Vannes (1995) also observed two 2 ellipses due to potential core and divergent cone when samples were fixed at less than l/d=6.2. Hence there should be optimum distance between nozzle exit and specimen.

Dosanjh and Humphery (1985) also found that greater turbulent intensity at inlet will have greater mixing of jet and hence faster spreading of jet (table 8.12.1). Similarly, due to the conservation of mass, in higher turbulence, the centre-line velocity decreases causing less impact energy.
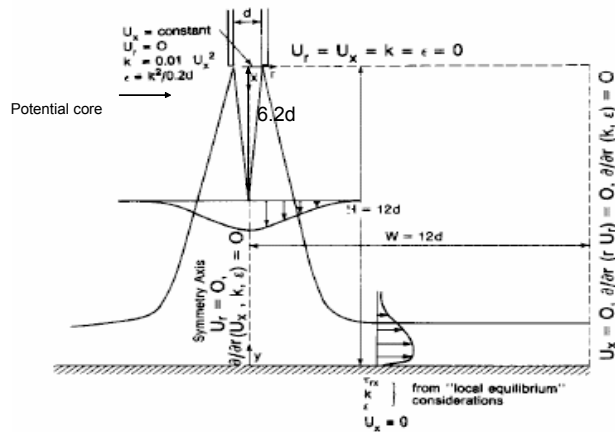
Figure 8.12.1 Particle-laden impinging jet flow configuration with relative dimensions and boundary conditions (based on Dosanjh and Humphery, 1985 and Chevallier et al. (1995)

Table 8.12.1 Comparison of the jet spreading rate and the decay of the center-line velocity (Dosanjh and Humphery, 1985)

l/d	Normalized width of the jet	Normalized centre line velocity
0	1.00	1.00
4	1.23	0.99
6	1.26	0.93
8	1.42	0.85
10	1.61	0.72

The impact of jet in the specimen sides introduces lot of uncertainties both in impact angle and surface quality especially in the coated specimens. The shapes of the eroded area were observed on aluminum specimens by polishing the eroded specimen by sand paper (grade 800). The specimens were eroded by striking 1500 gm of Baskarp-15 sand particles on 90° and 45° impingement angles. The sketches of observation of eroded surface on specimens are presented in figure 8.12.2 and 8.12.3. Frantzen and Haldogård (2000) also observed doughnut shape erosion pattern in which central area is relatively less eroded. Stachowiak (1993) defined the erosion concentrated straight to the jet and relatively unworn annular area surrounding wear scar in laminar flow as '*halo effect*', which seems to be opposite to the one observed in figure 8.12.3. But observation from both aluminium and elastomer specimens (Figure 8.7.1) shows clear area of erosion about 20 mm diameter in addition to minor effect outside this area. Hence the distance between the nozzle exit and the diameter of eroded area gives the divergence of jet inside the water pool with apex angle only about 7°, which is quite less than 25°-30° degrees, the one experienced by Chevallier and Vannes (1995). The inner annular circle is slightly offset with respect to outer circle, which may be

149

due to error in fixing specimen exactly at 90° or slight offset of inner tube for particles compared to nozzle. The eroded areas in acute angles are elliptical or egg shaped as shown in figure 8.12.3.
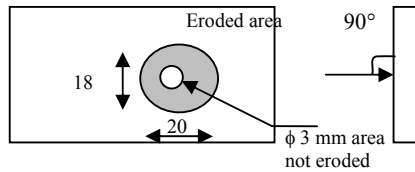
Figure 8.12.2: Observation of erosion area in aluminum specimens at 90° impact angle (1500 gm of Baskarp-15 sand and 70 m/s jet velocity)
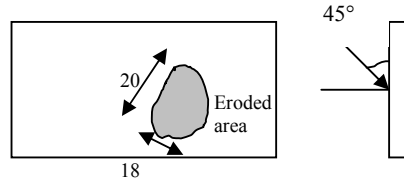
Figure 8.12.3: Observation of erosion area in aluminum specimens at 45° impact angle (1500 gm of Baskarp-15 sand 70 m/s jet velocity)

The orientations of three different specimens with respect to the jet are shown in figure 8.12.4. As shown in figure 8.12.4 (a), even largest specimen when tilted at 15° will miss about 13% of jet. At the two extreme ends of specimen, the impingement angels are between 13° to 18°. Figure 8.12.4 (b) shows that the jet hits directly to part of uncoated edge, which is about 5% of total coated surface faced towards jet. This uncoated surface has impact angel approximately 70° and distance of this surface compared to centre of specimen is small causing high erosion effect. To avoid such uncertainties, the coatings GES were tested by tilting along width, but in such case, even inclination up to 30° have missed some portion of jet as shown in figure 8.12.4 (c). To avoid the effect in the edges of GES specimens, shields of steel and aluminum were used, but these shields deformed or broken only after few tests (figure 8.12.5). This indicates the strength of jet on the sides of specimen and hence creates more doubts on the erosion in the uncoated sides of specimens. The edge effect have significant contribution in the error in the result of erosion rate because jet strength in the edge is high enough to remove the coating flakes from the edges as shown in figure 8.12.5.

Since the jet from nozzle is circular, to achieve uniform effect of jet strike in all direction, this author recommend circular specimen as shown in figure 8.12.6. Similar specimen was also used by Wu et al. (2003). The specimen edge should also be coated in same way as test surface and the specimens should be coated after they are cut in to required size. The thickness of specimen should be as low as possible to avoid edge effect, but edge effect and galling effect can also be avoided by leveling the specimen surface with that of clamping device. The covering of the specimen in the back side may also avoid erosion due to recirculation, but care should be taken to avoid any three body abrasion effect due to narrow gap in between specimen and base or cavitation effect due to vibration of the specimen due to jet strike.

All the tests are carried out l/d ratio more than 12, which means the jets are already fully developed. As seen from figure 8.12.4, for impingement angles 15° or lower, the specimen size should be larger than 65 mm.

150

a. GEC and 16Cr5Ni
specimens

b. Coatings M1, M2 and
M3 on duplex steel

c. GES coatings
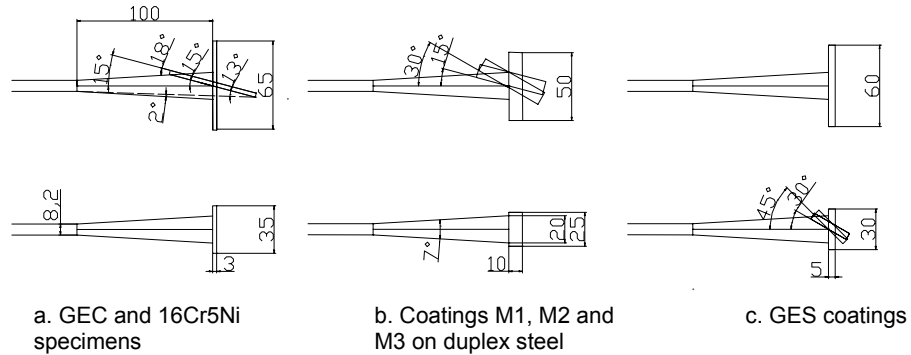
Figure 8.12.4 Orientation of specimens with respect to jet.

Damage of shield at edge by striking jet

Removal of coating at the edge
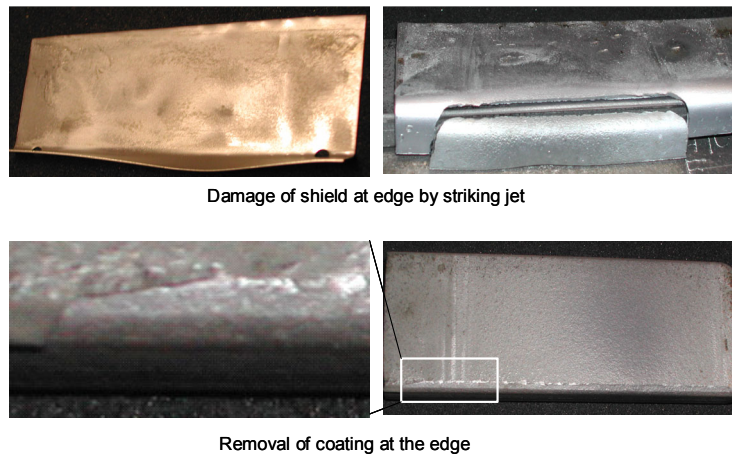
Figure 8.12.5 Protection at the edge of specimen and removal of coating at the edge

Several standard and non-standard test rigs are in use for erosion test by nozzle type test rig. ASTM G76 recommends the use of a nozzle 50 mm long with a bore of 1.50 mm; on the other hand DIN 50332 suggests the use of a 120 mm long nozzle with an internal diameter of 8 or18 mm. A long nozzle may give higher particle exit velocity and less divergence of the jet, leading to minimize the uncertainties of impingement angle and spread of velocities of particles. On the other hand, higher cost of production of long nozzle, friction loss associated with inner surface quality of bore and retardation of particle velocity due to collision of particle-wall favor for the smaller nozzle. The length to diameter ratio of nozzle is called "Aspect ratio" and it is even found up to 316 in test rig with long nozzles (detail in Appendix A1). In NTNU/SINTEF test rig, aspect ratio is only about 6; which is quite low compared to test rigs of gas jet. Stevenson and Hutchings (1995) studied the influence of nozzle length on the divergence of the erodent particle stream in a gas-blast erosion rig, but did not find any strong relation between particle velocity and nozzle length. Hence, the nozzle length in NTNU/SINTEF test rig may be appropriate design but, there could be

rotation of particles and swirl of water due to sharp 90° bend in short distance ahead of nozzle, even with the disc with 6 holes to make the flow straight. The sharp 90° bend is not a suitable design both for hydraulic and material stress point of view.
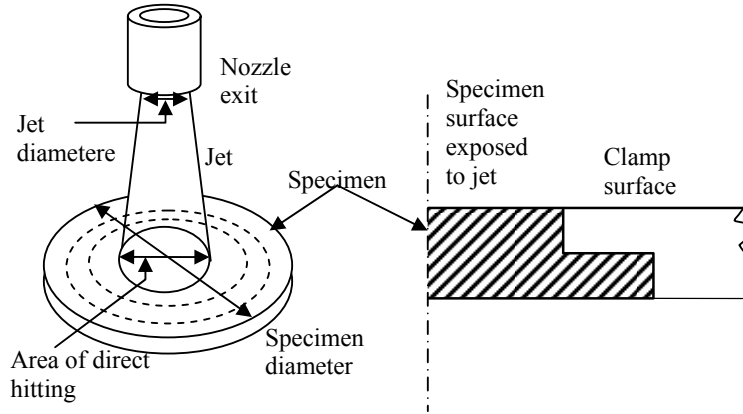
Figure 8.12.6 Proposed specimen shape for jet type of test rig

Even though enough attention is given in this test rig for filtration of the sand particle before water is recirculated, fine sands are passing through the pump, which is in one way increasing the uncertainties of total amount of particles striking the specimen and on the other hand they are eroding the pump itself. After the operation of the pump for about 150 hours by this author, the leakage in the pump was found unacceptable. The leakage could be due to damage of only seals or it could be due to wear of piston-cylinder due to abrasive effect. This can be avoided either by having longer water loop between tank and pump inlet with more chambers for particle settlement or introducing screen to filter particle from water.

Impingement angle

CFD analysis of particles released from nozzle shows spectrum of impingement angles due to deflection of incoming jet with deflected jet and gliding of particles. CFD analysis of this experimental set up by Svensson (1998) revealed that maximum particles strike the substrate with effective impact at 45° impingement angle. At low angles around 15°, most of the particles glide away without striking the specimen. Similarly at 90° impingement angle, some of the particle kinetic energy will be destroyed by rebounding jet. Compared to other angles, the larger spread of data is observed in the duplicate measurements at 90°. Hence most of the tests for erosion versus velocity are carried out only for 45° impingement angle, where minimum uncertainty is expected.

Velocity

Theoretically 3 cylinder reciprocating pump can have 13.4% flow fluctuation, which can be divided in to 6.7% on both side of mean value. After several experiments, the velocity fluctuation in the equipment is found less than theoretical fluctuation because of the effect of accumulator in the delivery side. The percentage deflections from mean value in both

sides are in the range of 3.2% to 3.9% at different velocity range as shown in figure 8.12.7 for same bypass flow adjustment.
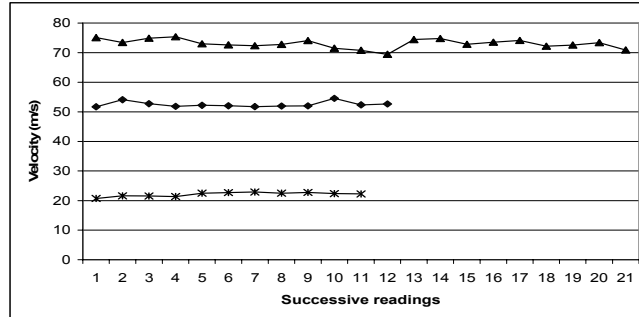
Figure 8.12.7 Fluctuation of jet velocity in high velocity jet erosion test rig

The error in the measurement of velocity will magnify the error in the estimation of erosion rate. Assuming the erosion rate = $f(V^3)$, 7% uncertainty in velocity measurement will magnify to 20% uncertainty in the calculated erosion rate. These velocities are calculated based on the flow reading on suction side of the pump. Compared to suction side less fluctuation is expected in delivery side of the pump due to damping of fluctuation by accumulator. Hence less that 7% uncertainty for flow measurement is expected in reality for relation between velocity and erosion rate presented in section 8.2.

The velocity fluctuation in the system can be minimized by introducing large tank as accumulator in the delivery side. The inlet for the pump at the tank has sharp edge, which could also be a cause of instability in the system and that may be reduced by making the inlet opening diverging toward tank.

Other uncertainties

The greatest human error is possible during measurement of weight loss, but this can be avoided by careful cleaning of specimen before weighing and precautions to avoid any mechanical damage during clamping specially for coatings.

Very thin film of oil was seen in the water surface during the tests in later stage after the pump worn out and leakage increased. But the oil level in lubricating oil tank of pump was not reduced beyond minimum level during entire test period. The wear of the pump could have caused this leakage of small amount of lubricating oil in the test rig. The effect of lubricating oil in the working fluid is discussed in section 3.3.1. Since all the tests were carried out at room temperature, the lubricant will not play any significant role in cooling and it will also not change the viscosity of the fluid such that the type of flow will change to laminar due to high viscosity.

Even though there are certain limitations in the jet type of test rig at NTNU/SINTEF, this rig gives realistic data of erosion rate for solid particle erosion and the rig can simulate the flow condition of Pelton turbine as well as low impingement angle erosion. However certain modification can improve the performance of the rig.

8.13 Application of experiment results

Estimation of weight loss of turbine

Estimation of weight loss of turbine component due to sand erosion as well as cavitation is a challenging task. The cavitation phenomenon and criteria are considered during tender contract of generation equipment, whereas sand erosion is not considered in performance guarantee in general, except few cases in turbine delivered to China from Norway (Hermod, 2004). IEC standard, publication 609 (Cavitation pitting evaluation of hydraulic turbines, 1978) on storage pump and pump turbines recommends evaluation of cavitation erosion based on electrodes used to repair damaged surface, which is not useful for prior estimation. The estimation of erosion, both in term of mass loss and dimensional change is very essential for operational and maintenance planning and total optimization process.

The analytical erosion models are not fully developed to incorporate material properties and operating variables to give material loss for a given condition. Hence normally erosion estimation is carried out on the basis of experimental observation on similar operating environment. Several types of test rigs are used for erosion tests; hence there is no single universal equation for estimation of erosion rate for hydraulic machinery. The experiment results on high velocity jet test rig at NTNU/SINTEF are used to establish the empirical relation of erosion rate. The erosion rate is presented in term of weight loss of specimen per kilogram of particles striking the specimen in a given operating condition. The validity of the experimental results and its practical application to estimate the erosion of turbine is discussed in this section.

The erosion rate in terms of weight loss of material with respect to weight of striking particle is proportional to velocity with the power n (V^n), assuming all other parameters are constant. Hence the relation can be written as:

$$W = K \times V^n$$

Where W is erosion rate in mg/kg and K is numerical constant for the given test condition and material.

This equation can be used to estimate the weight loss of turbine component operating in similar environment.

The loss of weight of turbine due to impact of sediment can be estimated by multiplying the amount of sediment passing through the turbines.

$$\text{Loss of weight of turbine} = W \times S$$

Where S is the amount of sediment (in kilograms) passed through turbine.

But all these sediment passing through turbine will not strike the turbine surface. The ratio of particle striking the surface depends upon movement of particles away from streamlines due to turbulence and wetted surface of the turbine. The wetted surface of the turbine varies according to turbine design and type. In general, Francis turbines will have larger wetted

surface compared to Pelton turbine. Among particles hitting the surface, all will not cause erosion with same intensity and only the fraction with hardness more than that of turbine material cause major erosion. Hence the equation for weight loss of material can be written as:

Loss of weight of turbine (kg) = q x S x W x 10^{-6}

Where, q is hard particle content of the sediment (kg/kg) and W is in mg/kg.

Comparison with erosion of Jhimruk turbine

The experimental observation from high velocity jet erosion test rig is compared with actual erosion of turbine of Jhimruk power plant (JHP), Nepal. The erosion of Francis turbines of JHP is discussed in section 6.3.2. This turbine is made up of stainless steel 16Cr5Ni and at each monsoon approximately 9000 tons of sediment is expected to pass through each unit. The absolute velocity at the outlet of guide vane is nearly 37 m/s and the relative velocity at the runner outlet is roughly 32 m/s. Considering erosion rate as function of velocity, this schematic variation of velocity gives some indication of extent of erosion damage of different components.

The relationship of erosion rate and velocity for the 16Cr5Ni can be seen in figure 8.2.2. Based on that for 45° impingement angle, the erosion rate equation can be written as y = $6E-05x^{3.13}$. Assuming laboratory test condition close to operating condition of JHP, interpolation of above equation gives erosion rate at guide vane and runner outlet. These values can be used to estimate the weight loss from these components. The validation of the estimated result is compared with the observation of erosion of actual turbine.

The interpolation of this curve gives erosion rate at guide vane outlet 4.25 mg/kg and that at the outlet of runner is 2.22 mg/kg. In the turbulent flow region, same particles may strike surface several times and the kinetics of particles is really complex. But in this research it is assumed that particles strike once at the guide vane system and then turbine blades. With this assumption, the weight loss due to 9000 tons of particles removes 38 kg material from guide vane system and 20 kg from blades. But from the mineralogical analysis of the sand of Jhimruk River, about 70% of the particles are harder than steel. With reference to this, if we consider only 70% particles cause active erosion, the weight loss for guide vane and runner blades can be estimated only about 26.6 kg and 14 kg respectively. Total weight loss of 40 kg from the 4 MW turbine with 0.8 m diameter could be high. This difference could be due to actual effective particles they are taking part in erosion. Finnie (1960) had assumed only 50% particles take part in erosion. The validity of this amount is compared with the observation of eroded turbine.

The loss of material from the actual turbine of Jhimruk power plant is estimated based on the observation of erosion damage of turbine. The assumptions and estimation of erosion for different components and total weight loss for this turbine is presented in Appendix D. Erosion estimate from experimental measurement is about 3.5 times higher than the one estimated from observation. The actual weight loss of eroded turbine component is not measured so far. Weighing whole of the turbine could be difficult, but separate components

like guide vanes, top and bottom covers can be weighed and actual weight loss can be found. The 3.5 times deviation of estimated loss of weight is due to all particles which is passing through turbine conduits but may not necessarily striking turbine surface. The ratio of wetted surface to volume of water may give some indication of this factor, which is not clearly understood. But the experimental measurement gives close estimation to the material removed from the turbines.

This method of estimation of loss of material of turbine components gives same value irrespective of type of turbine. Tsuguo (1999) have suggested different values of velocity exponent (n) for different types of turbines for example, n = 3 for Francis runner, n = 2.5 for guide vanes, n = 2.5 for Pelton nozzle and n = 1.5 for Pelton bucket. Same type of turbine can have different erosion damage depending upon profile and curvature of buckets or vanes. The actual relation of erosion and associated parameters are really complex. Hence the empirical equations obtained in section 8.2 on erosion rate and velocity can be used for approximate estimation of weight loss of turbine material.

8.14 Erosion test with river sand from Nepal

The findings of erosion test carried out at Kathmandu University on jet type of test rig with river sand from Nepal are presented in this section.

Mineral content

The percentage of main minerals present in the sediment sample for different rivers are presented in their respective basins in the order of their location from west to east of Nepal (figure 8.14.1). This result is based on average erosion rate by samples size 425-300 μm, 300-212 μm and less than 212 μm. Quartz is found as main constituent of the sediment in Nepalese rivers with more than 50% in almost all cases. Second largest constituent is the feldspar with average of 3-8%. Remaining hard minerals are Sillimanite, Garnet, Ilminite, Amphibole and Hematite and together they constitute up to nearly 7%. The remaining constituents of the sediment samples are minerals softer than 5 Moh's scale and rock fragments, clay minerals and others. The minerals harder than 7.5 Moh's scale are not found in the samples. On average, nearly 70% of the constituent of the sediment are hard mineral content with hardness more than 5 Moh's scale.

The rivers in the Koshi basin have almost 70% hard mineral content except sample from Roshi River. The sampling location Panauti is close to origin of this river and river itself flows through area rich with vegetation and soils. The yellowish colour of this sand sample had indicated presence of large quantity of soil on it. Several of the rivers of sampling location in this basin originate in high Himalayas. High Himalayan crystalline metamorphic rocks comprising gneisses, quartzite and marbles can be seen in geological formation map shown in figure 6.2.3 in the upstream of sampling location of Koshi basin. Compared to east, western parts of Nepal have shown varying quantity of quartz, but lesser quartz content than in the east. Figure 6.2.3 also indicates possibility of several types of rock groups in the river course in western part of Nepal. Some of these rivers originate in middle

mountains and hence the quartz contents may have varied because of local geology, through which the river is flowing. Similar to the Panauti, sediment from Pokhara have also shown low quartz contents. These samples with low quartz contents have almost 30-40% rock fragments consisting schist and quartzite. East Rapti and Bagmati basin which is almost in middle of the country, have quartz content some what in between eastern and western basins.

Muscovite and biotite are two major minerals which is present abundantly in several samples, but these minerals have hardness less than 3 Moh's scale and hence is not very harmful with respect to erosion. Sample from Bishnumati River at Kathmandu valley contains almost 50% of these two minerals. The quartz content in sample from Jhimruk is highest among all samples but this is in agreement with the quartz content for fine particles reported by Basnyat (1999). All these mineral analyses were carried out using sediment samples of size in between 212-90 μm. Small particles will have normally higher quartz content because of their mechanical and chemical stability. Before becoming small particles, other softer minerals will be weathered. Samples from suspended sediment will have smaller particle size distribution (PSD) and hence they may give higher percentage of quartz. Small particles may give higher quartz content than these values, but visual counting of small size particles are not accurate compared to Differential Thermal Analysis (DTA) process. On the other hand DTA has limitation that it can not identify other minerals present in the sediment except quartz. The general characteristic and hardness of minerals present in the sediment in Nepalese Rivers are presented in table 8.14.1 considering example of JHP. The detail data for all the sediment samples are presented in appendix D.

Particle size analysis

The particle size distribution obtained from VA Tube analysis of all sediment samples are presented in figure 8.14.2 (a-d). The particle size in terms of d_{50} for the sediment varied in between 0.1 mm for sample of Jhimruk to 0.5 mm for the sample from Pokhara at the downstream of Phewa Lake. The samples from Jhimruk and Modi are taken from sediment settling basins. Hence they might be finer than other samples taken from the river beds. The sediment collected in the Pokhara was very coarse with gravels. Most of the smaller particles may have settled down in the Phewa Lake and hence only coarser particles could be present in the downstream river bank. There is also quite variation in d_{50} size for the samples in the East Rapti and Bagmati basins. The samples from the Kathmandu valley have similar distribution. For example samples from Bagmati at Gokarna and Manahara have exactly similar distribution, which can be justified by the similar upstream flow condition of these two rivers. As expected, sample from Bagmati at Gaur have shown uniform particle size distribution compared to sample from location close to the origin of this river. This could be due to low gradient of river at plane land at Tarai and larger particles might have already settled down before they travel long distance. But interestingly both the samples have d_{50} almost equal to 0.2 mm. Except for Saptakoshi and Roshi, all the rivers in the Koshi basins have d_{50} in the range of 0.25 to 0.3 mm. Similar to the Bagmati at Gaur, the sediment from main river Saptakoshi is also more uniform and smaller in size compared to its tributaries. The sediment from Khimti adit-4 and Khimti River are almost similar with d_{50} approximately 0.25 mm.
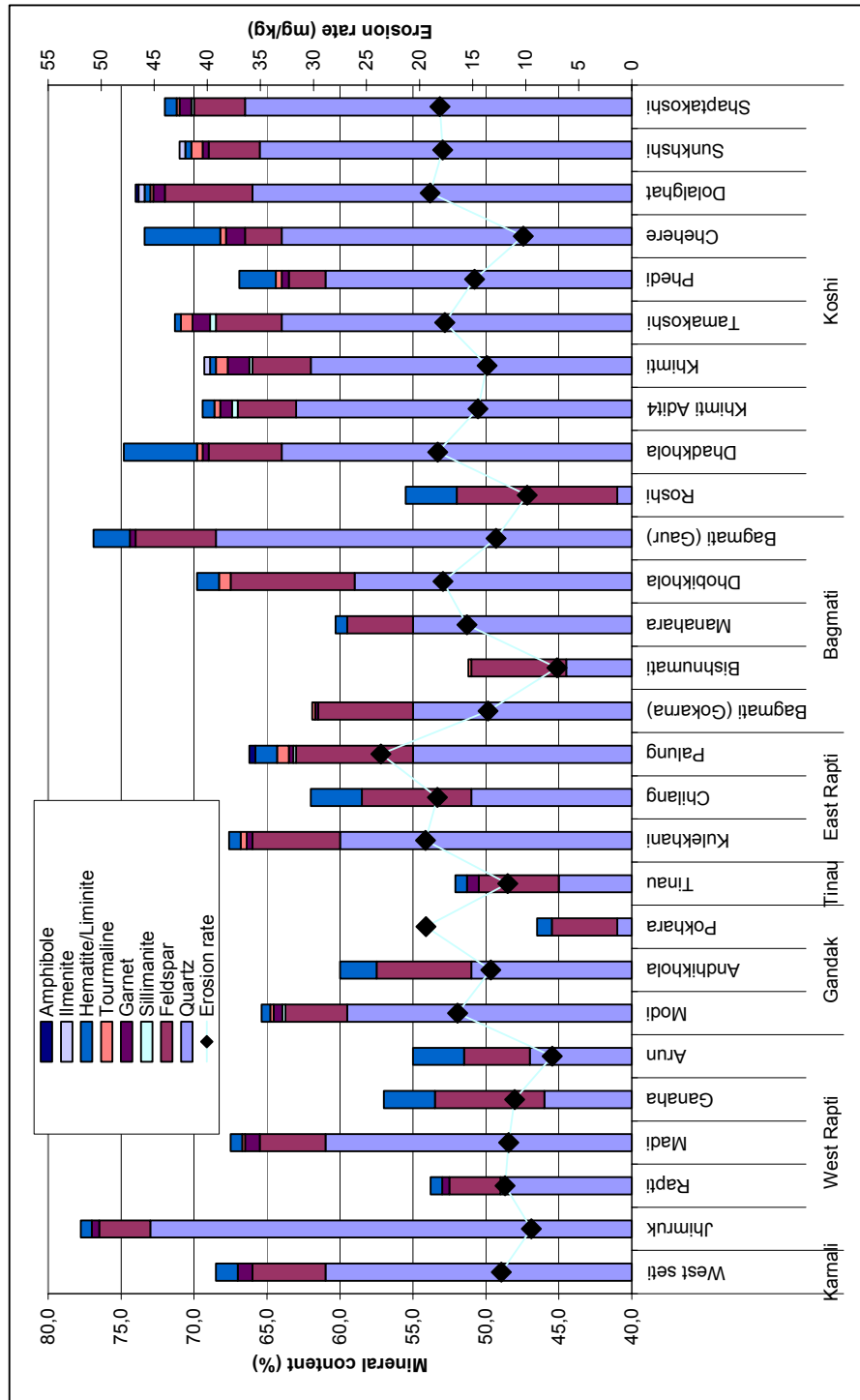
Figure 8.14.1 Percentage of minerals in sediment samples and average erosion rate

Erosion rate

The average erosion rate obtained from laboratory measurement at KU are also presented in figure 8.14.1 corresponding to hard mineral contents. The trend of erosion rate for different river basins can be observed from this figure. The erosion rates are very close to 10 mg/kg for all the samples in western basins. In the eastern basins, even if they are varying, the spread of results are less compared to middle part of the country. The overall trend of erosion rate is found increasing from western basins to eastern, which can also be justified by higher quartz content in eastern basins. The difference of erosion rate data in the middle region in East Rapti and Bagmati basins are high, but on average, the erosion rates are higher compared to both eastern and western basins. Since the rivers in these basins originate from middle mountains and are of short length, the properties of sediment particles in these rivers could be localized and may also have fresh sharp edges. Once the particles traverse certain distance by rolling and sliding, it will be rounded off and it will have less eroding capacity. Even if the sample from Bagmati River at Gaur is having higher hard mineral content, it showed less erosion compared to origin of this river at Gokarna. This could be due to smaller size particles as seen in particle size distribution (PSD) curve in figure 8.14.2. Since the erosion rate is presented in term of weight loss with respect of weight of striking particles, particle shape could have more influence than particle size. The particles could have traveled long distance from origins up to sampling location at Gaur by rolling and jumping numerous times, and hence may have become blunt. These particles could have less cutting ability compared to the one close to origin. The erosion rate by the sample from Palung is highest (22.5 mg/kg) and Bishnumati have shown lowest erosion rate (7 mg/kg) when they have difference of 15% of hard mineral content. Sediment from JHP has shown low erosion rate compared to the highest fraction (77%) of hard mineral. The reason of extreme erosion of turbines at Jhimruk power plant even if the erosion rate is not excessively high on lab test could be due to large quantity of sediment load passing through the turbines in every monsoon season. The additional settling basin at JHP to decrease suspended sediment load through turbines may reduce the damage of turbine components considerably.

The bigger particles have higher impact energy. Bitter (1962) have discussed threshold velocity below that erosion due to deformation does not take place. This threshold value is based on stress induced or impact energy due to striking particles. These are also dependent on mass of particles. Hence very fine particles will not cause erosion in principle and that is the reason settling basins are designed to extract particles greater than 0.15 or 0.2 mm. Since the effect of particles smaller than 90 μm can not be investigated accurately at 50 m/s velocity with less amount of particles, the particles smaller than 212 μm were mixed together for erosion tests. Similarly there were very less quantity of particles in between 500-425 μm and hence tests were not carried out with that range of sand. Even if most of the tests were carried out with 1000 gm particles are for 15 minute duration, some of the tests were carried out only with 500 gm (for example Chehere 425-300 μm and 300-212 μm, Phewa >500 μm) and 400 gm (for example Saptakoshi 300-212 μm, Bagmati-Gokarna>500) particles for 10 minutes test duration. This was done because sand of these categories was not sufficient. Even though erosion rate is presented with respect to striking particles, some uncertainties may prevail due to difference of quantity of striking particles. Figure 8.14.3 (a to d) shows the erosion rate for different size of sand particles. Even if

deviations in erosion rate are observed for different size particles, with the uncertainties associated in the test procedures, average values presented in figure 8.14.1 can be useful for general use. Most of the cases have shown almost equal erosion rate for all particle size such as in Jhimruk, Andhikhola, Tinau, Bagmati (Gokarna) and Tamakoshi. The result of Modi have shown increasing erosion rate with decrease in particle size but most of the other results have shown decreasing erosion rate with decreasing particle size.

Table 8.14.1 Minerals composition of sediment sample collected from settling basin of Jhimruk hydropower plant (JHP) and mineral characteristics

Minerals	Percentage (%)	Hardness Moh's scale)	Special characteristics of the minerals
Quartz	74-75	7	Hard mineral, resist weathering
Feldspar	3 – 4	6	Gets weathered white colored
Muscovite	4-5	2.0 – 2.5	Light colored soft flaky mineral
Biotite	12-14	2.5 – 3.0	Dark colored soft flaky mineral
Amphibole	ND	5.0 – 6.0	Green to dark green elongated grain / needle like crystals
Pyroxene	ND	5.0 – 6.0	Dark green to black grains
Chlorite	0.5-1	2.0 – 2.5	Soft flaky mineral, green
Olivine	ND	7.6 –7.0	Lemon yellow colored grain
Calcite/ dolomite	<0,5	3 /and 3.5 – 4.0	Light colored rhombic grains
Kyanite	ND	4.0 – 5.0 6.0 –7.0	Elongated blade like mineral (parallel) Elongated blade like mineral (transverse)
Sillimanite	ND	6.0 – 7.0	Colorless, transparent, elongated needle & blade like mineral
Magnetite	<0.5	3.5 – 5.0	Shining dark gray, magnetic
Hematite/ limonite	<1	5.0 – 5.5	Earthy redish brown iron oxide
Ilmenite	Rare	5.5 – 7.6	Shining black/ silver gray
Garnet	<0.5	7.6 – 7.5	Light pink to pinkish brown colored
Tourmaline	Rare	7.0 – 7.5	Fragments of black, green, pink
Rutile	Traces	6.0 - 7.6	Fine, colorless to pink, brown
Apatite	ND	5.0	Fine transparent needle like
Zircon	ND	7.5	Fine, colorless, brilliant tiny crystals
Corundum/ Topaz	ND	9.0	Very hard, transparent, brilliant
Clay minerals	Rare	1.5 - 2.5	Soft flaky, irregular mass, earthy

There are definitely certain uncertainties in these erosion experiments such as variation of performance of pump during tests, flow condition of particles and so on. The pressure at the outlet of the pump was monitored in all the tests and fluctuation was observed in between $4.8 - 5.4$ kg/m^2. In spite of thorough cleaning and precautions, human error could occur during weight measurement and in some cases even increase in weight were observed after the erosion test. Such increase in weight of specimen is possible in case of embedding of particles in soft specimen like aluminum, but it is not expected in 16Cr5Ni stainless steel. The increase in erosion rate can also be expected in case of corrosion of specimen. Even though the specimen holder was made of mild steel, the specimen was separated from the holder by nylon sheet. The duration of test is also so small and in most of the cases weight measurements were carried out immediately after the test. Hence the effect of corrosion is considered insignificant in these experiments. Similarly in some cases exceptionally high erosion rate was observed. This may be due to sudden removal of slightly bigger fragments during tests after several tests on same specimens. Unlike in coatings, such detachment of bigger fragment can not be distinguished in stainless steels by naked eye. Only simple way to minimize the uncertainty in such case is to carry out more than one test for same operating condition and identify any abnormal values. Some of the abnormal values are discarded in the results presented in figure 8.14.3.

Together with other properties, the percentage of hard mineral in sediment significantly affects the erosion rate. The scatter of the erosion rate with respect to percentage of hard minerals (>5 Moh's hardness) are presented in figure 8.14.4. The erosion rate has increasing trend with respect to percentage of hard particles. But the slope of the linear trend line is only about 0.5. The sharp and hard particles remove material by cutting action, on the other hand, even blunt and relatively softer material may cause erosion due to plastic deformation and fatigue due to repeated hitting of particles. The spread of erosion rate for same percentage of hard mineral content indicated that, it is not only the composition of hard mineral content which is important for erosion of material, but the difference could also be due to other properties. One of the very influential property is particle shape.

Shape

Sediment particles are defined in term of regular shapes based on visual observation during mineral analysis. These are qualitative indicators. The most often used shapes in sediment petrology are angular, sub-angular, rounded and sub-rounded. If the boundary of sand grain is not equal in different directions and has irregular sharp edges, the shape is called **angular**. If their boundary is partly smooth but not of equal dimension, it is called **sub-angular**. On the other hand, the grain with more or less equal dimensions in all the directions with smooth rounded edge is called **rounded.** If the boundary is more or less rounded with smooth edge but not with equal in dimension in all directions is called **sub-rounded**. An attempt has been made to illustrate these shapes by shapes of garnet grains used for abrasive jet machining as shown in figure 8.14.5.
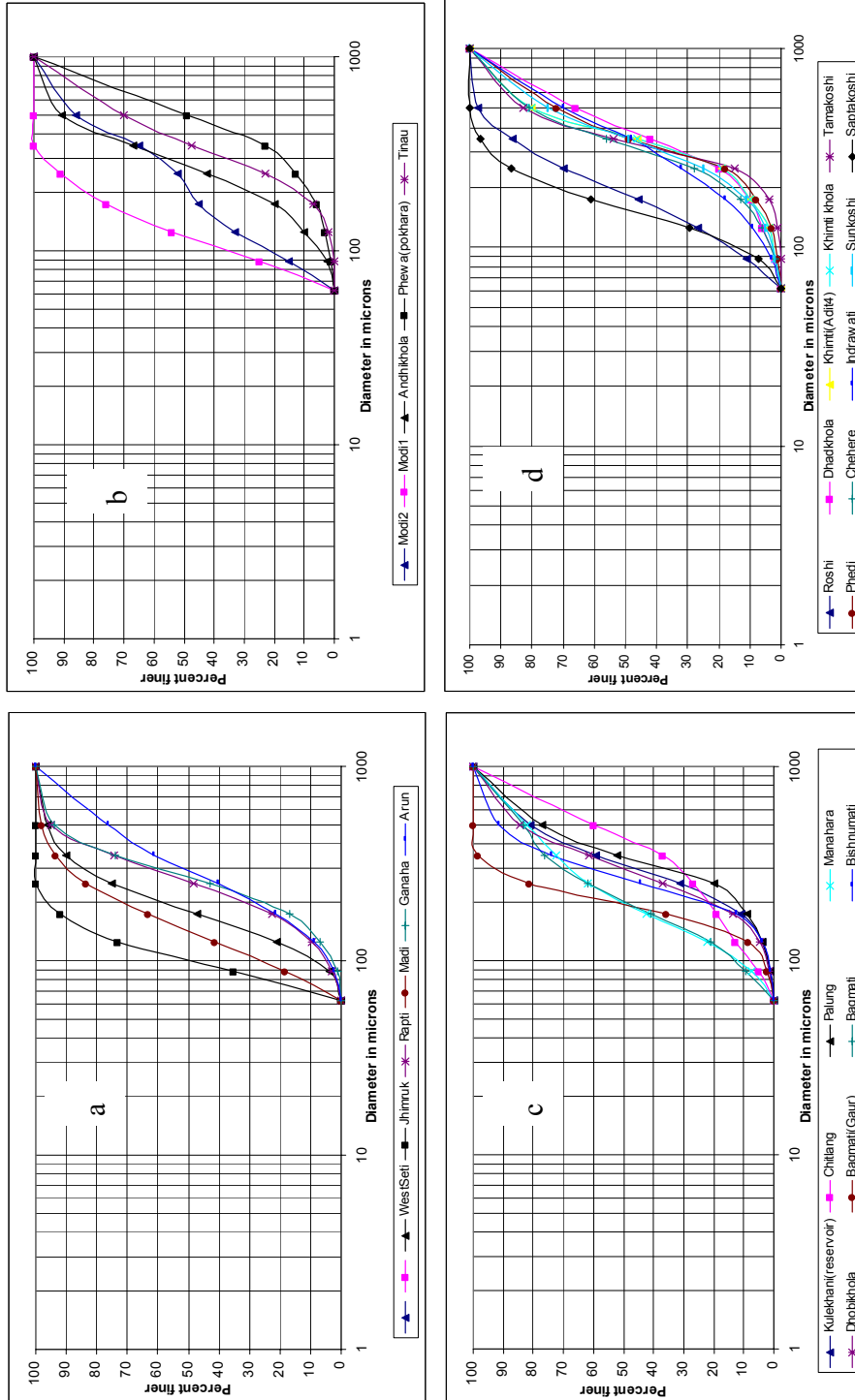
Figure 8.14.2 (a-d): Particle size distribution of sediment samples
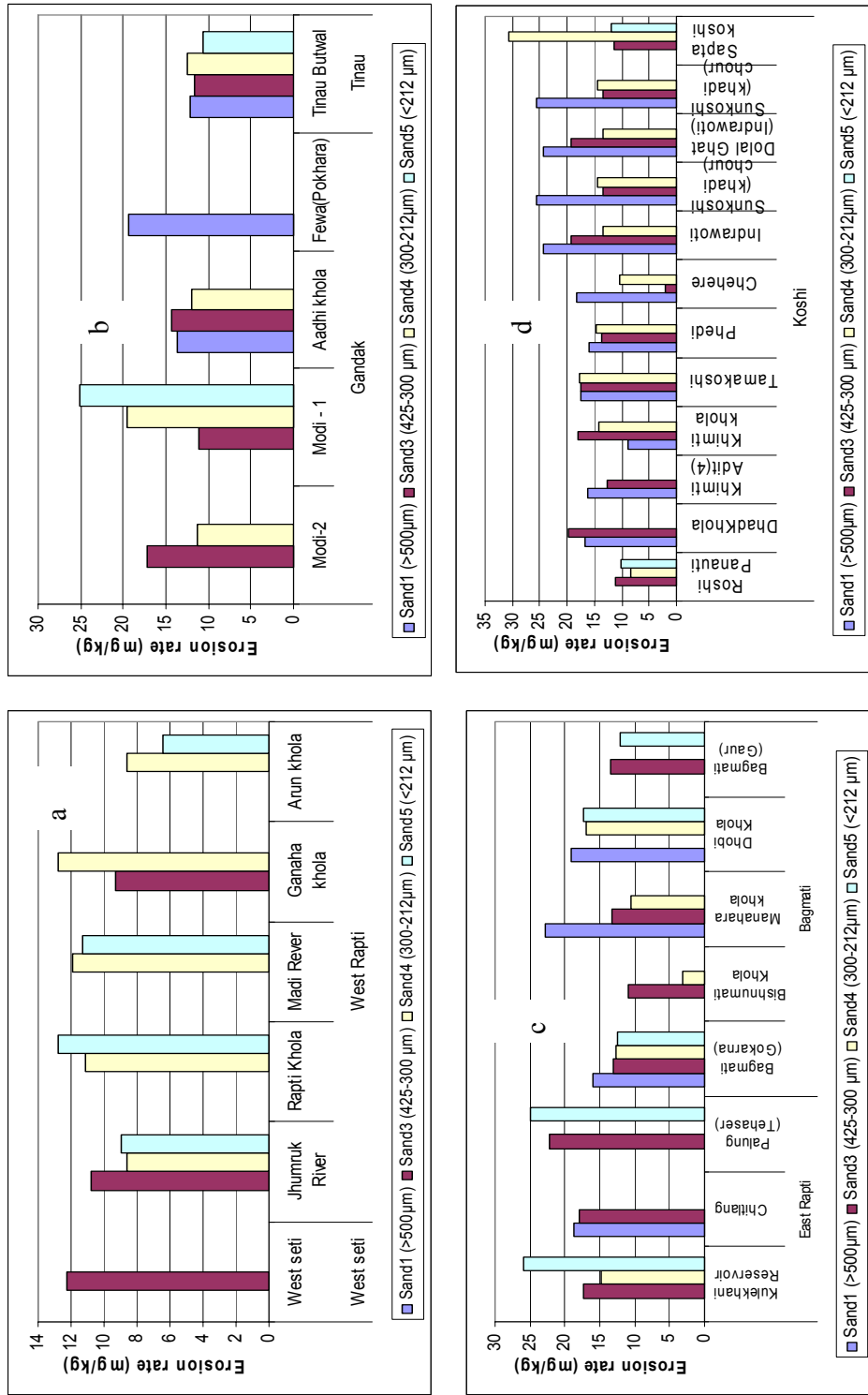
Figure 8.14.3 (a-d): Erosion rate from different size specimens
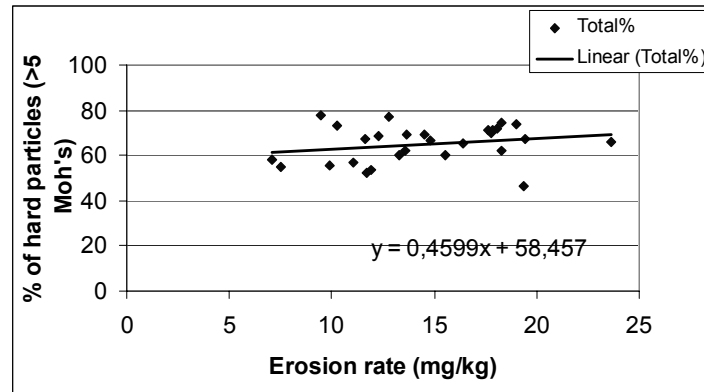
Figure 8.14.4 Relation of percentage of hard mineral content and erosion rate (Thapa B., Dahlhaug O.G. et al., 2004)

| Rounded | Square | Sub-rounded | Sub-angular | Angular to sub-angular | Angular | Angular |
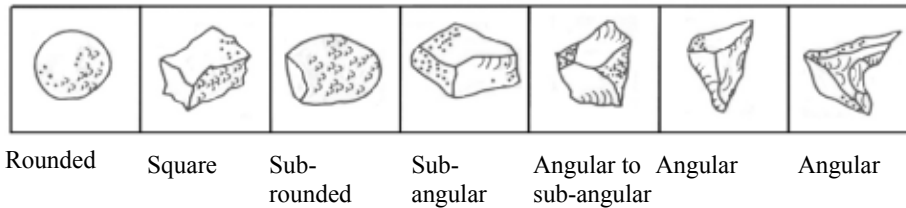
Figure 8.14.5 Shapes of Garnet grits used for abrasive jet machining (http://engr.smu.edu)

Basically three different shapes sub-angular to sub-rounded, angular to sub-rounded and angular to sub-angular were reported for entire samples. It seems the visual observation can not distinguish the average shape of all particles because same particles can have different shapes and it becomes more complex in the case of mixture of several mineral with different shapes. In such cases, considering shape factor in the erosion model may not give noteworthy meaning. The solution for this could be to analyse the particle shape by image processing techniques and statistical analysis to quantify shape parameter.

The analysis of particle shape by image processing technique is initiated by this author at Kathmandu University and it still is under progress. The particle image is captured by paper scanner (figures 8.14.6 a) and grain boundaries are developed to quantify shape and smoothness of the grains and count the number of sand grains. The project is not yet complete, but the figures 8.14.6 b shows the image of one of the sand sample from Sunkoshi River and boundary generated by image processing technique.

The relation between shape of particles with geographical locations, mineralogical content and erosion rate and so on can be used for ranking the erosivity of different existing and forthcoming power plants. The research activities at KU to investigate the properties of sediments and their effects on erosion of turbine material revealed the possibility of use of sediment from hydropower plants as by-product. Large quantity of quartz in sand of

Nepalese rivers makes it valuable for applications such as construction, foundry mould, production of glass, abrasive materials for sand paper, sand blasting and abrasive water jet machining and so on. Even though industrial use of the sand in Nepal is negligible at the moment, the data prepared from this research work initiated the awareness for use of sediment from hydropower plants both in term of economy and environment (Thapa et al., 2004).
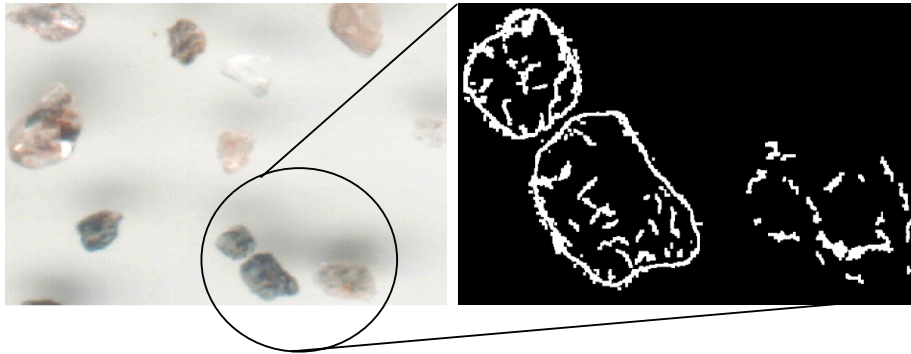
(a) Scanned sand particle shape   (b) Image generated from
                                             computer

Figure 8.14.6: Sand particle shape from Sunkoshi River (Thapa, Shrestha et al. 2004)

Chapter 9

Particle separation in swirl flow: Experimental

9.1 Background

Together with several parameters affecting erosion rate (discussed in section 3.3), the modification in design in term of turbine size, profile and curvatures also play vital role in reducing erosion rate. The separation of particles from streamline depends upon acceleration of particles, which further depends on profile of blade and bucket. This aspect is not explored at large. New test rig has been built at NTNU where the flow in guide vane cascade is simulated in order to verify the particles separation and to find the drag force of particle in the swirl flow. Newly developed test rig is descried in this section together with the concept of particle separation due to acceleration.

Few studies have been done in the field of particle transport and separation in erosion test rig together with cyclone separator and conveying of particles in process industry. Chevallier and Vannes (1995) carried out numerical and experimental study of interaction between particle and specimen. They studied the particle speed in non uniform flow by generalizing Basset, Boussinesq and Oseen's (in 1888) expression which gives an equilibrium of particle. The added weight effect, effect of static and viscous pressure, Archimedes thrust and gravity force are neglected in the case of air as flow medium (ρ/ρ_p $<10^{-3}$) and when particle and fluid acceleration are of the same order. Equation 9.1.1 is a simplified equation of equilibrium between acceleration and drag force obtained by neglecting all other terms (Chevallier and Vannes, 1995).

$$\frac{\pi d^3}{6}\rho_p\frac{dV}{dt} = \frac{\pi}{8}d_p^2\rho C_D\left(V - C\right)\left|V_p - C\right|$$

9.1.1

Here d is diameter of particle with density, ρ_p in fluid of density, ρ. The fluid velocity is C and particle velocity is *V*. The coefficient of drag (C_D) is obtained from equation 9.1.2 by Clift (in 1978).

$$C_D = \frac{24}{\mathrm{Re}_p}\left(1 + 0.15\,\mathrm{Re}_p^{0.687}\right)$$

9.1.2

Similarly Tabakoff et al. (1991) used simplified governing equation of force of interaction of particle motion in the turbo-machinery flow with reference to cylindrical coordinates relative to frame of reference fixed with respect to the rotating blades as (equation 9.1.3):

$$\overline{F} = \frac{3}{4}\frac{\rho}{\rho_p}\frac{C_D}{d}\left[\left(V_r - \frac{dr_p}{dt}\right)^2 + \left(V_\theta - \frac{d(r_p\theta_p)}{dt}\right)^2 + \left(V_z - \frac{dz_p}{dt}\right)^2\right]^{\frac{1}{2}}(\overline{V} - \overline{V_p})$$

9.1.3

Here r_p, θ_p and z_p define particle location in cylindrical coordinates. Similarly V_r, V_θ and V_z represent relative gas velocities in the radial, circumferential and axial directions respectively. This equation includes centrifugal force as well as Coriolis force. The forces due to gravity and inter particle interaction are negligible in the case of turbo machinery. The drag coefficient (C_D) is a function of particle Reynolds number. Deng et al. (2001) considered C_D=0.44 for large Re_p (>500), but that is given by equation 9.1.4 for Re_p in between 0.2 to 500.

$$C_D = 24\left(\mathrm{Re}_p^{-1} + 0.167\ \mathrm{Re}_p^{-1/3}\right)$$

9.1.4

In spite of several numerical and experimental study of particle flow in curved paths, analysis of particle flow in case of hydraulic machinery is not found.

9.2 Particle in swirl flow

When the particles travel in the curved path, for example in swirling flow towards an outlet located in the centre as shown in figure 9.2.1, the particles will be exposed to two main forces. Centrifugal force (F_c) moves the particle away from the centre, while drag force (F_D) pull them towards the outlet, which is in centre of the tank or towards the runner in case of Francis turbine (Thapa and Brekke, 2004 and Brekke, 2004). These two forces are given by following equations:

Centrifugal force, $F_c = \rho_p\dfrac{\pi d^3}{6}\dfrac{V^2}{r}$

9.2.1

Drag force, $F_D = C_D\rho\ \dfrac{C^2 A}{2}$

9.2.2

Following three conditions prevail in such case:

1. particle will stay at the orbit of radius r, if $F_c = F_D$
2. particle will strike outer wall, if $F_c > F_D$
3. particle will flow along with water towards the center of the tank, if $F_c < F_D$

At equilibrium, these two forces balance each other and a particle of a given diameter stay at orbit of radius (*r*) until either velocity components are changed or particles become smaller by fracture due to impact. The diameter of particle (d) for equilibrium condition is given by equation 9.2.3.

$$d = \frac{3}{4}C_D\frac{\rho}{\rho_p}\left(\frac{C}{V}\right)^2 r$$

9.2.3

The drag force is caused by absolute velocity of water (C) and centrigugal force is caused by velocity of the particle in tangential direction.

Even though the phenomenon of particle motion in the curved path discussed here is very similar to swirl flow in between guide vane outlet and runner inlet, the concept of particle separation due to high acceleration in curved path can be co-related with the other turbine components like flow in between guide vane cascade, runner blades of reaction turbines and flow through Pelton buckets. Direct application of this concept is operating strategy of turbine, for example manipulation of guide vane position to maintain velocity ratio in such a way that the particle of given size should flow along with water without striking the wall.
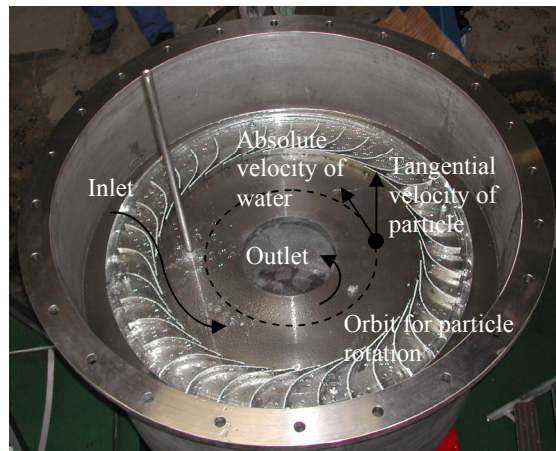
Figure 9.2.1 Illustration of particle flow in curved path due to swirl

Such phenomena and damage of Francis turbine guide vane is observed in Herva hydropower plant in State of California (Brekke, 2004). Particles larger than 0.2 mm are normally removed in hydropower plants. In some cases, larger particles may enter in to the swirl flow. Some of the causes for entering big particles are flooding near intake, sweeping of sand and gravel from the tunnel floor or sand trap due to mass oscillation in the water conduit. This is very likely situation in unlined tunnel with weak rocks. Once large particle enters in to the swirl flow, it will be rotating and hitting in between runner inlet and guide vane outlet damaging suction side of the guide vanes. It may be difficult to observe this type of erosion from the side of spiral casing during inspection. Figure 9.2.2 illustrates damage of guide vanes by this phenomenon.

9.3 Objective of experiment

The objective of development of test rig and experiment are as follows:

1. To study the particle separation process in the flow in the curved path
2. To study the forces on particle on rotational motion or swirl
3. To assess the drag coefficient for particle in swirl flow
4. To establish the operating strategy for Francis turbine operating on sand laden water

168

Figure 9.2.2 Erosion damage of guide vane by large particles (Photo courtesy: Hydro Energy Norway – DWR, State of California)

9.4 Description of test rig

The test rig is developed at Water Power Laboratory at NTNU to create strong swirl flow similar to the flow in between guide vane outlet and runner inlet. There is a provision to introduce particles in the swirl flow and observe the motion of particle. The construction of the test rig is described in this section.

The test rig shown in figure 9.4.1 consists of main tank, inlet pipe and outlet cone with valve. The main tank of rig has diameter 1100 m and height 1000 m. The tank and piping are dimensioned for 50 m water head in order to be able to carryout tests at high velocity. The main tank consists of two compartments with 250 mm diameter opening as outlet at the center of plate. This plate divides the tank in to two compartments as shown in figure 9.4.2. Thirty-six curved vanes (resembling guide vanes) are fixed at the plate around the perimeter of circle of diameter 900 m. The vanes with radius 100 mm towards inlet and 90 mm straight section towards outlet are fixed (as shown in exploded view in figure 9.4.2) in such a way that the inlet velocity direction is almost in radial direction and outlet makes 10° to the tangent. These vanes are sandwiched in between bottom plate and 50 mm thick, 950 mm diameter transparent Plexiglas plate. Due to this arrangement, the swirl flow in between Plexiglas and bottom plate can be clearly observed. The edges of the Plexiglas are made curved to ensure uniform flow. The arrangement of vanes inside the tank with Plexiglas plate can also be seen in figure 9.4.2.

The top cover of the tank is fitted with 4 transparent windows of Plexiglas of diameter 160 mm at the pitch circle diameter 700 mm. Through these four windows, the motion of particles in swirl flow can be observed. The particle injection point is at 250 mm from the centre. The particles are released at the bottom of Plexiglas through 15 mm diameter pipe and valve arrangement. The particles up to 10 mm can be injected from this arrangement.

169

Together with this injection pipe, one additional air bleeding valve is made at 390 mm from centre. The manometers are fitted in the air bleed valve which gives pressure at the inlet of the vanes and tank. Similarly, the manometer fitted on the injection pipe gives the pressure at the swirl flow field and gauge at the outlet cone gives pressure at outlet.
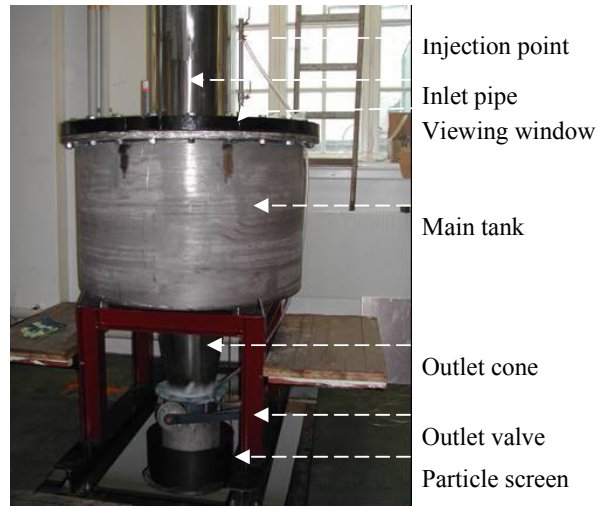

Injection point

Inlet pipe
Viewing window

Main tank

Outlet cone

Outlet valve
Particle screen

Figure 9.4.1 Photograph of test rig for at Water Power Laboratory, NTNU

9.5 Test Procedure

The particles are tracked by visual observation and filming particle motion inside the rig. The flow rate in the test rig can be obtained from electromagnetic flow-meter in the main control panel of the laboratory.

The main activity in this test is to find out the size of particle which will flow together with the water in a given flow condition. Any particle higher than equilibrium diameter will stay rotating in the tank until flow rate is decreased to reduce swirl. The steel balls from 1.5 mm to 10 mm are used for the observation. Steel balls are used because the coefficient of drag for spherical particles is available for comparison and calculation. Apart from steel balls, plastic ball of 6 mm diameter and plastic granular of specific gravity 1.41 and 1.42 of size 3-4 mm are also used as particle. These particles are used as material having density closer to density of sand. The small sand particles are not used in the test rig because of the safety of instrumentation of the laboratory, but gravels of 8 and 4 mm are tested because this can be filtered in the present system.

The particles are injected in to the swirl from the particle injector as shown in exploded view in figure 9.4.2. For particle injection, first lower valve is closed and particle is inserted from upper valve. Then, upper valve is closed and lower valve is opened. After the opening of lower valve, the particle sinks and slowly drops in between Plexiglas and steel plate. Depending upon velocity at the point of injection, the particle will either move towards

outer radius or follow flow direction heading towards outlet at the centre of the tank and ultimately sinks.
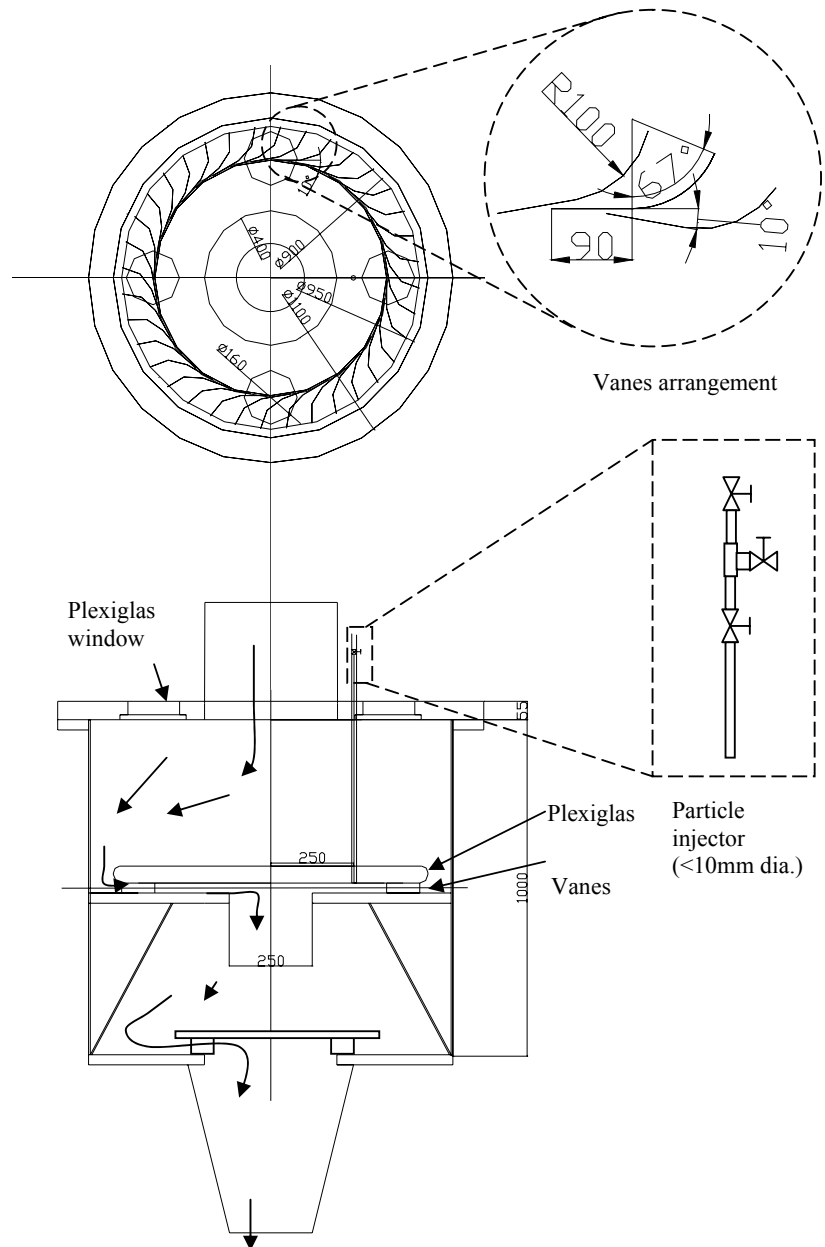

Figure 9.4.2 Schematic diagram of swirl flow particle separation test rig at Water Power Laboratory, NTNU

Chapter 10

Particle separation in swirl flow: Results and discussion

The results of the measurements carried out to meet the objectives presented in section 9.3 are presented in this chapter. This includes the investigation of flow in the test rig, swirl flow behind vanes and relationship between drag force and Reynolds number.

10.1 Flow in the test rig

This test rig is connected to laboratory pipe system of Water Power laboratory at NTNU. There is a provision of running the system in open loop and closed loop. The system operates at 16 m head in an open loop and 50 m head at closed loop. Even if the pumps have discharge capacity of 1000 l/s in 16 m head, maximum discharge is obtained only around 40 l/s due to small area of vanes opening. Each vane cascade have 30 mm x 6 mm opening and total 36 vane opening gives area 6.48×10^{-3} m^2. The acceleration of flow in vane cascade should theoretically give more than 16 m/s velocity and 110 l/s flow rate at free flow. The velocity at vanes outlet corresponding to valve opening are shown in figure 10.1.1. The absolute velocity (C) of water at the vanes outlet can be obtained from continuity equation. The peripheral component (C_u) of absolute velocity can be obtained from the orientation of blade angle, which is fixed at 10° in this case. This angle varies at different operating regimen in actual hydropower plant. The peripheral component causes centrifugal force of particle whereas the radial component causes the drag force.

The vanes causes swirl inside the tank, which simulate the swirl created by guide vanes in Francis turbine. Such swirl satisfies $C_u r$=constant towards vanes, whereas there will be whirl or forced vortex following C_u/r=constant towards centre of the rig, which is not of interest in this test. The distribution of peripheral velocity component and pressure at different radial positions inside the tank are shown in figure 10.1.2. The diagram shows that C_u at the end of vane is 6.17 m/s and at the point of injection is 8.45 m/s considering maximum flow rate (40 l/s). Similarly the pressure at the inlet of vane is measured 15 m and that at the outlet of vane obtained from Bernoulli's equation is 13 m. The pressure at the point of injection is measured around 11.3 m and that at outlet of tank is almost atmospheric pressure.

In the experiment in this test rig, firstly the operating condition is set at certain velocity level by controlling the valve opening. Then the particles are injected and motion of the particles is observed through the Plexiglas window. If centrifugal force and drag force on particle are equal, the particles rotate at the radius of 250 mm, which is an injection radius. But if those two forces are not equal, there are two possibilities. The particle can move

towards inner diameter and ultimately sink to the outlet if drag force is high. On the other hand, at higher velocity, the centrifugal force will be high and particle will move towards outer radius. The particle will be rotating within the tank hitting the sides of vanes. This phenomenon can be clearly observed for bigger particles at lower velocity.
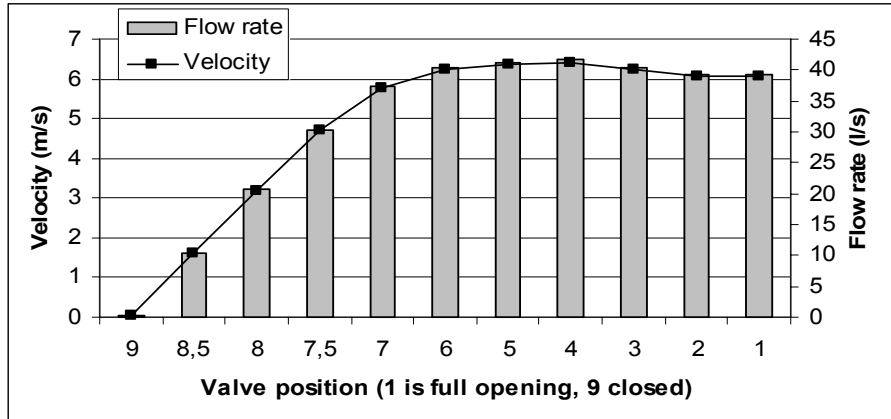
Figure 10.1.1 Flow characteristic of the test rig
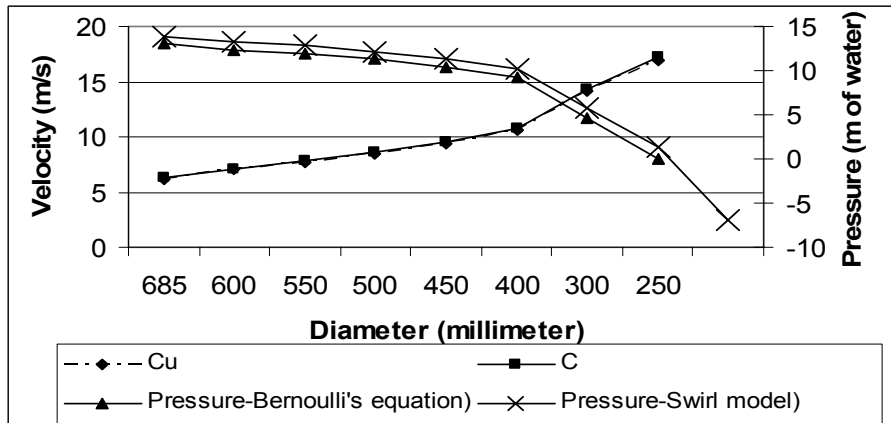
Figure 10.1.2 Velocity and pressure distribution at different radial position due to swirl based on calculation corresponding to maximum flow rate 40 l/s.

10.2 Swirl flow in the test rig

The swirl flow occurs in guide vane outlet-runner inlet gap and outlet of the draft tube of Francis turbine. The swirl flow contains energy which is utilized in runner, but this energy will be is lost in the draft tube. The test rig at NTNU creates swirl flow inside the tank to study the motion of particle in swirl flow. Unlike draft tube, the swirl flow in the test rig is only two dimensional. But basic theory of swirl flow in the test rig is similar to that for draft tube if inlet and outlet of draft tube is merged by freezing its length.

The theory of swirl flow is not well understood. Brekke (2000) have presented idealized swirl flow model for draft tube cone. The theory of swirl flow for draft tube is also valid for this test rig with following assumptions:

1. Constant ratio of peripheral to radial velocity at all radial position, C_r/C_u=constant.
2. Swirl flow formation with rigid body motion or constant vorticity circulation at core with C_u/r=constant and vortex free circulation (swirl) with C_ur=constant towards wall.
3. The flow is incompressible and inviscid.
4. Both continuity and energy conservation hold good.
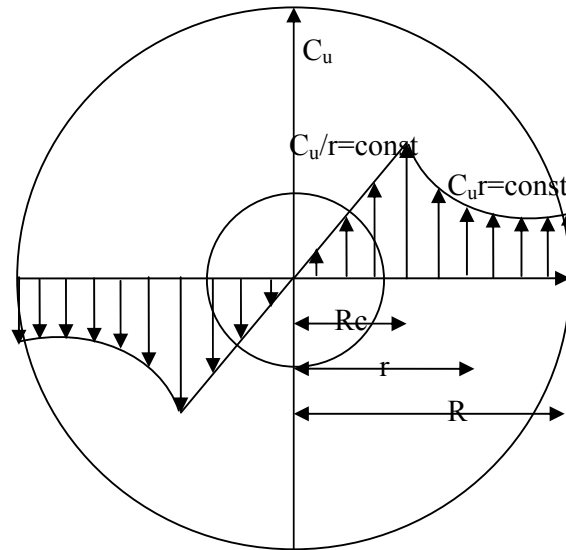
Figure 10.2.1 Illustration of vortex and swirl flow in the test rig

Among two rotational flow shown in figure 10.2.1, the flow in the outer region with C_ur=constant is of main interest in case of this test rig. The junction between vortex and swirl is the point of highest C_u, which occurs at radius R_c.

The distribution of pressure in the field of rotation can be obtained by equilibrium of forces in radial direction as shown by equation 10.2.1.

$$dp = \frac{\partial p}{\partial r} dr = \rho \frac{C_u^2}{r} dr$$ 10.2.1

The integration and substitution of boundary condition value in equation 10.2.1 gives the equation of pressure as:

For the region with vortex at core (*C_u/r*=constant) is:

$$p = p_0 + \frac{1}{2} \rho \left(\frac{C_u R}{R_C^2} \right)^2 r^2$$ 10.2.2

Here p_0 is pressure at the centre and ρ is density of water.

For the region with vortex free swirl ($C_u r$=constant) is:

$$p = p_0 + \frac{1}{2} \rho \left(\frac{C_u R}{R_C} \right)^2 - \frac{1}{2} \rho \left(\frac{C_u R}{r} \right)^2$$ 10.2.3

It is also assumed that there is no energy transfer across the system boundary and there is no loss of energy. Hence total energy flux at different radial section is constant.

The swirl in the test rig can be computed by using equation 10.2.4. The value of C_u at the outlet of the vanes can be calculated according to absolute velocity at that point obtained by continuity equation and angle of vanes with respect to tangent. The pressure at different section of vanes and radial position inside the vanes can be determined with the help of Bernoulli's energy equation (equation 10.2.5).

$$C_u r = const.$$ 10.2.4

$$P + \frac{C^2}{2g} + Z = const.$$ 10.2.5

The main challenge in using equation 10.2.3 and 10.2.4 to calculate the pressure at different radial position is to estimate the ratio of value of R_c/R. Compared to uncertainties associated in guessing the ratio (R_c/R), Bernoulli's equation (equation 10.2.5) gives realistic pressure distribution in the swirl flow region. There is only slight difference in pressure distribution based on Bernoulli's equation and swirl equation assuming $R_c/R = 0.5$. The distribution of pressure at different radial position can be seen in figure 10.2.2. The measured pressure at the point of injection and wall of cone at outlet is already presented in figure 10.1.2.

10.3 Flow visualization

The objectives of the tests on this rig are mainly accomplished by visualization of particle flow inside the test rig. The validity of equation 9.2.3 is also examined by flow visualization. Large particles rotating at low velocity can be clearly seen by naked eye. But as the speed of particle increases or as the size of particle becomes smaller, it is not possible to distinguish the particles in the flow field and the location of particle rotation can not be visualized. The rotation of steel balls up to 8 mm diameter at highest velocity can be seen with naked eye and rhythm of hitting at the vanes can also be heard. The locus of stone, plastic granular and steel balls of different size in different flow velocity are presented in table 10.3.1 and 10.3.2.
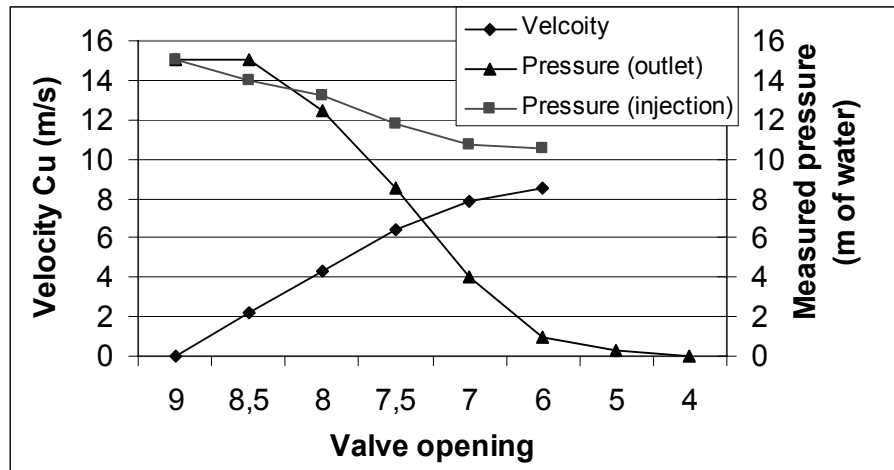
Figure 10.2.2 The measured pressure at the point of injection and wall at outlet

The motion of small particles at higher velocity can be visualized from high speed video camera. High speed video camera is used to compare the location of rotation of particle of different size and determine which size of particles sinks and which size remains rotating in the rig. The use of high speed video camera is very effective for identifying particle rotation and drag coefficient is calculated based on this observation. The images of high speed camera can also be used for assessing speed of particles. Figure 10.3.1 shows the position of steel balls of diameter 10 mm, 7 mm and 4 mm at high flow rate (37 l/s). The locus of all these particles are close to vanes but the observation from high speed video clearly indicates locus at different diameters. Steel ball of 10 mm diameter regularly hits on the wall of vanes and locus of motion changes, but remains rotating inside the tank. Similarly figure 10.3.2 shows the locus of 7 mm particle at low flow rate (0.2 l/s). This particle is moving along the flow direction and ultimately sinks. Figure 10.3.3 shows picture frames from high speed video camera of 10 mm steel ball in less than 1 l/s flow rate, which remain rotating in the test rig. Some additional picture frames with time is shown in appendix E.

From observation with naked eye, the velocity of particle is found close to 0.43 m/s for 6 mm steel particle and 0.39 m/s for 8 mm steel ball at the valve position 8.5 with flow rate 10.4 l/s. The velocity of water computed at this diameter is about 1.6 m/s. This difference in water and particle velocity can be explained by higher frictional force between particle and steel plate at low velocity range. At high velocity region (valve position 8 with flow rate 20.6 l/s), the effect of friction is negligible because there may not be direct contact between particle and surface. The particles may be floating, which is also observed by shadow of balls in the video image. With the naked eye observation, the velocity of sand particle of 4 mm is found about 3.34 m/s and that of 8 mm steel ball was found 2.83 m/s. This velocity is closed to the one calculated from continuity (figure 10.1.1 valve position 8) that is 3.17 m/s. The calculation of velocity of particle using images of high speed video camera is about 5.75 m/s for 10 mm particle at valve position 7 with flow rate 37.3 l/s, which gives velocity same as calculated from continuity equation. This observation verifies the assumption that particles have same velocity as that of water.

Table 10.3.1 Visual observation of particle flow at 10.4 l/s
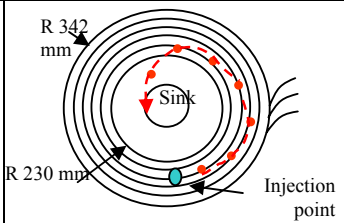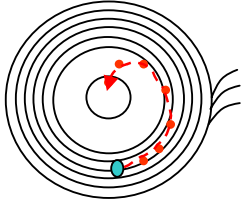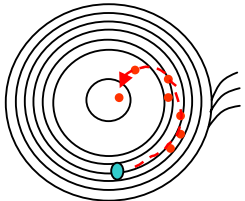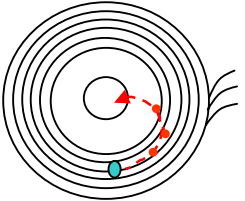
Particles	Comments	Sketch (dotted lines-particle locus)
Stone 4 mm (not completely spherical)	Slightly moves outward and then sinks. Not able to complete 1 revolution.	R 342 mm / Sink / R 230 mm / Injection point
Plastic spherical ball 6 mm	Completes 1 round at the radius in between 270-290 mm.	
Plastic granular (black) specific gravity 1.42	Can not complete 1 revolution and sink	
Plastic granular (white) specific gravity 1.41	Completes half the revolution and sinks	
Steel ball 2 mm diameter	Completes ¼ revolution and sinks	

Table 10.3.1 Continued
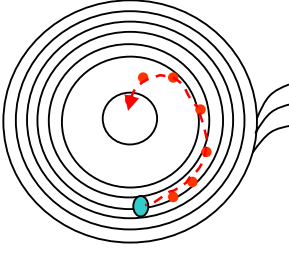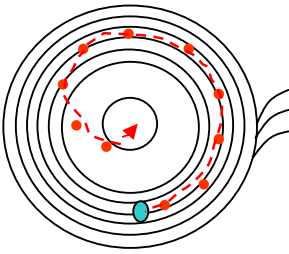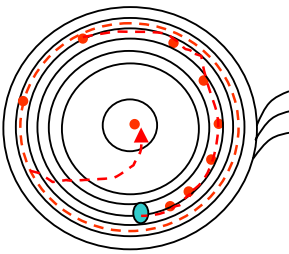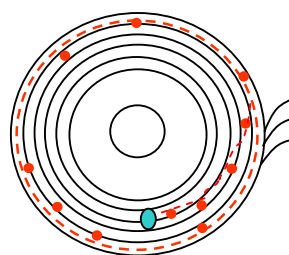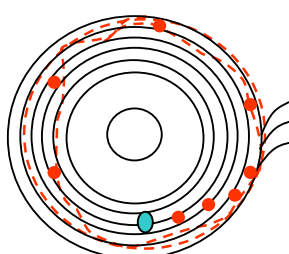
Steel ball 3 mm diameter	Completes ½ revolution and sinks	
Steel ball 4 mm diameter	Completes ¾ revolution and sinks	
Steel ball 5 mm diameter	Rotates 6-7 revolutions in between radius 290-310 mm and sinks	
Steel ball 6 mm diameter	Rotates continuously at the radius 342 mm hitting the vanes. Remains rotating. 24 revolutions in 2 minute.	
Steel ball 8 mm diameter	Rotates continuously at the radius 342 mm hitting the vanes. Remains rotating. But direction changes rapidly due to hitting on the vane wall 22 revolutions in 2 minute.	

Table 10.3.2 Visual observation of particle flow at 20.6 l/s

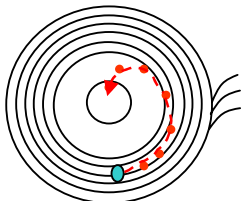| Flow rate increased to 20.6 l/s		
Steel ball 8 mm diameter	79 revolution in 1 min.	Rotate at vanes
Steel ball 3 mm diameter	77 revolution in 1 min.	Rotate at vanes
Steel ball 2 mm diameter	Invisible	
Stone 4 mm	101 revolutions in 65 sec	Rotates almost at vanes
Plastics ball & granular	Invisible or sinks	
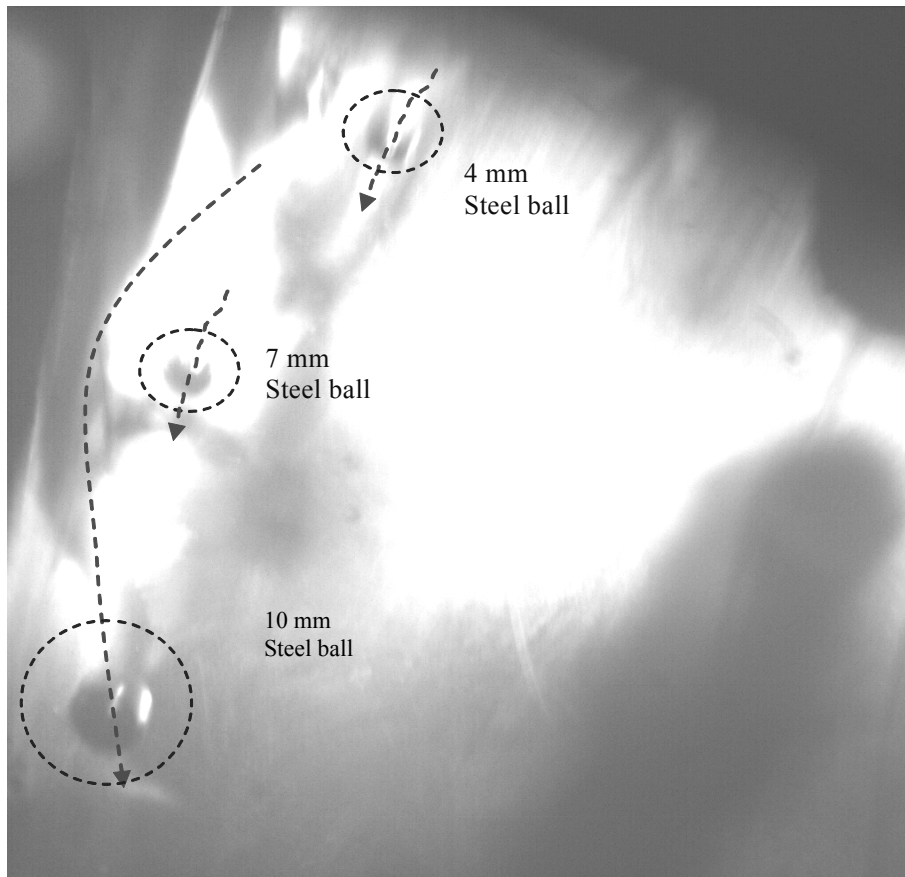
Figure 10.3.1 Motion of steel balls of different sizes observed from high speed video camera at flow rate about 37 l/s.
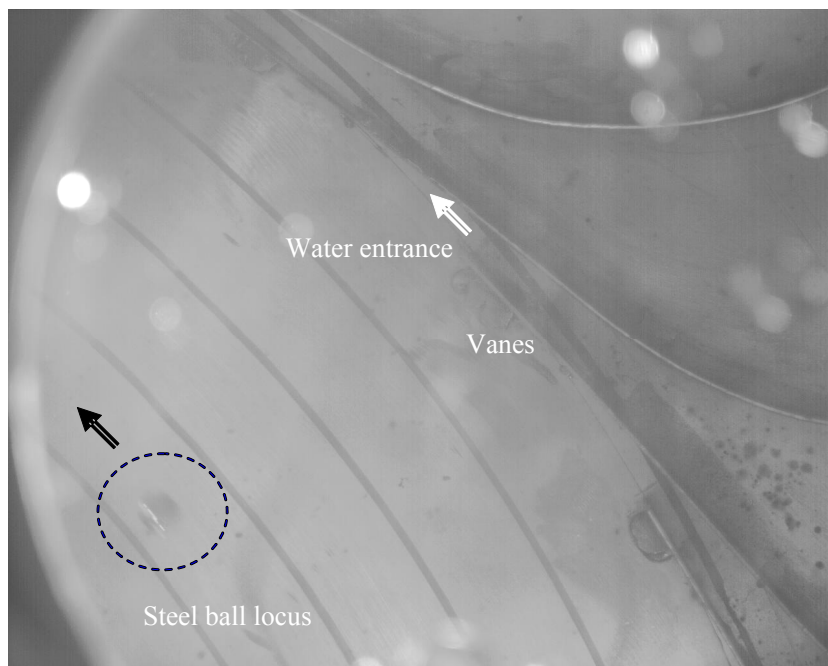
Figure 10.3.2 Motion of steel ball of 7 mm diameter rolling at the diameter of injection point at very low flow rate (0.2 l/s)

10.4 Reynolds number and drag coefficient

The calculated value of drag coefficient (C_D) from equation 9.2.3 depends on particle size, specific gravity of particle, vane angle and radius at which particle is moving. As discussed in previous section, the value of calculated C_D depends upon diameter of particle and radius of locus for equilibrium between drag force and centrifugal force. The ratio of particle velocity in peripheral direction and absolute velocity of water can be obtained from orientation of vane angle. The directions of flow at different radial positions were analyzed by observing direction of wool threads fixed at Plexiglas. The movement of 8 mm stone particle at different flow condition and corresponding Reynolds number is presented in table 10.4.1.

The comparison can be made for the C_D presented on literature based on Reynolds number and calculation from this test. The flow Reynolds numbers at different valve opening at the point of injection and just outside the vanes are presented in figure 10.4.1. Similarly the Reynolds numbers for particles of different sizes are presented in figure 10.4.2 for same valve opening positions. The flow Reynolds number is calculated considering hydraulic diameter at the point of injection and vane outlet as characteristic dimension, whereas Reynolds number for particle is calculated considering diameter of particle as characteristic

dimension. There are differences in opinion for calculating particle Reynolds number. Tabakoff et al. (1991) have considered the difference of particle and fluid stream velocity for calculating Re. But in this test fluid stream velocity is considered as incident velocity as suggested by Spurk (1997) and Re_p is calculated by using equation 10.4.1

$$Re_p = \frac{Vd}{\nu}$$ 10.4.1

Frame 1	Frame 4
Frame 2	Frame 5
Frame 3	Frame 6
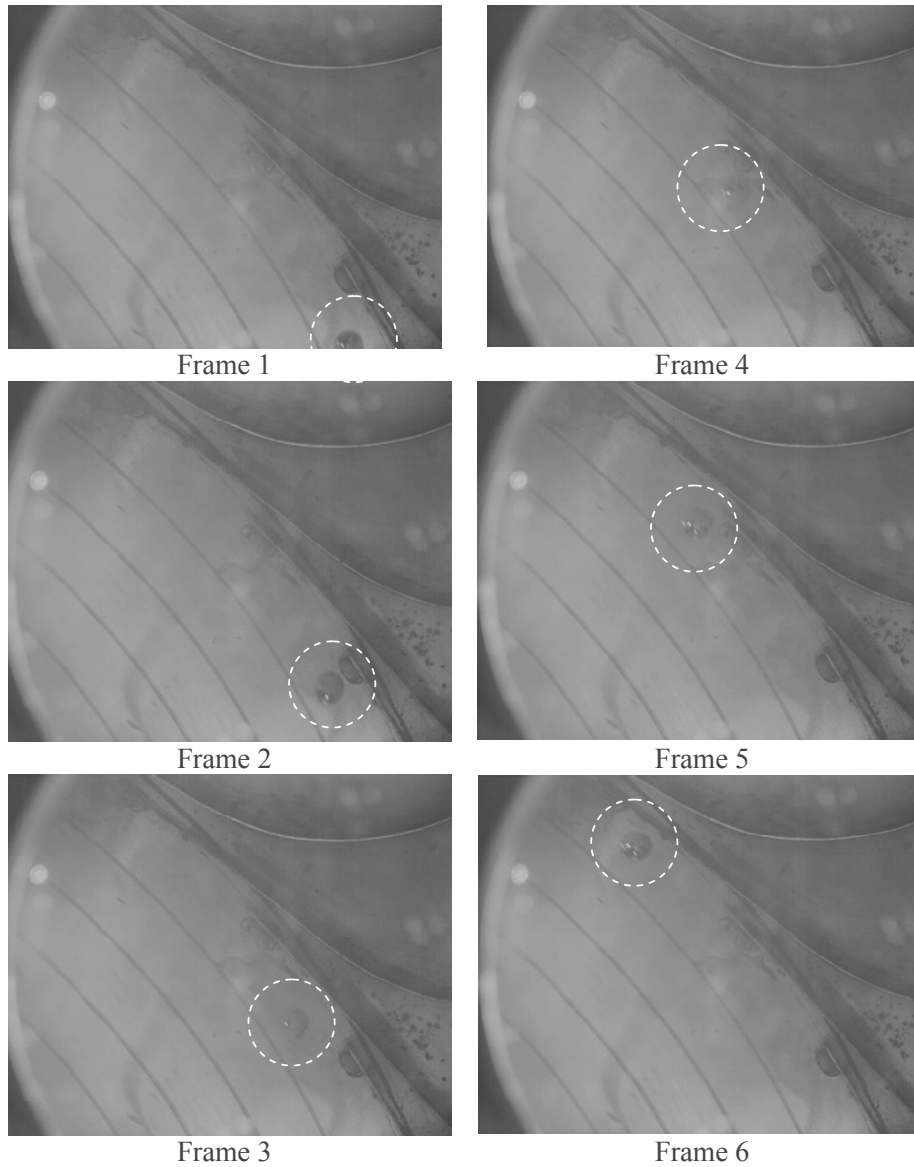
Figure 10.3.3 Picture frames of high speed video camera with 10 mm steel ball at flow rate less than 1 l/s
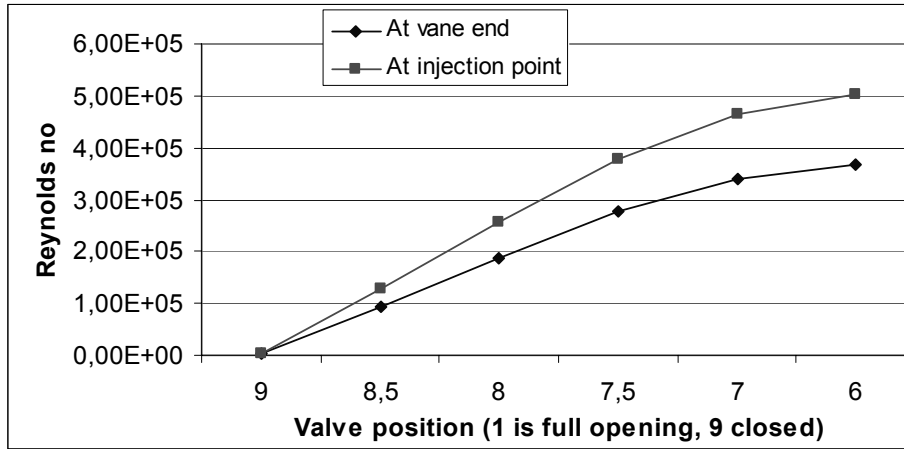
Figure 10.4.1 The flow Reynolds number for different valve opening at end of vane and at the point of injection
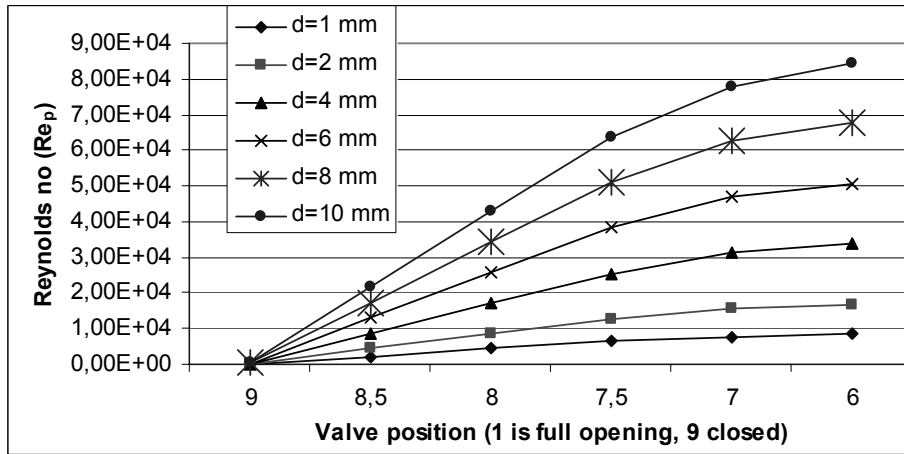
Figure 10.4.2 (b) Particle Reynolds number for different valve opening at the point of injection

At low velocity, the Reynolds number is low and inertia force is smaller than the friction force. In such cases, particles are pulled by surrounding water and carried towards stagnation point. It is hard to achieve smooth streamlines as shown in figure 10.4.3 for $Re=10^0$ and 10^2 in case of flow of water in the test rig. The velocity should be extremely low to achieve this condition. In fact the flow inside the rig is turbulent and even with the minimum discharge condition, for instance 0.2 l/s, the Reynolds number reaches almost 2500. The highest flow Re at point of injection corresponding to 40 l/s flow is almost $5X10^5$ and the Reynolds number beyond 6th valve opening position is almost same because of constant flow rate thereafter. But the particle Reynolds number (Re_p) is only about 60 for 1.5 mm particle on velocity around 0.04 m/s and highest value is for 10 mm particle at highest velocity (8.5 m/s) is about $8.5X10^4$.

As the Reynolds number increases, there will be a separation of flow field with the formation of vortex behind the body and further increase in Reynolds number causes unstable and unsteady wake formation. The drag coefficient depends upon the flow pattern behind the object. But for incompressible flow, the drag coefficient is only a function of particle Reynolds number as shown in figure 10.4.3 by Spurk (1997). The sudden drop of value of C_D around Reynolds number $3X10^5$ is due to transition of laminar boundary layer on spherical surface to turbulent boundary layer. The shear stress in the turbulent boundary layer is larger; hence fluid at outer layer is dragged close to the wall. This retards the flow separation and wake becomes narrower. The non-separated flow in the back side of the particle exerts force against the flow direction and hence C_D becomes smaller. This transition can occur in lower Reynolds number when the surface is made rough as in golf ball. Sand particle surface being rougher than the regular spherical surface may have value of C_D in this region.

The observation of Reynolds number at different flow condition and direction of flow components are presented in table 10.4.1. The values of C_D from the experiment in the swirl flow are smaller than that shown in figure 10.4.3 given by Spurk (1997), where the value of C_D observed from experiment is plotted on dots. From experimental observation, C_D for small particle is small and lies towards the transition region compared to large particle. The hypothetical situation with particle of 4 mm size at the high velocity (for example 85 m/s) may just cross the transition region. With these observations, the assumption that at equilibrium condition the drag force is balanced by centrifugal force can be confirmed and equation 9.2.3 is valid for particle moving in rotational flow.

Some of the uncertainties that may come across are:

- assumption of equal particle and flow velocity
- difference in friction force between particle and surface in rolling, sliding and gliding condition of particles
- irregularity of stone and plastic granular compared to perfect spherical shape
- flow direction in test rig is different than the one shown in figure 10.4.3 (which is across the streamline)

In spite of these uncertainties, the value of C_D around 0.1-0.2 could be appropriate for estimation of particle that will stay rotating in the swirl flow due to centrifugal force at high Re region.
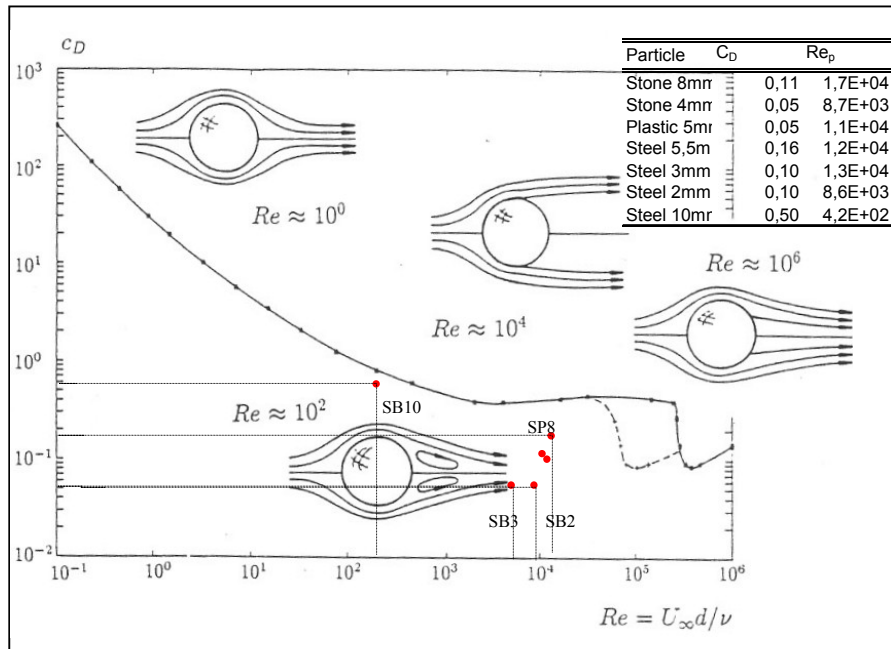
Figure 10.4.3 Drag coefficient of spherical particle (after Spurk, 1997) and experimental value calculated based on observation of rotation of steel ball, plastic and granular and stone on swirl flow in test rig at NTNU (SB-Stainless steel ball and SP is stone particle, number indicate diameter in mm)

10.5 Discussion and conclusion: particle separation

The erosion of Francis turbine guide vanes by large particles support phenomenon of particle separation. Similarly the work of Tabakoff et al. (1991) also confirmed the concept of particle separation. They have also observed the deviation of particle trajectory from streamline in the gas turbine with increasing size of ash particles. The observation by naked eye and with high speed video camera on newly built test rig at NTNU verified the concept. Following conclusion can be drawn from the experiment on this test rig.

- The equilibrium of particle between centrifugal force and drag force holds true in case of swirl flow.
- Coefficient of drag depends upon Reynolds number.
- Theory of swirl flow is true in case of test rig. The measured and computed pressure distribution in the swirl flow is very close.
- The visualization of flow direction in the swirl flow confirms assumption that flow direction is same in all radial positions.
- The radial position of rotation of particles of various sizes confirms that the drag coefficient is function of particle Reynolds number. The experimental observation reveals that drag coefficient for particles is in between 0.1-0.2.

The particles of higher size are settled down or removed before it enters turbine. The unsettled large size particles, especially in the monsoon season pass thorough turbines in hydropower plant. The guide vanes of Francis turbine can have maximum angle up to as low as 10°-12° at full load in normal operating condition. Whereas this angle could go up to 30° - 40° in some of the turbine design. The illustration of guide vane angle and the value of that for some of the power plants are given in figure 10.5.1. Such inclination of guide vanes creates swirl flow in Francis turbine and the magnitude of swirl depends upon angle of inclination of guide vanes. Even though irregular shape of sand particles could have higher drag coefficient compared to spherical steel balls, the observation from the test rig can be utilized for determining the size of particle which will remain rotating in the swirl flow in between guide vane outlet and runner inlet. Any particles higher than this size continuously hit the guide vane outlet region at suction side and damage them severely.

The guide vane maximum angle at full load

Powerplant	n_s	α
Skjærka	66	12
Nedre Vinstra	69	12
Hol I	72	13
Mesna	78	13
Røssåga	104	18
Grønsdal	113	23
Nore II	198	34
Dynjafoss	208	27,5
Oltesvik	264	38,5
Iverland	269	31,5
Fiskumfoss	308	40,5
Fiskumfoss	308	36,5
Gravfoss	346	37
Solbergfoss	365	38
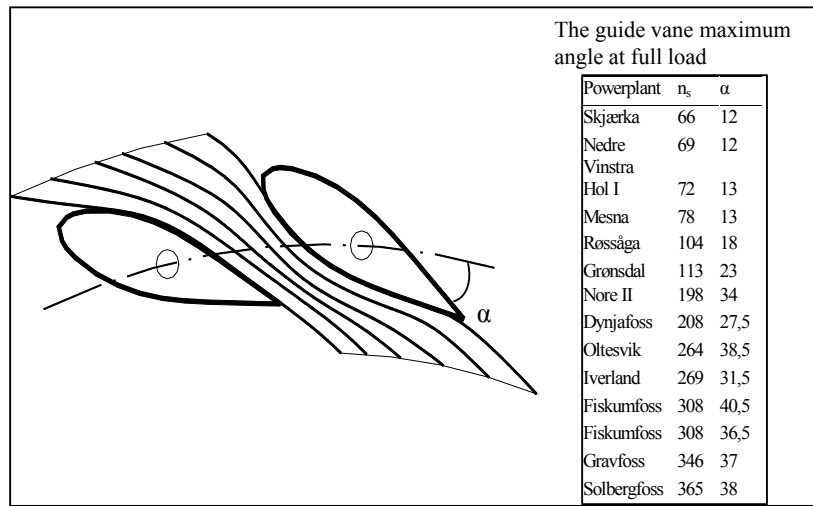
Figure 10.5.1 The illustration of guide vane in open position and guide vane maximum angle at full load for different power plants (based on lecture notes by Dahlhaug, Ole G.)

The diameter obtained from equation 9.2.3 can be considered as critical diameter. All the particles larger than critical diameter will remain rotating in the swirl flow hitting the guide vane wall. On the other hand all the particles smaller than critical size flows through turbines. The relation between particle size and drag coefficient for turbine of radius 1 m at inlet is shown in figure 10.5.2. This figure indicates that the sand particles of diameter higher than 2 mm will stay rotating in the swirl flow and damage guide vanes positioned around 10°. At higher Reynolds number, the drag coefficient is around 0.1, which shows even particle size around 1 mm will stay rotating. Similarly the relation between critical diameter and runner inlet diameter is shown in figure 10.5.3 (considering drag coefficient 0.2). This figure also shows that smaller turbines are more prone to sand erosion because smaller turbines are having small critical diameter, for example particles as small as 0.35 mm may remain rotating in the turbines of inlet diameter 800 mm. This is a likely case at Jhimruk hydropower project in Nepal.

Figure 10.5.2 and 10.5.3 is suggested as guidelines for operating strategy for Francis turbine operating with large sand particles. If the particle size in the water is larger than critical particle sizes given in these figures, the turbine should not be operated at low guide vane opening.
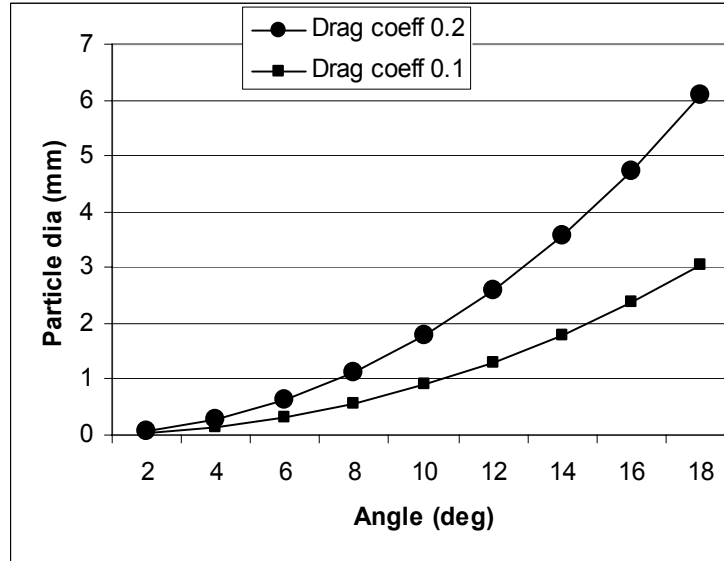
Figure 10.5.2 The critical diameter of particle for turbine runner with radius 1 m
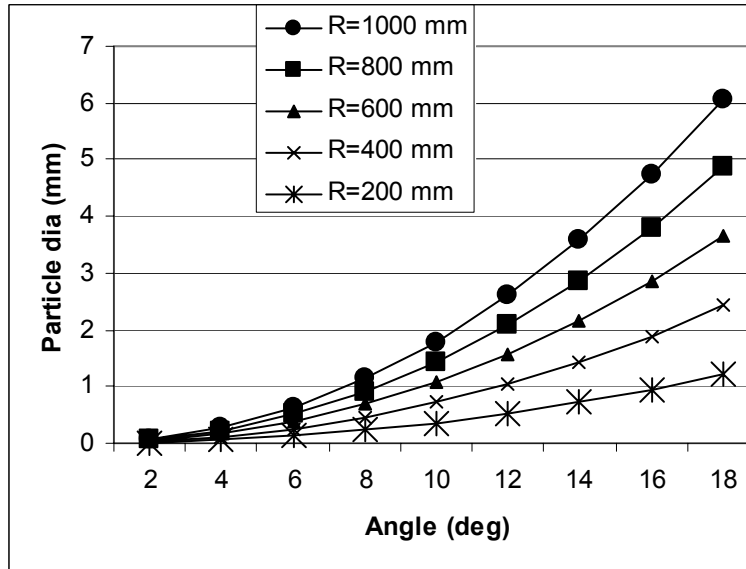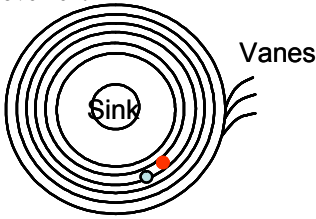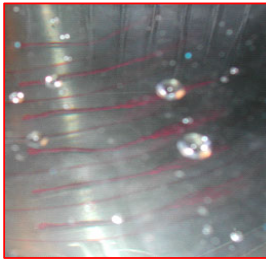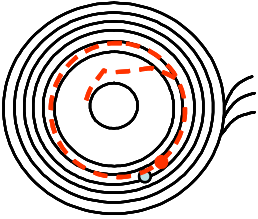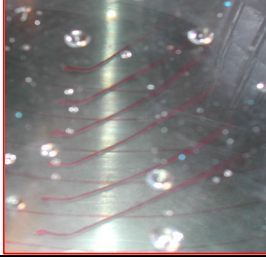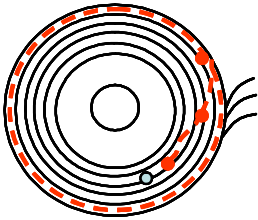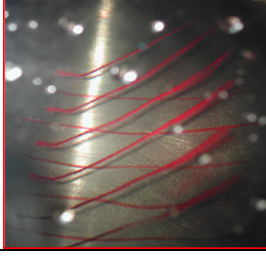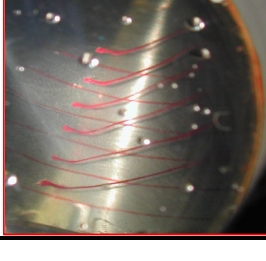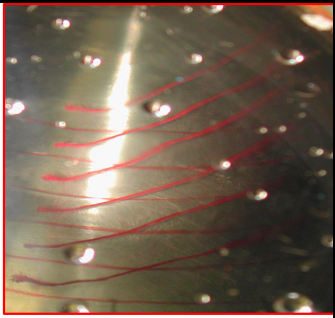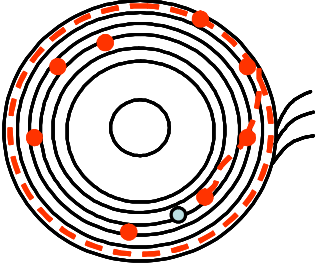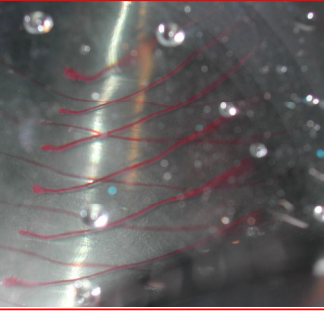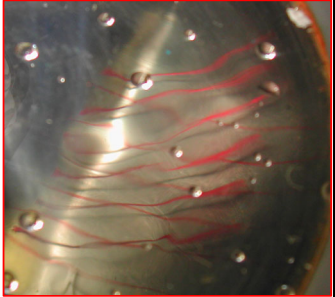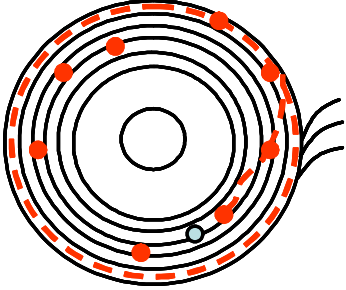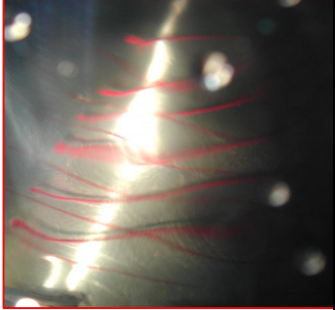
Figure 10.5.3 The critical diameter of particle considering drag coefficient 0.2

Table 10.4.1 Flow visualization and Reynolds number at different flow condition using 8 mm stone particle

Valve position	Flow rate l/s	Reynolds number and remarks (dots – particle trace)	Flow direction (represented by thread)
9	0.2	$Re_p \approx 335$ No movement Vanes Sink 	
8.5	10.4	$Re_p \approx 17416$ Circulates 4-5 round and sinks 	
8	20.6	$Re_p \approx 34497$ Starts striking on vane wall 	
7.5	30.4	$Re_p \approx 50908$ Continue striking on vane wall	

7	37.3	Re$_p$≈62463 Continue striking on vane wall	
6	40.4	Re$_p$≈ 67654 Continue striking on vane wall 	
4	41.6	Re≈503940 Particle its the wall violently and particle path depends upon impact. Some stone particles break and small fraction flow with water	
2	39.2	Re≈503940 	

Chapter 11

Further work

This research on sand erosion on hydraulic machinery is one of the few efforts in the problem area. As discussed in main text of this thesis, this problem area is related to technological, management and economical matters. The attempt to investigate and solve all the issue would have been day dream. Even then attempts have been made to explore as much as issues related to sand erosion of hydraulic machinery. The ideas which were emerging during this work are also discussed in respective sections. Following are specific suggestions for future work.

Model development

There are several parameters associated with erosion of turbine. In this research, measurements were carried out for only few parameters to develop erosion model for application to hydraulic machinery. Hence more tests should be carried for various parameters and more number of tests at same test condition for statistical confidence. The development of method for sand particle shape analysis is specifically recommended for the purpose of erosion model. Combined effect erosion and cavitation is not explored much. The rotating disc apparatus to study cavitation at Water Power Laboratory can be used to study synergy between cavitation and sand erosion for the purpose of hydraulic machinery.

Lastly, with the convinced erosion model, computational fluid dynamic (CFD) analysis can be carried out for sand erosion problem in hydraulic machinery together with numerical analysis of mechanics of material and fracture.

Field Inspection

Inspection and measurement of eroded turbine is dubious. The inspection procedure for sand erosion should be developed. The inspection by boroscope is one of promising techniques, but this author recommends for image processing of such images and develop decision making tool for repair based on operation database of total discharge and sediment load passed through turbine units. Such tool can incorporate cutoff limits for concentration, efficiency drop and so on.

High velocity jet erosion test rig

The suggestions for modification and improvement of high velocity jet erosion test rig are discussed in section 8.12. In principle following recommendation are made for the measurement on jet type of test rig.

1. The jet with bigger hydraulic radius and closest distance in between nozzle exit and specimen should be made to ensure effective hitting of particles and get analogous condition of flow in hydraulic machinery.
2. Use of jet and particle velocity measurement.
3. Further tests on specimens with different roughness and pre-stressed specimens for understanding their role in erosion model.
4. Test at very high velocity with similar abrasive and environment by using high pressure abrasive jet machining gives additional data to extrapolate laboratory data for erosion rate for high head turbines.
5. Establishing relation between experimental model and weight loss of turbine in given operating condition.

Swirl flow test rig

Following are the recommendation for further work in newly develop test rig:

1. Computational fluid dynamics (CFD) simulation of flow in test rig and verification of particle motion in such flow is necessary to supplement the knowledge of separation of large particle in turbine components.
2. The modifications suggested in newly built test rig are: (i) adjustable vanes (ii) addition of window for light source close to observation window (iii) provision to measure velocity components by knife edge pitot (iv) improvement in air bleeding system.
3. Regarding further tests on this test rig, measurements at high velocity (using pressurized system) for fine sand (smallest possible size to observe from high speed camera) and particles of known geometry (cubical, triangular) can be carried out to have clear understanding of relation between Reynolds number and drag coefficient.

References

Abrahamson G.R. (1961) J. Appl. Mech. E 3, pp. 519–528

Adhikari M.S. (1999) NHE experience in the sand wearing problems of the hydraulic turbines and their parts, Proc. Int. Seminar on sediment handling technique, NHA, Kathmandu

Anderws P., Illson T.F. and Mathews S.J.(1999) Erosion-corrosion studies on 13 Cr steel in gas well environments by liquid jet impingement, Wear (233-235) pp 568-574

Arnold J.C and Hutchings I.M. (1990) The mechanisms of erosion of unfilled elastomers by solid particle impact, Wear (138) pp 33-46

Arnold J.C and Hutchings I.M. (in 1989) Flux rate effects in the erosive wear of elastomers, Jr. of material science (24) pp 833-839

ASTM G40-88 (1988) Standard terminology related to wear and erosion, American society for testing and materials (ASTM)

Aunemo H. (1992) Utprøving av erosjonsbestandige belegg for nål og munnstykke I Mel kraftverk, Prosjekt nr VF0083, Kværner Eureka a.s (Report in Norwegian)

Bahadur S. and Badruddin R. (1990) Erodent particle characterization and the effect of particle size and shape on erosion, Wear (138) 189-208

Bardal E. (1985) Korrosjon og korrosjonsvern, Tapir, Trondheim (In Norwegian)

Basnyat S. (1999) Monitoring sediment load and its abrasive effects in Jhimruk hydropower plant Nepal, Proc. Optimum use of run-off-river conf., Trondheim

Basnyat S. (1999a) Internal report - BPC Hydroconsult – Recommended actions on sediment control at Jhimruk power plant, Proc. Int. seminar on sediment handling technique, NHA, Kathmandu

Bergeron P. and Dollfus J. (in 1958) The influence of nature of the pumped mixture and hydraulic characteristics on design and installation of liquid/solid mixture pump, Proc. 5th conf. on hydraulics, turbines et pumpes Hydrauliques, pp 597-605

Berget J. (1998) Influence of powder and spray parameters on erosion and corrosion properties of HVOF sprayed WC-Co-Cr Coatings, Dr. Ing. Thesis, NTNU

Berget J. (2004) Private communication

Berget J. and Rogne T. (2004) Erosion and erosion-corrosion properties HVOF sprayed tungsten carbide (WC) coatings with high alloy binders, Proc. International thermal spray conference, Osaka

Bhushan B. (2002) Introduction to Tribology, John Wiley & Sons, New York

Bishwakarma M.B, Dhakal G.P. and Pradhan P. (2003) Headworks design in Himalayan rivers: case study of Khimti I hydropower project Nepal, Int. Conf. Hydro 2003, Croatia

Bishwakarma M.B. (1999) Sediment exclusion optimization study, Jhimruk hydropower plant Nepal, Proc. Optimum use of run-off-river Conf., Trondheim

Bitter J. G. A. (1963) A Study of Erosion Phenomena, Part I and II, Wear (6) pp 5 - 21 and 169 - 190

Bjordal M. (1995) Erosion and corrosion of ceramic-metallic coatings and stainless steel, Dr. Ing. Thesis, Universitetet I Trondheim, NTH

Brekke H (2004) Personal communication

Brekke H. (1978) Discussion of Pelton turbine versus Francis turbines for high head turbines, IAHR, Colorado

Brekke H. (1984) Choice of material for water turbines and the influence this has on design manufacturing, testing and operation, General doctoral lecture notes for NTH, Trondheim

Brekke H. (1986) Design and material quality for high head turbine, IAHR symposium, Montreal

Brekke H. (1988) The influence from guide vane clearance gap on efficiency and scale effect for Francis turbine, IHAR, Trondheim

Brekke H. (1994) State of art in Pelton turbine design, Hydropower and dam (March), pp 21-28

Brekke H. (1998) Operational safety, reliability and life time of hydraulic machines, IAHR, Singapore

Brekke H. (2000) Hydraulic turbines, design, erection and operation, Compendium, NTNU

Brekke H. (2002) Design of hydraulic machinery working in sand laden water, In: Duan C.G. and Karelin V.Y. (eds), Abrasive erosion and corrosion of hydraulic machinery, pp 155-181, Imperial college press, London

Brekke H. (2004) Design and operation of medium and high head turbines, Hydro vision 2004, Montreal

Brekke H., Bardal E. and Rogne T. (1994) Norwegian research work on erosion resistive coating for water turbines, XVII IAHR Symposium, Beijing

Burwell, John T. Jr. (1957/58) Survey of possible wear mechanisms, Wear (1) pp 119-141

Castberg T. (2002) Private communication

Chaudhary C.S. (1999) Impact of high sediment on hydraulic equipment of Marsyangdi hydropower plant, Proc. Int. seminar on sediment handling technique, NHA, Kathmandu

Chen Q. and Li D. Y. (2003) Computer simulation of solid particle erosion, Wear (254) pp 203-210

Chevallier P. and Vannes A.B. (1995) Effect on a sheet surface of an erosive particle jet upon impact, Wear (184) pp 87-91

Chevallier P., Vannes A. B. and Forner A. (1995) New parameters in erosion for study of bulk materials and coatings, Wear (186-187) pp210-214

Chopra V. and Arya S. (1996) Silt-Its effect on hydro power components and remedial measures, Proc. Silt damages to equipment in hydro power stations and remedial measures, New Delhi, pp 101-109

Clark H. M. and Hartwich R. B. (2001) A re-examination of the `particle size effect' in slurry erosion, Wear (248) 147-161

Clark H. McI, Tuzson J. and Wong K. K. (2000) Measurements of specific energies for erosive wear using a Coriolis erosion tester, Wear (241) pp 1-9

Clark., Hawthorne H. M. and Xie Y. (1999) Wear rates and specific energies of some ceramic, cermet and metallic coatings determined in the Coriolis erosion tester, Wear (233-235) pp 319-327

Clift R. Grace J.R. and Weber M.E. (1978) Bubbles, drops and particles, Academic press, New York, pp 77-78

Dahlhaug O.G. and Thapa B. (2004) Sand erosion in Francis turbine: A case study from Jhimruk power plant, Nepal, IAHR symposium on hydraulic machinery and systems, Stockholm

Das S., Mondal D. P., Modi O. P. and Dasgupta R. (1999) Influence of experimental parameters on the erosive-corrosive wear of Al-SiC particle composite, Wear (231) pp 195-205

Deng T., Bradley M.S.A. and Bingley M.S. (2001) An investigation of particle dynamics within a centrifugal accelerator type erosion tester, Wear (247) pp 55-65

Dosanjh S. and Humphery J.A.C. (1985) The influence of turbulence on erosion by a particle-laden fluid jet, Wear (102) pp 309-330

Drolon H. and Druaux F. and Faure A. (2000) Particle shape analysis and classification using wavelet transforms, Pattern recognition letters (21) pp 473-482

Duan C.G. (1988) Sand erosion of hydraulic turbine, Press of Tsinghua University, Beijing (in Chinese)

Duan C.G. and Karelin V.Y. (eds) (2002) Abrasive erosion and corrosion of hydraulic machinery, Imperial college press, London

Fang Q. and Sidky P.S. and Hocking M.G. (1998) Microripple formation and removal mechanism of ceramic materials by solid-slurry erosion, Wear (223) pp 93-101

Feng Z. and Ball A. (1999) The erosion of four materials using seven erodent – towards an understanding, Wear (233-235) pp 674-684

Field J.E. (1999) Liquid impact: theory, experiment, applications, Wear (233-235) pp 1-12

Field, J.E., Sun, Q. and Jilbert, G.H. (1995) Solid particle erosion of IR-transmitting materials and diamond composites, Wear (186-187) pp 195-202

Finnie I. (1960) Erosion of surfaces by solid particle, Wear (3) pp 87-103

Finnie I. (1995) Some reflections on the past and future of erosion, Wear (186-187) pp 1-10

Frantzen R. and Haldogård G. (2000) Project report - Fastlegging av erosjonsforhold i høyhastighets prøveutstyr, HIST (in Norwegian)

Galay V., Schreier H. and Bestbier R. (2002) Himalayan sediments: Issues and Guidelines, CD publication, Water and Energy Commission Secretariat, Nepal

Gandhi B.K., Singh S.N. and Seshadri V. (1999) Study of parametric dependence of erosion wear for the parallel flow of solid-liquid mixtures, Tribology International (32) pp 275-282

Ghosh A and Mallik A.K. (1986) Manufacturing Science, Ellis Horwood, page 261, 309

Goel D.B. and Sharma M.K. (1996) Present state of damages and their repair welding in Indian hydroelectric projects, Proc. Silt damages to equipment in hydro power stations and remedial measures, New Delhi, pp 137-152

Haakon K. (1999) Khimti I hydropower project, Proc. Optimum use of run-off-river Conf., Trondheim

Halg R. and Krause M. (1996) Ceramic coating as an efficient measure against erosion at the Francis turbine in the Pradella power plant, Proc. Silt damages to equipment in hydro power stations and remedial measures, New Delhi, pp 153-158

Hana M. (1999) Numerical analysis of non-stationary free surface flow in a Pelton bucket, dr. ing. Thesis, NTNU

Haugen K., Kvernvold O., Ronold A. and Sandberg R., Sand erosion of wear-resistant materials: Erosion in choke valves, Wear 186-187(1995) 179-188

Hawthorne H. M. (2002) Some Coriolis slurry erosion test developments, Tribology International (35) pp 625-630

Head W.J. and Harr M. E. (1970) The development of model to predict the erosion of materials by natural contaminants, Wear (15) pp 1 – 46

Hengyun Z.F., Shiyun L. and Chenzhao H. (1986) The role of sand particles on the rapid destruction of the cavitation zone of hydraulic turbines, Wear (112) 199-205

Hojo H., Tsuda K. and Yabu T. (1986) Erosion damage of polymeric material by slurry, Wear (112) pp 17-28

Horszczaruk E. (2003) The model of abrasive wear of concrete in hydraulic structures, Wear

Hu X. G., Momber A. W. and Yin Y. G. (2002) Hydro-abrasive erosion of steel-fibre reinforced hydraulic concrete, Wear (253) 848-854

Hubner W. and Leitel E. (1996) Peculiarities of erosion- corrosion processes, Tribology International (29) pp 199-206

Hussainova I. (2001) Some aspects of solid particle erosion of cermets, Tribology International (34) pp 89-93

Hussainova I., Kubarsepp J. and Pirso J. (2001) Mechanical properties and features of erosion of cermets, Wear (250) pp 818-825

Hussainova I., Kübarsepp J. and Shcheglov I. (1999) Investigation of impact of solid particles against hardmetal and cermet targets, Tribology International, (32) pp 337

Jain A.K (1999) Silting problems in hydropower projects: Indian scenario, Proc. of 1ˢᵗ Int. conf. on Silting problems in hydro power plants, New Delhi, pp 37-54

Jilbert G.H. and Field J.E. (2000) Synergistic effect of rain and sand erosion, Wear (243) pp 6-17

Kang Z. and Chenqing G. et al. (1993) Study on mechanism of combined action of abrasion and cavitation erosion on some engineering steels, Wear (162-164) pp 811-81

Karelin et al. (2002) Fundamental of hydroabrasive erosion therory, In: Duan C.G. and Karelin V.Y. (eds), Abrasive erosion and corrosion of hydraulic machinery pp 1-52, Imperial college press, London

Karimi A. and Schmid R.K. (1992) Ripple formation in solid-liquid erosion, Wear 156 33-47

Karimi A., Verdon C., Martin J. L. and Schmid R. K. (1995) Slurry erosion behavior of thermally sprayed WC-M coatings, Wear (186-187) pp 480-486

Kayastha G.P. (1999) Silting problems in hydro power plants in Nepal, Proc. of 1st Int. conf. on Silting problems in hydro power plants, New Delhi, pp 23-30

Khanna R. (1996) Ceramic wear resistance coatings for needle tips and nozzles used in Pelton machines, Proc. Silt damages to equipment in hydro power stations and remedial measures, New Delhi, pp 159-165

Kjell O.H. (2002) Sand erosion in hydraulic machinery, Project report, Inst. of energy and process engg, NTNU

Krause M. and Drtina P. (1996) applied abrasion research- prediction of damage, Proc. Silt damages to equipment in hydro power stations and remedial measures, New Delhi, pp 192-202

Krzyzanowski J.A., Kowalski A.E. and Shubenko A.L. (1994) Some aspects of erosion prediction of steam turbine blading, Trans. ASME, Jr. of eng. for gas turbines and power, pp 442-451

Levy A. and Man F.Y. (1986) Surface degradation of ductile metals in elevated temperature particle gas streams, Wear (111) pp 173-186

Levy A.V. (1981) Solid particle erosion behavior of steels as a function of microstructure, Wear (68) pp 269-287

Lin H. C., Wu S. K. and Yeh C. H. (2001) A comparison of slurry erosion characteristics of TiNi shape memory alloys and SUS304 stainless steel, Wear (249) pp 557-565

Lynn, R. S., Wong K. K. and Clark H. M. (1991) On the particle size effect in slurry erosion, Wear of Materials, ASME, pp 77 - 82

Lysne D.K., Glover B., Støle H. and Tesaker E. (2003) Hydropower development book series number 8 - Hydraulic design, NTNU

M.S. Yalin (1971) In: (4th edn. ed.), Proc. 14th Congr. International Association for Hydraulic Research, Paris, 1971 Vol. 3, Société Hydrotechnique de France (SHF), pp. 101–108

Madsen B. W. (1988) Measurement of erosion-corrosion synergism with a slurry wear test apparatus, Wear (123) 127-142

Mann B. S. (2000) High-energy particle impact wear resistance of hard coating and their application in hydroturbines, Wear (237) pp 140-146

Mann B. S. and Arya V. (2002) An experimental study to correlate water jet impingement erosion resistance and properties of metallic materials and coatings, Wear 253 pp 650-661

Maozhong Y., Baiyun H. and Jiawen H. (2002) Erosion wear behavior and model of abradable seal coating, Wear 253 pp 9-15

Matsumura M. and Chen B.E. (2002) Erosion-resistant materials, In: Duan C.G. and Karelin V.Y. (eds), Abrasive erosion and corrosion of hydraulic machinery, pp 235-314, Imperial college press, London

Meng H.C. and Ludema K.C. (1995) Wear models and predictive equations: their form and content, Wear (181-183) pp 443-457

Ministry of water resources (MWR) (2003), Nepal Country Report presented by Minister for Water Resources at 3rd World water forum, Kyoto

Murthy J. K. N., Rao D. S. and Venkataraman B. (2001) Effect of grinding on the erosion behavior of a WC–Co–Cr coating deposited by HVOF and detonation gun spray processes, Wear (249) pp 592-600

Naidu B.K.S. (1996) Silt erosion problems in hydropower stations and their possible solutions, Proc. Silt damages to equipment in hydro power stations and remedial measures, New Delhi, pp 1-53.

Naidu B.K.S. (1999) Developing silt consciousness in the minds of hydro power engineers, Proc. of 1st Int. conf. on Silting problems in hydro power plants, New Delhi, pp 1-32

Nanda V.K. (1999) Parameters affecting abrasion and remedial measures, Proc. of 1st Int. conf. on Silting problems in hydro power plants, New Delhi, pp V 43-52

Nayak, J.N. and Chaudhary C.S. (1996) Repair of hydro turbine with high resistance materials, Proc. 3rd Int. Conf. on power development in Afro-Asian countries, Kathmandu, 1996, pp 407-413

Nepal Electricity Authority (NEA) (2002/2003) Annual Report

Neville A. and McDougall B. A. B. (2001) Erosion– and cavitation–corrosion of titanium and its alloys, Wear (250) 726-735

Neville, A., Reyes, M. and Xu, H. (2002) Examining corrosion effect and corrosion/erosion interactions on metallic materials in aqueous slurries, Tribology International (35) 634-650

Palgrave R. (1990) Process pump design for hot abrasive service, Porc. of seminar of IME, Application of advanced material technology in fluid machinery (ed), pp 1-10

Pande V.K. and Ramanathan S.M. (1999) Prediction of erosion severity for hydro turbine components operating in silty conditions, Proc. Int. seminar on sediment handling technique, NHA, Kathmandu

Parajuli R. (2003) 'Theoritical hydroelectric capacity can be more', Kantipur Daily (28.01.2003) (in Nepali)

Peterson B., Rishel D. M. et al. (1995) The development of surface features on nickel during erosion-corrosion, Wear (186-187) pp 56-63

Pool K.V., Dharan C.K.H. and Finnie I. (1986) Erosive wear of composite materials, Wear (107) pp 1-12

Pradhan P., Dahlhaug O., Joshi P.N. and Støle H. (2004) Report on Sediment and efficiency measurement at Jhimruk hydropower plant – monsoon 2003, Hydro Lab, Nepal

Preece C.M. and Brunton J.H. (1980) Comparison of liquid impact erosion and cavitation erosion, Wear (60) pp 269-284

Pugsley V.A. and Allen C. (1999) Microstructure/ property relationships in the slurry erosion of tungsten carbide-cobalt, Wear (225-229) pp 1017-1024

Rajesh J., Bijwe J., Tewari U. S. and Venkataraman B. (2001) Erosive wear behavior of various polyamides, Wear (249) pp 702-714

Rayan M.A., Shawky M. (1989) Evaluation of wear in a centrifugal slurry pump, Proc. Inst. Mech. Eng. (203) pp 19-23

Reyes M. and Neville A. (2003) Degradation mechanisms of Co-based alloy and WC metal–matrix composites for drilling tools offshore, Wear (255) pp 1143-1156

Schneider C. and Kachele, T. (1999) Recent research results on predicting and preventing silt erosion, Proc. of 1st Int. conf. on Silting problems in hydro power plants, New Delhi, pp III-2 – 13

Sehadri V., Gupta R. and Singh S. N. (1995) Prediction of uneven wear in a slurry pipeline on the basis of measurements in a pot tester, Wear (184) pp 169-178

Sharma M.K. (1996) Problems in repair welding of 13/4 Stainless Steel and their remedial measures, Proc. Silt damages to equipment in hydro power stations and remedial measures, New Delhi, pp 166-181

Sheldon G.L. and Finnie I. (1966) On the ductile behavior of nominally brittle material during erosive cutting, Transaction of ASME (88B) pp 387-392

Shida Y. and Fujikawa H. (1985) Particle erosion behavior of boiler tube material in elevated temperature, Wear (103) pp 121-139

Shrestha S.B. (2003) Importance of small hydropower in Nepal, Proc. Int. Conf. on hydropower, Hydro Africa 2003, Arusha, Tanzania

Speyer A.J., Wood R. J. K. and Stokes K. R. (2001) Erosion of Aluminum based cladding on steel by sand in water, Wear (250) pp 802-808

Spurk J.H. (1997) Fluid mechanics, Springer, Berlin

Srinivasan S. and Scattergood R. O. (1991) R curve effects in solid particle erosion of ceramics, Wear (142) pp115-133

Stachowiak G. W. (2002) Particle angularity and its relationship to abrasive and erosive wear, Wear (241) pp 214-219

Stachowiak G.W. and Batchelor A. W. (1993) Engineering Tribology, Elesevior, Amesterdam

Stack M. M. and Peña D. (2001) Mapping erosion of Ni–Cr/WC-based composites at elevated temperatures: some recent advances, Wear (251) 1433-1443

Statistical year book (SYB) (2002) Central bureau of statistics, Kathmandu Nepal

Stevenson A. N. J. and Hutchings I. M. (1995) The influence of nozzle length on the divergence of the erodent particle stream in a gas-blast erosion rig, Wear (189) pp 66-69

Støle H. (1993) Withdrawal of water from Himalayan Rivers, sediment controls at intake, Dr. Ing. thesis, Universitetet I Trondheim, NTH

Stringer J. and Wright I.G. (1987) In: Proc. 7th Int. Conf. on Erosion by Liquid and Solid Impact (4th edn. ed.), J.E. Field and J.P. Dear (eds) Paper 47, Cavendish Laboratory, Cambridge, Cambridgeshire.

Suchánek J., Blaskovic P. and Grinberg N. A. (1999) Erosive and hydroabrasive resistance of hardfacing materials, Wear (233-235) pp 229-236

Svensson A.M. (1998) Report on Modeling of erosion process, SINTEF Material Technology

Tabakoff W. and Metwally M. (1992) Coating effects on particle trajectories and turbine blade erosion, Jr. of engg. for gas turbines and power, pp 250-257

Tabakoff W., Hamed A. and Metwally M. (1991) Effect of particle size distribution on particle dynamics and blade erosion in axial flow turbines, ASME Jr. of Engg. for gas and power (113) pp 607-615

Takagi et al. (1987) Effect of suspended solids on the performance of a model hydraulic turbine, 2nd China-Japan joint conf. on fluid machinery, pp 302-309

Tewari U. S., Harsha A. P., Häger A. M. and Friedrich K. (2002) Solid particle erosion of unidirectional carbon fiber reinforced polyetheretherketone composites, Wear (252) pp 992-1000

Thakur T. N. (1996) Rehabilitation of Hydropower Equipments, Proc. 3rd International Conference on Power Development in Afro-Asian Countries, Kathmandu, ,pp 538 - 545.

Thapa B. (1999) The effect of sediments on wear of hydroelectric turbines in Nepal and repair of turbine runners, ME dissertation, BITS-Pilani, India

Thapa B. and Brekke H. (2004) Effect of sand particle size and surface curvature in erosion of hydraulic turbine, IAHR symposium on hydraulic machinery and systems, Stockholm

Thapa B. and Dahlhaug O.G. (2003) Sand erosion in hydraulic turbines and wear rate measurement of turbine materials, Proc. Int. Conf. on hydropower, Hydro Africa 2003, Arusha, Tanzania

Thapa B. and Skåre P.E. (2002) Inspection report: Fortun power plant, SINTEF Energy Research; Trondheim

Thapa B. Shrestha R., Dhakal P. and Thapa B. S. (2004) Sediment in Nepalese hydropower projects, Proc. Int. Conf. on the great Himalayas: climate, health, ecology, management and conservation, Kathmandu

Thapa B., Dahlhaug O.G., Shrestha R. and Kafle K.P. (2004) Sediments of Nepalese rivers with respect to sand erosion in hydraulic turbines, Proc. 9th Int. Symposium on river sedimentation ISRS, Yichang, China

Thapa, B. et al. (2000), Report on Demonstration of energy conservation in cooking, Kathmandu University-Water and Energy Commission Secretariat, Kathmandu, Nepal

Truscott G. F. (1972) Literature survey of abrasive wear in hydraulic machinery, Wear (20) pp 29-50

Tsuguo N. (1999) Estimation of repair cycle of turbine due to abrasion caused by suspended sand and determination of desilting basin capacity, Proc. Int. seminar on sediment handling technique, NHA, Kathmandu

Wensink H. and Elwenspoek M.C. (2002) A closer look at the ductile–brittle transition in solid particle erosion, Wear (253) pp 1035-1043

Wheeler D.W. and Wood R.J.K. (2001) Solid particle erosion of diamond coatings under non-normal impact angles, Wear pp 795-801

Winter R.E. and Hutchings I.M. (1975) The role of adiabatic shear in solid particle erosion, Wear (34) pp 141-148

Wood R. J. K. and Wheeler D. W. (1998) Design and performance of a high velocity air–sand jet impingement erosion facility, Wear (220) pp 95-112

Wood R. J. K. (1999) Sand erosion performance of coatings, Materials and Design (20) pp 179-191

Wood R. J. K., D. W. Wheeler, D. C. Lejeau and B Mellor. G. (1999) Sand erosion performance of CVD boron carbide coated tungsten carbide, Wear (233-235) pp 134-150

Wood R. J. K., Mellor B. G. and Binfield M. L.(1997) Sand erosion performance of detonation gun applied tungsten carbide/cobalt-chromium coatings, Wear (211) 1997 pp 70-83

Wood R.J.K, Wharton J.A. et al. (2002) Investigation of erosion-corrosion processes using electrochemical noise measurement, Tribology International (35) pp 631-641

Wu P., Yao Q. et al (1996) Effects of water carrying solid particles on Francis turbine performance and operation, Hydropower '96, Beijing, pp 466-472

Wu X., Jing H., Zheng Y., Yao Z. and Ke W. (2004) Erosion–corrosion of various oil-refining materials in naphthenic acid, Wear (256) pp133-144

Xie Y., H. McI. Clark and H. M. Hawthorne (1999) Modelling slurry particle dynamics in the Coriolis erosion tester, Wear (225-229) pp 405-416

Xie Y., Llewellyn R. J. and Stiles D. (2001) Amorphous diamond coating of tungsten carbide and titanium carbonitride for erosive slurry pump component service, Wear (250) pp 88-99

Yabuki A., Matsuwaki K. and Matsumura M. (1999) Critical impact velocity in the solid particles impact erosion of metallic materials, Wear (233-235) pp 468-475

Yashima S., Kanda Y. and Sano S. (1987) Relationship between particle size and fracture energy or impact velocity required to fracture as estimated for single particle crushing, Powder technology (51) pp 277-282 (in http://engr.smu.edu)

Yust C.S. and Crouse R.S. (1978) Melting at particle impact sites during erosion of ceramics, Wear (51) pp 193-196

Zahavi J. and Schmitt G. F. (1981) Solid particle erosion of polymer coatings, Wear (71) pp 191-210

Zhang J., Richardson M. O. W., et al. (1996) Assessment of resistance of non-metallic coatings to silt abrasion and cavitation erosion in a rotating disk test rig, Wear (194), pp 149-155

Zouari B. and Touratier M. (2002) Simulation of organic coating removal by particle impact, Wear (253) pp 488-497

Zu J.B. (1990) Wear of materials by slurry erosion, Dissertation, Univ. of Cambridge

Appendix A

A Literature survey: The experimental study of erosion

1. Introduction

Finnie's (1960) paper on "Erosion of Surfaces by Solid Particles" is a milestone in the understanding of erosion behavior with respect to the relation of the erosion rate and the parameters that influence it. The literature before the 1950's concerned specific erosion problems and practical solutions for erosion resistance (Finnie, 1995). Finnie (1995) also traced the history of publication on erosion mechanisms to 1807, citing Rayleigh (in 1912), who discussed the topic of sand blasting and drew on comments made by Young (in 1807) in his lecture on Natural Philosophy. Interest in the mechanism of erosion expanded during 1960's with applications in hydraulic turbines, steam turbines, and the mining and airlines industries.

This paper presents a literature survey of research trends during the last century in the field of experimental erosion. The findings of this study could be useful for the design or selection of test rigs for erosion in general and for hydraulic turbine erosion investigations in particular. Literature reviews are occasionally published on issues such as wear models, wear of hydraulic machinery and so on, but literature survey concerning experimental studies has yet been conducted. Although this survey has been conducted following the references of the published papers, the information presented here is not exhaustive. This paper present and compare erosion experimental setups with respect to construction, instrumentation, test environment, test materials and presentation of results. Based on this literature survey, classification for erosion test setups is also proposed to accommodate most of the setups in use, and that this author has not found in the literature to date.

2. Erosion test rigs and equipment

Erosion can be simulated in the laboratory either by the particle, the specimen or both in motion, where relative velocity between these is important. A wide variety of erosion test rigs which are used by researchers. This section briefly describes the construction features of the experimental setups.

Finnie (1960) believes the origin of experimental erosion research is from Germany as a result of the work by Siebel and Brockstedt (in 1941), in which they eroded a plate with quartz to compare the weight loss of different steels and alloys. But their result was not in agreement with the practical experience of the steel pipe transporting abrasive particles. Bitter (1962) conducted free fall rebound tests using hardened steel balls dropped from an evacuated tower. Head and Harr (1970) used a miniature sandblasting apparatus with a 3 inch square specimen size based on the "Sandblast" apparatus for an erosion test. Hence the 70's may be considered as the infancy stage for experimental erosion studies, but fundamental concepts have been developed during this period.

Jet type of test rig

Zahavi et al. (1980) used an air-blast sand erosion test rig with compressed air at room temperature. A similar jet-type erosion tester, as shown in Figure 1, was used by Pool et al. (1985). The particles are accelerated in a 0.3 m long and 5 mm diameter nozzle and strike the specimen inside the erosion chamber. Under the Norwegian Research Program for multiphase flow, erosion of needle valves was tested, with the purpose to rank erosion resistance of materials and to establish data for the estimation of erosion rate of materials (Haugen et al., 1995). The test rig consisted of sand tank and accelerator pipe of 10 mm diameter and 2 m length. Similarly, Chevallier et al. (1995) also developed a test bench using compressed air for the study of jet flow impact. Tabakoff et al. (1995) used a high temperature test setup (Figure 2) to compare gas and steam turbine blade material erosion. After injection, the particles are heated by steam and accelerated in a long pipe to strike the specimen placed at the bend section.
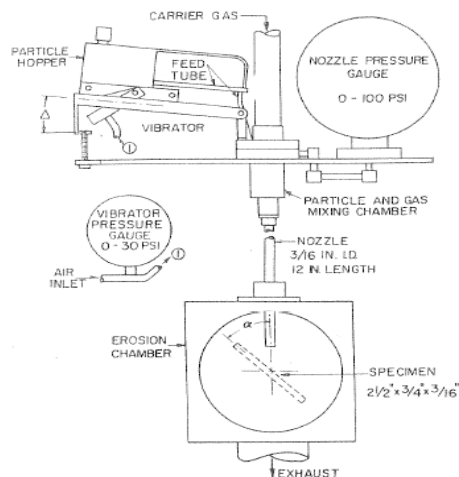
Figure 1 Air-blast sand erosion test rig (Pool et al., 1985)
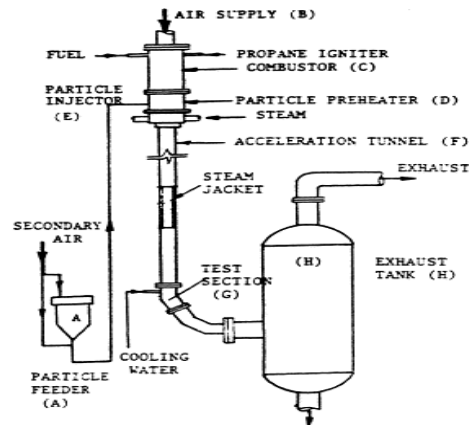
Figure 2 High temperature erosion test (Tabakoff et al., 1995)

Cavendish laboratory's sand erosion test facility (Figure 3) used a rotating disc to feed particles from a pressurized hopper, from which they are sucked in to the barrel through a syringe attached to a vibrator (Field et al., 1995). Wensink et al. (2002) also used this setup for the study of the transition between the ductile and brittle modes of erosion. The air from the compressor accelerates the particles in a 10 mm diameter and 4 m long barrel before

striking the target. The acceleration pipe in this setup is one of the longest found in such experiment. Beside the sand erosion test facility, Jilbert et al. (1999) used Cavendish Laboratory's multiple impact jet simulator (MIJA) to study the synergistic effect of rain and sand erosion. The rapid insertion of a titanium shaft into the nylon piston pumps water and produces a high velocity water jet from the nozzle.

Pugsley et al. (1999) compared the wear response of WC-Co with standard material in a slurry erosion environment by use of a jet impingement rig (Figure 4). The principle of suction at the nozzle is used to mix eroding particles into the working fluid inside the test chamber itself. The slurry mixture is accelerated through a short ejector. A funnel-type container and test chamber acts as a particle collector, and particles at the funnel are re-circulated during the tests. The particle screening capacity of the system can be doubtful because of splashing of the jet after strike.
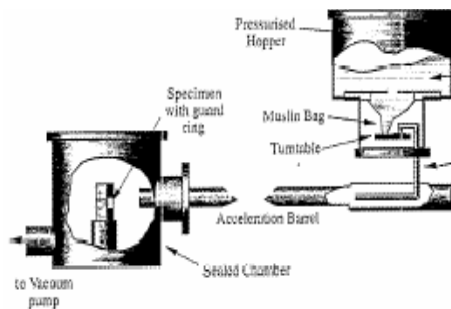
Figure 3 Cavendish laboratory sand erosion test facility (Field et al 1995)
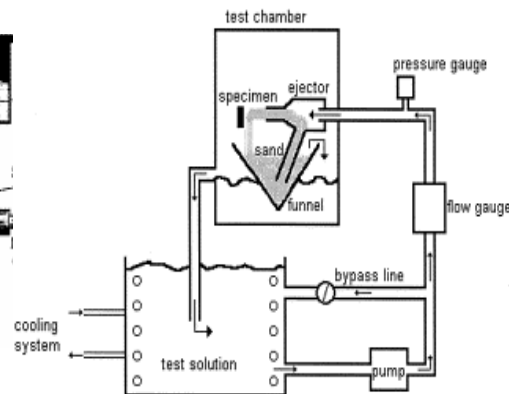
Figure 4 Schematic of the slurry jet erosion rig (Pugsley et al., 1999)
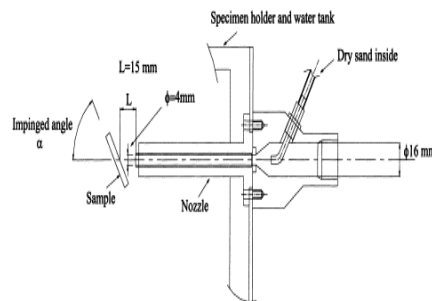
Figure 5 Jet type equipment (Lin et al. (2001)

Lin et al. (2001) also used jet type equipment (Figure 5) with a high speed water jet sucking in abrasive particles and accelerating them through a 4 mm diameter nozzle. Similarly, Neville et al. (2001) and Neville et al. (2002) studied the erosion-corrosion and cavitation of several materials with submerged jet with 4 mm diameter nozzle and distance between the nozzle and the specimen only 5 mm.

Wood et al. (1998) and Wood et al. (1999) used a sonic velocity air/sand erosion facility. The rig consists of a supply of compressed dry air with sand sucked through the venturi pipe as shown in Figure 6. The sand is accelerated at the 1 m long tube which is either 16 or 20 mm in diameter. An erosion-corrosion study on 13 Cr steel was done by liquid jet impingement in a gas well (Figure 7) to compare the erosion-corrosion damage in material with the industry standard (Andrews et al. 1999). Four samples were tested at the same time with separate nozzles and specimens were isolated with the holder by alumina spaces.
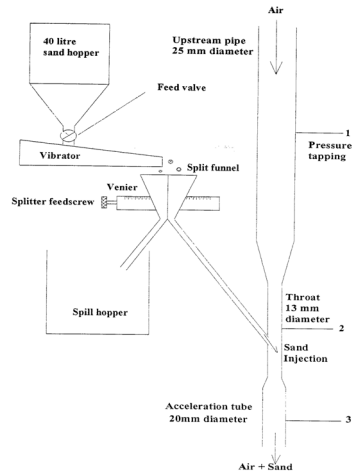
Figure 6 Venturi section for particle suction (Wood et al., 1998)
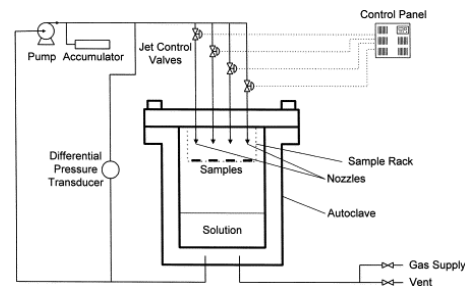
Figure 7 Erosion-corrosion test rig (Andrews et al., 1999)

Rotating type test rig

Madsen et al. (1988) used a slurry wear test set up for the measurement of erosion, corrosion and combined wear. The set-up consists of a dry sand hopper, from which abrasive particles fall in to the slurry hopper and are pumped to the slurry pot at constant rate. Contrary to jet type of test rigs, the pump handles abrasive slurry in this system, meaning that pump erosion could decrease the performance of the pump over a period of time. The slurry pot is made up of 16 sides to accommodate 16 specimens measuring 24X32X10 mm. The concentric impeller inside the slurry pot (Figure 8) rotates the slurry, exposing the specimen to the slurry at a high velocity. The impeller is also exposed to the slurry in the same condition; hence it is made up of extremely high wear-resistant ultrahigh molecular weight polyethylene. The tests in this setup can be carried out with a continuous flow of fresh sand, which gives a constant wear rate as a function of time. This slurry pot with 16 sides is comparable to the spiral casing wall of hydraulic machines.

Lynn, et al. (1991) used slurry erosion pot to study collision efficiency of particles. Clark et al. (2001) used the same equipment to investigate particle size effect in slurry erosion. This rig (Figure 10) consists of a cylindrical slurry pot with baffles in the wall. Two cylindrical specimens are held in the arm and rotated by central shaft.
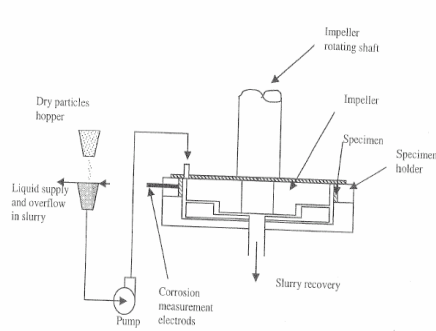
Figure 8   Slurry pot Apparatus
(based on Madsen et al.1988)
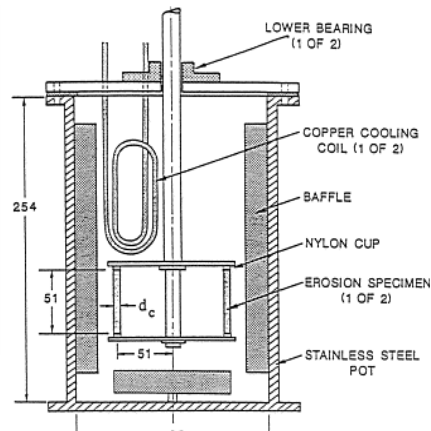
Figure 9 Surry erosion pot (Clark et al., 2001)

Several erosion/corrosion tests have been carried out in Rotating Disc Apparatus (RDA) and Co-axial Rotating Cylinder Apparatus (CRCA) (Figure 10) at NTNU/SINTEF (Bjordal, 1995). The rotating disc or cylinder is placed inside the oval tank and rotated with a motor. Six cylindrical specimens that project into the disc in the RDA or six rings in CRCA can be tested at the same time. The rotation of disc or cylinder at different speeds exposes the specimen to sand, electrolyte and water mixtures at different operating conditions. These setups also consist of instrumentation for corrosion; hence tests for pure corrosion, sand erosion and the synergy between them can be performed. The SAPHYR test rig used by Sulzer group (Krause and Drtina, 1996) is also ring type of test rig similar to CRCA, but in this case the sand and water mixture is not enclosed in a container.
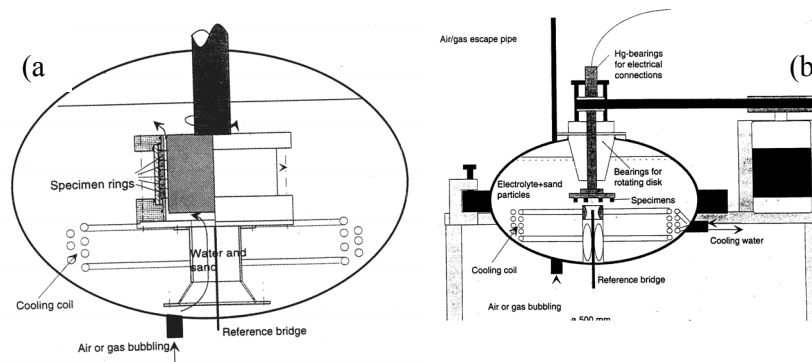
Figure 10   SINTEF Erosion/Corrosion Test Equipment (a) Rotating cylinder (b) Rotating disc (Bjodal, 1995)

Similar to the principle of slurry erosion pot, Sehadri et al. (1995) redesigned a slurry pot erosion tester with a propeller at the end of the shaft, which maintains the suspension of solid particles in the mixture. The exposure surface and angle of attack on the specimen is different in this set up as compared to other rotating specimen testers. Gandhi et al. (1999)

204

modified the specimen holder to study the parametric dependence of erosion for parallel flow. The rectangular edge of the specimen holder was changed to 45^0 (Figure 11) to avoid separation. Without this, erosion can not be observed at the leading edge. Flow visualization of this set up confirmed that the flow is parallel to the specimen surface, which is an indicator of low impingement angle.

Karimi et al. (1995) tested WC coatings for sand erosion in the apparatus, which produced a rotating tangential flow of abrasive slurry and water over the specimen using a helical gear-type impeller. Dry abrasive is fed from the hopper above the mixing unit and slurry is pumped either in a closed or open loop through the impeller center and comes out at a radial direction from the specimen holder. Hubner et al. (1996) used an erosion-corrosion simulator (EKS) (figure 12) similar to one used by Karimi et al. (1995) to study the erosion, corrosion and their combined effect under wide range of conditions. The impact velocity is controlled by rotation of the disc, but flow of erosive particles and corrosive media is controlled by the central opening in the disc. This system (Figure 12) is similar to the RDA with the difference that being the specimen is fixed and the impingement angle can be adjusted.
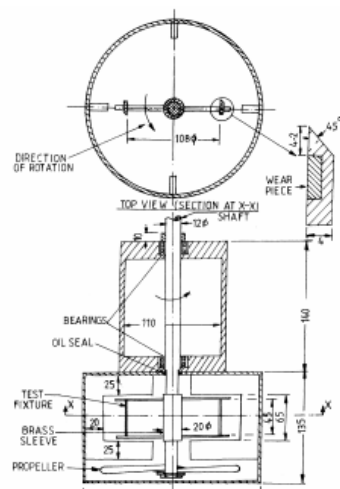
Figure 11 Pot tester for slurry parallel flow (with tapered specimen holder) (Gandhi et al., 1999)
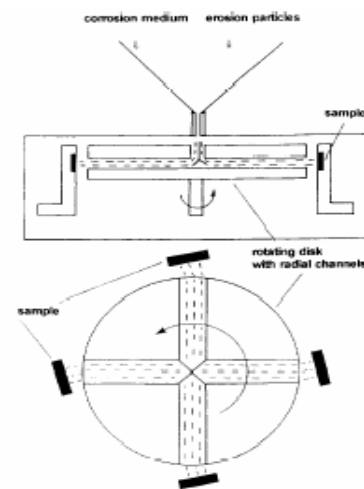
Figure 12 Erosion-corrosion simulator (EKS) (Hubner et al., 1996)

Hussainova et al. (2001) also used a setup similar to EKS to study material removal of hard metal and cermet. Particles are centrifugally accelerated in four channel devices. A similar type of test rig, centrifugal erosion tester CUK-3, was used by Suchanek et al. (1999) for a dry erosion test. They have also used Sand-hydroblast apparatus EO-2. CUK-3, which works on the principle of centrifugal acceleration of particles. The EO-2 (Figure 13) consists of conical tank for sand and water, which is pumped to the four delivery bodies by a screw pump. The jet from the nozzle at the end of delivery body strikes the specimen at different angles. Das et al. (1999) fixed the specimens at the rotating disc inside the slurry tank in an erosion-corrosion environment (Figure 14). The specimens are fixed at a radius

of 35 mm, 55 mm and 75 mm at 0°, 45° and 90° relative to the rotational direction. The advantage of this rig over the rig by Lynn et al. (1991) is that different angles and velocities can be tested at the same time.
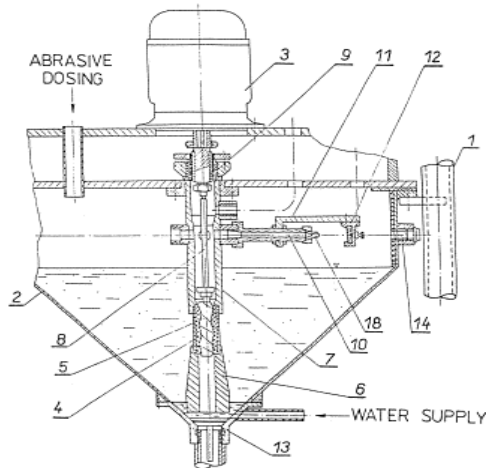
Figure 13 Sand-hydroblast apparatus EO-2 (1: supporting frame, 2: tank, 3: electric motor, 4: pump body, 5: rotor, 6: suction, 7: body, 8: connecting rod, 9: packing, 10: feed pipe, 11: holder, 12: specimen, 13: sledge sluice, 14: plug, 18: nozzle) (Suchanek et al., 1999)
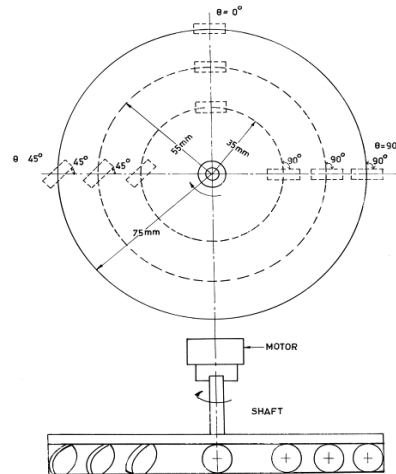
Figure 14 Schematic representation showing the location of samples placed on the disc (Das et al., 1999)

Mann (2000) used a rotary test setup (Figure 15) to test coatings. Sand particles are mixed with water and injected inside the chamber. A cylindrical specimen (12.76 mm in diameter and 12.76 mm long) is fixed in the rotating disc inside the housing. The sand particles are fed continuously to ensure constant concentration. Velocity of test condition is changed by changing the rotational speed or changing the radial location of the specimen. Mann et al. (2002) modified this setup to allow water jet impingement by accelerating particles from a 4.24 mm micro-jet nozzle. The jet strikes cylindrical specimens fixed in the rotating disc.

Stack et al. (2001) studied the erosion behavior of composite materials at room temperature and elevated temperatures in erosion-corrosion fluidized bed apparatus (Figure 16). The specimens, measuring 4X6X10 mm, are fixed in a rotating specimen holder. A pre-heater can supply hot gas for the test at elevated temperatures up to 600^0C.

Xie et al. (2001) carried out abrasion and slurry erosion tests. The mechanism in these two was assumed similar and hence they used the micro-abrasive wear test procedure proposed by Kassman (1991). A commercial dimple grinder is used for test where specimen is rotated in axis normal to flat surface.

The erosion test of an abradable seal coating on CMS-100 (Figure 17) by Maozhong et al. (2002) consists of specimens fixed at the end of a four bar rotating device inside a vacuum

chamber. The abrasive particles, supplied through a hopper, strike the rotating specimens for 1 hour.
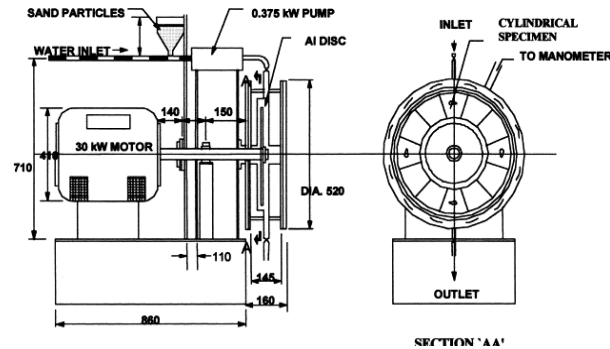
Figure 15 Cross sectional view of wear test facility (Mann, 2000)
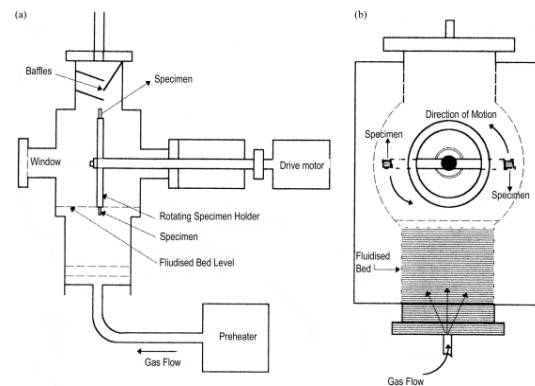
Figure 16 erosion-corrosion fluidized bed apparatus (Stack et al. 2001)

Unlike other rotating test Preece et al. (1980) used a water jet on rotating specimen to compare the impact of liquid erosion to a cavitation test (Figure 18). Even though there are similarities between the liquid impact and cavitation tests, the data are not interchangeable, but erosion resistance can be ranked in same order for both cases. This study was carried out with clean water but erosion can be tested by inserting erosive particles in front of the jet. This study also reflects that jet-type erosion testing is also affected by collapsing cavities. However, the number of impacts needed for the deformation to be effective is fairly high.
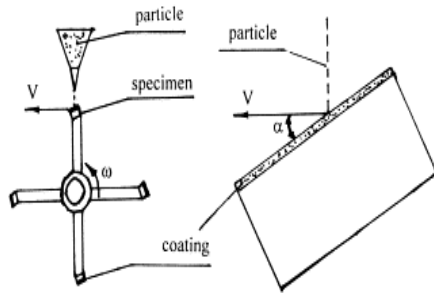
Figure 17 Schematic diagram of CMS-100 erosion tester (Maozhong et al. 2002)
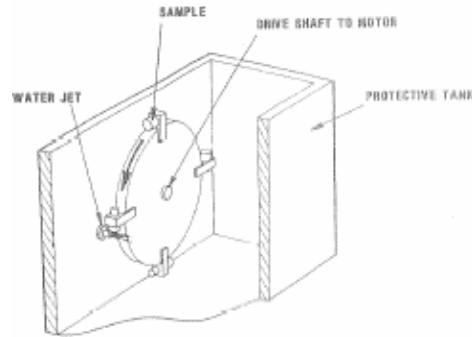
Figure 18 Wheel and jet apparatus for erosion studies (Preece et al.,

The Coriolis slurry erosion test was proposed by Tuzson (1984) to simulate the action of slurries in pumps and pipelines (in Clart et al. 1999). Slurry is fed through small pipe specimens attached 180° apart to a rotating bowl. Centrifugal force accelerates the slurry outwards while the Coriolis force increases the slurry interaction with the wall of the specimen. Coriolis test setup was modified with simpler flat specimen (Clark et al., 2000) measuring 29X15X6 mm. They are placed on either side of a diametric slot with a bore of 12.7 mm in a 150 mm diameter solid rotor. Hawthorne (2002) used a Mark II Coriolis tester (Figure 19) to develop a wear map of mild steel.
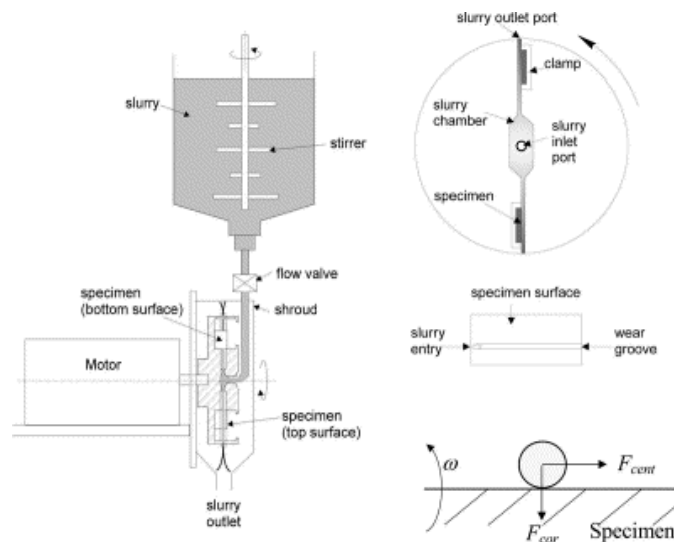
Figure 20 Schematics of the Mark II Coriolis slurry erosion tester, rotor assembly, worn specimen and main forces acting on erodent particles in the tester Hawthorne (2002)

Test Loop

In contrast to laboratory test rigs, Hengyun et al. (1986) used the sand water venture device at an actual tunnel of a hydropower plant for a combined test of erosion and cavitation. The aerofoil shape is placed at the centre of venturi to produce cavitation in a 70 mm diameter and 11 mm thick specimen. Similarly, Rayan et al. (1989) investigated the erosion of actual centrifugal slurry pump on the simple open loop hydraulic circuit. They used a 13 kW hydraulic pump with a 80 mm inlet and a 280 mm outlet diameter cast steel impeller (Figure 20). The pump discharges to a 1 m diameter and 3 m deep tank from where the slurry is re-circulated. Apart from laboratory test on small test rig, occasionally erosion tests are carried out on large test loop where flow condition may be simulated in more realistic way.

Sehadri et al. (1995) used closed test loop of 55 mm diameter and 60 m length pipe with particle mixing and a measuring tank with stirrer arrangements to generate data of uneven wear (Figure 21a). A special test fixture of 900 mm in length (Figure 21 b) is used to hold the specimen at the surface level of the pipe. Four specimens are placed at each end of the test fixture at an interval of 90° and offset by 45° between two ends. The correlation was developed and compared to measured values from the pot tester as well as predicted wear at the pilot plant. Similar test loop was used by Wood et al. (2003) (Figure 22) with the aim to determine the distribution of the erosion rate and the mechanism that occurs over a wetted surface within a loop that handles a solid liquid mixture. Pipes are made of AISI 304L stainless steel with a nominal wall thickness 5 mm and 80 mm diameter.

Apart from metallic and coating materials including polymers, tests of other materials are very rare. Hu et al. (2002) have performed hydro-abrasive erosion tests on construction materials using an abrasive jet device with a mixing chamber and orifice. Horszczaruk (2003) tested concrete erosion resistance on a device with 36 specimens rotating in the arms inside a horizontal drum of 155 cm in diameter and 228 cm long filled with a mixture of aggregate and water (Figure 23).

3. Instrumentation

The reliability, quality and quantity of data collected in erosion research work depend on instrumentation. With the development of automatic sensors, reliability and accuracy of the data have increased, while measurement procedures have become easier. The process variables in an erosion test, such as fluid and particle velocities, particle flux rate, weight loss due to erosion, surface damage, temperature, and so on must be maintained or measured during test. The use of modern instruments in erosion experiments has not increased that much compared to other research areas. Instruments used by researchers for erosion experiments are discussed in this section.

Head et al. (1970) had already used several measurement techniques before the 1970s. They used flow meters and pressure regulators to monitor and control the volume of airflow. They also used an air solenoid valve to control the timing of the test in a miniature sandblast apparatus. Particles discharge velocities as from a nozzle were assessed by measuring the total pressure at several locations. They used a photographic technique, with special light source and a timing device to determine the particle impact and rebounding

speed. Particle shape analysis is not carried out very often. Head and Harr (1970) used the Zeiss TGZ-3 Particle analyzer, where shapes were compared through photomicrographs and counts were entered manually, whereas Bahadur et al. (1990) photographed the particles in a scanning electron microscope and analyzed the shapes of those particles with scientific image analyzer to characterize the particle shapes used for erosion tests. The differences in the instruments used for velocity, concentration, weight, surface, corrosion, and cavitation and so on are discussed in this section.
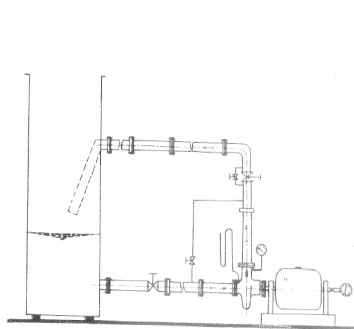

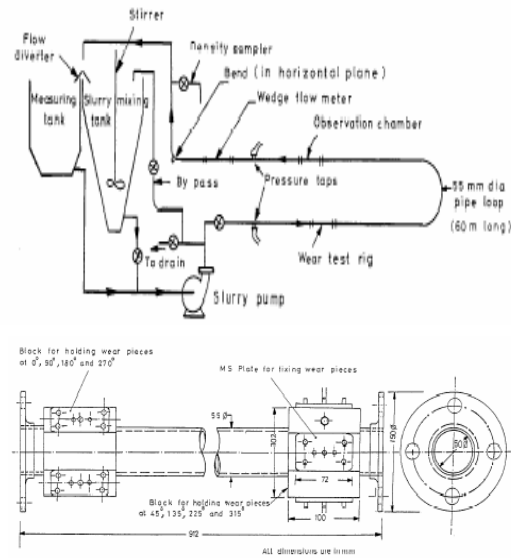Figure 20 Centrifugal slurry pump experiment Rayan et al. (1989)

Figure 21 (a) Schematic diagram of pilot plant (b) assembled view of test specimen fixture (Sehadri et al., 1995)
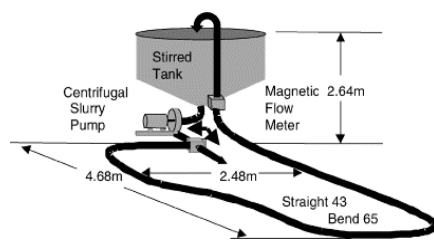

Figure 22 pilot-scale sand/water rig with pipe loop Wood et al. (2003)
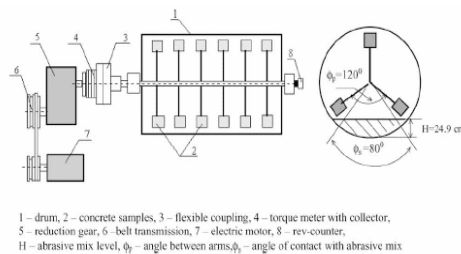

Figure 23 Scheme of the device for testing abrasive erosion of concrete (Horszczaruk , 2003)

Velocity

Zahavi et al. (1981) have used instruments such as a pressure and a temperature gauge and a moisture indicator in an air-blast sand erosion rig circuit. They measured air velocity with an orifice flow meter. They also inserted a sand velocity calibration system as suggested by Ruff and Ives (1975) in the test chamber as a way to measure particle velocity with a time-of-flight device. After Zahavi et al. (1981), Pool et al. (1985) also monitored pressure at the nozzle inlet to control the air flow rate. They calibrated the particle velocity with two parallel plates rotating at a constant angular velocity with the accuracy within 10%. The velocity of impact is controlled by the rotational speed of disc in most rotating type rigs. Hydraulically actuated valves operate the jets sequentially in the Erosion-corrosion test rig used by Andrews et al. (1999) in which the jet velocities are regulated by a differential pressure set between the pump outlet and the autoclave.

Some of the latest measurement techniques are being used in recent research. A series of light beams is used between optical fibers to measure jet velocities. The entire process in MIJA is computer-controlled. Hussainova (1999) and Hussainova et al. (2001) studied the details of particle impact using a Laser Doppler Anemometer (LDA).

Normally, flow meters are installed before the insertion of abrasive particles in most test rigs, but thermocouples and pressure gauges are shown in the circuit after that in the sonic air-sand test rig used by Wood et al., (1999). Although the velocity at these sections is quite lower than the jet velocity, erosion of these instruments can also be expected.

Concentration and particle feeding

The control and measurement of particles being fed to the flow is one of erosion experiment's most challenging tasks. The simplest method to control the particle flow is by changing the opening size in free fall as used by Maozhong (2002). The erosive particles feed rate to the air stream is controlled by vibrator frequency and the inclination of hopper in the erosion tester used by Pool, et al. (1986). A similar mechanism is used in a sonic velocity erosion facility by Wood et al. (1998) with a split funnel controlled by a splitter feed screw with vernier scale. The rate of particle flow is controlled by longitudinal grooves engraved in the rotating drum (Karimi et al. 1995) and size and radius of the groove in the disc in Cavendish laboratory's sand erosion test facility, together with the drum or disc speed. The suction pressure at the venturi or nozzle section is also used for controlling the flow rate, for which accurate dimensioning of the section is very important. The instrumentation used to monitor the concentration itself erodes over the period of time and sometimes even the sensors can be clogged. Hence there is a problem of short life and a drop in the accuracy of data over the period of time when instruments are working with solid particle slurries. Automation and online monitoring of particles are both difficult in such situations.

Although it is not clear from the literature, it seems that data such as the velocity, pressure and sand concentration are used from the instrumentation of the actual power plant itself for tests carried out in actual hydropower plants (Hengyun et al. 1986). Rayan et al. (1989) used the simplest technique for measuring the discharge of the pump by weighing the mixture. The mixture sample is collected at the end of the discharge pipe and the

concentration is determined by drying and weighing. Measuring the discharge by weighing is one of the most reliable methods, if there is the ability to measure the weight of such a large volume of water.

Weight measurement

Most researchers have used an electronic weighing balance with 0.1 mg least count to measure weight loss of specimens after erosion tests. Normally, the weighing balance with this accuracy has a maximum capacity of around 200-400 gm. But Rayan et al. (1989) reported a relative error in the erosion rate as $\pm$ 1 % in a pump impeller erosion test. The impeller is heavy compared to a maximum weight loss rate of 4 g/h. They did not mention in their paper the type of weighing balance they used. Accurate sensitive weighing can be difficult when weighing such a heavy test piece. Turbines, pumps and pipes erosion are measured in term of loss of thickness in actual practice. Since the loss of thickness is so small, this method is not normally followed in the laboratory tests. But Stack et al. (2001) measured the thickness loss of a specimen using a micrometer with 1μm precision.

Surface morphology

Aside from weight loss, measurement of surface roughness is one of most commonly used methods for quantifying the extent of damage due to erosion. Zahavi et al. (1981) measured surface roughness before and after a test by using a Talysurf machine. They also used scanning electron microscopy (SEM) to visualize the eroded surface and make a qualitative comparison of the nature and extent of damage. Most researchers who are interested in material technology are using SEM to evaluate specimens after erosion tests. Along with SEM, Karimi et al. (1995) used X-ray diffraction and Transmission Electron Microscopy (TEM) to study the microstructure of damaged surfaces. Clark et al. (1999) and Clark et al. (2000) used a computer- controlled LVDT based needle probe to measure surface height at several places to determine wear scar for a specimen tested on a Coriolis erosion tester.

Erosion, corrosion and cavitation

Pure erosion and combined erosion are measured in terms of the total weight loss whereas the effect of corrosion is monitored by use of a polarization curve (Madsen, 1988). Wood et al. (2002) used an electrochemical potential noise measurement facility with computerized data logging and analysis. Preece et al. (1980) used an Ultrasonic Cavitation Device and Neville et al (2001) used a Branson Ultrasonic Sonifier Cell Disrupter Model 450 for producing the cavitation in the test specimens, whereas Hengyun et al. (1986) used a simple aerofoil profile.

4. Operating Environment

The properties of sand particles (grain size, shape, hardness, material) and operating environment (velocity, impingement angle, concentration, temperature) will be discussed in this section. Another factor, base material (substrate) will be discussed in the next section. These parameters can change the result of the experiment to a great extent and should be controlled or monitored throughout the experiment.

There are great non-homogeneities in the shape and size of natural abrasive particles. It is almost impossible to segregate different shapes of particles and screen particles of same size. Hence, whenever the knowledge of exact shape and size of particles is needed, standard steels balls are used as particles, such as in 300 μm balls in Bitter (1962) and 300-500 μm size balls in Tiwari et al. (2002).

Head and Harr (1970) used three types of artificial dusts, angular shaped silica carbides, round shaped glass beads and less angular aluminum oxide of approximate particle diameter 105 μm. Zahavi et al. (1981) simply used round and elongated natural sand particles (96% weight SiO_2) from the Mediterranean Sea sieved in a size between 210-297 μm. Hengyun et al. (1986) used the natural sand from a hydropower plant with a concentration 0.603 kg/m3, and Haugen et al. (1995) used sand from the North Sea. The mineralogical composition and particle size distribution of foundry sands are normally known. Hence many researchers have used foundry sand as erosive particles in their tests (Suchanek et al. 1999; Wood et al. 1997).

In addition to sand, zinc (max. size 1.18 mm) (Gandhi et al. 1999) and copper tailing material (between 0.37-0.45 mm size) (Gupta et al. 1995) with specific gravity 2.82 have been used. Lin et al. (2001) used quartz, Maozhong et al. (2002) used corundum powder and Hu et al. (2002) used garnet as abrasive particles in their tests. Tabakoff et al. (1995) used chromite particles for testing erosion in gas turbine blades at high temperatures. Liquid particle erosion tests have been carried out without particles by Jilbert et al. (2000), Preece et al. (1980), Andrews et al. (1999).

Except in a few cases, air or water are the most frequently used fluid for carrying particles in erosion tests, because most of the erosion damage occurs in these medium and they are abundantly available. Lynn et al. 1991 and Clark et al. (2001) used diesel oil in slurry pot erosion to avoid corrosion during tests. Oils of different viscosities can be easily used for collision efficiency in different media, but this has not been found in the literature so far. Sodium chloride solutions at different concentrations are the most frequently used corrosive medium in erosion-corrosion tests. Das et al. (1999) has used sulfuric acid and hydrochloric acid to create corrosive environments.

Even though erosion tests are normally carried out under atmospheric pressure, a few tests have been conducted under pressurized and vacuum conditions. Evacuated free fall of steel balls avoids the problem of non-uniform particle velocity. On the other hand, aerodynamic perturbations in the proximity of the target are reduced in such an environment, which ensures the precision of impact velocity and angle. Particularly in Bitter's (1962) rebound test there will not be any air friction loss. But vacuum in the liquid environment may cause cavitation close to the specimen and hence material damage may not be entirely due to solid particle erosion. Bitter (1962) carried out tests in 1 mm Hg and Maozhong et al. (2002) in 1.3-6.5 Pa in vacuum pressure. Haugen et al. (1995) studied erosion of different steel chokes at a moderate pressure of 10 bars, where the actual working pressure is around 700-800 bars. Tabakof et al. (1992) and Stack et al. (2001) have carried out tests at elevated temperatures up to 600^0C. The temperature of the mixture in recirculation or enclosed fluids increases due to the mechanical work input in to the system. Some of the tests have incorporated cooling arrangements, but for short duration tests the rise in temperature is not significant. Studies have shown that the temperature of material up to the softening

temperature (for steel 600^{0}C) does not significantly affect the erosion rate (Stachowiak, 1993).

Velocity is a very important parameter that affects erosion rate by approximately a power of 3. As discussed in the instrumentation section, it is difficult to monitor the actual effective velocity of a particle just before it strikes the specimen. This velocity is interpreted as the velocity of flow, jet or the rotational velocity of specimens. The lowest velocity used in erosion testing was found in the slurry pump test by Rayan et al. (1989) as 0.64 and 0.85 m/s. The velocities in rotating types of experiments may reach up to approximately 30-40 m/s. Similarly, the rotational speeds reported in the literature range upwards of about 5000 rpm in the Coriolis tester (Clark et al. 2000). Jet type erosion tests can have a wide range of velocities beginning at a few m/s to the sonic range of 400 m/s (Wood et al. 1998) or 600 m/s (Jilbert et al. 2000). For the purpose of hydropower turbines, the maximum jet velocity that is possible for the highest head power plant could be about or even less than 80 m/s in Pelton turbine based on existing strength of steels. Hence the jet types of test rig can conduct erosion testing at the actual working velocity ranges of hydraulic turbines. The range of particle acceleration reported in the literature is 18000 times the acceleration due to gravity (Mann 2002), when the particle acceleration in the Pelton buckets falls between 5000-10000 times that of gravity (Brekke et al., 1994). The impact frequency of jets with a rotating type of specimen is about 76 cycles/sec in Mann (2002).

The 4X3X3 matrix of 4 particle size (35, 90, 200, 300 μm), 3 different concentrations of alumina (5, 10 and 15 %) and 3 different velocities (3000, 5000 and 7000 rpm) have been used by Hawthorne (2002) to develop specimen wear maps.

Bjordal (1995) have used low concentrations (0.025% by weight) whereas Gandhi et al. (1999) have used concentrations as high as 40%. Low concentration mixture requires a long test duration and vice versa. Another factor that affects test times is the velocity of impact. The test duration varies from 2 minutes (Lynn et al. 1991) to several days in different tests. Normally jet type tests have low test periods compared to rotary test rigs. All these are accelerated tests and have to be interpreted in some manner with respect to actual working conditions. Tests in actual hydropower plants can extend for as long as 500 hours (Hengyun et al. 1986). This long test period allows a specimen to experience the cavitation effect and may have been the result of specimen placement only during a removal of the plant maintenance period.

5. Specimen material

The reasons for selecting materials for erosion tests vary widely. Wellinger and co-workers (from 1942-1958) carried out tests on steel St. 37 (Vicker's hardness from 127 -840 kN/mm^2) to clear up the contradictory evidence regarding erosion resistance of materials for different impingement angles (in Finne 1960). Preece et al. (1980) compared the erosion rate and mechanisms of material removal from liquid impact and cavitation erosion on normal and heat treated pure aluminum, 99.999% iron, Al-Mg alloy and Cu-Zn alloys specimens. Lynn et al. (1991) used annealed copper rod specimens for a short period test and polished API P110 casing steels for a longer period to study collision efficiency. Simple mild steel was used by Hawthorne (2002) to develop a wear map of specimens in a

Coriolis tester. Almost all materials used to study erosion mechanisms and the effects of variable parameters are pure and soft metals with known properties in which the effects of erosion can quickly be seen and erosion can be differentiated from other material failure mechanisms.

Occasionally, erosion models are developed based on laboratory tests. Bitter (1962) carried out tests on annealed aluminum plates to obtain data for his erosion model. Similarly, Head et al. (1970) used heat-treated aluminum alloy, beryllium copper, and normal stainless steel as ductile material, but glass was used as the brittle material to develop a statistical erosion model. The materials selected for developing erosion models behave in a completely opposite manner in terms of ductile and brittle properties.

Erosion and corrosion act together in several industrial applications. But generally corrosion is the subject that is at the forefront of the search for new material development. Several research groups around the globe are working on the investigation of pure corrosion, pure erosion and the synergy between erosion and corrosion of existing and newly developed materials. Madsen (1988) used typical low cost, corrosion and wear resistant materials like low alloy steel (A514), stainless steel (type 316) and commercial abrasion resistant low alloy steel in a slurry wear test. Several metals, coatings and treatment processes were tested as part of the project "Corrosion and erosion resistant surface/coatings" at NTNU/SINTEF (Brekke et al. 1994). Coatings from processes like diffusion, laser treatment, ion-nitrated and sintered thermal spray of different matrices of Fe, Cr, W, Co, Ni, Ti, C and B were compared with the reference materials SAF 2205 stainless steel and structural steel. Similarly, 28 different materials including standard steel grades, solid tungsten carbide, coating materials and ceramics were tested by Haugen et al. (1995). Hubner et al. (1996) tested erosion-corrosion behavior of martensitic steels and duplex steels. The metals other than steels tested for erosion-corrosion are Al-alloy based composite material (Das et al. 1999), pure Ti and Ti alloys (Neville et al. 2001), Co-base Stellite X-40 and austenitic cast iron BS 3468 S2W (Neville et al. 2002), WC metal matrix (Reyes et al. 2003) and so on.

Tabakoff et al. (1995) compared AISI 410 stainless steel erosion with coatings like Cr_3C_2 and a (80%Cr20%Ni) matrix in different proportions sprayed by a D-gun and plasma for high temperature application of gas and steam turbines. Similarly, Stack et al. (2001) studied the erosion behavior of Ni-Cr/WC based composites at various temperatures as a function of reinforcement, particle velocity and size and exposure time in an erosion-corrosion fluidized bed apparatus. Some of the high temperature application coatings are tested at room temperature or low temperature as opposed to actual operating environments such as abradable seals for high temperature, which were tested at room temperature by Maozhong (2002). Results from such tests can not be interchanged for actual high temperature applications; hence materials should be treated at actual operating conditions to have a clear understanding of erosion.

The development of new coatings is making rapid progress with various aims. These coatings differ from each other based on chemistry, powder properties and spray process. Many of these coatings are tested for solid particle erosion under different operating conditions. Karimi et al. (1995) tested WC coatings with different metal matrices along with Cr_2O_3 sprayed on with an air plasma spraying technique and HVOF. Hussainova et al. (1999) and Hussainova (2001) also tested WC-Co hard metal and TiC-base cermet to

215

investigate the features of surface damage and the material removal process. Wood et al. (1997) have studied D- Gun sprayed WC-Co-Cr coating materials whereas Wood et al. (1999) tested chemical vapor deposited (CVD) boron-carbide coatings. Some other materials tested for erosion are aluminum-based claddings on steel (Speyer et al. 2001), diamond coatings (Wheeler et al. 2001), amorphous diamond coating of tungsten carbide and titanium carbonitride for an erosive slurry pump component (Xie et al. 1999), TiNi (Lin et al. 2001). Similarly IR-transmitting solids (ZnS, germanium, calcium lanthanum sulphide, diamond etc.) used in aircraft and polycrystalline diamond (PCDs) are tested for their erosion behavior by Field et al. (1995). This survey revealed that most of the combinations of coating material, spraying process and test rig can be found in the literature. Aside from coatings, other special purpose materials have also been tested for both performance comparisons to further understand failure mechanism.

Chevallier et al. (1995) developed a new test bench to study the jet flow impact, along with a profile of the erosion area and rate. Although they have discussed results from the experiment, they did not describe the materials that were used as specimens. Therefore it is doubtful that all material will have a similar profile of crater as they have shown. Gupta et al. (1995) and Gandhi et al. (1999) used soft materials like brass and mild steel to see the effect of erosion on modified equipment. In general, simple cheap materials with known characteristics are used to verify the performance of newly developed test rigs or improvements in existing test rigs.

Although nonmetallic polymer coatings show poor erosion resistance compared to metallic material in general, they are used in machine components because of other advantages such as light weight, high specific strength, stiffness, corrosion resistance and so on. Zahavi et al. (1980) tested protective polymer coatings of hard polyurethane and elastomeric polyurethane used in aerospace and the general purpose paint elastomeric fluorocarbon. Pool et al. (1985) also studied the erosive wear behavior of four composite materials: (i) unidirectional continuous-graphite-fiber-reinforced polymide laminate, (ii) woven graphite-fiber-reinforced epoxy laminate, (iii) woven aramid-fiber-reinforced epoxy laminate and (iv) chopped-graphite-fiber-reinforced thermoplastic. These composite materials are also preferred over conventional metals in aircraft industries. Along with different grade steels, Wood et al. (1998) tested Cupro-Nickel, medium density polyethylene and gas reinforced plastics used as pipe materials subject to fluid-born sand particle erosion in marine industry. Rajesh et al. (2001) studied various polyamides including aromatic polyamides, which are used in tribo-applications such as bearings and gears. Similarly, Tiwari et al. (2002) studied unidirectional carbon fibre (CF) reinforced polyetheretherketone (PEEK) composite, which has generally better erosion resistance compared to unreinforced polymer matrix. Abradable seal coatings, used in aircraft turbine engines, which are composed of a metal phase, self-lubricating non-metal phase and many pores are studied by Maozhong et al. (2002). Hu et al (2002) conducted hydro-abrasive erosion tests on plain concrete (PC) and steel-fiber reinforced concrete (FRC) used in dams, canals and tunnels, which are affected by river sediments. Basically all the nonmetallic materials tested are developed considering some other properties and investigations of their performance are done for solid particle erosion. Interestingly, most of the non-metals found in this survey are tested on jet type equipment. The reason for this could be to analyze the effect of high velocities at different impingement angles, which is difficult to achieve with rotating specimens.

6. Presentation of results

Erosion is one type of wear; hence there are many similarities in parameters for both general wear and erosion. In accordance with the ASTM definition of wear, many researchers represent erosion experiment results in terms of mass, volume or thickness loss per unit time or mass of eroding particles. This is a quantitative representation of erosion, whereas most results obtained from a material point of view use visualization of surface morphology and microstructure (scanning electron microscope and optical electron microscope) to understand the damage pattern and the extent of damage. Although it is a qualitative method, it is very useful for material ranking and comparison.

This is because the number of individual particle impacts varies with the change in particle diameter for the same mass of erodent. Some researchers have even used a relative index for presenting results based on standard material. Haugen et al. (1995) used the ratio of volume loss of material by that of carbon steel as the relative erosion resistance (REF). Zahavi et al. (1981) quantified the surface damage due to erosion by measuring surface roughness in terms of center-line-average.

Since there are several factors that affect results and not all can be controlled during an experiment, the spread in experimental data is quite large. Haugen et al. (1995) reported that erosion rates have differed by a factor of 10^3 under their test conditions.

7. Classification

This survey of experimental studies on erosion showed a variety of test rigs that are in use. The experimental set up and operating conditions described earlier in this paper gives idea of the similarities and differences between them. Except for a few general efforts (Chevallier 1995, Wood et al. 1998), the classification of erosion test rigs has not been found in the literature. Wood et al. (1998) proposed the classification such as sand or gas-blast rig, recirculation liquid slurry loop, centrifugal accelerator and whirling arm rig. However not all experiments in the literature fit in one of those categories, hence this author propose the classification of erosion test rigs in the following categories:

Basis for classification	Type
Relative motion between mixture and specimen	Jet type
	Rotating specimen type
	Rotating fluid type
Particle carrier (normally for jet type)	Air
	Gas
	Water
	Other liquid
Type of wear	Solid particle erosion
	Solid particle erosion-corrosion
	Solid particle erosion – cavitation
	Liquid particle erosion
Use of fluid and particles	Continuous
	Re-circulating
	Batch

Material removal mechanism	Cutting
	Deformation
	Fatigue
	Combination
Particle forces on specimen	Linear inertia
	Rotational inertia
	Coriolis force

Each test rig presented in section 2 falls under one or more than one of above classifications, and hence they can be specified in combination according to the basis for classification. For designing and selecting an erosion test rig, the best combination from the proposed classification can be used, which shows the most resemblance to an actual working environment.

8. Conclusion

The experimental study of erosion has been a specific problem and the source for practical solutions in the past. Most recently, experiments have been conducted for all aspects of erosion such as the investigation of the effects of variable parameters, materials and processes. There is however no standard procedure or test rigs for the purpose. As a result, the disparity in construction, instrumentation and operating environment of test rigs is very high. Since the interaction between the variables is not clearly known, it is difficult to exchange and interpret results from different tests. The selection of proper type of test rig for specific erosion application is very important. This paper proposes the classification of erosion test rigs into 21 different types based on 6 typical bases for classification. Each particular test rig should fall under some combination of classification presented. Conversely, for particular applications, a set of the proposed classification can be selected for most appropriate match with actual operating conditions.

The monitoring of operating variables in an erosion test rig is difficult. Modern and automatic sensors are not used to a great extent due to degradation of sensors by particle impact. Generally erosion rates are presented in terms of the ratio of weight loss of the specimen to the weight of striking particles. But the ranking or comparison of the erosion behavior of materials with respect to a standard reference material under the same operating conditions is also widely used. Since there are large uncertainties in the variables in erosion tests, the qualitative ranking of different materials is a good option for presenting the findings of erosion experiments.

Appendix B

Photographs of eroded components of small turbine

Figure C2 The eroded top cover of 240 KW Francis runner

Figure C1 The 640 KW eroded Pelton bucket of Sundarijal hydropower plant (head 228 m and discharge 0.37 m³/s)

Figure C3 Eroded guide vane of 240 KW Francis turbine
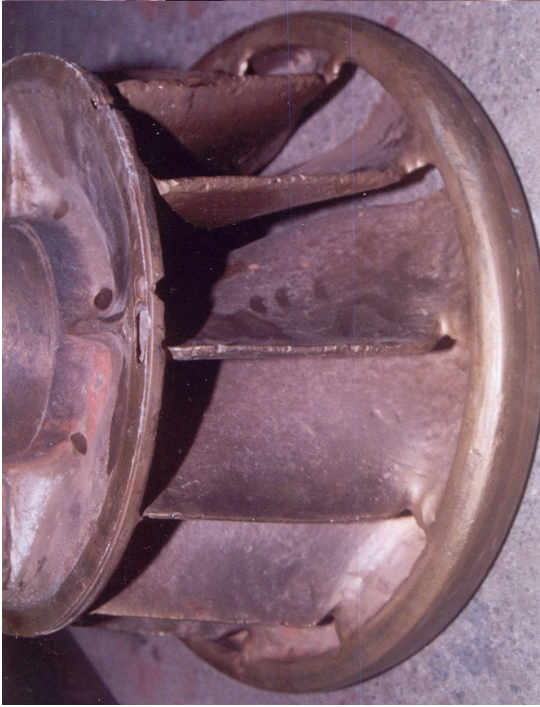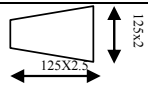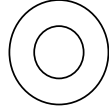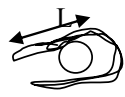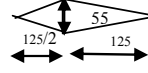
Figure C4 The 240 KW eroded Francis runner made up of bronze (head 23.5 m and discharge 1.35 m^3/s)

Appendix C

Weight loss estimation of eroded turbine

Summary of calculation of weight loss of Francis turbine components due to erosion based on observation at workshop during maintenance

Part Name	Assumption	Area (mm^2)	Volume (mm^3)	Quantity	Total Volume (mm^3)	Weight loss (kg)	
Runner Blade	Erosion of 1mm uniform thickness all around	78125	78125	16	1250000	9,75	
Face plate	Face plate erosion 1mm (0.5mm top + 0.5mm bottom	130310	130310	1	130310	1,02	
Horse shoe	L*W*D L= (70+60)*2 W=12 D=4	3120	12480	20	249600	1,95	
Guide vane Face	125X125	15625	15625	20	312500	2,44	
Guide vane top-bottom	1mm in total	5156,25	5156,25	20	103125	0,80	
Grooves	groove length = dia of shaft	39,25	2158,75	2X20	86350	0,67	
Sum						16,63	

Appendix D

Detail data of sand sample analysis

Table D1 Mineral content of sand samples from different rivers and power plants of eastern region of Nepal

	Roshi	Dhad	Khimti	Kimti	Tamakoshi	Phedi	Dolal Dhat	Sukoshi	Sapta
Quartz	40 - 42	63 - 65	62 - 64	61 - 63	63 - 65	60 - 62	65 - 67	65 - 66	65 – 68
Feldspar	10 - 12.	4 - 6.	3 - 5.	3 - 5	4 - 5.	3 - 5.	5 - 7.	3 - 4	3 - 4.
Muscovite	<1	8 - 10.	8 - 9.	6 - 7	7 - 8.	8 - 10.	8 - 9.	7 - 8	9 - 10.
Biotite	<2	13 - 15.	15 - 16.	18 - 20	15 - 16.	12 - 14.	12 - 14.	15 - 16	14 - 15.
Amphibole(Hornblende, Actinolite)	ND	<0.5	Rare	Rare	Rare	ND	<0.25	Rare	Rare
Pyroxene	ND	ND	ND	ND	ND	ND	Traces	Traces	ND
Chlorite	1 - 2.	1 - 2.	<1	<1	<1	1.5 - 2	<1	<1	1 - 2.
Olivine	NI	ND	ND	Traces (?)	ND	ND	ND	ND	NI
Calcite/dolomite	<0.5	<0.5	ND	<0.5	<0.25	<0.25	<0.25	<0,5	Rare
Kyanite	ND	ND	ND	ND	ND	ND	ND	ND	ND
Sillimanite	ND	ND	<0.5	<0.25	<0.5	Rare	Rare	<0.5	<0.25
Magnetite	<0.5	<1	<0.5	0.5-1	<1	<1	<0.25	<1	0.5 - 1
Hematite/limonite	3 - 4.	<1	<1	<0.5	<0.5	2 - 3.	<0.5	<0.5	<1
Ilmenite	ND	Rare	Traces	<0.5	Rare	Rare	<0.5	rare	Rare
Garnet	Traces	<0.5	<1	1 - 2	1 - 1.5	0,5	0.5 - 1	<1	<1
Tourmaline	Traces	<0.5	0,5	<1	<1	<0.5	<0.25	<0.5	<0.25
Rutile	ND	Rare	Rare	Rare	Rare	Rare	Rare	<0.25	Rare
Apatite	ND	ND	ND	ND	ND	ND	ND	ND	ND
Zircon	ND	ND	ND	ND	Traces	ND	NI	Traces	Very rare
Corundum/Topaz	ND	ND	ND	ND	ND	ND	ND	ND	ND
Clay minerals	2 - 3.	Rare	Rare	Rare	Rare	Rare	Rare	rare	Rare

Table D2 Mineral content of sand samples from different rivers and power plants of middle region of Nepal.

	Kulakhani	Chitlang	Palung	Bagmati	Manahara	Dhobi	Gaur (Bagmati)
Quartz	58 - 61	50 -52	54 - 56	54 – 56	54 - 56	58 - 60	67 – 70
Feldspar	5 - 7	7-8	7 -9	6 - 7.	4 - 5.	8 - 9.	5 - 6.
Muscovite	7 - 8	7-8	9-10	16 - 17.	18 - 20.	12 - 14.	4 - 5.
Biotite	13 - 14.	10 -13	12-14.	17 - 18.	20 - 22.	14 - 16.	7 - 8.
Amphibole(Hornblende, Actinolite)	Rare	rare	<0.5	ND	Traces	ND	ND
Pyroxene	ND	ND	ND	ND	ND	ND	ND
Chlorite	2	2-3	1-2.	1 - 2.	<1	<1	2 - 3.
Olivine	ND	ND	ND	ND	ND	ND	ND
Calcite/ dolomite	<0,5	<0.5	<0.5	ND	ND	ND	<0.5
Kyanite	Very rare	ND	ND	NI	NI	ND	ND
Sillimanite	Very rare	ND	<0.25	rare	ND	ND	ND
Magnetite	1-2	<1	1-1.5	<0.25	<0.25	<0.25	<0.5
Hematite/ limonite	<1	3-4	1-2.	<1	<1	1 - 2.	2 - 3.
Ilmenite	Rare	rare	rare	rare	Rare	Rare	Rare
Garnet	<0.5	ND	0.25-0.5	<0.25	Rare	Rare	<0.5
Tourmaline	<0.5	ND	0.5-1	<0.25	Rare	<1	Very rare
Rutile	Rare	ND	rare	Very rare	Traces	Traces	Very rare
Apatite	ND	ND	ND	ND	ND	ND	ND
Zircon	ND	ND	Traces	ND	ND	ND	ND
Corundum/ Topaz	ND	ND	ND	ND	ND	ND	ND
Clay minerals	Rare	8-10	rare	rare	<0.5	Rare	Rare

Table D3 Mineral content of sand samples from different rivers and power plants of western region of Nepal

Minerals	Rivers West	Jhimruk	Rapti	Madi	Ganaha	Arun	Modi-2	Modi - 1	Andhi	Tinau
Quartz	60 -62	72 -74	48 -50	60 -62	45 - 47	46 - 48	60 - 62	56 - 58	50 - 52	44 – 46
Feldspar	4 - 6	3 -4	3 -4	4 - 5	7 -8	4 - 5	3 - 4	3 -4	6-7	5 -6
Muscovite	5 -6	4 - 5	<1	6-7	1 - 2	<1	10 - 12	12-14	<1	<1
Biotite	8 -10	12 - 14	<1	10 -12	1 - 1.5	<1	16 -18	21-23	<1	<1
Amphibole(Hornblende, Actinolite)	Rare	ND	Traces	Rare	ND	ND	Rare	Rare	Traces	Rare
Pyroxene	ND	ND	NI	Traces	ND	ND	Traces	Traces	NI	ND
Chlorite	1.5 - 2	0.5 -1	<1	1 - 2	3-4	0.5 - 1	1-2	2	<1	<1
Olivine	ND	ND	ND	ND	ND	ND	ND	NI	ND	ND
Calcite/ dolomite	<0.5	<0.5	<0.5	<0.1	<1	<0.5	<0.25	<0,5 -1	<0.25	1-2
Kyanite	ND	ND	ND	ND	ND	ND	ND	ND	ND	ND
Sillimanite	Rare	ND	ND	ND	ND	ND	<0.25	Traces	Traces	ND
Magnetite	<1	<0.5	<0.5	0.5 -1	<0.25	<0.25	<1	<0.5	<0.25	<0.25
Hematite/ limonite	1 - 2	<1	<1	<1	3 - 4	3 - 4	<0.5	<1	2-3	<1
Ilmenite	Traces	Rare	Rare	Rare	ND	ND	Rare	Rare	ND	ND
Garnet	<1	<0.5	0,5	<1	Rare	Rare	<1	<0.5	Rare	<1
Tourmaline	Rrare	Rare	Traces	<0.25	ND	Traces	<0.25	<0.25	Traces	NI
Rutile	Rrare	Traces	Traces	Rare	ND	Traces	Rare	Rare	ND	ND
Apatite	ND	ND	ND	ND	ND	ND	ND	ND	ND	ND
Zircon	ND	ND	ND	ND	ND	ND	Traces	Traces	ND	ND
Corundum/ Topaz	ND	ND	ND	ND	ND	ND	ND	ND	ND	ND
Clay minerals	Rrare	Rare	<1	Rare	<1	1 - 2	ND	<1	1-2	Rare

Appendix E

Supplementary photos of high speed video images

Time 00:000 sec

Time 00:009 sec

Time 00:003 sec

Time 00:012 sec

Time 00:06 sec

Time 00:015 sec
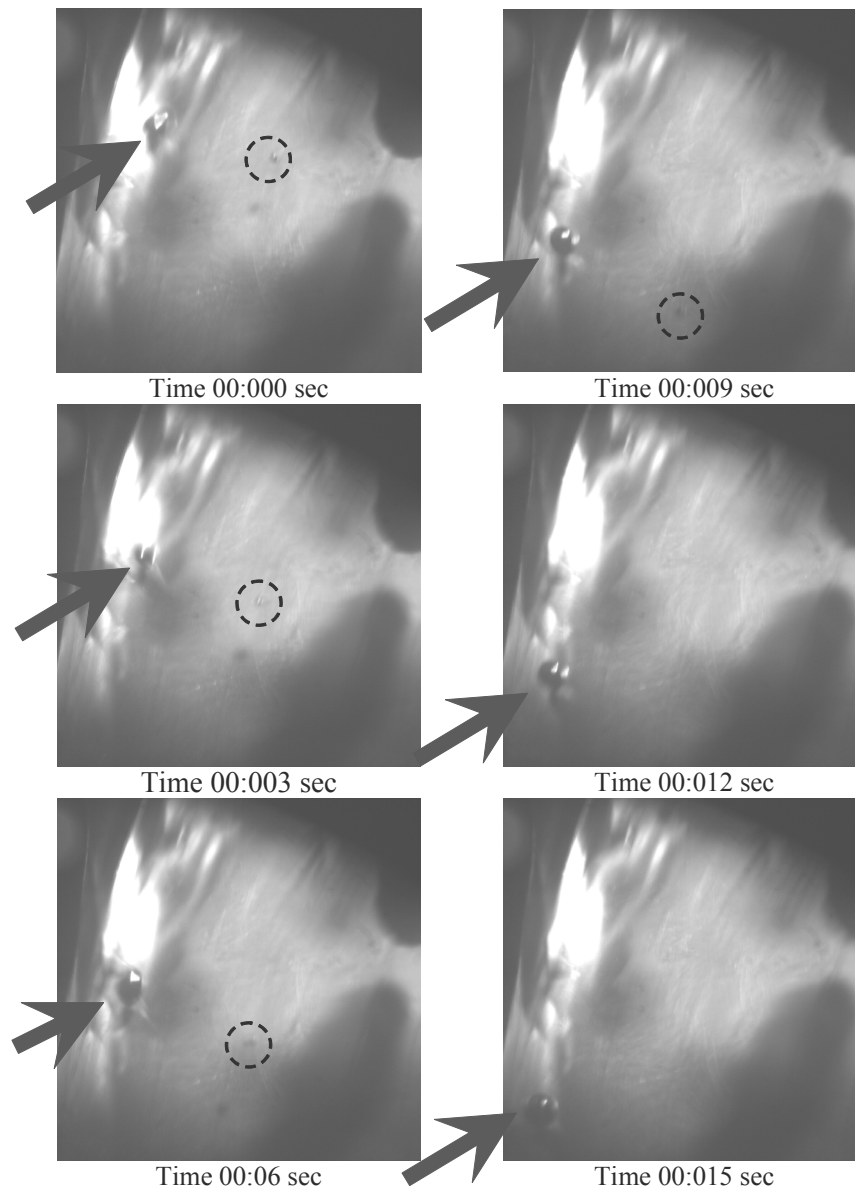
Figure E1 High speed video picture frames

Arrow - 10 mm steel ball   Dotted circle – 4 mm steel ball

Frame 1

Frame 4

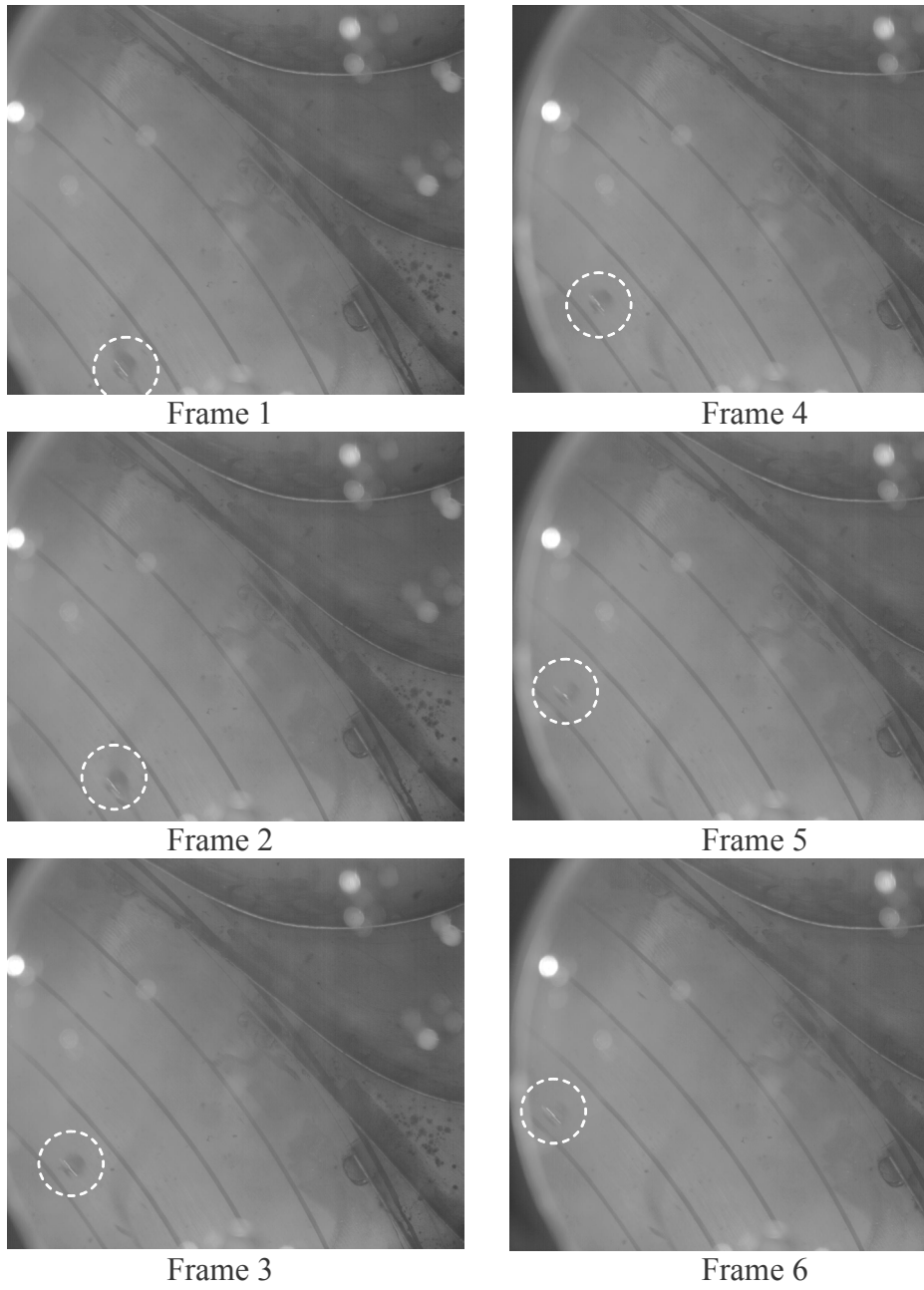Frame 2

Frame 5

Frame 3

Frame 6

Figure E2 High speed video picture frames

Steel ball of 7 mm diameter on frames